UNIVERSIDADE DE LISBOA

INSTITUTO SUPERIOR TÉCNICO

Evaluation of the seismic vulnerability of the unreinforced masonry buildings constructed in the transition between the 19th and 20th centuries in Lisbon, Portugal

Ana Gabriela Gaspar Simões

Supervisor: Doctor Rita Maria do Pranto Nogueira Leite Pereira Bento

Co-Supervisors: Doctor Sergio Lagomarsino

Doctor Paulo José Brandão Barbosa Lourenço

Thesis approved in public session to obtain the PhD Degree in Civil Engineering

Jury final classification: Pass with Distinction

2018

UNIVERSIDADE DE LISBOA
INSTITUTO SUPERIOR TÉCNICO

Evaluation of the seismic vulnerability of the unreinforced masonry buildings constructed in the transition between the 19th and 20th centuries in Lisbon, Portugal

Ana Gabriela Gaspar Simões

Supervisor: Doctor Rita Maria do Pranto Nogueira Leite Pereira Bento
Co-Supervisors: Doctor Sergio Lagomarsino
Doctor Paulo José Brandão Barbosa Lourenço

Thesis approved in public session to obtain the PhD Degree in Civil Engineering
Jury final classification: Pass with Distinction

Jury

Chairperson: Doctor Eduardo Nuno Brito Santos Júlio, Instituto Superior Técnico, Universidade de Lisboa

Members of the Committee:

Doctor Rita Maria do Pranto Nogueira Leite Pereira Bento, Instituto Superior Técnico, Universidade de Lisboa
Doctor Romeu da Silva Vicente, Universidade de Aveiro
Doctor Luís Manuel Coelho Guerreiro, Instituto Superior Técnico, Universidade de Lisboa
Doctor Xavier das Neves Romão, Faculdade de Engenharia da Universidade do Porto
Doctor António Manuel Candeias de Sousa Gago, Instituto Superior Técnico, Universidade de Lisboa

Funding Institution
Fundação para a Ciência e a Tecnologia

2018

ABSTRACT

The main objective of this work is to evaluate the seismic vulnerability of the unreinforced masonry buildings constructed in the transition between the 19th and 20th centuries in Lisbon, Portugal. It is proposed to define the seismic vulnerability based on the derivation of fragility functions supported on detailed numerical models and displacement performance-based assessment approaches.

A detailed architectural and structural characterization of the buildings is performed based on a multidisciplinary approach. A group of three buildings, representative of a sub-type of buildings, is defined as case of study in order take into account the effect of the block of buildings. The main variations within the typology, in terms of geometry, constructive details and materials are identified. These variations are assumed as epistemic uncertainties and treated through the logic-tree approach.

The analysis of the seismic behaviour addresses the global response of the structure, mainly governed by the in-plane capacity of the walls, and the local response, related to the activation of out-of-plane collapse mechanisms of parts of the structure. The assessment comprehends the comparison between the displacement capacity of the structure, identified for different performance limit states, and the seismic demand, expressed by a properly reduced acceleration-displacement response spectrum. The evaluation of the corresponding seismic intensity measure is obtained from the application of the Capacity-Spectrum Method.

The global seismic behaviour is determined through non-linear static (pushover) analyses considering the equivalent frame model approach. Different parameters are assumed as aleatory variables and treated by the Monte Carlo Method. The combination between epistemic and aleatory uncertainties results in the definition a group of 1000 buildings representative of the typology. Non-linear static (pushover) analyses are performed to define the capacity of the structures. Non-linear dynamic time-history analyses are performed in order to verify the reliability of the load distributions considered in the non-linear static (pushover) analyses. The values of the seismic intensity measure compatible with the attainment of the performance limit states are treated to derive the parameters for the definition of the fragility functions.

The local seismic behaviour of out-of-plane collapse mechanisms are evaluated by non-linear kinematic analyses considering the macro-block modelling approach. The reliability of each mechanisms is analysed as an epistemic uncertainty and treated through the logic-tree approach. As the out-of-plane behaviour is mainly related to the geometric stability rather than to the strength of materials, the geometry of the elements and the actions involved in the mechanisms are assumed as aleatory variables. These variables are combined through a full factorial analysis in order to define the input parameters for the set of mechanisms. In addition, considering that the mechanisms under study are located in the upper level of the buildings, the seismic action is defined through a floor response spectrum that takes into account the dynamic filtering effect of the buildings. The values of the seismic intensity measure compatible with the attainment of the performance limit states are treated in order to derive the parameters for the definition of the fragility functions. This includes the determination of the dispersion related to the definition of the capacity of the mechanisms based on the Response Surface Method.

The fragility functions for the sub-type of masonry buildings studied in this thesis are determined considering the combination between the global and local seismic behaviour. The expected distribution of damage is presented for different seismic events. These fragility functions are then compared with other functions available in the literature for similar masonry buildings. The methodology adopted in this thesis for the evaluation of the seismic vulnerability of masonry buildings may be considered for the analysis of other building typologies.

Key-words: unreinforced masonry building, seismic vulnerability, fragility functions, performance-based assessment, non-linear analyses

RESUMO

O principal objetivo deste trabalho consiste na avaliação da vulnerabilidade sísmica dos edifícios de alvenaria não armada construídos entre os séculos XIX e XX em Lisboa, Portugal. Propõe-se definir a vulnerabilidade sísmica com base na definição de funções de fragilidade baseadas em modelos numéricos detalhados e em abordagens com base no desempenho estrutural em termos de deslocamentos.

É realizada uma caracterização arquitetónica e estrutural detalhada dos edifícios com base numa abordagem multidisciplinar. Um grupo de três edifícios, representativo de um subtipo de edifícios, é definido como caso de estudo para ter em consideração o efeito do quarteirão. As principais variações dentro da tipologia, em termos de geometria, detalhes construtivos e materiais são identificadas. Estas variações são assumidas como incertezas epistémicas e tratadas através da abordagem da árvore lógica.

A análise do comportamento sísmico aborda a resposta global da estrutura, principalmente governada pela capacidade das paredes no seu plano, e a resposta local, relacionada com a ativação de mecanismos de colapso de partes da estrutura para fora do plano. A avaliação compreende a comparação entre a capacidade de deslocamento da estrutura, identificada para diferentes estados limite de desempenho, e a ação sísmica, expressa por um espectro de resposta de aceleração-deslocamento devidamente reduzido. A avaliação da medida de intensidade sísmica correspondente é obtida a partir da aplicação do Método do Espectro de Capacidade.

O comportamento global é determinado através de análises estáticas não-lineares (“pushover”) considerando o modelo de pórtico equivalente. Diferentes parâmetros são assumidos como variáveis aleatórias e tratados por meio do Método de Monte Carlo. A combinação entre incertezas epistémicas e aleatórias resulta na definição de um grupo de 1000 edifícios representativos da tipologia. Análises estáticas não-lineares (“pushover”) são realizadas para definir a capacidade das estruturas. Análises dinâmicas não-lineares com integração no tempo são realizadas para verificar a fiabilidade das distribuições de cargas consideradas nas análises estáticas não-lineares (“pushover”). Os valores da medida de intensidade sísmica compatíveis com a obtenção dos estados limite de desempenho são tratados para definir os parâmetros para a definição das funções de fragilidade.

O comportamento local dos mecanismos de colapso para fora do plano são avaliados através de análises cinemáticas não-lineares de acordo com a abordagem de modelação macro-bloco. A fiabilidade dos mecanismos é analisada como uma incerteza epistémica e tratada através da abordagem da árvore lógica. Uma vez que o comportamento para fora do plano é principalmente relacionado com estabilidade geométrica e não com a resistência dos materiais, a geometria dos elementos e as ações envolvidas nos mecanismos são assumidas como variáveis aleatórias. Estas variáveis são combinadas através de uma

análise fatorial completa para definir os parâmetros a atribuir ao conjunto de mecanismos. Para além disso, considerando que os mecanismos em estudo estão localizados no nível superior dos edifícios, a ação sísmica é definida através de um espectro de resposta ao nível do piso que tem em conta o efeito de filtragem dinâmico dos edifícios. Os valores da medida de intensidade sísmica compatíveis com a obtenção dos estados limite de desempenho são tratados para definir os parâmetros para a definição das funções de fragilidade. Isto inclui a determinação da dispersão associada à definição da capacidade dos mecanismos com base no Método de Superfície de Resposta.

As funções de fragilidade para o subtipo de edifícios de alvenaria estudados nesta tese, são determinadas considerando a combinação entre o comportamento sísmico global e local. A distribuição esperada do dano é apresentada para diferentes eventos sísmicos. Estas funções de fragilidade são depois comparadas com outras funções disponíveis na literatura para edifícios de alvenaria semelhantes. A metodologia adotada nesta tese para a avaliação da vulnerabilidade sísmica de edifícios de alvenaria pode ser considerada para a análise de outras tipologias de edifícios.

Palavras-chave: alvenaria não armada, vulnerabilidade sísmica, funções de fragilidade, avaliação com base no desempenho, análises não-lineares

ACKNOWLEDGEMENTS

I would like to express my sincere gratitude to Professor Rita Bento, my supervisor, for the full support, dedication and guidance throughout these years of research work and for the patience during the writing and correction of this thesis.

I would like to acknowledge to Professor Sergio Lagomarsino, my co-supervisor, for the dedication, valuable scientific contribution and discussions that enrich the work herein presented.

I would like to acknowledge Professor Paulo B. Lourenço, my co-supervisor, for the support, encouragement and comments.

I would like to acknowledge Professor Serena Cattari for the dedication, valuable scientific contribution and constant enthusiasm.

I would like to acknowledge Professor Miguel Castro and Luís Macedo for their contribution regarding the selection of the ground-motion records.

I would like to acknowledge Professor Mário Lopes and Professor António Gago for the support during my first years of research and for the help with the flat-jack tests. Here, I would also like to acknowledge the help from Fernando Alves, Fernando Costa and João Lopes.

I would like to acknowledge Jelena Milošević for the full support and friendship throughout these years of research work.

I would also like to acknowledge my colleagues Rita Peres, André Belejo, Mauro Monteiro, Mohsen Kohrangi, Helena Meireles, Claudia Caruso, Sofia Real, Jorge Pontes, Daria Ottonelli, Stefania Degli Abbati, Jamil Haddad, Salvatore Marino and Daniela Camilletti and my colleagues from the first year of the FTC PhD Program InfraRisk-, Despoina Skoulidou, Leonardo Rodrigues, Pedro Narra, João Mário, Tiago Ferradosa and Hugo Guimarães for all the help during this period.

I would like to acknowledge the Board of Studies from the FTC PhD Programme InfraRisk- for providing me the opportunity to develop this research work and for the grants awarded PD/BI/52584/2014 (1 year) and PD/BD/106076/2015 (3 years).

I would like to express my deepest acknowledgement to my parents, to my sister, to my husband and to my dearest friends, for the full support, encouragement and love.

This page was intentionally left blank

LIST OF CONTENTS

LIST OF FIGURES

LIST OF TABLES

LIST OF SYMBOLS

1. Introduction

im	Value of the seismic intensity measure
p_{LS}	Probability that a generic performance limit state is reached or exceeded given a value of the seismic intensity measure
d	Displacement representative of the building seismic behaviour
D_{LS}	Displacement representative of the performance limit state
Φ	Standard cumulative distribution function
IM_{LS}	Median value of the lognormal distribution of the seismic intensity measure that produces the attainment of the performance limit state
β_{LS}	Dispersion of the lognormal distribution of the seismic intensity measure im_{LS} that produces the attainment of the limit state threshold
β_H	Dispersion in the definition of the hazard curve
β_D	Dispersion in the definition of the seismic demand
β_T	Dispersion in the definition of the performance limit state
β_C	Dispersion in the definition of the capacity

3. Analysis of the global seismic behaviour

H_{eff}	Effective height
V	Acting shear force
V_u	Ultimate shear force
β_i	Residual strength for damage level i
δ_i	Drift for damage level i
k_{in}	Ratio between the elastic and the secant stiffness at the point where the ultimate shear force is reached
k_{el}	Elastic stiffness
k_{sec}	Secant stiffness
k_0	Ratio between the acting shear force and the ultimate shear force
N	Axial force
M	Bending moment

E	Modulus of elasticity
J	Inertia
h	Height of the element
u	In-plane displacement of the element
w	Out-of-plane displacement of the element
φ	Rotation of the element
G	Shear modulus
M_u	Ultimate bending moment
D	Length of the element
t	Thickness of the element
σ_0	Vertical compressive stress
f_c	Compressive strength
h_0	Distance between the section of maximum flexural capacity and the contra-flexure point
f_t	Tensile strength
τ_0	Equivalent shear strength
F_u	Ultimate test load
A_d	Diagonal failure surface area
Int	Interlocking
μ_{loc}	Coefficient of friction in the mortar joints
X_k	Aleatory variable *k*
$X_{k,low}$	Lower value of the aleatory variable *k*
$X_{k,up}$	Upper value of the aleatory variable *k*
μ	Ductility
μ''	Mean value of the updated interval
σ''	Standard deviation of the updated interval
μ'	Mean value of the *a priori* interval
σ'	Standard deviation of the *a priori* interval
$\bar{x}$	Mean value of the test results
$\bar{s}$	Standard deviation of the test results
ε	Standard deviation associated to the uncertainty of the testing method
A	Area of the link beams

I	Inertia of the link beams
t_{eq}	Equivalent thickness
G_k	Permanent load *k*
Q_k	Variable load *k*
ψ_2	Reduction factor
$X_{k,med}$	Median value of the aleatory variable *k*
β	Dispersion
$f_X(x)$	Probability density function
V_b	Base shear force
W	Weight of the model
E[X]	Mean value of X
d	Average displacement of the roof weighted by the seismic modal mass of all nodes
K	Initial stiffness
V_{max}	Maximum base shear force
ξ	Equivalent viscous damping
T_1	Fundamental period
M	Mass matrix
D	Damping matrix
ω	Pulse
d_y	Yielding displacement
d_u	Ultimate displacement
$\Lambda_{P,DLk}$	Cumulative rate of damage in piers that reach damage level *k*
A_p	Cross section of the pier
N_p	Total number of piers in the building
H	Heaviside function
Λ_P	Cumulative rate of damage in piers threshold
θ_{DLk}	Inter-storey drift for damage level *i*
$\Lambda_{P,WL,DLk}$	Cumulative damage of piers in a given wall and level for damage level *k*
k_G	Ratio between the acting base shear force and the maximum base shear force
T^*	Equivalent period
Γ	Transformation factor
m_i	Mass of node *i*
Φ_i	Modal displacement of node *i*

V^*	Equivalent base shear force
d^*	Equivalent displacement
S_a	Spectral acceleration
S_d	Spectral displacement
ξ_{el}	Elastic viscous damping
ξ_{hyst}	Hysteretic damping
d_{PLk}	Displacement of performance level k
E_D	Dissipated energy
E_0	Strain energy
η	Damping correction factor
PGA_{PLk}	Peak ground acceleration that produces the attainment of the performance level k
$PGA_{50\%}$	Median value of the lognormal distribution of the peak ground acceleration that produces the attainment of the performance level k
β_C	Dispersion in the definition of the capacity
T	Period
β_H	Dispersion in the definition of the hazard curve
β_D	Dispersion in the definition of the seismic demand
$PGA_{84\%}$	Peak ground acceleration corresponding to the 84% percentile
$PGA_{16\%}$	Peak ground acceleration corresponding to the 16% percentile
β_G	Dispersion in the global seismic behaviour
w	Weight of the model

4. Analysis of the local seismic behaviour

P_R	Vertical load transmitted by the roof to the piers
μ	Coefficient of friction
P_1	Weight of the parapet
P_2	Weight of the pier
P_3	Weight of the pier below the hinge
α	Static seismic multiplier
$t_{parapet}$	Thickness of the parapet
t_{pier}	Thickness of the pier
γ_R	Self-weight of the roof

$X_{k,low}$	Lower value of the aleatory variable *k*
$X_{k,med}$	Median value of the aleatory variable *k*
$X_{k,up}$	Upper value of the aleatory variable *k*
N	Number of aleatory variables
d_C	Horizontal displacement of a control node
S_d	Spectral displacement
S_a	Spectral acceleration
g	Acceleration of gravity
Γ	Transformation factor
$e*$	Rate of total mass that participates in the mechanism
δ_{Cx}	Horizontal component of the virtual displacement of the control node
n_b	Number of blocks
W_k	Weight of block *k* plus the other masses it carries during the activation of the kinematism
Q_k	Total weight of masses that not carried by block *k* but are connected to it during the activation of the kinematism
$\delta_{Qx,k}$	Virtual horizontal displacement of the barycenter of weights W_k and Q_k
T_e	Elastic period
T_s	Secant period
d_e	Displacement corresponding to the elastic period
d_s	Displacement corresponding to the secant period
α_{med}	Median value of the static seismic multiplier
z	Height of the hinge
ξ	Equivalent viscous damping of the mechanism
ξ_{el}	Elastic viscous damping
ξ_{hyst}	Hysteretic damping
Z	Height of the mechanism
T	Period of the mechanism
$S_a(T,\xi)$	Ground motion response spectrum
$S_{aZ,k}(T,\xi)$	Acceleration response spectrum at position Z due to k^{th} mode of N modes considered
$PFA_{Z,k}$	Peak floor acceleration
f_k	Factor of amplification
T_k	Period of the main structure

ξ_k	Equivalent viscous damping of the main structure
γ_k	Modal participation coefficient of mode k
$\psi_k(x,y,z)$	Modal shape of mode k
$PGA_{50\%}$	Median value of the lognormal distribution of the peak ground acceleration that produces the attainment of the performance level k
β_C	Dispersion in the definition of the capacity
β_{Ci}	Partial dispersion in the definition of the capacity
β_D	Dispersion in the definition of the seismic demand
β_{FS}	Dispersion in the definition of the floor response spectrum
β_L	Dispersion in the local seismic behaviour
w	Weight of the model

5. Analysis of the local seismic behaviour

P_{PLk}	Probability of the performance limit state k
$P_{G,PLk}$	Probability of the performance limit state k related to the global seismic behaviour
$P_{L,PLk}$	Probability of the performance limit state k related to the local seismic behaviour
w	Weight of the model
β_G	Dispersion in the global seismic behaviour
β_L	Dispersion in the local seismic behaviour
β_{FS}	Dispersion in the definition of the floor response spectrum

LIST OF ACRONYMS

FTC	"Fundação para a Ciência e a Tecnologia"
InfraRisk-	Analysis and Mitigation of Risks in Infrastructures
HAZUS	Hazard United States
GIS	Geographic Information System
RISK-UE	An advanced approach to earthquake RISK scenarios with applications to different EUropean towns
LESSLOSS	Risk mitigation for earthquakes and landslides
SYNER-G	Systemic Seismic Vulnerability and Risk Analysis for Buildings, Lifeline Networks and Infrastructures Safety Gain
GEM	Global Earthquake Model
GDP	Gross Domestic Product
INE	"Instituto Nacional de Estatísticas"
RC	Reinforced Concrete
URM	Unreinforced Masonry
RSCCS	"Regulamento de Segurança das Construções Contra os Sismos"
RSEP	"Regulamento de Solicitações em Edifícios e Pontes"
IREBA	"Instruções Regulamentares para o Emprego do Beton Armado"
EC8-3	Eurocode 8 – Part 3
KL	Knowledge Level
CF	Confidence Factor
CEN	"Comité Européen de Normalisation"
SDOF	Single-Degree-Of-Freedom
ADRS	Acceleration-Displacement Response Spectrum
EC8-1	Eurocode 8 – Part 1
IDA	Incremental Dynamic Analysis
NTC	"Norme tecniche per le costruzioni"
MIT	"Ministero delle Infrastrutture e dei Trasporti"
PERPETUATE	Performance-Based Approach to Earthquake Protection of Cultural Heritage in European and Mediterranean Countries

SAC	Structural Engineers Association of California (SEAOC), Applied Technology Council (ATC), California Universities for Research in Earthquake Engineering (CUREe)
FEMA	Federal Emergency Management Agency
CNR	“Consiglio Nazionale delle Ricerche”
LS	Limit State
IM	Intensity Measure
PGA	Peak Ground Acceleration
AML	“Arquivo Municipal de Lisboa”
RSEU	“Regulamento de Salubridade das Edificações Urbanas”
RGEUL	“Regulamento Geral das Edificações Urbanas em Lisboa”
LNEC	“Laboratório Nacional de Engenharia Civil”
SEVERES	Seismic Vulnerability of Old Masonry Buildings
IPQ	“Instituto Português da Qualidade”
GNDT	“Gruppo Nazionale per la Difesa dai Terremoti”
FEM	Finite Element Method
DL	Damage Level
DS	Damage State
RILEM	“Reunion Internationale des Laboratoires et Experts des Materiaux, Systemes de Construction et Ouvrages”
ASTM	American Society for Testing and Materials
NZSEE	New Zealand Society for Earthquake Engineering
SRSS	Square Root of Sum of Squares
CQC	Complete Quadratic Combination
CoV	Coefficient of Variation
MDOF	Multiple-Degree-Of-Freedom
NLDA	Non-linear dynamic analyses
NLSA	Non-linear static analyses
PL	Performance Level

1. INTRODUCTION

1.1. Motivation

The PhD thesis now presented has been developed within the scope of the FTC PhD Programme in Analysis and Mitigation of Risks in Infrastructures – InfraRisk- (http://infrarisk.tecnico.ulisboa.pt/). The aim of this programme is to analyse the main risks to infrastructures due to the exposure to different natural hazards (e.g. earthquakes, hurricane winds, floods, etc.). As stated in the objectives of the programme: "in Portugal, earthquakes are the phenomena with the largest human and economic impact" and "the scale of devastation they can induce is so spread to cause decades of economic stagnation". Therefore, it is fundamental to conduct the seismic risk analysis in Portugal in order to introduce measures that reduce potential losses due to future earthquakes.

Despite some variations present in the literature, seismic risk results from the combination of three components (McGuire, 2004; Vicente et al., 2011): seismic hazard, exposure and seismic vulnerability. Seismic hazard represents the susceptibility of a region for the occurrence of earthquakes. It is defined as the probability of exceeding a certain intensity of a seismic event, during a specified recurrence period. Exposure refers to the elements exposed to the seismic hazard (e.g. people and assets). Seismic vulnerability represents the susceptibility of the elements to suffer damage or loss due to a seismic event. It can be defined in the form of fragility functions, as the probability of reaching or exceeding a specified damage limit state as a function of a certain intensity of a seismic event, or in the form of vulnerability functions, as the expected value of loss evaluated in terms of replacement cost of buildings or number of fatalities, as an example. As a result, seismic risk reflects the probability of exceeding a certain level of damage/loss of an exposed element in the occurrence of a seismic event of certain intensity.

In the past decades, the field of seismic risk analysis has witnessed remarkable improvements (Calvi and Pinho, 2006). The development of fragility functions for the seismic risk analysis as started in the early 1990s, following the 1971 San Fernando earthquake in the USA, where catastrophic damages were observed in almost every type of lifeline (Pitilakis, Crowley and Kaynia, 2014). Major earthquakes that followed, such as the 1985 Mexico City earthquake, the 1989 Loma Prieta earthquake, the 1994 Northridge earthquake, the 1995 Kobe earthquake, the 1999 Chi-Chi and Turkey earthquakes revealed important lessons, leading to the development of new methods for estimating risk and identify ways to mitigate future earthquake damages and losses. The HAZUS application represents the first comprehensive methodology to estimate potential losses due to earthquakes, hurricane winds, floods and tsunamis (https://www.fema.gov/hazus). This application is implemented in the Geographic

Information System (GIS) software to map and display hazard data and the results of damage and economic loss estimates for buildings and infrastructures. The first edition of the application dates from 1997 – HAZUS97. Although it has been developed within USA, HAZUS has also been adopted by emergency management organizations worldwide such as Singapore, Canada, Australia, Pakistan and Portugal, between others.

Attempts to establish a methodology for the seismic risk analysis of buildings and infrastructures in Europe include, for example, the research projects RISK-UE (Mouroux and Le Brun, 2006) and LESSLOSS (Calvi and Pinho, 2004). In both projects, the seismic hazard and vulnerability of several European cities (including Lisbon) were evaluated in order to estimate the associated seismic risk. The SYNER-G project (Pitilakis, Crowley and Kaynia, 2014) developed an integrated methodology for the seismic vulnerability and risk analysis of buildings, infrastructures and networks, including the evaluation of the physical and socio-economic systemic vulnerability. At a global scale, reference as to be made to the Global Earthquake Model, GEM (Pinho, 2012). This initiative has the objective of developing best practises, datasets, models and tools for the seismic risk assessment at a national and regional scale, through the collaboration with local experts worldwide.

Silva et al. (2015a) has proposed an integrated model for the assessment of the seismic risk of the building stock in mainland Portugal. The three components of risk were defined based on previous studies, up-to-date models and data, and provided as input to the OpenQuake engine (Silva et al., 2014), an open-source program within the Global Earthquake Model. It was estimated that a future seismic event, with a return period of 475 years, has the potential to produce mean economic losses to the current residential building stock in Portugal of approximately 32% of the Portuguese Gross Domestic Product (GDP) from 2011 (reference year of the study). As expected, it was concluded that the Lower Tagus Valley (Lisbon and Setúbal districts) and the southwest of Portugal have the highest seismic risk. The economic losses per building typology indicated that masonry buildings are the most seismically vulnerable, and therefore the ones for which strengthening/retrofitting campaigns should be first addressed.

The exposure model used by Silva et al. (2015a), combines information from the Building Census of 2011 (INE, 2012) with other building statistics, to create a dataset capable of providing the geographic distribution of building typologies as a function of the type of construction, number of storeys and date of construction. A detailed vulnerability model for the reinforced concrete (RC) building stock was derived based on an analytical methodology (Silva et al. (2015b)). In contrast, a simplified approach was adopted for the masonry building stock, starting from the capacity curves proposed by Carvalho et al. (2002) for different typologies categorized by the number of storeys and seismic design approach. Despite the general conclusions of the study, it highlights the importance of conducting a detailed seismic vulnerability analysis for the masonry building typologies in Portugal; which are the most vulnerable and the most common typology, representing half of the building stock (INE, 2012).

The seismic vulnerability assessment of masonry buildings is a complex task because it refers to a wide variety of constructions, characterized by different types of masonry and structural systems that depend on the geographical area and period of construction (Cattari and Lagomarsino, 2013). Masonry is a heterogeneous material defined by units (stone, clay brick, adobe, etc.) and joints (filled or not by mortar). The mechanical properties of the material are thus related to the properties of the constituents and to the dimension, shape and interlocking of the units. In regards to the structural system, a distinction as to be made between engineered and non-engineered masonry buildings. The former have been specifically conceived to withstand seismic loads, either as unreinforced, confined or reinforced masonry (CEN, 2005). The latter refer to the traditional masonry buildings constructed based on local materials, traditional construction processes and empirical rules. These are usually characterized by unreinforced masonry (URM) walls and timber floors and roof structure. In some cases, the systematic introduction of earthquake-resistant elements (e.g. steel tie-rods, timber frames reinforcing the masonry walls) is observed, following the occurrence of medium or high intensity seismic events. Despite this, the seismic vulnerability of URM buildings has been testified worldwide.

The development of detailed vulnerability models at territorial scale requires the identification of different building classes/typologies. This is supported on the idea that buildings with similar architectural and structural features and located in similar geotechnical conditions are expected to have a similar seismic performance. With focus on the residential buildings from Lisbon district, one with the highest seismic risk in Portugal, four masonry typologies are usually recognized: 1) buildings that resisted to the 1755 earthquake, fire and tsunami, 2) buildings constructed afterwards, under the plan of the Marquis of Pombal, later known as “Pombalino” buildings, 3) buildings constructed in the end of the 19th century and in the beginning of the 20th century, called in a depreciatory way as “gaioleiro” buildings, and 4) buildings with a mixed masonry-RC structure, named in a colloquial way as “placa” buildings (due to the use of RC slabs). Here, it is important to refer that all these masonry typologies were constructed before the publication of the first design codes regarding the quantification of the seismic action in Portugal (RSCCS, 1958; RSEP, 1961).

The first typology referred is quite heterogeneous as it results from different periods of construction (and reconstruction after the 1755 earthquake). In contrast, “Pombalino” buildings were constructed in a standardized way and making use of earthquake-resistant practises (Ramos and Lourenço, 2004; Lopes et al., 2014; Meireles et al., 2014). The third typology represents a period of downgrade of the construction quality in Lisbon. There are, in fact, records of collapsed buildings during the construction phase which originated a public demonstration against the “gaioleiro”, the name given to the contractors responsible for these buildings. A few years after, the buildings got to be known as “gaioleiro”, meaning “bird cage” in the sense they were more adequate for birds than for people (Appleton, 2005; Simões et al., 2017). The fourth typology of buildings is characterized by the introduction of the first RC elements, beams, columns and slabs (Lamego et al., 2017; Milošević, Cattari and Bento, 2018) along with the publication of the first RC code in Portugal (IREBA, 1918).

Masonry buildings are the most seismically vulnerable and the most common building typology in Portugal. With the focus on Lisbon district, particular attention should be given to the buildings constructed in the transition between the 19th and 20th centuries considering the downgrade of the construction quality in comparison with the preceding “Pombalino” buildings. In addition, the increase of the urban regeneration in Lisbon in the last decades requires better knowledge about the existing stock of buildings and the application of proper analysis procedures for the seismic assessment and retrofitting in order to guarantee safety, functionality and the maintenance of cultural features. The importance of conducting a comprehensive assessment of the seismic vulnerability of the residential masonry buildings in Lisbon is therefore clear, starting from the URM buildings constructed in the transition between the 19th and 20th centuries. This frame the work proposed for this PhD thesis along with the research focus, objectives and methodology presented in the following sections.

1.2. Research focus and background

The seismic response of URM buildings is mainly related to the mechanical properties of masonry, geometry of the elements, construction details and type of horizontal diaphragms – floors and roof (Lourenço et al., 2011; Cattari and Lagomarsino, 2013; Penna, 2014). URM buildings are quite prone to local mechanisms related to the out-of-plane behaviour of walls or parts of the structure; in particular when connections between perpendicular walls and between walls and floors/roof are not effective. In case local mechanisms are prevented (through the introduction of tie-rods or ring beams, as an example), and the walls disintegration cannot occur, the seismic behaviour is mainly governed by the in-plane capacity of walls and by the in-plane stiffness of horizontal diaphragms. However, URM buildings usually have timber floors and roof, exhibiting a quite flexible diaphragm behaviour and providing a lower degree of coupling to the walls, limiting the distribution of forces between vertical structural elements and the activation of a global box-type behaviour. The assessment of URM buildings with timber floors/roofs requires therefore the use of proper methods of analysis and verification procedures, which take into account both the local (out-of-plane) and global (in-plane) seismic response and the flexible behaviour of diaphragms.

The methodology proposed in Part 3 of Eurocode 8, EC8-3 (IPQ, 2017) for the seismic assessment/retrofitting of existing buildings considers a performance-based assessment supported on a displacement- or deformation-based approach, to determine the level of safety of the structure. It comprehends: 1) selection of limit states for the structural performance, 2) definition of a knowledge level (KL) based on the number of tests and inspections performed on the building addressing the identification of the geometry, constructive details and materials, 3) identification of the method of analysis (as a function of KL), 4) application of a Confidence Factor (CF) to the mean properties of materials (as a function of KL), 5) safety verification where the conformity of each element/mechanism is checked involving procedures which depend on the nature of the mechanism (i.e. ductile or brittle).

The methods of analysis are divided in linear (lateral force analysis and modal response spectrum analysis), non-linear (static pushover analysis and time-history dynamic analysis) and q-factor approach. In case of masonry structures, linear methods may be used when "floors possess enough in-plane stiffness and are sufficiently connected to the perimeter walls to assume that they can distribute the inertia forces among the vertical elements as a rigid diaphragm" (IPQ, 2017). It also states that "the need to check the attainment of the limit state of near collapse can only be applied when the analysis is non-linear" (IPQ, 2017). On the other hand, the application of the q-factor approach is not reliable since existing buildings are not capacity designed (Lagomarsino and Cattari, 2015a), stressing the impossibility of applying the ductile/fragile mechanism concept proposed in the EC8-3 (IPQ, 2017), also due to the absence of specific q-factors for different masonry typologies. In this framework, the assessment of masonry buildings must rely on non-linear methods of analysis (static and dynamic).

The development of performance-based concepts has led to an increasing use of non-linear static (pushover) analyses. These simplified procedures comprehend the comparison between the displacement capacity of the structure (identified for different performance limit states) and the seismic demand, which depends both on the structure and on the characteristics of the seismic action (Freeman, 1998; Fajfar, 1999). The displacement capacity of the structure is described by a force-displacement curve (the pushover curve) that provides the overall inelastic response of the structure under horizontal seismic loads in terms of stiffness, overall strength and ultimate displacement capacity. This curve may be obtained by a non-linear incremental static (pushover) analysis, i.e. by subjecting the structure to a static lateral load distribution of increasing intensity (simulating the seismic inertial forces). The pushover curve is then converted into the capacity curve of an equivalent single-degree-of-freedom (SDOF) system and compared with the seismic demand, obtained by a properly reduced acceleration-displacement response spectrum (ADRS). Different methods are available for the evaluation of the displacement demand on the capacity curve (Lagomarsino and Cattari, 2015a): 1) the Capacity-Spectrum Method and the Displacement-Based Method (Freeman, 1998; Calvi, 1999; Priestley, Calvi and Kowalsky, 2007), 2) the N2 Method (Fajfar, 2000) adopted in the Eurocode 8 – Part 1, EC8-1 (CEN, 2004), 3) the Coefficient Method (ASCE, 2014), or 4) the Modified ADRS Method (FEMA, 2005).

Non-linear dynamic time-history analyses are the most accurate method for the seismic assessment, as the dynamic behaviour of the structure is directly considered (while in case of non-linear static analyses the behaviour of the structure is analysed under a predefined mode, induced by a lateral load distribution, monotonically increased; thus the effects of higher modes, which induce a widespread diffusion of damage are not taken into account). Another advantage is that the conventional conversion to an equivalent SDOF system is not required. The capacity of the structure, associated with different performance limit states, is evaluated, for example, by performing Incremental Dynamic Analysis, IDA (Vamvatsikos and Cornell, 2002). IDA curves are obtained by scaling a proper set of acceleration time-history records until the reaching of a specific performance limit state. An alternative consists in performing non-linear dynamic analyses with higher number of records, here without any scaling (cloud method). The seismic intensity measure compatible with a specific performance limit state is analysed based on a statistical evaluation, for example through the Multiple Stripe Analysis, as proposed by Jalayer and Cornell (2009). The higher computational effort (time consuming, treatment of results), the additional modelling features (e.g. cyclic hysteretic behaviour of structural elements, not required for non-linear static analyses) and the difficulty in the definition of performance limit states make the application of non-linear dynamic methods feasible only in a limited number of cases or their application to prove the reliability of the non-linear static analyses results.

Several problems have been raised in the last years regarding the application of the EC8-3 (IPQ, 2017) to masonry buildings (Cattari and Lagomarsino, 2009; Magenes and Penna, 2009, 2011). This has motivated the development of a number of research projects aiming to provide consistent alternative solutions and the publication of parallel codes, as the case of the Italian Building Code, NTC (2008) and subsequent commentary (MIT, 2009). Some of the issues are related to: 1) the analysis of the local mechanisms associated with the out-of-plane behaviour of walls or parts of the structure, 2) the behaviour of the buildings as structural units that are part of building aggregates, which is the common case in historic city centres, 3) the definition of performance limit states addressing masonry buildings with flexible diaphragms or 4) the definition of the KL and the need to introduce specific criteria for masonry buildings. In regards to the first two points, these are simply not addressed in the EC8-3 (IPQ, 2017).

Regarding the analysis of local behaviour, Ferreira et al. (2015) and Sorrentino et al. (2017) present a critical overview of the out-of-plane assessment techniques for masonry buildings available in literature and in codes, including force-based, displacement-based and energy-based approaches. Aiming to evaluate the capabilities of different approaches, around the 9th International Masonry Conference, in 2014, a blind prediction was proposed regarding the out-of-plane response of two masonry structures subjected to shaking table tests (Mendes et al., 2017). In general, the predictions were carried out using limit analysis based on the kinematic approach, and the assessment of the collapse was based on the force-based and displacement-based approaches. Good predictions were obtained for the stone structure, while only fair results were obtained for the brick structure.

As referred, the EC8-3 (IPQ, 2017) makes no reference to the analysis of local mechanisms. The Italian Building Code (NTC, 2008; MIT, 2009) suggests the use of limit equilibrium analysis for the assessment of the out-of-plane behaviour. The method is based on the application of the Principle of the Virtual Works to selected mechanisms and on the evaluation of the seismic capacity in terms of resistance (linear kinematic analysis) or infinitesimal displacement (non-linear kinematic analysis), allowing therefore the consideration of both force-based and displacement-based approaches. Additional studies have been carried out by Lagomarsino (2015) and Degli Abbati and Lagomarsino (2017) regarding the calibration of the methodologies based on experimental tests and parametrical numerical analyses. Moreover, considering that the mechanisms are usually located at the upper levels of the building, the seismic input should be defined through a floor response spectrum that takes into account the dynamic filtering effect of the building. Improved formulations for this floor response spectrum have been proposed by Degli Abbati et al. (2017) starting from the formulation on the commentary to the NTC (MIT, 2009).

In what concerns the analysis of building aggregates, the Italian Building Code (NTC, 2008; MIT, 2009) proposes some simplifications. It states for instance, that for buildings bonded on both sides by other building units, the structural analysis may be performed by neglecting torsional effects. It also suggests that for buildings with flexible diaphragms, the analysis of single walls or of systems of coplanar walls can be carried out, each analysed as an independent structure subjected to relevant vertical loads and seismic action in the direction parallel to the wall (Magenes and Penna, 2009). However, additional research on the structural interaction between buildings is still needed. Regarding the analysis of building aggregates, reference to the works related to the analysis of complete blocks of "Pombalino" buildings in Lisbon (Ramos and Lourenço, 2004; Oliveira, 2009; Simões, 2010).

In regards to the third point, the EC8-3 (IPQ, 2017) recommends the consideration of three performance limit states directly defined on the pushover curve based on conventional displacement thresholds. The definition of performance limit states in buildings with box-type behaviour and rigid floors is quite trivial, as it is reasonable to assume that a number of elements and walls reach a specified limit state almost at the same time. However, the presence of flexible diaphragms (timber floors and roof) leads to a more independent behaviour of the walls. As a consequence, the reaching of serious damage in a wall may not appear evident on the pushover curve, when this wall offers a small contribution to the total base shear. In addition, the attainment of a limit state should also consider the lack of homogeneity on damage distribution and its possible premature concentration in some walls. Due to these reasons, Lagomarsino and Cattari (2013), within the PERPETUATE project (http://www.perpetuate.eu/), proposed to define performance limit states based on a multi-scale approach that correlates the response of the structure at three scales: structural elements (piers and spandrels), macro-elements (walls and horizontal diaphragms) and global (represented by the pushover curve).

PERPETUATE project had as main objective to produce European Guidelines for the evaluation and mitigation of seismic risk to cultural heritage assets (D'Ayala and Lagomarsino, 2015). The displacement-based approach is adopted as the standard method of analysis. Static and dynamic non-linear verification procedures were defined to evaluate the seismic intensity measure compatible with the attainment of specific performance limit states (Lagomarsino and Cattari, 2015a). This includes both the global seismic behaviour of structures (Lagomarsino and Cattari, 2015b) and the seismic behaviour of independent macro-elements (Lagomarsino, 2015), such as rocky structures (e.g. archaeological remains, obelisks, columns), arch-piers systems, out-of-plane mechanisms of walls (e.g. standing out walls, façades in buildings) and artistic assets prone to overturn (e.g. pinnacles, statues).

Finally, the fourth issue is related to the definition of the KL and the need to introduce specific criteria for masonry buildings, taking into account that: 1) the majority of buildings were built in absence of design regulations (often no drawings or structural details are available) and 2) experimental tests to buildings' materials are usually not feasible or unreliable due to the intrinsic variability of the material within the building. The KL methodology has been studied by many authors (Franchin, Pinto and Rajeev, 2010; Jalayer et al., 2011; Tondelli et al., 2012; Rota, Penna and Magenes, 2014; Cattari, Lagomarsino, Bosiljkov, et al., 2015) showing in general the inadequacy of the present format. Although a Confidence Factor (CF) is applied to the properties of materials, it is intended to cover different sources of uncertainty related to knowledge of the construction details, variation of mechanical properties in the structure, methods of analysis and modelling approaches. One alternative to overcome these shortcomings is to pass from a semi-probabilistic approach, as the one proposed in the EC8-3 (IPQ, 2017), to a fully probabilistic approach capable of considering, in an accurate way, the propagation of uncertainties in the seismic response of the structure. In this framework, reference to the recommendation documents such as the SAC-FEMA guidelines (Cornell et al., 2002; Jalayer and Cornell, 2003) and to the Italian provisions CNR-DT 212/2013 (CNR, 2014; Pinto and Franchin, 2014). Uncertainties are usually divided into epistemic and aleatory related, respectively, to the state of knowledge and to the intrinsic randomness of a phenomena.

Fully probabilistic approaches require the definition of fragility functions that provide the probability that a specified performance limit state (LS) is reached or exceeded given a value *im* of the seismic Intensity Measure (IM). Fragility curves are often described by a lognormal cumulative distribution function, as in Equation (1.1):

$$p_{LS}(im) = P(d \geq D_{LS} \mid im) = P(im_{LS} < im) = \Phi\left(\frac{1}{\beta_{LS}} \log\left(\frac{im}{IM_{LS}}\right)\right) \tag{1.1}$$

where, d is a displacement representative of the building seismic behaviour, D_{LS} is the displacement limit state threshold, Φ is the standard cumulative distribution function, IM_{LS} is the median value of the lognormal distribution of the intensity measure im_{LS} that produces the attainment of the limit state threshold and β_{LS} is the dispersion.

Fragility functions are thus defined by two parameters: IM_{LS} and β_{LS}. The first may be obtained from the statistical analysis of data from multiple models accounting for different uncertainties or variations within a building class/typology. The second describes the uncertainty associated with the fragility function for each limit state. The dispersion β_{LS} may consider different contributions related to (Lagomarsino and Cattari, 2014): 1) the uncertainties in the definition of the seismic demand, including i) epistemic uncertainties (β_H) related to the derivation of the hazard curve, and ii) intrinsic/aleatory uncertainties (β_D) related to the variability of the seismic input (here described only by a value of the seismic intensity measure), 2) the uncertainties in the definition of the performance limit states (β_T) and 3) the uncertainties in the definition of the capacity (β_C) of buildings belonging to the same class/typology. Assuming that these contributions are statistically independent, dispersion β_{LS} is given by Equation (1.2).

$$\beta_{LS} = \sqrt{\beta_H^2 + \beta_D^2 + \beta_T^2 + \beta_C^2} \tag{1.2}$$

There are several methods available in the literature for the derivation of fragility functions for building typologies. These are conventionally classified into four categories (Porter, Kennedy and Bachman, 2007; Pitilakis, Crowley and Kaynia, 2014): empirical, expert elicitation/judgement, analytical (based on simplified or detailed models) and hybrid. Regarding the derivation of fragility functions for masonry buildings supported on analytical procedures and detailed models, reference to works of Erberik (2008) and Rota et al. (2010). Erberik (2008) proposed the generation of fragility functions for the masonry typologies in Turkey, taking into account structural variations within each building typology (e.g. number of storeys, load-bearing wall material, regularity in plan and the arrangement of walls). The mechanical properties of masonry were considered as aleatory variables and treated by the Latin Hypercube Sampling Method. The buildings capacity curves were obtained through non-linear static (pushover) analyses. Rota et al. (2010) proposed a methodology for the derivation of fragility functions for masonry buildings based on the convolution between the probability density function of specified damage limit states, determined based on non-linear static (pushover) analyses, and the probability distribution of the seismic demand obtained from non-linear dynamic time-history analyses. In this case, the mechanical properties of masonry were considered as aleatory variables and treated by the Monte Carlo Method.

Other important factors for the derivation of fragility functions are the definition of performance limit states (LS) and the choice of the seismic intensity measure (IM). In regards to the first, one option, in case of URM buildings with flexible diaphragms, is to adopt the multi-scale approach proposed by Lagomarsino and Cattari (2013). In regards to the second, the Peak Ground Acceleration (PGA) is frequently adopted, due to the large amount of information (strong motion records) and models (ground motion prediction equations) available. In addition, it is a good parameter in the case of masonry buildings as they are usually characterized by short natural period (Lagomarsino and Cattari, 2015a).

In summary, the seismic assessment of URM buildings should consider both local (out-of-plane) and global (in-plane) response and the flexible behaviour of timber diaphragms. The assessment may be supported on displacement performance-based approaches and non-linear analyses procedures. Although non-linear dynamic analysis represents the most accurate analysis technique, non-linear static (pushover) analysis still remains the best option for the assessment of masonry buildings. The analysis of the local seismic behaviour may rely on incremental non-linear limit analysis of rigid blocks and consider the amplification of the seismic input when the mechanisms are located at the upper levels of the building. Moreover, the propagation of uncertainties in the seismic response of the structure may be considered through a fully probabilistic approach. This requires the knowledge of the fragility functions associated with specific performance limit states and the determination of the corresponding seismic intensity measure, usually defined by the peak ground acceleration. Finally, the analysis of buildings in historic city centres should consider the structural interaction between building units constructed in aggregates. However, limit research has been conducted in this regards.

1.3. Objectives, methodology and outline of the thesis

The main goal of this PhD thesis is to evaluate the seismic vulnerability of the URM buildings constructed between the 19th and 20th centuries in Lisbon, Portugal. It is proposed to define vulnerability based on the derivation of fragility functions. The following objectives are proposed:

1. Characterization of the buildings following a multidisciplinary approach to increase the knowledge about the typology and to identify the variations between buildings.

2. Definition of representative cases of study for the analysis of a sub-type of buildings considering in addition the effect of building aggregates.

3. Analysis of the seismic behaviour considering both global response and the possible occurrence of local out-of-plane mechanisms, by neglecting their interaction, supported on displacement-based approaches and non-linear analysis procedures.

4. Derivation of fragility functions for a sub-type of buildings considering the different contributions that influence the seismic behaviour of the typology.

In order to accomplish these objectives, the thesis is organized in six chapters and five annexes. The main tasks and methodologies adopted are described next:

1. Introduction, presents the motivation, the research focus and background and highlights the objectives, methodology and outline of the work proposed to evaluate the seismic vulnerability of the masonry buildings constructed between the 19th and 20th centuries in Lisbon, Portugal.

2. Masonry buildings in the 19th and 20th centuries in Lisbon, compiles the main characteristics of the typology and defines the cases of study for the analysis of the seismic vulnerability.

The characterization is based on the information available in the literature and on a detailed study to a block of buildings and includes: 1) the analysis of the period of construction, 2) the identification of architectural and structural features, and 3) the identification of the main structural and construction weaknesses. The expected seismic behaviour of the buildings is then approached making reference to previous numerical and experimental studies.

The cases of study address a sub-type of buildings constructed as part of building aggregates. A prototype building is defined and replicated in order to define a block of buildings. This aims to account for the structural interactions between buildings and the block effect in the seismic response. In addition, the main variations between buildings, in terms of geometry, constructive details and materials are treated as epistemic uncertainties following the logic-tree approach in order to define representative building models for the analysis of the seismic vulnerability of the typology.

3. Analysis of the global seismic behaviour, defines the global capacity of the sub-type of buildings taking into account the main variations within the typology and estimates the parameters for the definition of the fragility functions considering the contribution of the global seismic response.

Three-dimensional models of the different cases of study are defined according to the equivalent frame model approach making use of TREMURI program (Lagomarsino et al., 2013) for the non-linear seismic analyses of masonry buildings. The main modelling assumptions adopted are discussed, including the quantification of some parameters as aleatory variables. This aims to account for the uncertainties in the definition of the parameters and the intrinsic variations between buildings belonging to the same typology. The following aleatory variables are considered: mechanical properties of masonry, strength and deformability characteristics of masonry piers and spandrels, mechanical properties of interior timber "tabique" walls, quality of connections between walls and in-plane stiffness of timber floors. These variables are defined within plausible intervals of values, based on the information available in the literature and results from experimental tests. In particular, the Bayesian update approach is applied to define the mechanical properties of the different types of masonry present in these buildings. The Monte Carlo Method (Rubinstein, 2011) is then used to sample the variables and define the input parameters for the set of numerical models.

The global seismic behaviour is addressed to the group of buildings resulting from the combination between: 1) the cases of study identified based on the logic-tree approach (epistemic uncertainties) and

2) the parameters defined based on the Monte Carlo Method (aleatory uncertainties). The analysis of the global seismic behaviour is supported on the following steps (Lagomarsino and Cattari, 2015a): 1) evaluation of the pushover curve based on non-linear static (pushover) analyses, 2) definition of performance limit states in terms of displacement thresholds and related values of equivalent viscous damping, 3) evaluation of the capacity curve, by the conversion to an equivalent SDOF system, 4) definition of the seismic demand, in terms of an over-damped elastic ADRS, and 5) evaluation of the values of the seismic intensity measure compatible with the specified performance limit states. Moreover, non-linear dynamic analyses with time integration are performed with the objective of verifying if the load distributions considered in the non-linear static (pushover) analyses are able to capture the seismic response of the buildings. The results of the different sets of analyses performed are presented and discussed, highlighting the main features and vulnerabilities of the building typology.

4. Analysis of the local seismic behaviour, defines the capacity of the sub-type of buildings taking into account possible out-of-plane mechanisms and estimates the parameters for the definition of the fragility functions considering the contribution of the local seismic response.

The chapter includes the identification of the possible out-of-plane mechanisms in the sub-type of buildings. These are defined based on the geometry of the building, layout of openings, constructive details and restrains given by the structure. These are treated as epistemic uncertainties following the logic-tree approach in order to quantify the reliability of each mechanism. The different mechanisms are modelled according to the macro-block approach making use of MB-PERPETUATE program (Lagomarsino and Ottonelli, 2012). The main modelling assumptions are discussed, including the quantification of some parameters as aleatory variables, such as the geometry of the elements involved in the mechanism and the external loads applied. These aleatory variables are defined within plausible intervals of values and treated by a full factorial combination in order to define the input parameters for the set of mechanisms.

The local seismic behaviour is addressed to the group of mechanisms resulting from the combination between: 1) the mechanisms identified based on the logic-tree approach (epistemic uncertainties) and 2) the parameters defined based on the full factorial combination (aleatory uncertainties). The analysis of the local seismic behaviour is supported on the following steps (Lagomarsino, 2015): 1) evaluation of the pushover curve based on non-linear kinematic analyses, 2) definition of performance limit states in terms of displacement thresholds and related values of equivalent viscous damping, 3) evaluation of the capacity curve, through the conversion to an equivalent SDOF system, 4) definition of the seismic demand, in terms of an over-damped elastic ADRS, modified from the seismic input at the ground level for mechanisms located at the upper levels of the building (floor response spectrum), and 5) evaluation of the values of the seismic intensity measure compatible with the specified performance limit states. Even if local mechanisms typically occur before the activation of the global seismic response, in this work their analysis is presented afterwards, as the analysis of the local seismic behaviour takes into account the dynamic filtering effect provided by the main structure.

5. Derivation of fragility functions, combines the global and local capacity of the buildings and estimates the parameters for the definition of the fragility functions of the sub-type of buildings.

The fragility functions proposed take into account the main variations of the sub-type of buildings and the block effect in the seismic response. The expected distribution of damage is presented for different seismic events. These fragility functions are then compared with other functions available in the literature for similar masonry buildings.

6. Final remarks and future work presents the main conclusions from the work developed and identifies the issues that need further development.

Considering the amount of results generated in the work, mainly in reference to chapter 3, for a matter of simplicity and interpretation of the main outcomes, part of these results are presented in annex:

Annex A provides the results from the modal analyses performed with the three-dimensional models of the buildings.

Annex B presents the results from non-linear static (pushover) analyses carried out with the models defined by the median properties of the aleatory variables.

Annex C specifies the results from non-linear dynamic analyses used to analyse the reliability of the load distributions considered for the non-linear static (pushover) analyses.

Annex D provides the results from non-linear static (pushover) analyses carried out with the models defined by aleatory properties obtained with the Monte Carlo Method.

Annex E contains the results for the median seismic intensity measure and dispersion in the capacity obtained for each group of models.

This page was intentionally left blank

2. MASONRY BUILDINGS IN THE 19TH AND 20TH CENTURIES IN LISBON

2.1. Introduction

This chapter presents the main features of the residential masonry buildings constructed between the 19th and the 20th centuries in Lisbon. The period of construction is analysed in terms of political, economic and social conditions. The main architectural and structural features are described based on the information available in the literature and on a detailed survey carried out to a block of buildings in the area of "Avenidas Novas". This block was previously studied by Appleton (2005). In the course of the present work, the 19 masonry buildings were analysed starting from the original drawings available at the Municipal Archive of Lisbon (Arquivo Municipal de Lisboa, AML, http://arquivomunicipal.cm-lisboa.pt/) and *in situ* visits to the majority of the buildings and flats (Simões et al. (2016a)). From these visits, it was also possible to confirm the geometry and the materials used and to catalogue the main structural alterations introduced in the buildings. The expected seismic behaviour of the buildings is approached making reference to previous numerical and experimental studies carried out. This comprehensive characterization aims to increase the knowledge about the buildings, to identify the variations within the typology and to highlight the main structural and construction weaknesses.

Different cases of study are afterwards set with the objective of conducting the seismic analysis of the typology. Considering that these buildings are assembled in aggregates, a prototype of a sub-type of buildings is defined and replicated in order to define a block and take into account the structural interactions between buildings. In addition, the main variations within the typology, in terms of geometry, constructive details and materials are identified. These variations are assumed as epistemic uncertainties and treated through the logic-tree approach aiming to define representative models for the analysis of the seismic vulnerability of the typology of buildings. Part of the content of this chapter has been published in Simões et al. (2017, 2018).

2.2. Historical background

Lisbon was founded in an undetermined time during the pre-Roman period (França, 2009). The morphology of the city has been influenced by many centuries of history, by the occurrence of natural disasters and by the implementation of urban plans. Until the mid-19th century, the urban settlement was mainly concentrated in the downtown area surrounded by the hill of St. Jorge and of St. Catarina and by the Tagus River on the south (Figure 2.1). This part of the city was severely destroyed by the 1755 Lisbon earthquake and tsunami. It was rebuilt afterwards following the plan proposed by the engineering/architectural team of Manuel da Maia and under the political support of Sebastião José de

Carvalho e Melo, later nominated Marquis of Pombal. The urban design, commonly addressed as "Baixa Pombalina" or "Pombalino" Downtown, represents a landmark in history. The centre of Lisbon was entirely constructed in a standardized way and making use of solutions designed to provide resistance to seismic actions (Lopes et al., 2014).

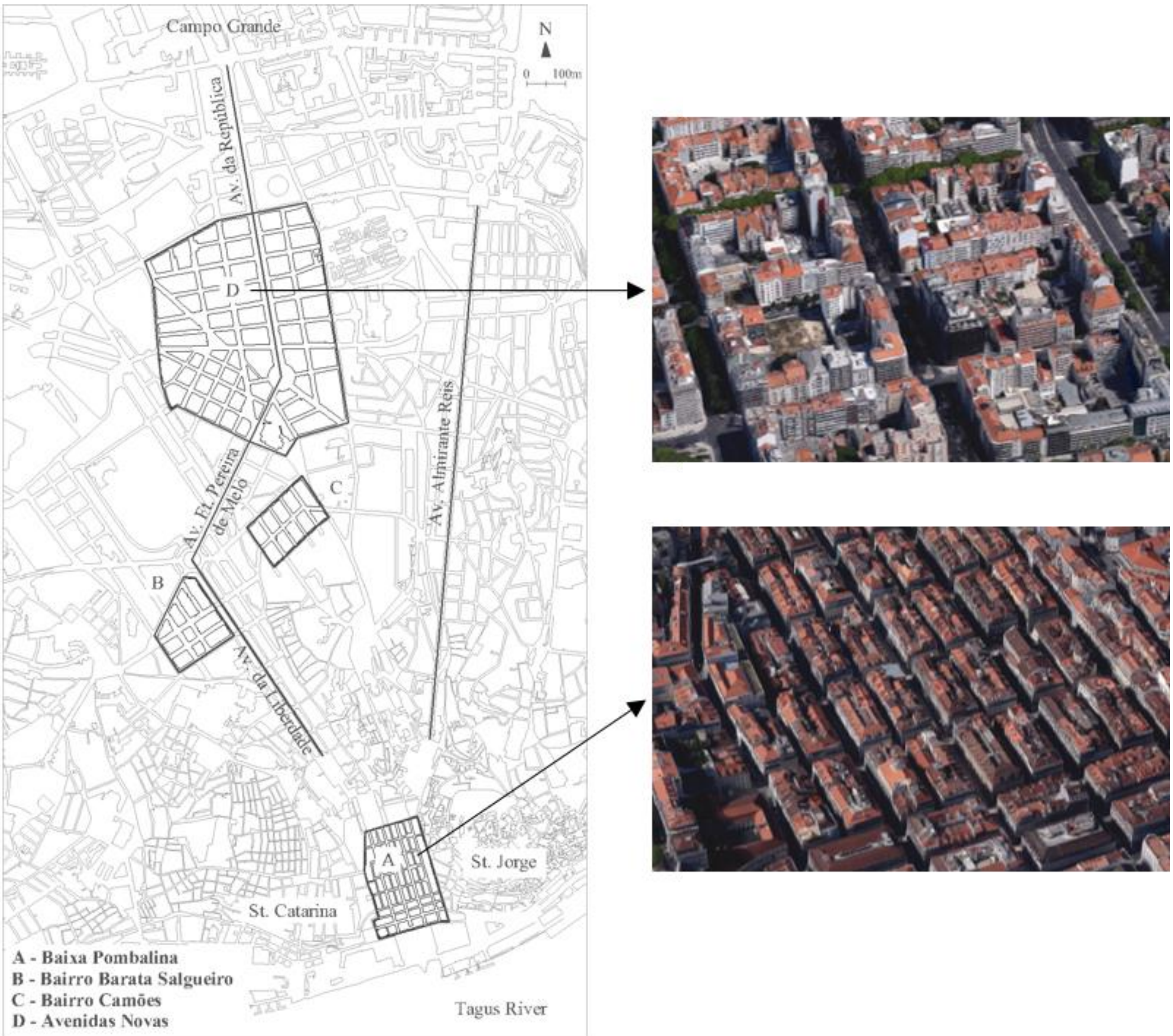

Figure 2.1 – Map of Lisbon illustrating the new avenues proposed by Frederico Ressano Garcia to connect "Baixa Pombalina" to the outskirts of the city

Only after one century, a public commission was nominated to deal with the renewal of the city following the law from 1864, the Decreto No. 10, 31/12/1864, Título III, Secção I, cited in (Appleton, 2005). This law was mainly focused on urban issues, such as the relation between the width of the streets and the height of the buildings. Notwithstanding, the actual renewal of the city was characterized by two main moments. First, the approval, in 1877, of the project of a boulevard connecting "Baixa Pombalina" to the outskirts of the city, with the opening of "Avenida da Liberdade" (where "Avenida" means avenue or boulevard). The works began in 1879. Second, the presentation to the municipality, ten years later, of a plan that allowed the growth of the city to the north upland, the opening of new streets and neighbourhoods. This plan took advantage of the law from 1885 that doubled the urban area by merging Lisbon’s municipality with the adjacent municipalities of Belém and Olivais (Silva, 1989).

In both moments, the chief engineer of Lisbon’s municipality, Frederico Ressano Garcia, had an important role. Firstly, by correcting and adapting the project of the boulevard to the extension of the city that he had already in mind. Secondly, because the new plan was designed by the municipality services under his direction. This resulted on the construction of the neighbourhoods of “Barata Salgueiro” and “Camões”, connecting “Avenida da Liberdade” to the existing city, during the 1880’s, and of the area of “Avenidas Novas” (meaning New Avenues), during the 20th century, representing the core of that extension of the city (Figure 2.1). The construction of new buildings was also spread to other parts of the city, namely to “Avenida Almirante Reis” and the adjacent neighbourhoods.

In the last quarter of the 19th century, the population in Lisbon increased significantly. The census to the population estimated a total of 301 206 inhabitants in 1890, 356 009 inhabitants in 1900 and 435 359 inhabitants in 1911 (Rodrigues and Ferreira, 1993). This represents an increase of 45% in 21 years. This change was more motivated by the political reforms implemented in Portugal aiming at the improvement of the economic condition and the modernization of the transport system, than by the Industrial Revolution, as in other European cities. After 1890, the population continued to increase, with exception to the period between 1910 and 1920, due to the social and political turbulence of the beginning of the Portuguese Republic (1910), and to the First World War (1914-1918).

The construction industry benefited from both urban and population growth. The construction of new buildings was controlled by private entities following the contemporary Liberalism political ideals. During the 19th century, multi-storey residential buildings were commonly constructed and rented flat by flat by the landlord. These buildings are commonly called “prédios de rendimento” (rentable buildings). On the transition to the 20th century, the idea of rentable buildings changed in Lisbon. The liberal “bourgeois” (who ascended to the top of the social hierarchy) prefer to buy the already finished buildings and use them as a “financial product”. In this case, the developer, which was often the contractor, was in charge of the construction and sale of the building. The new landlord was responsible for the renting, but also for the maintenance and other problems due to project or construction flaws. Thus, most of the surplus value was made in the transaction between the first and the second landlord, and not over a long time of renting, as before.

Filius Populi (anonymous author under a pseudonym), claims that the contractors from Tomar, a small city 150 km from Lisbon, were responsible for this new system of buildings “for sale”, where the profit of the transaction would be maximized by the use of cheaper materials and construction processes (Populi, 1946). For many, this is the main reason for the decline of the construction quality in the first decades of the 20th century in Lisbon. Other possible reasons are related to the economic and political conditions of the country. Portugal had a bankruptcy in 1892 and passed from a monarchy to a republic in 1910. The devaluation of the currency, the subsequent inflation in material prices and the shortage of bank credit, forced contractors to purchase cheaper materials and to simplify the construction processes as a way to avoid bankruptcy (Populi, 1946; Fernandes, 1993).

All these factors contributed to the downgrade of the construction quality during this period, being in the ultimate case, proved by the collapse of some of these buildings during the construction phase. For example, Figure 2.2 a) shows the ruin of a building in 1921 which killed twelve workers. This event caused a public demonstration against the so-called "gaioleiros", the name given to the contractors which were seeking for fast profit and making buildings without guarantying minimum safety conditions (Figure 2.2 b)).

a)

b)

Figure 2.2 – Downgrade of construction quality: a) collapse of a masonry building and b) public demonstrations against "gaioleiro" contractors (Ilustração Portugueza, 1921)

A few years after, these buildings were known as "gaioleiro" buildings in a pejorative way. This etymology derives from the transition from "gaiola" to "gaioleiro" system, but it has probably a double sense. Firstly, referring to the simplification of the timber structures (known as "gaiola"), which defined the inner skeleton in Lisbon masonry construction and was used in a generalized way in the "Pombalino" buildings after the 1755 earthquake. Secondly, referring to the fragile, oversized, speculative, non-hygienic buildings, similar to cages and more adequate for birds than for people. The designation of "gaioleiro" was subsequently extended to all buildings constructed in the end of the 19th century and in the beginning of the 20th century in Lisbon.

2.3. Architectural characterization

2.3.1. Urban design and image

New aggregates of buildings were defined to accompany the streets and avenues designed to connect the new boulevard and the plan of Frederico Ressano Garcia to the existing city. The blocks are squared, rectangular or irregular in shape because they were conditioned by the pre-existent routes or buildings and by the slope of the hills. The urban design was also sustained by the law from 1889, i.e. the Decreto

04/10/1889, cited in Appleton (2005), which allowed the City Hall to expropriate a strip of 50 m for each side of the axis of the street. This was particular effective in the area of “Avenidas Novas”. As the land was flat (rural plateau), the blocks could have a regular geometry and maximized dimensions as there were few existing constructions (see Figure 2.1).

After the 1864 law, the City Hall technicians defined a plan for the general improvement of the living conditions in the city. The new blocks were divided in lots obeying to a hierarchical criterion: large lots (with more than 13 m of width) in the main avenues, medium lots and small lots (with 7 m to 8 m of width) in secondary avenues. The depth of the lots varies with the block, but it is in general high, especially in “Avenidas Novas” where it can reach 50 m. The buildings were located along the perimeter of the lot, with entrances facing the street and private courtyards in the rear of the building. The buildings were constructed side by side or with small passageways to access the courtyards.

The main difference between the new buildings and the preceding “Pombalino” buildings is that the image in “Baixa Pombalina” was fully controlled by the engineering/architectural team of Manuel da Maia. The blocks were also divided in lots with variable width for the construction of rentable buildings. However, the blocks resemble a single building. The buildings were constructed side by side with the same depth and number of floors, while the street façades were designed by the city planners in a sober way (França, 1977; Santos, 2005). In the end of the 19th century, no specifications were provided regarding the aesthetics of the new urban areas, the configuration of the buildings or the health conditions of the houses. The architectural image in “Avenidas Novas” was controlled by private developers/contractors which could construct as far as they wanted in the depth of the lot.

During the 19th and 20th centuries, there was a division between the technical (urban) and artistic (architectural) domains. Only in exceptional cases, buildings were designed by architects, such as Ventura Terra (1866-1919), Álvaro Machado (1874-1944), Norte Júnior (1878-1962), Miguel Nogueira (1883-1953) or Pardal Monteiro (1897-1957), especially those located in the main avenues or in the corner of the blocks. Thus, most of the references to the “Eclecticism” and “Art Nouveau” or revival architectural movements in this period were made by contractors in a quite naive way, due to the absence of a solid formation in architecture studies (Simões et al., 2017). This resulted on the design of façades characterized by a diversity of proportions and architectural or decorative solutions (Figure 2.3) following the requests of an emerging bourgeoisie (Portas, 1980).

Despite this, the street façades obey to a “classical” tripartite composition. The lower level is the socle or pedestal where large size entrance doors and stores are located. It is usually coated with bush-hammered limestone (Figure 2.4 a)). The medium level is the largest one, as it corresponds to most of the flats. It is often plastered and painted or coated with ceramic tiles (“azulejos” – Figure 2.4 b)). The top level includes the cornice and parapet (sometimes a balustrade) and the roof with dormer windows or mansards.

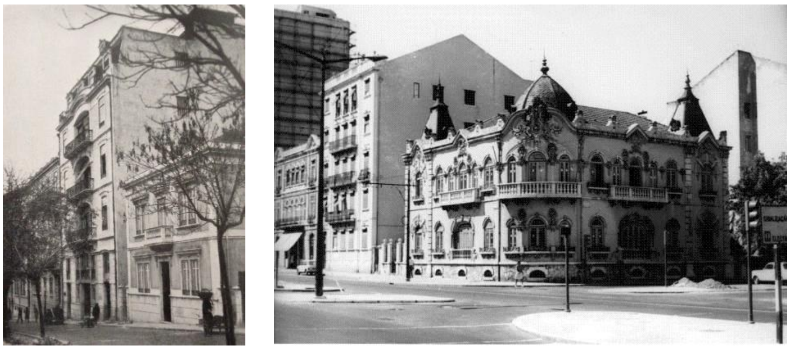

Figure 2.3 – Buildings from the beginning of the 20th century showing different types of façade walls (AML; Populi 1946)

a) b)

Figure 2.4 – Street façade: a) bush-hammered limestone socle and b) ceramic tiles ("azulejo")

The openings are mainly elongated but showing different shapes: simple casement or French windows; scattered, twinned or differently grouped; arched or with straight lintels, etc.. The street façades are also recognized by the exuberant steelwork, in cast or wrought iron, used in doors, fences, balustrades and gates or by the terracotta/moulded reliefs or glazed tiles with floral motifs, in friezes/bands or around the windows (Figure 2.5). In contrast, the rear façades are much simpler and functional. These are mainly intended for service functions: kitchen and laundry. The finishing of the walls is made of plaster and painting. Jack arch balconies with steel profiles are placed in the rear façade with staircases to access the courtyards (Figure 2.6). These are some examples of cast-iron elements in residential architecture in Lisbon.

Figure 2.5 – Decorative details in two different buildings from "Avenidas Novas"

Figure 2.6 – Balconies and staircases in the rear façades in “Avenidas Novas”

2.3.2. Configuration of the buildings

The Health Regulation for Buildings (RSEU, 1903) was an attempt to control housing conditions. However, since the beginning, this regulation was considered to be outdated and undemanding, when compared to foreign health regulations for buildings. Yet, until 1930, this was the only construction regulation in Lisbon. The Health Regulation for Buildings (RSEU, 1903) redefined the relation between the height of the façades and the width of the streets and minimum ceiling heights (Table 2.1).

Table 2.1 – Limits imposed by the Health Regulation for Buildings (RSEU, 1903)

Street Width	Building Height
< 7 m	< 8 m (2 floors)
7 – 10 m	< 11 m (3 floors)
10 – 14 m	< 14 m (4 floors)
14 – 18 m	< 17 m (4 floors)
> 18 m	< 20 m (5 floors)

Floor	Ceiling Height
Ground and 1st	3.25 m
2nd	3.00 m
3rd	2.85 m
4th	2.75 m
5th	2.75 m

Buildings from “Avenidas Novas” have in average four to six storeys with one or two flats on each floor. The range of building types was determined by the width of the lots (Figure 2.7): type I – buildings with small size façades and one flat per floor, type II – buildings with medium size façades and one flat per floor, type III – buildings with medium to large façades and two flats per floor, and type IV – buildings on the corner of the block with one or two flats per floor. This classification, used here in a generalized way, has been previously proposed by Appleton (2005), based on a detailed study of a block of buildings in “Avenidas Novas”.

Buildings of type I to III are characterized by long corridors connecting the rooms adjacent to the street and the rear façades (Figure 2.7 and Figure 2.8 a)). The flats have several lateral rooms, sometimes with insufficient natural light and ventilation, as these depend on the depth of the lot and on the size of the airshafts (“saguões” in Portuguese or “courettes” in French – Figure 2.8 b) and c). On this, the Health Regulation for Buildings (RSEU, 1903) defined minimum ventilation conditions for sleeping rooms. For instance, it imposed minimal areas for the airshafts: 9 m^2 when serving kitchens and 4 m^2 when serving stairs and antechambers (small room leading to a main room, but with no restriction for its usage as bedroom). Due to this, buildings of type I and II have one or two airshafts in asymmetrical position. Buildings of type III have one to three airshafts in symmetrical position. In buildings of type IV, airshafts are organized in other ways. However, it is very unusual to have more than three airshafts.

Figure 2.7 – Typical street façades and floor plan of buildings type I, II, III and IV (Simões et al., 2014a). Airshafts are marked with grey colour

a) b) c)

Figure 2.8 – Examples of a) longitudinal corridor, b) and c) airshafts

As to the staircases, the regulation only states that they should “allow a comfortable ascending” and also to have an “empty space on its axis” in order to provide to all floors natural light from a skylight on the roof and to allow firefighter’s hoses to pass through. The staircases were arranged in two flights separated by a half-landing. Staircases with three flights are less common. In buildings of type I and II, staircases are generally aligned with the main entrance, close to one side wall. In buildings of type III, the staircases are generally in the axis of the building to access both flats.

Ventilation boxes were used on the ground floor to prevent the rising damp from the soil and the rotten of the timber floors. These boxes can be identified by the presence of steel or masonry grids on the façades and by the presence of a first flight of masonry stairs on the entrance hall of the buildings, to access the floor level (Figure 2.9). The 1903 regulation recommends a minimum of 0.60 m height for the ventilation boxes.

Figure 2.9 – Ventilation box on the ground floor

2.3.3. Layout of the flats

In contrast with the eclectic language from the street façades, the layout of the flats is very repetitive (also visible in the plan views from Figure 2.7). Buildings of types I, II and III have similar distribution of the rooms: private areas mainly in the centre of the flat; social areas on the street façade; dining/family room and service areas on the rear façade and sometimes with WC and/or bathroom close to an airshaft. Only after the 1903 regulation, a WC and a slop sink in each house or flat were mandatory.

An example of the extreme "speculative" construction in Lisbon is the building in "Rua Braancamp" No. 10, constructed in 1921. The building has 18 m of width and 36 m of depth and two flats on each floor – building of type III (Figure 2.10a). Each flat has eight rooms depending from a narrow airshaft. It has a drawing room and an antechamber on the street façade and a kitchen and a dining room on the rear façade. All other compartments of the flat (with more than 300 m^2) are interior and depend on the airshafts, demonstrating the idea that developers/contractors could build as far as they wanted in the depth of the lot (referred in §2.3.1).

The interesting feature is that the same layout of the flat was adapted for many lots in "Avenidas Novas". The distribution of the rooms is almost the same, but the number varies as a function of the depth of the building. This is, for instance, the case of the building in "Avenida Visconde Valmor" No. 32 (Figure 2.10b). The building was constructed in 1908 and has 14 m of width and 22 m of depth. Here only four rooms depend on the airshaft. Larger lots (generally for buildings of type III) were also used to construct two buildings of type I. The side walls and the airshaft are shared between buildings, but the street access is independent. The building in "Avenida Elias Garcia" No. 79 and No. 81 is an example of this (Figure 2.10 c)).

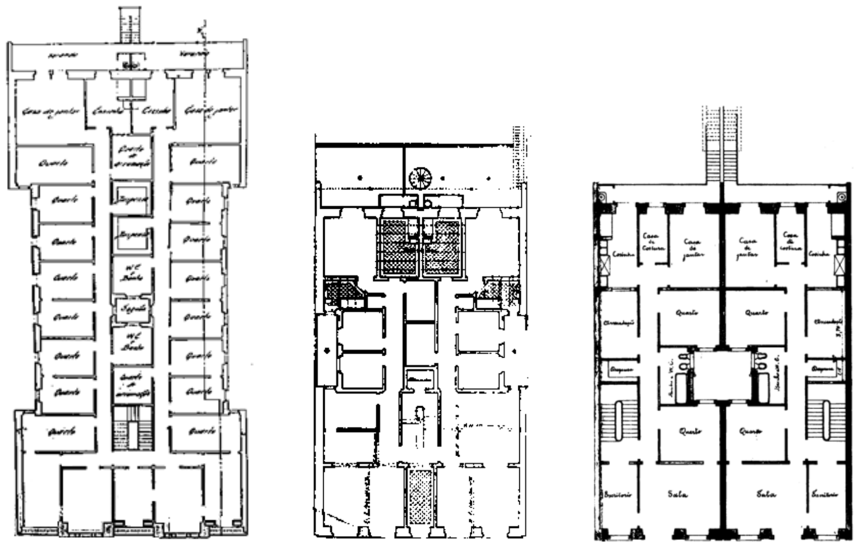

a) b) c)

Figure 2.10 – Layout of buildings in Lisbon (AML): a) "Rua Braancamp" No. 10, b) "Avenida Visconde Valmor" No. 32 and c) "Avenidas Elias Garcia" No. 79 and No. 81

Buildings of type IV are a particular case because of their position on the corner of the blocks and the use of two street façades. These buildings have quite variable dimensions and shapes (in L or closer to a square). Thus, it is not possible to define a specific pattern in comparison with types I to III. Some of these lots, due to their privileged location and value, were occupied by single houses commissioned by richer owners. These houses are, generally, among the buildings that were designed by architects (as referred in §2.3.1). One example is the house in the intersection of "Avenida da República" No. 38 with "Avenida Visconde de Valmor" No. 22 construed in 1905. This house was designed by the architect Ventura Terra for the widow of the Visconde de Valmor. Another example is the house located in "Avenida da República" with "Avenida de Berna" No. 1 designed by the architect Norte Júnior and constructed in 1909.

2.4. Structural characterization

The building activity was based in local materials and traditional construction processes. Due to the Portuguese bankruptcy in 1892, there were few contractors that could use imported materials. Clay brick, limestone, lime mortar, pinewood and tiles, were from Lisbon surroundings or from the centre of Portugal. There is the exception for timber, which could be imported, following the long tradition of acquiring it on the North of Europe for ship-building and to overcome the deforestation in Portugal (Reboredo and Pais, 2012). The structural system is also repetitive. Although there were some French construction manuals in Portugal, the most influential ones were written by Segurado (1908). These were, in many ways, an adaptation of foreign manuals to the national context.

2.4.1. Foundation

The ground soil foundation in the area of "Avenidas Novas" is classified as type B – deposits of very dense sand, gravel or very stiff clay (CEN, 2004). The typical foundation system is characterized by continuous rubble limestone masonry walls with higher thickness than the load-bearing walls (shallow foundation). The thickness of the foundation varies between 0.70 m and 1.50 m on the façades and between 0.30 m and 0.80 m on the side walls and airshafts. Usually, hard limestone masonry and air lime mortar was used. The mortar binder:sand ratio was 1:2 or 2:5. In some cases, in particular when the resistant soil is at lower levels, the foundation is made with stone or brick masonry arches supported on masonry columns, as shown in Figure 2.11. This structure is now visible in this building due to the opening of a basement.

Figure 2.11 – Foundation with masonry arches and columns

2.4.2. Exterior walls

The façades were made of rubble limestone masonry and air lime mortar (with the same binder:sand ratio used in the foundation). The thickness of the walls varies with the height of the building, decreasing between 0.05 m and 0.10 m in each floor. The façades have typically 0.60 m to 0.90 m thickness at the ground floor level. The wall below the windows has lower thickness and is made of clay brick masonry. Above the windows there are clay brick relieving arches and lintels (Figure 2.12).

Figure 2.12 – Rubble stone masonry walls and windows with brick lintels and reliving arches and (examples from "Avenidas Novas")

According to the law from 1867, i.e. the Código Civil, Decreto 01/07/1867, cited in Appleton (2005), the side walls could be shared between adjacent buildings. The arrangement of the side walls may depend on the time of construction, on the dimension of the lot and on the position of the building inside the block, but it seems that there was no clear rule. Nevertheless, when a new building and a new side walls were constructed, frequently the side wall has a lower thickness than the side wall from the adjacent building. The side walls can be made of rubble stone masonry or clay brick masonry and air lime mortar. When clay brick masonry is used, the units can be solid or hollow and, in some cases, they are solid on the lower levels and hollow on the upper levels of the building. The walls from the airshafts have the same material and thickness as the side walls. The thickness of these walls varies between 0.20 m and 0.50 m and is constant between floors.

2.4.3. Interior walls

The interior load-bearing walls are placed parallel to the façades to support the floor timber beams. In Portuguese construction, these load-bearing walls are known as "frontal" walls, while the partition walls are known as "tabique" walls. In Lisbon, the composition of interior walls in old masonry buildings has changed over the time.

During the "Pombalino" construction, "frontal" walls were composed by vertical, horizontal and diagonal timber joists assembled to define Saint Andrew's Crosses ("Cruzes de Santo André") filled in the gaps by rubble masonry (Figure 2.13). These walls were distributed in the two main directions of the building, defining a tri-dimensional timber structure, known as "gaiola Pombalina" (meaning cage) intended to withstand the horizontal seismic loads (Lopes et al., 2014). In the mid-19th century, other types of "frontal" walls were designed (e.g. "frontal forrado" where the Saint Andrew's Crosses were covered on both sides by timber boards and "frontal à galega" with vertical and horizontal timber joists).

Figure 2.13 – Interior "frontal" walls with "Cruzes de Santo André" in "Pombalino" buildings (Appleton, 2003; Lopes et al., 2014)

Partition or "tabique" walls were usually constructed on top of the timber floors (there is no continuity between floors). These walls were generally made of vertical timber boards (the non-serviceable boards from the outer part of the log, "costaneiras"), with 0.10 m or 0.15 m of width, and horizontal laths (half-opened branches from chestnut, "arco de castanho") filled in the gaps by rubble masonry (Figure 2.14 a)). These walls may also have diagonal boards, directing the loads to perpendicular walls (known as "tabique aliviado" or "tabique aspeado" – Figure 2.14 b)). These partition walls have approximately 0.10 m of thickness divided, as shown in Figure 2.14 c), between the thicknesses of the vertical boards (e), horizontal laths (c) and rendering on both sides.

a) b) c)

Figure 2.14 – Timber “tabique” walls with a) vertical boards, b) vertical and diagonal boards, and c) section cut (adapted from Pires (2013))

In the beginning of the 20th century, “frontal” walls started to be constructed in clay brick masonry. The thickness of the walls decreases with the height of the building by changing the orientation of the brick units, as exemplified in Figure 2.15 (0.23 m x 0.11 m x 0.07 m is the standard dimension of the bricks). This variation is also on the use of solid brick units on the lower floors and hollow brick units on the top floors (Figure 2.16 a) and b)). In some cases, these clay brick walls were reinforced by timber frames (Figure 2.16 c)). As to the timber “tabique” walls, these were constructed with more standardized timber elements (trapezoidal horizontal laths and boards with regular dimension).

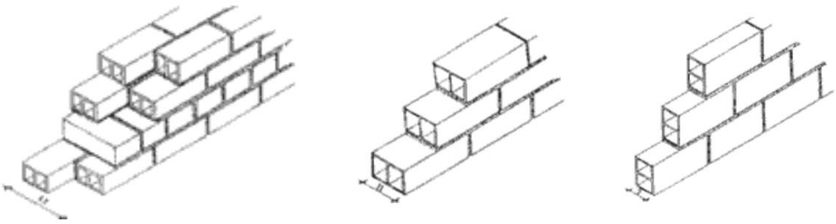

Figure 2.15 – Clay brick masonry walls with different thickness

a) b) c)

Figure 2.16 – Clay brick masonry walls (Gomes, 2011): a) solid units, b) hollow units, and c) reinforced by timber frames

In this period, the contractors kept the terms “frontal” and “tabique”, but now to designate, respectively, the walls parallel and perpendicular to the façades, nor the type of structure/material, as before. In addition, the composition of the interior walls varies between buildings and between two extreme cases: all interior walls are made of clay brick masonry or all interior walls are made with a timber "tabique" structure (Figure 2.14 a) shows for example the use of timber "tabique" walls in the staircase). In the 1930's, after the publication of the new building regulation (RGEUL 1930), the timber frames were eliminated from clay brick masonry walls, while the construction of timber "tabique" walls was limited to the last floor of the buildings.

2.4.4. Floors

Floors are mainly made of *Pinus pinaster Ait.* ("pinho bravo" or "pinho nacional") wood type (Segurado, 1903). The main joists are set perpendicular to the façades and positioned with a distance of 0.35 m to 0.45 m between each other. The geometry of the joists ranges between 0.07 m and 0.08 m for the width and 0.16 m and 0.22 m for the height. These joists are restrained in the perpendicular direction by smaller joists (named "tarugos") or by diagonals (Figure 2.17 a) and b)). The main joists are simply embedded on the walls (pocket holes) or supported on transition joists with squared sections (0.07 m to 0.10 m) running inside the wall (named "frechais"), as shown in Figure 2.18.

a) b)

Figure 2.17 – Timber floors main joists restrained by a) smaller joists and by b) diagonals

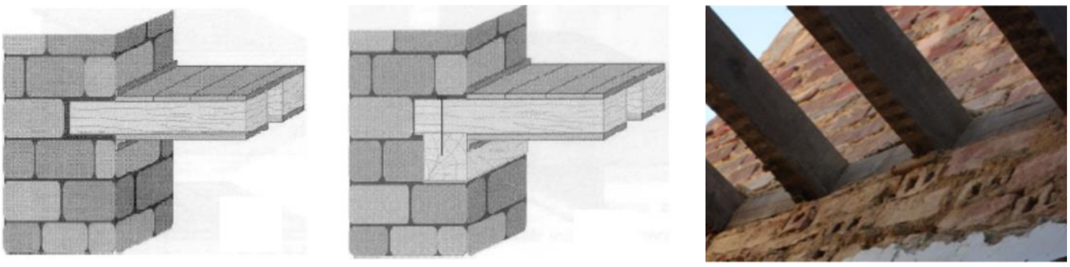

a) b) c)

Figure 2.18 – Connection of the main joists to masonry wall: a) simply embedded (pocket hole), b) and c) connection to a transition joist (Appleton, 2003; Gomes, 2011)

Floors are covered by timber boards with 0.12 m to 0.22 m of width and usually with 0.022 m of thickness or by hydraulic tile paving on kitchens and bathrooms. Hydraulic tiles were applied with mortar, frequently over shorter boards embedded between beams, in order to maintain the same ceiling height. Ceilings are finished by timber laths (“arco de castanho”) and covered with plaster and decorative elements.

These buildings are characterized by the presence of jack arch balconies with steel profiles in the rear façade which, in some cases, is also extended to the kitchen floor. This flooring system was developed in the United Kingdom, in the end of the 19th century, and was mainly used to cover large floor areas at warehouses, factories and other industrial buildings. It is composed by clay brick masonry arches supported by I or T steel section beams, spacing between 0.50 m and 0.65 m (Figure 2.19 and Figure 2.20). The span of the balconies varies between 1.00 m and 2.20 m. The steel sections are embedded on the façade wall and supported on the opposite side by I, L or U section beams and by circular cast-iron columns (Figure 2.20 and Figure 2.6). The balconies are then covered by mortar and hydraulic tiles. The staircases to access the courtyards (exemplified in Figure 2.6) are made with I or T steel sections and textured steel plates.

a) b) c)

Figure 2.19 – Jack arch balcony with steel profiles: a) section cut (Appleton, 2005), b) and c) examples in “Avenidas Novas”

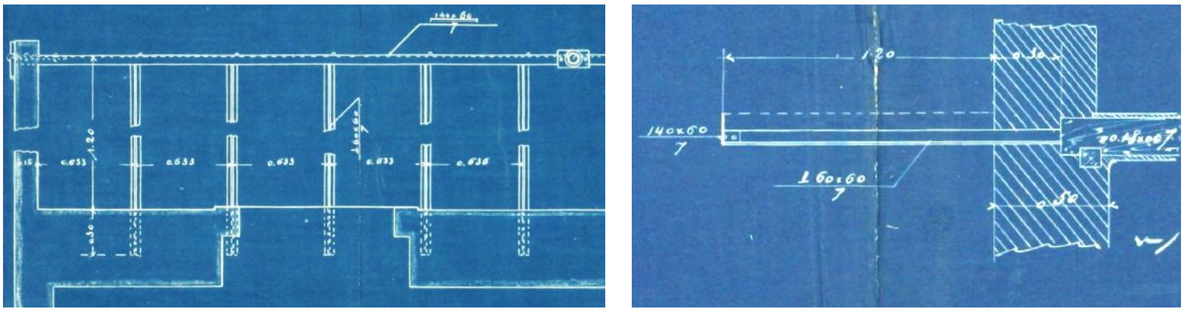

a) b)

Figure 2.20 – Original drawings from AML showing the connection of the T steel sections to the façade wall: a) plan view and b) section cut

2.4.5. Roofs

The buildings have pitched roofs with the slope perpendicular to the façade walls. The roof is covered by ceramic roof tiles (“Lusa” type). The roof structure is quite simplified (the use of timber trusses was not very common), as shown in Figure 2.21. It is composed by a number of purlins (“madres”), usually 3, 5 or 7 as maximum, disposed parallel to the façades and supported by timber posts (“prumos”) or struts ("escoras"), transferring the loads to the main interior walls. A range of rafters ("varas" or "varedo"), distancing 0.40 m to 0.60 m, are placed on top of the purlins. Small section battens ("ripas" or "ripado") are disposed on top, to support the roof tiles. When the attic was used for housing, a board covering layer ("guarda-pó") was used under the battens. *Pinus pinaster Ait*. wood type is often used as in floors.

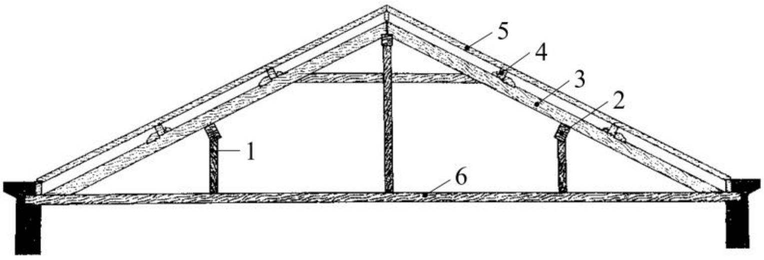

a)

b)

Figure 2.21 – Typical timber roof structure: a) adapted from (Appleton, 2005) indicating 1 – post, 2 – purlin, 3 – rafter, 4 – batten, 5 – roof tiles and 6 – tie beam, and b) picture of a roof (López, 2013)

2.4.6. Structural alterations

These masonry buildings have experienced several alterations induced from human activity, motivated by different needs of occupation and changes of usage. Initially, the buildings in the area of "Avenidas Novas" were fully residential or used for commerce at the ground floor level. Nowadays, due to the location of the buildings in the city centre, several flats have been converted into offices and archives (Figure 2.22), increasing the loads on the structure. The jack arch balconies on the rear façade have also been transformed into galleries and are used for archive/storage or to place additional bathrooms. The corrosion and deformation of the steel elements is also frequent; thus, in the last years several balconies have been replaced by new RC structures.

Figure 2.22 – Examples of flats and balcony in "Avenidas Novas" converted to offices and archives

It is common to observe the cut of masonry elements at the ground floor to have larger shop windows (Figure 2.23). The removal of interior walls to have larger rooms (Figure 2.24) is also quite frequent. This type of interventions introduces local weaknesses and stiffness variations on the building. The removal of interior walls results on the excessive deformation of the overlying walls and the loss of the original support system of the floors. These alterations decrease the strength capacity of the building to horizontal actions and generate artificial soft-storeys, which can be particular damaging to the buildings in case of an earthquake. In addition, the removal of interior walls perpendicular to the s, increases the vulnerability to the out-of-plane overturning and collapse of the façades.

Figure 2.23 – Removal of masonry elements to have large shop windows in “Avenidas Novas”

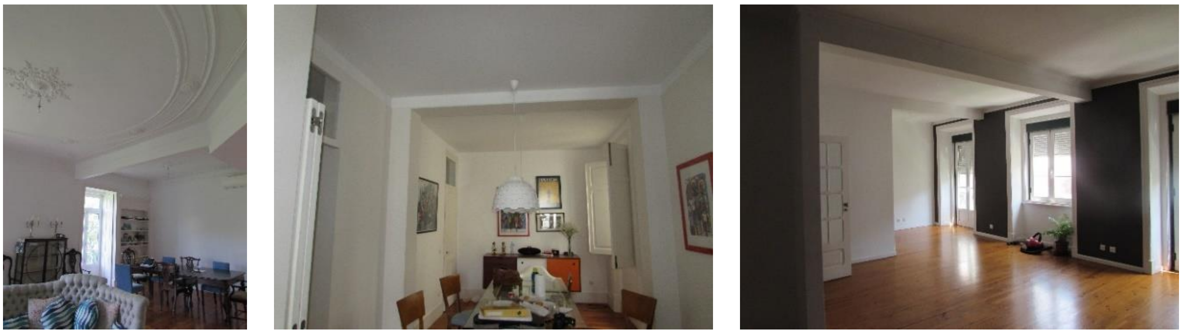

Figure 2.24 – Cases from “Avenidas Novas” showing the removal of interior walls

New floors were added to these buildings, even only a few years after being constructed, following the idea of rentable buildings (as referred in §2.2). Figure 2.25 shows, as an example, the original drawings of a building and the addition of two new floors (marked in red). The opening of basements starting from the ventilation boxes on the ground floor is also usual (as shown in Figure 2.11). Both cases have an impact on the foundation system and on the stability of the building and of the adjacent buildings. In fact, one of the main causes of cracking in masonry buildings is caused by differential settlements of the foundation.

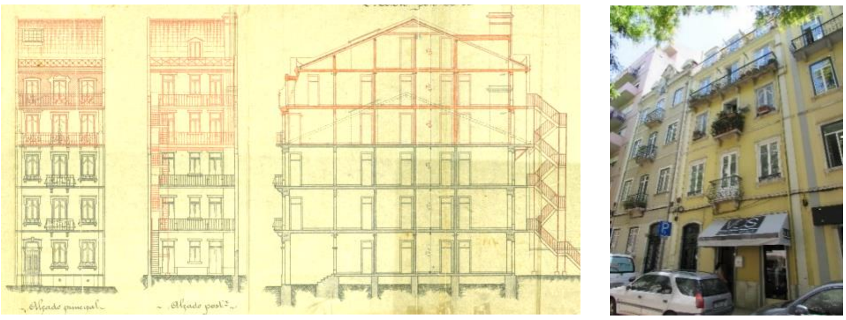

a) b) c) d)

Figure 2.25 – Original drawings from AML showing the addition of two floors (marked in red): a) front façade wall, b) rear façade wall, c) section cut and d) picture of the building

The present condition of the buildings derives from the combination between the structural and construction weaknesses, the alterations induced from human activities and the extended service lifetime of the buildings (new buildings are designed for 50 years lifetime, whilst these masonry buildings are in average 100 years old). The ageing of materials, the lack of maintenance and the action of external agents (e.g. the action of fungi and termites on timber elements) may lead to the sudden or gradual decay of mechanical properties of materials.

The limited performance of these masonry buildings, in terms of functionality and safety, has supported the demolition of several buildings in the last decades. Nowadays in the area of "Avenidas Novas", 55% of the buildings have RC structure, 10% have a mixed masonry-RC, 30% are multi-storey masonry buildings and 5% are single masonry buildings. This survey included the analysis of 18 blocks and 323 buildings limited by the following avenues (Figure 2.26): "Avenida de Berna", "Avenida Defensores de Chaves", "Avenida da República" and "Avenida Marquês de Tomar". The point is that the majority of the RC buildings are replacing old masonry buildings. The construction of RC buildings introduces structural irregularities within the behaviour of the block related to the increment of the plan eccentricity between mass and stiffness, which may originate major torsional effects during the action of an earthquake.

Figure 2.26 – Distribution of buildings in 18 blocks from "Avenidas Novas"

2.5. Seismic behaviour and vulnerabilities

As referred, the seismic behaviour of URM buildings is usually divided between the out-of-plane response and the in-plane response. The first is related to local mechanisms, typically consisting on the overturning of parts of the structure insufficiently connected to the rest of the building (Figure 2.27 a)).

The second is related to the occurrence of a global (box-type) behaviour controlled by the in-plane capacity of walls and the in-plane stiffness of horizontal diaphragms (Figure 2.27 b)).

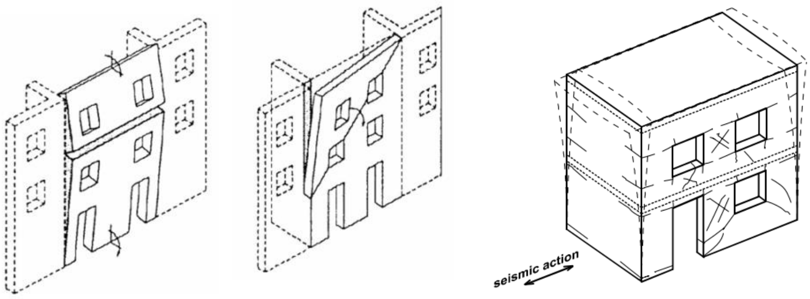

a) b)

Figure 2.27 – Seismic performance of URM buildings: a) local damage mechanisms (D’Ayala and Speranza, 2003) and b) global response (Magenes and Penna, 2009)

It is to expect that the seismic response of the masonry buildings constructed in Lisbon between the 19th and the 20th centuries is mainly governed by local mechanisms. The buildings were constructed based on an empirical approach (i.e. according to the experience of the contractor) and without considering specific constructive details to prevent the out-of-plane behaviour of the façade walls as in the preceding “Pombalino” buildings (e.g. the use of a tri-dimensional timber structure reinforcing the masonry walls (“gaiola Pombalina”), steel tie rods connecting opposite exterior walls or steel elements connecting floors to masonry walls). At the end of the 19th century, the timber floors and roofs are simply supported on the façade walls or supported on transition joists (Figure 2.18). The interlocking between the rubble stone façade walls and the clay brick side/interior walls is questionable due to the use of different materials. In both cases, the friction developed in the contact surface (wall-to-floor and wall-to-wall) provides limited restrain to the out-of-plane behaviour of the façade walls. Moreover, the presence of interior timber “tabique” walls provides no restrain.

Results from dynamic tests on reduced scale models representative of the buildings under study have confirmed the out-of-plane failure of the masonry elements from the last floors (Candeias, 2008; Mendes, Lourenço and Campos-Costa, 2014), as shown in Figure 2.28. The tests were performed on the tri-axial shaking table from the “Laboratório Nacional de Engenharia Civil”, LNEC (http://www.lnec.pt/) considering a prototype with four storeys, façade walls with openings, side walls without openings and timber floors. In the first case, the walls were constructed in self-compacting bentonite-lime concrete (Candeias, 2008), while in the second, in rubble stone masonry (Mendes, Lourenço and Campos-Costa, 2014). In both cases, different solutions to improve the out-of-plane response of the walls and the in-plane stiffness of timber floors were tested.

In case proper strengthening/retrofitting measures have been implemented to improve the connection between elements and to prevent local mechanisms, the seismic response of the buildings is then governed by global failures modes. The response of masonry buildings depends on the capability of the structure to redistribute the horizontal loads between the elements in order to explore the maximum in-plane strength of masonry walls (Lourenço et al., 2011). However, the presence of flexible diaphragms (timber floors and roofs) provides lower degree of coupling between walls, which tend to vibrate more independently (Cattari and Lagomarsino, 2013), compromising the activation of the global box-type behaviour. Mendes and Lourenço (2014) presented a sensitivity analysis taking into account possible variations on the features of this typology of masonry buildings, concluding that the in-plane stiffness of the timber floors significantly affects the strength capacity of the structure and the type of collapse mechanism.

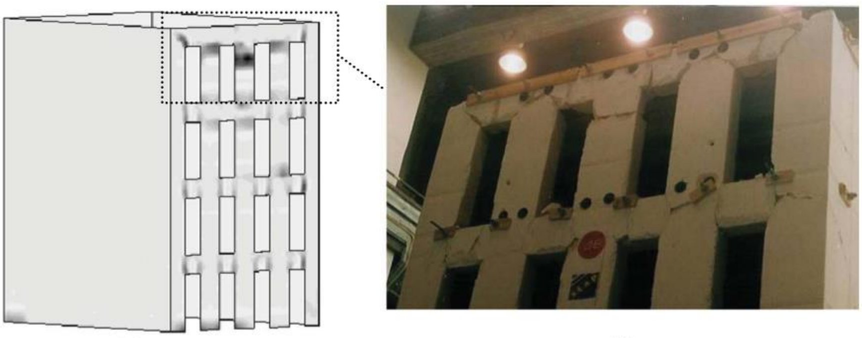

a) b)

Figure 2.28 – Damage to the model in the end of the test (Lourenço et al., 2011): a) numerical representation and b) picture of the prototype

The in-plane strength of masonry walls is dominated by flexural or shear failure modes (Magenes and Calvi, 1997; Calderini, Cattari and Lagomarsino, 2009), which in turn depends on the geometry of the elements and on the mechanical properties of the material. The mechanical properties of masonry are related to the mechanical properties of the constituents – units and mortar – and to the characteristics of the assembly – dimension/shape of the units and interlocking in the exterior leafs and across the thickness. The proper characterization of the mechanical properties is difficult due to the heterogeneity of the material and the variability from element to element, but also due to the limitations in performing *in situ* destructive tests. The number of experimental campaigns for the characterization of the mechanical properties of masonry in Lisbon is quite limited. In the following, reference is made to some of the tests carried out to the buildings constructed in the transition between the 19th and 20th centuries.

Lopes (1996) conducted monotonic shear-compression tests on the façade rubble stone masonry walls, clay brick masonry walls from the staircases and timber "tabique" walls from a masonry building from the early 1920's that was being demolished. Branco and Correia (2003) performed laboratory compression tests on a clay brick masonry specimen, extracted from Praça de Touros do Campo Pequeno, in Lisbon (constructed in 1890). Within SEVERES project (http://www.severes.org/), Simões et al. (2016b) performed double and shear flat-jack tests on the exterior rubble stone masonry walls from a "Pombalino" building and from a masonry building constructed in 1911 (Figure 2.29). The objective of the tests was, respectively, the evaluation of the masonry deformability properties in compression and the shear strength parameters following a new testing technique. It was concluded that the stiffness and strength of the exterior walls from the later building were much lower in comparison to the ones from the “Pombalino” building (e.g. the modulus of elasticity is in average equal to 0.39 GPa, which is 81% lower than the obtained in the “Pombalino” building, whereas the compressive strength is in average equal to 0.63 MPa, which is about 67% lower). Flat-jack tests were also conducted on the interior clay brick masonry walls from the building constructed in 1911.

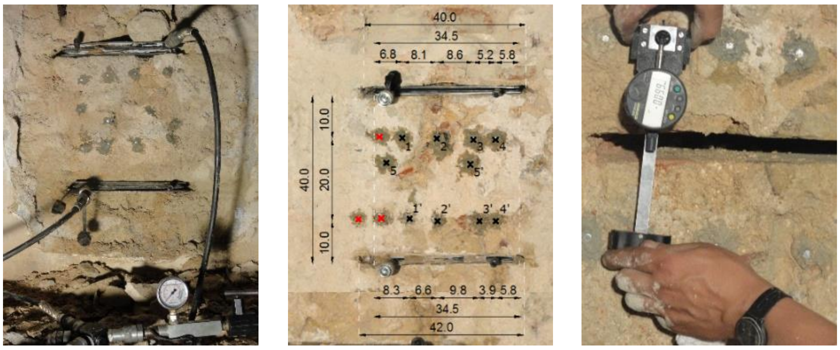

a) b) c)

Figure 2.29 – Double flat-jack tests (Simões et al. (2016b)): a) flat-jacks positioned in parallel holes in the wall and hydraulic pump to control the pressure in the flat-jacks, b) measuring points, and c) removable mechanical meter to record the displacements in the wall during the test

Other experimental results are related to laboratory tests on masonry specimens constructed to represent the traditional masonry walls. Pinho et al. (2012) carried out compression tests and monotonic shear-compression tests on rubble stone and air lime mortar masonry specimens aiming to evaluate the performance of different strengthening solutions. Unreinforced specimens were also tested. Within SEVERES project, Milošević et al. (2013, 2014) performed compression, triplet, diagonal compression and cyclic compression-shear tests on rubble stone masonry specimens with two types of mortar: air lime and hydraulic lime. As expected, the hydraulic lime mortar specimens presented higher stiffness and strength in comparison to the air lime mortar specimens. However, what is noteworthy is to compare the behaviour of the masonry specimens in the end of the diagonal compression tests. The specimens with hydraulic mortar got divided in two parts along a vertical crack, while the specimens with air lime mortar were simply disintegrated.

These references highlight the general low strength capacity of the rubble stone and air lime mortar masonry used on the construction of masonry buildings in the beginning of the 20th century, when compared to other typologies of masonry buildings in Lisbon. In one hand, this may be a consequence of the social-economic conditions during the period of construction of the buildings (§2.2), which “forced contractors to purchase cheaper materials and to simplify the construction processes as a way to avoid bankruptcy” (Simões et al., 2017). On the other hand, this conclusion is supported on a limited number of *in situ* tests, raising also the importance of investing in more experimental campaigns for the mechanical characterization of masonry walls.

According to Appleton (2003), the lack of structural integrity (due to the weak connections between elements), the use of low quality materials and the reduced thickness of masonry walls and timber joists, can be a simple and just explanation for the number of partial collapsed buildings in the beginning of the 20th century in Lisbon. Even nowadays, in case of harsh winters, these masonry buildings are the most damaged and, it is not rare, that few of them partially collapse (Soares, 2013). Thus, the assessment of the seismic vulnerability of these buildings can be a quite complex problem considering the structural and construction weaknesses identified, the alterations induced from human activities (§2.4.6) and the state of conservation of the buildings.

There are some studies focused on the seismic behaviour of the masonry buildings constructed in the transition between the 19th and 20 centuries in Lisbon. These are mainly addressed to specific building cases of study (Branco and Guerreiro, 2011; Monteiro, 2012; Frazão, 2013; Simões et al., 2014a, 2014b) exploring different options in terms of modelling (finite elements based on solid, shell and frame elements), methods of analysis (linear dynamic and non-linear static) and verification procedures. Nevertheless, they only consider the behaviour of single buildings and are mainly focused on the assessment of the global behaviour and less on the out-of-plane behaviour of parts of the structure, as initially approached in Simões et al. (2014b).

Simões et al. (2014a) compared the seismic behaviour of buildings of type I to IV (Figure 2.30). The global seismic behaviour was analysed by non-linear static (pushover) analyses. The seismic performance-based assessment was carried with the application of the N2 Method (CEN, 2004; NTC, 2008). The behaviour of the four building types was then compared in terms of fragility functions, by assuming conventional parameters for the definition of the lognormal dispersion (β_{LS}), as indicated in Equation (1.1). It was estimated that for the seismic demand in Lisbon (action type 1.3 with PGA=1.5 m/s^2 (IPQ, 2010)) there is 60% to 90% probability of near collapse of the buildings and that building of type I is the most vulnerable structure. In a latter work (Simões et al., 2015), the fragility functions derived for building of type I were compared with the fragility functions derived for the other typologies of masonry buildings in Lisbon, namely “Pombalino” building and mixed masonry-RC building, concluding that building of type I have higher probability of near collapse.

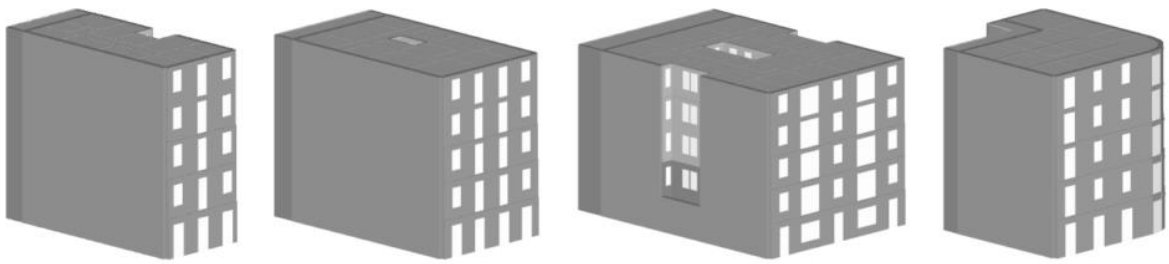

Figure 2.30 – Three-dimensional view of the four building types (Simões et al. (2014a))

Simões et al. (2016a) carried out the seismic vulnerability assessment of 19 masonry buildings from a block in the area of "Avenidas Novas" constructed in the beginning of the 20th century. The assessment was based on the attribution of a vulnerability index to each building, supported on the evaluation of fourteen parameters that classify the vulnerability of the buildings. The method is based on the vulnerability index formulation presented by the "Gruppo Nazionale per la Difesa dai Terremoti" – GNDT II level approach (GNDT, 1994), proposed to evaluate the seismic vulnerability of masonry buildings, with the modifications proposed by Vicente et al. (2011). Figure 2.31 illustrates the block of buildings and the vulnerability index obtained for the 19 buildings analysed, showing that buildings located in the end of a row usually have higher vulnerability index values. The corresponding vulnerability and fragility functions, for the average vulnerability index of the block, were derived following the methodology suggested by Vicente et al. (2011). This simplified assessment indicated that for the seismic demand in Lisbon (action type 1.3 with PGA=1.5 m/s^2 (IPQ, 2010)): 28% of the buildings are expected to have heavy damage, 34% are near to collapse and 9% are expected to collapse.

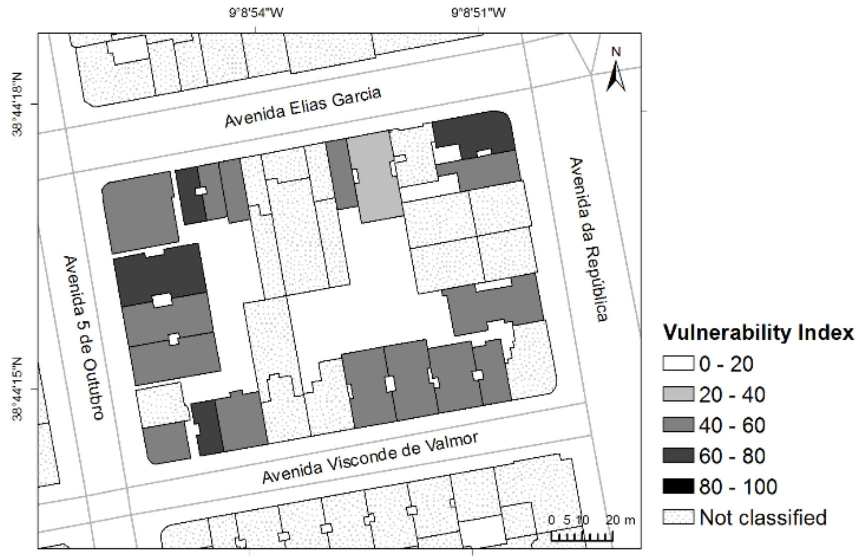

Figure 2.31 – Vulnerability index for the 19 masonry buildings analysed (Simões et al. (2016a))

Comparing the probability of near collapse for the code seismic demand in Lisbon, determined from the detailed numerical assessment (Simões et al., 2014a) and from the simplified index vulnerability assessment (Simões et al. (2016a)), it is evident that these are quite opposite: between 60% an 90% in the first case and 43% in the second case (defined as the sum of probabilities for near collapse and collapse). In the first case, the buildings were analysed as isolated structures, while in the second case, the vulnerability index takes into account the position of the buildings inside the block. Notwithstanding the differences between the two approaches, the above mentioned studies have demonstrated in a quantitative way the seismic vulnerability of these URM buildings; in particular of buildings of type I – buildings with small size façades and one flat per floor. It can also be concluded that the assessment of the seismic performance of the masonry buildings should consider both the local and global seismic response. In the first case, particular attention should be given to the out-of-plane failure modes of the last floors following the results from shaking table tests from (Candeias, 2008; Mendes, Lourenço and Campos-Costa, 2014). In the second case, the limited strength capacity of the connections between walls and the flexible behaviour of horizontal diaphragms should be accounted in analysis, considering that these factors compromise the activation of the global box-type behaviour.

2.6. Definition of the cases of study

The assessment of a building typology should take into account the variations between buildings in terms of geometry, constructive details and materials. In this work, these variations are considered as epistemic uncertainties and are herein treated by the logic-tree approach in order to define all possible combinations and set different building models for the analysis of the seismic vulnerability of the typology. An expert judgement probability is attributed to each branch of the tree to quantify the reliability of the building model within the typology. It is proposed to focus the study on the seismic assessment of buildings of type I supported by the high probability of near collapse associated (highlighted by previous studies §2.5), and by the representativeness of the buildings in the existing stock[1]. A prototype building is defined based on the architectural and structural features of the buildings and, in particular, on the characteristics of the six buildings of type I from the block in "Avenidas Novas" studied (Simões, Bento, Lagomarsino, et al., 2016) and identified in Figure 2.32.

Figure 2.32 – Identification of the building types within the block in "Avenidas Novas"

The geometry of the prototype building is presented in Figure 2.33 and Figure 2.34. It is characterized by plan irregularity due to the position of the airshaft close to one of the side walls. Buildings of type I

[1] The survey to the 18 blocks of buildings in the area of "Avenidas Novas", indicated in §2.4.6, revealed that within the URM buildings: 34% are of type I, 18% of type II, 39% of type III and 9% of type IV.

have in average five storeys high. The ceiling height and the ventilation box height adopted for the prototype building follow the minimum dimensions recommended by the Health Regulation for Buildings (RSEU, 1903): the ventilation box has 0.60 m height, the ground floor and the first floor have 3.25 m, the second floor has 3.00 m, the third floor has 2.85 m and the fourth floor has 2.75 m. In this case, the prototype building has a total height of 17 m.

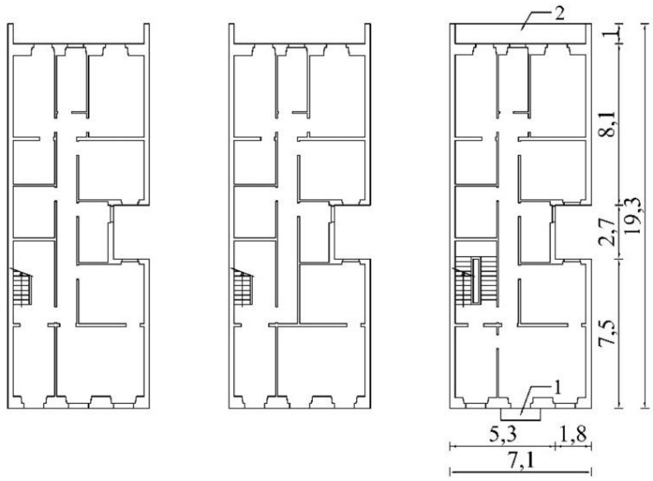

a) b) c)

Figure 2.33 – Plan of the prototype building: a) ground floor used for housing, b) ground floor used for commerce/shop, and c) regular floors with dimensions in meters (1 – stone balcony in the street façade and 2 – jack arch balcony with steel profiles in the rear façade)

a) b) c)

Figure 2.34 – View of the prototype building: a) street façade with ground floor used for housing, b) street façade with ground floor used for commerce/shop, and c) rear façade

In this typology of buildings, the ground floor level may be used for housing or for commerce/shop, with few implications on the openings in the front part of the building, as exemplified in Figure 2.33 and Figure 2.34 a) and b). In some buildings, the ground floor has also been converted from housing to shop. Taking into account the reference block of buildings from “Avenidas Novas”, the ground floor of 33% of the buildings is used for housing and 67% is used for commerce/shop. The regular floors are used for housing in both cases (the plan of the floor is presented in Figure 2.33 c)).

In what concerns the type of material and constructive details, the façade walls are made of rubble stone masonry and air lime mortar. The walls have 0.60 m of thickness at the ground floor (including the rendering with 0.04 m of thickness) and decrease 0.05 m in each floor. The wall below the windows is made of solid clay brick masonry and air lime mortar with 0.27 m of thickness (here the brick units were considered with a standard dimension of 0.07 x 0.11 x 0.23 m). Above the windows there are clay brick relieving arches and lintels. The side walls and the airshaft walls are made of clay brick masonry and air lime mortar with 0.27 m of thickness. The wall below the windows on the airshafts has 0.15 m of thickness.

There is limited information in the buildings' process (in AML) about the type of unit, meaning if it is made of solid bricks or hollow bricks. The Building Regulation from 1930 (RGEUL, 1930) recommended the use of hollow bricks on the last two floors of the building and solid bricks on the lower floors. Considering that this regulation was published at the end of the construction of these buildings, a lower probability was attributed to this option. Therefore, it was considered that in 70% of the cases, the side walls are made of solid clay brick masonry and on 30% of the cases, the side walls are made of solid clay brick masonry on the first three floors and hollow clay brick masonry on the last two floors.

The interior walls are made of clay brick masonry or have a timber "tabique" structure. The main load-bearing walls are placed parallel to the façades to support the floor timber beams. Other walls are designated as partition walls. The thickness of the interior clay brick masonry walls is: 0.15 m for main walls and 0.10 m for partition walls (including the rendering with 0.04 m of thickness). It was assumed that in 40% of the buildings the main interior walls are made of solid clay brick masonry and that in 40% these are made of solid clay brick masonry on the ground floor and hollow clay brick masonry on the other floors. It was also considered that in 20% of the buildings the main interior walls have a timber "tabique" structure, however this case was limited to the last floor of the building considering the recommendation from (RGEUL, 1930). As to the material used in the partition walls, it was considered that in 50% of the buildings these are made of hollow brick masonry and that in 50% are made of timber "tabique" structure.

The floors and roof are made of timber elements: *Pinus pinaster Ait.* ("pinho bravo" or "pinho nacional") wood type. The joists are set perpendicular to the façades with a distance of 0.40 m between each other and covered by one layer of timber boards. The joists have 0.18 m of height and 0.07 m of width, while the boards have 0.022 m of thickness. The pitched roof structure is supported on purlins disposed parallel to the façade walls (as exemplified in Figure 2.21). The pitched roof is usually behind a parapet in the street façade. These are made of clay brick masonry with 0.15 m of thickness and 0.80 m of height.

In the street façade there are stone balconies on the middle French windows, while in the rear façade there are jack arch balconies with steel profiles. In the first case, these are composed by a limestone blocks with 0.60 m of width, 0.15 m of thickness and 2.00 m of length. In the second case, these are composed by jack arches made of hollow clay brick masonry, supported on steel T section beams with 0.07 m x 0.07 m with a distance of 0.55 m between each other and covered by a layer of mortar with 0.06 m. The balconies have 1 m span and are embedded in the façade wall in one end and supported on steel U sections beams with 0.14 m x 0.06 m on the other end (this section is then embedded in the side brick walls). These balconies are subsequently covered by a layer of mortar with 0.040 m of thickness.

Buildings of type I do not exist as isolated structures. They are located in the middle or in the end of a row of buildings (Figure 2.32). It is also frequent to find buildings of type I adjacent to each other, occupying larger lots (generally for buildings of type III). In this case, the dimension of the buildings and the layout of the flats is very similar and usually the side walls are shared between buildings. Therefore, it is proposed to replicate the prototype building and define a block of three buildings of type I in order to take into account: 1) the effect of the adjacent buildings and, 2) the possibility that the side walls are shared or independent between buildings, as shown in Figure 2.35.

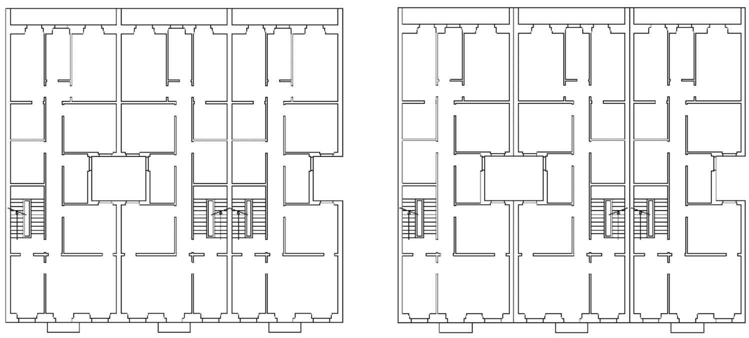

a) b)

Figure 2.35 – Plan view of the case of study (regular floors): a) block of buildings with shared side walls and b) block of buildings with independent side walls

The main variations inside the typology are summarized in the following:

1. Ground floor configuration: use of the building for i) housing (H) or for ii) shop (S).
2. Side walls solution: i) side walls shared between adjacent buildings (S) or ii) independent (I).
3. Side walls material: i) solid clay brick masonry (S) or ii) solid clay brick masonry in the first two floors and hollow clay brick masonry in the last three floors (SH).
4. Main interior walls material: i) solid clay brick masonry (S), ii) solid clay brick masonry in the first two floors and hollow clay brick masonry in the last three floors (SH), or iii) solid clay brick masonry in the first two floors, hollow clay brick masonry in the medium two floors and timber “tabique” walls on the last floor (T).
5. Partition walls material: i) hollow brick masonry (H) or ii) timber “tabique” walls (T).

The combination of these variations is presented in the logic-tree from Figure 2.36, resulting in a total of 32 possible building models and corresponding probabilities that quantify their reliability/weight within the typology. Each model is identified by an acronym in reference to the capital letters indicated in the list above. These 32 building models define the cases of study and should be considered for the numerical analyses of the seismic vulnerability of buildings of type I. In future work, it is suggested to adopt an equivalent procedure for the analyses of buildings of type II, III and IV and perform the overall seismic assessment of the URM building typology constructed in Lisbon in this period.

2.7. Conclusion

The buildings constructed in the area of "Avenidas Novas" represent the core of the urban development of Lisbon in the transition between the 19^{th} and 20^{th} centuries. The new city blocks were divided in lots with variable width originating four types of buildings (from I to IV). Despite this variation, within each type, the configuration of the buildings and the layout of the flats are practically identical. The buildings have in average four to six storeys high and are characterized by unreinforced masonry walls and timber floors and roof structure. The structural system and materials used in this period are also repetitive and based on traditional construction processes and local materials.

The analysis of the seismic behaviour of these URM buildings should consider both local and global seismic response. In the first case, particular attention should be given to the out-of-plane failure modes involving the last floors following the results from shaking table tests on reduced scale models representative of the buildings under study. In the second case, the limited strength capacity of the connections between walls and the flexible behaviour of horizontal diaphragms should be accounted, considering that these factors compromise the activation of the global box-type behaviour. Additional studies should be carried out for the characterization of the mechanical properties of traditional masonry walls. Nevertheless, the few results available indicate in general the reduced strength capacity of the materials used on the construction in the transition between the 19^{th} and 20^{th} centuries in Lisbon.

With the objective of conducting the seismic vulnerability analysis of this typology of masonry buildings, the most vulnerable type was defined as the case of study: type I – buildings with small size façades and one flat per floor. Considering that these buildings are assembled in aggregates, a prototype building was defined and afterwards replicated in order to set a block of three buildings aiming to take into account: 1) the effect of the adjacent buildings and, 2) the possibility that the side walls are shared or independent between buildings. In addition, the main variations within the typology, in terms of geometry, constructive details and materials were identified. These variations were assumed as epistemic uncertainties and treated by the logic-tree approach, resulting in the definition of 32 building models for the comprehensive assessment of buildings of type I.

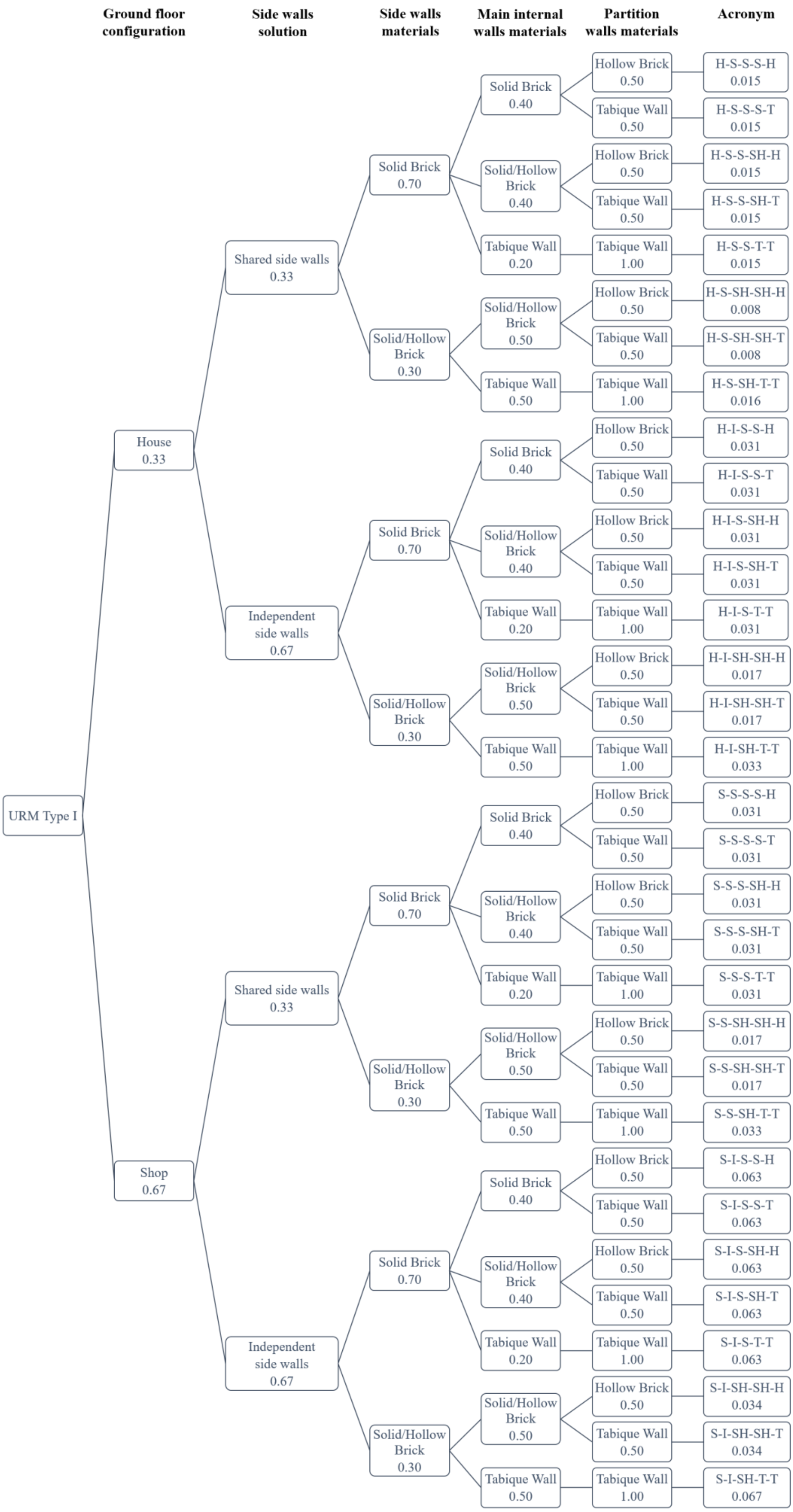

Figure 2.36 – Logic-tree with the definition of the possible building models

This page was intentionally left blank

3. ANALYSIS OF THE GLOBAL SEISMIC BEHAVIOUR

3.1. Introduction

The global seismic behaviour of URM buildings is based on the assumption that the connection between walls and the connection between walls and floors/roof are effective to prevent the occurrence of local mechanisms associated with the out-of-plane response of walls. In this context, the response of the structure is mainly governed by the in-plane capacity of the walls and by the in-plane stiffness of horizontal diaphragms that rules the distribution of the horizontal loads between vertical structural elements. However, the presence of flexible horizontal diaphragms (timber floors and roof) provides lower degree of coupling between walls, compromising the activation of the global box-type behaviour. In this thesis, the analysis of the global seismic behaviour is supported on non-linear static procedures and three-dimensional models able to capture the response of the structure.

Different modelling approaches are available for the analysis of masonry structures (Lourenço, 2002). Structural element models represent the simplest approach. These are based on the identification of macroscopic structural elements, defined from a geometrical and kinematic point of view through finite elements (solid, shell or frame) and described from a static point of view by their internal generalized forces (Lagomarsino et al., 2013). Finite Element Method (FEM) numerical models, based on the macro-modelling approach comprehend several simplifications, in terms of geometry and material properties, with respect to the real non-linear dynamic behaviour of the structure. Nevertheless, these require a moderate number of degrees of freedom, allowing the analysis of three-dimensional models with a reasonable computational effort.

In this framework, three-dimensional models of the 32 cases of study identified in §2.6 are modelled according to the equivalent frame approach making use of TREMURI program (Lagomarsino et al., 2013) for the non-linear seismic analyses of masonry buildings. Various parameters are assumed as aleatory variables aiming to account both the uncertainties in the quantification of the values and the intrinsic variations between buildings belonging to the same typology. The following variables are considered: mechanical properties of masonry, strength and deformability characteristics of masonry piers and spandrels, mechanical properties of interior timber “tabique” walls, quality of connections between walls and in-plane stiffness of timber floors. A detailed characterization of all parameters is conducted in order to define plausible ranges of variation. In regards to the mechanical properties of masonry, the limited knowledge about the materials in this typology prevents the definition of reference values with reasonable degree of confidence. The Bayesian update approach is applied to this end. This takes into account the experimental results from tests carried out in masonry walls in Lisbon, and the reference values proposed in the commentary to the NTC (MIT, 2009) for different types of masonry. The Monte Carlo Method is then used to sample all aleatory variables considered and with this define the input parameters for the set of building models.

The global seismic behaviour is addressed to the group of buildings resulting from the combination between: 1) the 32 cases of study identified based on the logic-tree approach (epistemic uncertainties) and 2) the parameters defined based on the Monte Carlo Method (aleatory uncertainties). It is proposed to analyse the global seismic behaviour of the buildings according to a displacement-based assessment approach (Lagomarsino and Cattari, 2015a). This aims to define the seismic intensity measure compatible with specific performance limit states. Non-linear static (pushover) analyses are performed to define the capacity of the different building models. The analyses are first carried out with the building models, defined by the median properties of the aleatory variables, in order to compare the global behaviour of the different cases of study and identify the main features and differences of the seismic response. Non-linear dynamic time-history analyses are also carried in order to verify the reliability of the load distributions considered in the pushover analyses. Pushover analyses are afterwards performed with the building models, defined by the aleatory properties of the various parameters.

Four performance limit states are defined on the pushover curves in terms of displacement thresholds. In a previous work about these URM buildings in Lisbon (Simões et al., 2014b), the criterion proposed by the EC8-3 (IPQ, 2017) and the multi-scale approach proposed by Cattari and Lagomarsino (2013) were compared. Based on these results, in the present work, the definition of the performance limit states is based only on the multi-scale approach. In fact, this approach is particularly effective for buildings with flexible diaphragms as it correlates damage in the structure at different scales, namely single elements, macro-elements and global. Moreover, in this thesis, a new criterion for the verification at the macro-element scale is adopted.

The performance-based assessment comprehends the comparison between the displacement capacity of the structure, identified for different performance limit states, and the seismic demand, expressed by a properly reduced acceleration-displacement response spectrum (ADRS). The Capacity-Spectrum Method with over-damped spectrum is adopted in this work. The values of the seismic intensity measure compatible with the attainment of the performance limit states are treated in order to derive the parameters for the definition of the fragility functions. This includes the determination of the dispersion related to the definition of the capacity of the structure and the dispersion related to the definition of the seismic demand. Finally, the fragility functions associated with the global seismic behaviour of the typology of buildings are derived and the damage distribution is estimated for different seismic scenarios.

3.2. Modelling assumptions

In order to analyse the global seismic behaviour of buildings of type I, the 32 building models identified with the logic-tree approach (Figure 2.36) are modelled making use of TREMURI program (Lagomarsino et al., 2013). This program is based on the equivalent frame modelling approach for the non-linear seismic analysis of masonry buildings. The commercial version of the program – 3Muri release 5.5.110 (http://www.stadata.com/) – is used to generate the mesh of elements, while the research version – TREMURI (Lagomarsino et al., 2012) – is used to perform the non-linear analyses considering a more detailed force-deformation law for the characterization of the masonry elements. In TREMURI program, the three-dimensional model of building is obtained by assembling: 1) the walls modelled as an equivalent frame and, 2) the horizontal diaphragms (floors and roof) modelled as membrane elements. Figure 3.1 presents the plan view of the block of buildings and the three-dimensional view of one of the models.

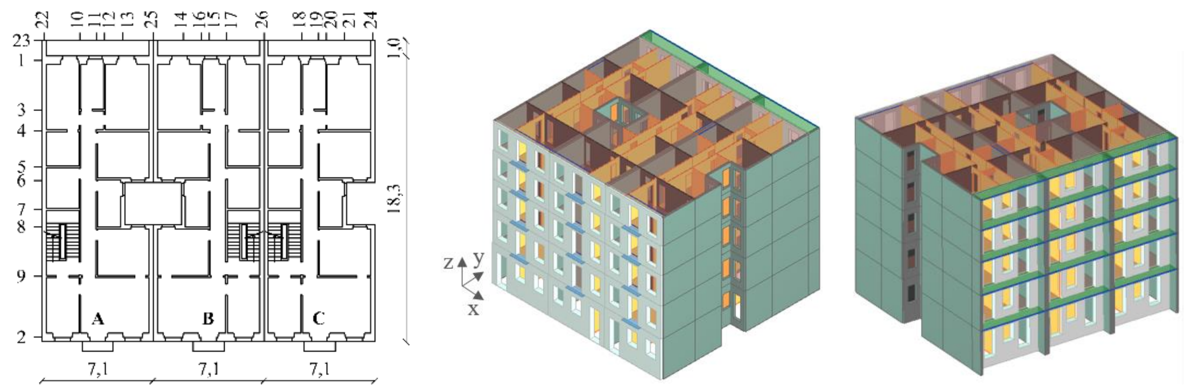

a) b) c)

Figure 3.1 – Block of three buildings of type I: a) plan view with identification of buildings A, B and C and wall numbering (dimensions in meters), and three-dimensional model in 3Muri b) street view and c) rear view

The main modelling assumptions considered are presented in the next sections. This includes the options for the quantification of some parameters as aleatory variables (X_k). Each aleatory variable is defined within a plausible interval of values, based on the information available in the literature and results from experimental tests, and described by a continuous probability distribution function. The Monte Carlo Method is then used to sample the aleatory variables and define the input variables for the group of numerical models.

3.2.1. Masonry walls: non-linear equivalent frame model

The equivalent frame model approach comprehends the discretization of the masonry walls with openings into a set of panels (Figure 3.2): 1) piers, which are the main vertical elements carrying both vertical and horizontal loads, 2) spandrels, which are the horizontal elements coupling piers and limiting their end-rotations in case of horizontal loads, and 3) rigid node/portion, undamaged elements confined between piers and spandrels. The geometry of these panels is defined by the distribution of openings and by the damage observation in URM buildings after past earthquakes and experimental tests. The height of interior piers corresponds to the height of the openings. The height of exterior piers is assumed as the average between the height of the opening and the inter-storey height, considering the possible development of inclined cracks starting from the opening corners (identified as H_{eff} in Figure 3.2). The height and length of spandrels is defined by the vertical and horizontal alignment of openings.

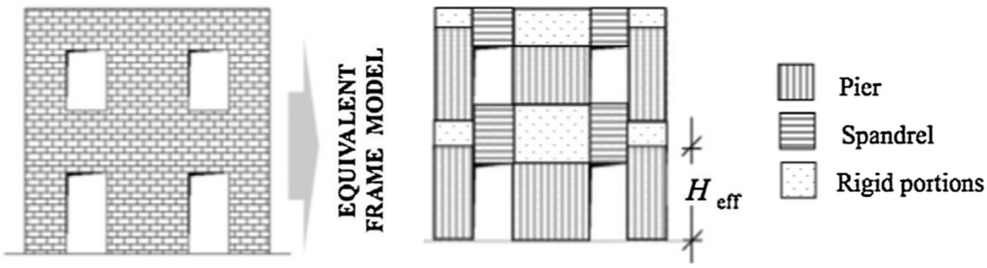

Figure 3.2 – Idealization of a URM wall with openings into an equivalent frame model (adapted from Lagomarsino et al. (2013))

In TREMURI program, the behaviour of masonry panels is modelled by non-linear beam elements with lumped (concentrated) inelasticity. These elements are directly characterized in terms of stiffness, strength and displacement capacity by a multi-linear force-deformation constitutive law, represented in Figure 3.3. This piecewise constitutive law is based on a phenomenological approach that aims to describe the non-linear response of masonry panels for increasing Damage Levels (DLi, with i=1,…,5). Each DL represents the point after which the element experiences a Damage State (DS). These DS are defined in accordance to the European Macroseismic Scale, EMS-98 (Grünthal, 1998): DS0 – no damage, DS1 – slight, DS2 – moderate, DS3 – heavy, DS4 – very heavy, and DS5 – collapse.

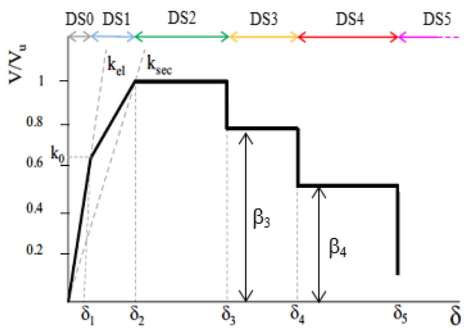

Figure 3.3 – Multi-linear force-deformation constitutive law for the characterization of the in-plane behaviour of masonry panels (adapted from Cattari and Lagomarsino (2013))

The response of the elements is determined from the comparison between the acting shear force (V) and the ultimate shear force (V_u) considering the occurrence of flexural, shear or mixed failure modes (DL2). This multi-linear constitutive law assumes a progressive strength degradation (defined in Figure 3.3 in terms of residual strength β_i) at pre-determined drift levels (δ_i), coincident with DL3, DL4 and DL5. Once DL5 is reached, the panel only keeps its capacity to support vertical loads. Mixed failure modes are also possible, when the prediction between flexural and shear modes is close. In this case, the drift limits (δ_i) are evaluated as a linear combination of those associated with the basic failure modes. The ultimate shear force (V_u) may be interpreted by simplified criteria based on mechanical and phenomenological hypotheses, proposed in structural codes and literature (the criteria adopted in this thesis are discussed in §3.2.2).

The multi-linear constitutive law describes, in addition, the initial stiffness degradation of the panel (after DL1) by two parameters (Figure 3.3): 1) k_{in} which gives the ratio between the elastic (k_{el}) and the secant (k_{sec}) stiffness at the point where V_u is reached, and 2) k_0 which gives the ratio between the shear force at the end of the elastic phase and V_u. The elastic stiffness (k_{el}) is directly determined by the shear and flexural stiffness contribution, as summarized in the stiffness matrix indicated in squared brackets in Figure 3.4.

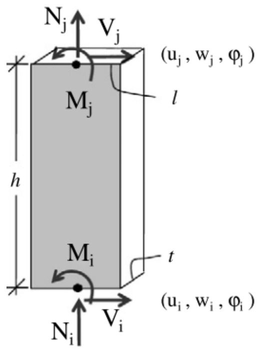

$$
\begin{Bmatrix} V_i \\ N_i \\ M_i \\ V_j \\ N_j \\ M_j \end{Bmatrix} =
\begin{bmatrix}
\frac{12EJ}{h^3(1+\psi)} & 0 & -\frac{6EJ}{h^2(1+\psi)} & -\frac{12EJ}{h^3(1+\psi)} & 0 & -\frac{6EJ}{h^2(1+\psi)} \\
0 & \frac{EA}{h} & 0 & 0 & -\frac{EA}{h} & 0 \\
-\frac{6EJ}{h^2(1+\psi)} & 0 & \frac{EJ(4+\psi)}{h(1+\psi)} & \frac{6EJ}{h^2(1+\psi)} & 0 & \frac{EJ(2-\psi)}{h(1+\psi)} \\
-\frac{12EJ}{h^3(1+\psi)} & 0 & \frac{6EJ}{h^2(1+\psi)} & \frac{12EJ}{h^3(1+\psi)} & 0 & \frac{6EJ}{h^2(1+\psi)} \\
0 & -\frac{EA}{h} & 0 & 0 & \frac{EA}{h} & 0 \\
-\frac{6EJ}{h^2(1+\psi)} & 0 & \frac{EJ(2-\psi)}{h(1+\psi)} & \frac{6EJ}{h^2(1+\psi)} & 0 & \frac{EJ(4+\psi)}{h(1+\psi)}
\end{bmatrix}
\begin{Bmatrix} u_i \\ w_i \\ \varphi_i \\ u_j \\ w_j \\ \varphi_j \end{Bmatrix}
$$

with $\psi = 24\left(1+\frac{E-2G}{2G}\right)1.2\frac{b^2}{12h^2} = 1.2\frac{E}{G}\frac{b^2}{h^2}$

Figure 3.4 – Modelling of a masonry panel as a beam element: kinematic variables, generalized forces and geometric properties

In Figure 3.4, V, N and M are, respectively, the acting shear force, axial force and bending moment at the element end nodes i and j, E is the modulus of elasticity of masonry, J is the inertia of the element section, h is the height of the element, u, w and φ are, respectively, the horizontal displacement, vertical displacement and rotation at the element end nodes i and j and G is the shear modulus of masonry. The redistribution of internal forces is made according to the element equilibrium, while the rigid node/portion is used to transfer the static and kinematic variables between elements.

The drift of the element is computed from the contribution of the horizontal displacement and rotation according to Equation (3.1):

$$\delta = \frac{(u_j - u_i)}{h} + \frac{(\varphi_j - \varphi_i)}{2} \tag{3.1}$$

In the next section, the strength criteria adopted for piers and spandrels are discussed, along with the identification of the parameters considered as aleatory variables.

3.2.2. In-plane behaviour of masonry panels

Masonry piers subjected to in-plane loading typically show two types of behaviour: flexural and shear (Figure 3.5). The response of the panels depends on the geometry, boundary conditions, axial load, mechanical properties of masonry and type of masonry (i.e. block aspect ratio, in-plane and cross-section masonry pattern). The behaviour of spandrels depends, in addition, on the interlocking phenomenon originated at the end-sections of the panel with the contiguous masonry, type of lintels (e.g. masonry arches or architraves in stone, timber, steel or RC), and interaction with other elements coupled to them (in particular if tensile resistant, such as steel tie-rods).

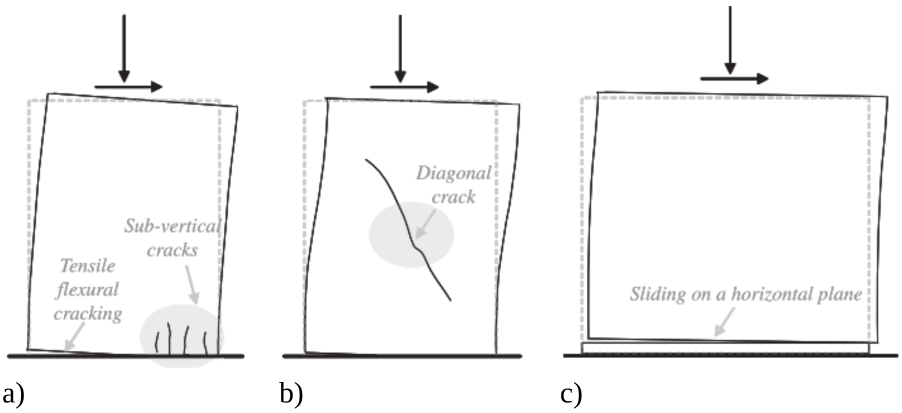

Figure 3.5 – Typical in-plane failure modes of masonry piers (Calderini, Cattari and Lagomarsino, 2009): a) rocking, b) diagonal cracking, and c) sliding shear

The flexural behaviour of piers combines both rocking/bending and crushing/compression failure modes (Figure 3.5 a)). In the former, the panel behaves as a nearly rigid body, rotating around the toe, and in the latter, the panel is subjected to a widespread damage with sub-vertical cracks oriented towards the compressed toe. The flexural failure is described by the beam theory, following the common criteria proposed in codes (NTC, 2008; IPQ, 2017). The ultimate bending moment (M_u), at the panel end section, is determined according to Equation (3.2) by neglecting the tensile strength of masonry and assuming a non-linear distribution of stresses at the compressed toe. This distribution of stresses is approximated to a rectangular stress diagram with a factor equal to 0.85.

$$M_u = \frac{D^2 t \sigma_0}{2}\left(1 - \frac{\sigma_0}{0.85 f_c}\right) \tag{3.2}$$

In Equation (3.2), D and t are the length and the thickness of the panel, σ_0 is the vertical compressive stress and f_c is the compressive strength of masonry. If the ultimate bending moment is attained, the shear force must be recalculated according to Equation (3.3) to satisfy the equilibrium of the element.

$$V_i = -V_j = -\frac{M_i + M_j}{h} \tag{3.3}$$

The ultimate shear associated with flexural failure ($V_{u,Flexural}$) is given by Equation (3.4):

$$V_{u,Flexural} = \frac{D^2 t \sigma_0}{2h_0}\left(1 - \frac{\sigma_0}{0.85 f_c}\right) \tag{3.4}$$

where h_0 is the distance between the section of maximum capacity and the contra-flexure point. The compressive strength of masonry (f_c) may be determined based on compression tests (ASTM, 2004; RILEM, 2004) or double flat-jack tests (RILEM, 1994; ASTM, 2002). These tests comprise the uniaxial loading of the panel aiming to determine the strength and deformability characteristics of the material: compressive strength (f_c) and modulus of elasticity (E).

The shear behaviour of piers may be governed by diagonal cracking failure or sliding failure (Figure 3.5 b) and c)). In the first type of failure, the peak resistance leads to the formation of inclined diagonal cracks, which may follow the path of bed- and head-joints or may go through the units, depending on the relative strength of mortar joints, unit-mortar interface, and units. The second type of failure occurs due to the formation of tensile horizontal cracks in the bed-joints. This may occur for low levels of axial load and/or low coefficient of friction.

The EC8-3 (IPQ, 2017) states that the shear behaviour of masonry piers may be described as a function of the cohesion and coefficient of friction of masonry (Mohr-Coulomb criterion), which is more consistent with the sliding type of failure. The commentary to the NTC (MIT, 2009) states that for masonry piers made of irregular units or characterized by not particularly resistant units, the shear behaviour may be governed by the diagonal cracking failure according to the criterion proposed by Turnšek and Čačovič (1970) and Turnšek and Sheppard (1980). Taking into account the characteristics of the masonry present in the buildings studied in this work, it is assumed that the shear behaviour of piers is characterized by diagonal cracking failure. In this case, the ultimate shear associated with diagonal cracking shear failure ($V_{u,Shear}$) is given by Equation (3.5):

$$V_{u,Shear} = Dt\frac{f_t}{b}\sqrt{1 + \frac{\sigma_0}{f_t}} = Dt\frac{1.5\tau_0}{b}\sqrt{1 + \frac{\sigma_0}{1.5\tau_0}} \tag{3.5}$$

where f_t is the tensile strength of masonry due to diagonal cracking, τ_0 is the equivalent shear strength of masonry, conventionally defined as $\tau_0=f_t/1.5$, and b is a corrective factor related to the distribution of the loads in the element. The corrective factor b depends on the slenderness of the panel (ratio between height and length, h/D) and is limited as in Equation (3.6):

$$1.0 \le b = h/D \le 1.5 \tag{3.6}$$

The commentary to the NTC (MIT, 2009) refers that the tensile strength of masonry (f_t) may be derived from diagonal compression tests (RILEM, 1994; ASTM, 2002) and determined according to Equation (3.7):

$$f_t = \frac{F_u}{2A} = \frac{F_u}{t \times (D+h)} \tag{3.7}$$

where F_u is the ultimate test load and A_d is the diagonal failure surface area, being t, D and h, respectively, the thickness, length and height of the panel.

The in-plane behaviour of spandrels is commonly characterized by the same criterion as that of piers mainly because, appropriate models for their force-deformation relationships were not available until recently (Beyer and Mangalathu, 2014). The EC8-3 (IPQ, 2017) makes no specific reference to the behaviour of spandrels, whereas the NTC (2008; MIT, 2009) defines the strength criterion taking the contribution of tensile strength of the elements coupled to them (e.g. steel tie-rods or RC beams). In the last decade, several tests have been performed to characterize the behaviour of masonry spandrels (Gattesco et al., 2008; Beyer and Dazio, 2012; Graziotti, Magenes and Penna, 2012). These experimental results have shown, for example, that spandrels have greater deformation capacity in comparison with piers and that their behaviour is influenced by the presence and type of lintel. In Cattari and Beyer (2015) the effect of spandrel modelling on the behaviour of masonry buildings is discussed.

In this context, it is proposed to model the flexural behaviour of spandrels according to the criterion proposed by Cattari and Lagomarsino (2008) assuming an equivalent tensile strength on the elements. Such assumption is motivated by the interlocking of masonry units at the panel end sections. The reliability of this criterion has been demonstrated by Beyer (2012). In addition, in a previous work about these URM buildings in Lisbon (Simões et al., 2014b), a sensitivity analysis was carried considering the flexural behaviour of spandrels modelled with no tensile strength (analogously to the criterion assumed for piers) and considering an equivalent tensile strength, following the criterion proposed by Cattari and Lagomarsino (2008). The behaviour of the building was compared in terms of pushover curves showing that the initial stiffness increases approximately 20%, as a result of the equivalent tensile strength attributed to spandrels. In this case, spandrels also provided a better coupling to piers in the beginning of the non-linear static (pushover) analyses, yet the type of damage failure in the building suffers few variations. Due to this reason, in this work, it is proposed to describe the flexural behaviour of spandrels assuming an equivalent tensile strength on the elements.

The criterion proposed by Cattari and Lagomarsino (2008) is characterized by two parameters: 1) interlocking (*Int*), defined as the ratio between the length and the height of the units, and 2) coefficient of friction in the mortar joints (μ_{loc}) at the element end section. In this work, the interlocking (*Int*) is assumed equal to 2.00, for clay brick masonry spandrels (defined directly from the brick size) whereas, for rubble stone masonry spandrels, lower values are expected due to the irregular pattern and variable dimension of the units. Due to this reason, the interlocking (*Int*) is set as an aleatory variable ranging between 0.50 and 2.00. The coefficient of friction (μ_{loc}) is also set as an aleatory variable for both types of masonry and assumed to vary between 0.40 and 0.70, starting from the values proposed by Eurocode 6 (CEN, 2005).

The shear behaviour of spandrels is supposed to be governed by the diagonal cracking failure, as in the case of piers.

In each step of the non-linear analysis, TREMURI program updates the ultimate shear force (V_u) in the elements taking into account the axial load variation. A verification for the ultimate compressive strength is also implemented. It considers that the ultimate compression strength of the element is limited as presented in Equation (3.8):

$$N = Dt\sigma_0 \leq 0.85Dtf_c \tag{3.8}$$

In this work, the mechanical properties of masonry – modulus of elasticity (E), shear modulus (G), compressive strength (f_c) and tensile strength (f_t) – are assumed as aleatory variables. On the other hand, the limited knowledge and experimental results regarding rubble stone and clay brick masonry walls in Lisbon, prevents the definition of a reference interval of values with reasonable degree of confidence. It is proposed to minimize this problem with the application of the Bayesian update approach, as discussed in §3.2.3.

The parameters defining the initial stiffness degradation (k_{in} and k_0) and the progressive degradation of strength (δ_i and β_i), in agreement with the multi-linear constitutive law (Figure 3.3), are also assumed as aleatory variables. The corresponding interval of values are defined based on experimental test results, reference values and expert judgement. In addition, due to the limited information available, the same values are adopted for rubble stone masonry and clay brick masonry.

In what concerns the definition of k_{in}, structural codes (NTC, 2008; IPQ, 2017) recommend to adopt a 50% reduction of the elastic stiffness properties (corresponding to k_{in} = 2), unless more detailed information is available. Previous parametrical studies have indicated this level of reduction leads to very conservative estimate of the non-linear behaviour of the panels (Cattari, 2007; Calderini, Cattari and Lagomarsino, 2009). Therefore, it is proposed to vary k_{in} between 1.00 and 1.50, in order to simulate the extreme cases in which there is no stiffness degradation and the case in which this reduction is approximately 67% due to the expected cracked state of the buildings. As to k_0, it is proposed to consider a range between 0.50 and 0.80.

Table 3.1 summarizes the lower and upper values ($X_{k,low}$ and $X_{k,up}$) adopted for the residual strength (β_i) and drift (δ_i) for piers and spandrels as a function of the possible failure modes (F – flexural or S –

shear). The values are defined based on experimental test results and reference values (Kržan et al., 2015; Haddad, Cattari and Lagomarsino, 2017; Vanin et al., 2017) and expert judgement. For instance, in case of piers, the ultimate drift levels (DL4) reflect the recommendations from structural codes (NTC, 2008; IPQ, 2017): between 0.4% and 0.6% in case of shear failure and between 0.8% and 1.2% in case of flexural failure. In case of spandrels, the experimental results from Beyer and Mangalathu (2014) are taken into account to characterize the behaviour of the shallow brick arches present in the façade walls (faç) and of the timber elements in the clay brick masonry walls. In case of spandrels with shallow brick arches, DL3 threshold is not defined in terms of drift, but in terms of ductility (μ), considering the greater deformation capacity of the elements observed during the experimental tests (Beyer and Mangalathu, 2014).

Table 3.1 – Residual strength, drift and ductility thresholds for piers and spandrels

Element	Parameter	X_k	$X_{k,low}$	$X_{k,up}$
Pier	Residual strength	β_{F4}	0.80	0.90
		β_{S3}	0.60	0.80
		β_{S4}	0.25	0.55
	Drift	δ_{F3}	0.0046	0.0074
		δ_{F4}	0.0078	0.0122
		δ_{F5}	0.0120	0.0180
		δ_{S3}	0.0023	0.0037
		δ_{S4}	0.0039	0.0061
		δ_{S5}	0.0056	0.0084
Spandrel	Residual strength	β_{F4}, β_{S3}, β_{S4}	0.40	0.70
		β_{F4}, β_{S3}, β_{S4} |faç	0.20	0.60
	Drift	δ_{F3}, δ_{S3}	0.0015	0.0025
		δ_{F4}, δ_{S4}	0.0045	0.0075
		δ_{F5}, δ_{S5}	0.0151	0.0249
	Ductility	μ |faç	3.21	5.19

3.2.3. Mechanical properties of masonry by the Bayesian update

Masonry is, in general, characterized by high specific mass, low tensile strength (due to the weak mechanical properties of mortar and low adherence with blocks) and low shear strength (diagonal or stepwise cracks occur in masonry panels subjected to vertical compression and shear forces). The mechanical properties of masonry are related to the mechanical properties of the constituents – blocks and mortar – and to the characteristics of the assembly – dimension, shape and interlocking of the blocks. The proper characterization of the mechanical properties of buildings' materials is difficult because, in many practical cases, it is not feasible or allowed to perform *in situ* destructive tests. Moreover, the heterogeneity of the material and the variability from panel to panel, requires performing several tests to have a significant statistical sample.

As referred in §2.5, the number of experimental campaigns for the characterization of the mechanical properties of masonry walls in Lisbon is quite limited. Table 3.2 to Table 3.4 summarize, for different masonry typologies, the values available in the literature for the modulus of elasticity (E), compressive strength (f_c) and tensile strength (f_t), including results from *in situ* tests on URM buildings in Lisbon and similar such as, the *in situ* double flat-jack tests performed on rubble stone masonry walls in Coimbra (Vicente et al., 2015), and the results from laboratory tests on masonry specimens constructed to represent the traditional masonry walls (identified in the tables as "Lab").

Table 3.2 – Rubble stone masonry and air lime mortar compression properties

Type of Test		Reference	E (GPa)	f_c (MPa)
Compression	*In situ*	Ramos (2002)	1.000	0.88 0.85 0.81
	Lab	Moreira (2015)	--	1.60
		Simões (2015)	--	0.50
		Martins (2014)	--	0.46 0.44
		Miloševič et al. (2013)	0.560	7.41
		Pinho et al. (2012)	0.239 0.409 0.267	0.42 0.40 0.46
		Morais (2011)	--	0.744
		Correia (2011)	--	0.60
		Carvalho (2008)	0.250	2.48
Double Flat-Jack	*In situ*	Simões et al. (2016)	2.000 0.205 0.420 0.510	1.89 0.47 0.67 0.75
		Vicente et al. (2015)	3.309 1.197 1.719 3.084 1.356 0.261 0.346 0.409 4.061	1.547 0.942 0.894 1.186 1.219 0.870 0.878 1.755 1.124
	Lab	Carvalho (2008)	0.080	2.38
Reference Values		Cóias e Silva (2007)	0.700 – 1.500	0.80 – 1.50
		Segurado (1908)	--	0.50 – 1.00

Table 3.3 – Rubble stone masonry and air lime mortar tensile strength

Type of Test	Reference	f_t (MPa)
Diagonal Compression (Lab)	Miloševič et al. (2013)	0.017 0.017

Table 3.4 – Clay brick masonry compression properties

Unit	Type of Test	Reference		E (GPa)	f_c (MPa)
Solid	Compression (*In situ*)	Branco and Correia (2003)		0.330	--
	Reference Values	Segurado (1908)	Regular brick	--	0.60 – 0.80
			Hard brick	--	0.80 – 1.00
		Ferreira and Farinha (1974)		--	0.59 – 0.98
Hollow	Reference Values	Ferreira and Farinha (1974)		--	0.49 – 0.59

The sample puts in evidence the variability and the reduced number of the test results, in particular for the characterization of the tensile strength (f_t). This shows the difficulty of defining an interval of values with reasonable degree of confidence. Moreover, the results from *in situ* tests, are affected by the experimental error and are very much dependent on the panel selected for the test, as well as, on its damage state; this is particularly true for rubble stone masonry due to the irregularity of the assembly.

In this thesis, it is proposed to define the mechanical properties of masonry by the Bayesian update approach, as suggested in the final draft of the EC8-3 (to be published, CEN 2018). A similar approach has been considered by Bracchi et al. (2016). The Bayes' Theorem is applied to update the probability of *a priori* distribution given that new evidences are available. In this case, the *a priori* distribution is defined by the interval of values proposed in the commentary to the NTC (MIT, 2009) for the relevant masonry types, whereas the new evidences are defined by the experimental test results collected. The updated interval of values is computed from the application of Equation (3.9) and Equation (3.10) that define, respectively, the mean value (μ") and standard deviation (σ") of the updated interval. In Equation (3.10), k is given by Equation (3.11).

$$\mu'' = \frac{\overline{x} + k\mu'}{1+k} \tag{3.9}$$

$$\sigma'' = \sigma' \sqrt{\frac{nk}{n+k}} \tag{3.10}$$

$$k = \frac{\varepsilon^2 + \overline{s}^2}{\sigma'^2} \tag{3.11}$$

Here, μ' and σ' represent the mean value and standard deviation of the *a priori* interval, n is the number of tests results, $\bar{x}$ and $\bar{s}$ are the mean value and standard deviation of the test results, ε is the standard deviation associated with the uncertainty of the testing method (and their correlation with the mechanical property in question). In this case, it is considered that the testing error (ε) and the variability of the mechanical properties in the building are statistically independent. In this work, the testing error (ε) was assumed equal to $0.3\bar{x}$ for compression and double flat-jack tests and equal to $0.4\bar{x}$ for diagonal compression tests.

Table 3.5 presents the initial and the updated interval of values for the compressive strength (f_c), modulus of elasticity (E) and tensile strength (f_t). As in the commentary to NTC (MIT, 2009) there is no specific reference for hollow clay brick masonry, the interval for solid clay brick masonry defines the initial range. The modulus of elasticity is representative of the not cracked state. The shear modulus (G) is assumed equal to 1/3 of the modulus of elasticity, following the recommendation from (MIT, 2009). As referred before, the mechanical properties of masonry are considered as aleatory variables.

Table 3.5 – Reference values for the mechanical properties of different types of masonry

Type of masonry	Reference	E (GPa)	f_c (MPa)	f_t (MPa)
Rubble stone masonry and air lime mortar	*A priori*	0.690 – 1.050	1.00 – 1.80	0.045 – 0.072
	Updated	0.615 – 0.882	0.84 – 1.07	0.027 – 0.039
Solid clay brick masonry and air lime mortar	*A priori*	1.200 – 1.800	2.40 – 4.00	0.090 – 0.138
	Updated	0.716 – 0.987	0.95 – 1.21	0.090 – 0.138
Hollow clay brick masonry and air lime mortar	*A priori*	1.200 – 1.800	2.40 – 4.00	0.090 – 0.138
	Updated	0.716 – 0.987	0.87 – 1.18	0.090 – 0.138

3.2.4. Interior timber "tabique" walls

The cases of study presented in §2.6 include different models where the interior walls are made of clay brick masonry and/or made of timber "tabique" structure. Common practise is to neglect the contribution of the partition timber "tabique" walls to the lateral resisting system of the building. However, with the objective of analysing the structural variations within this typology of buildings, the timber "tabique" walls are also considered in the numerical models in order to have a comparable distribution of the vertical loads in the buildings, especially for the walls positioned perpendicular to the floor timber joists, supporting therefore vertical loads.

The timber "tabique" walls have 0.10 m of thickness. These walls are modelled in TREMURI program following the equivalent frame model approach and considering an equivalent thickness of 0.04 m (Pires, 2013), corresponding to the average thickness of the vertical boards (Figure 2.14). The behaviour of the panels is modelled by non-linear beam elements with lumped (concentrated) inelasticity and by assuming a bi-linear force-deformation constitutive law. The elastic branch is directly determined by the shear and flexural stiffness, computed based on the geometric and mechanical properties of the element (as presented in Figure 3.4 for the case of masonry elements). The behaviour of the elements is determined from the comparison between the acting shear force (V) and the ultimate shear force (V_u) considering only shear failure modes. The hypothesis of having flexural failure modes is disregarded taking into account that these walls were constructed directly on top of the timber floors (i.e. there is no continuity between floors).

The mechanical properties of timber "tabique" walls – modulus of elasticity (E), shear modulus (G) and compressive strength (f_c) – are defined based on the experimental results from compression and shear tests performed by Rebelo et al. (2015) in similar walls. These parameters are treated as aleatory variables and assumed to vary within the range of values indicated in Table 3.6. A low value was assumed for the equivalent shear strength (τ_0), equal to 0.01 MPa, in order to neglect the contribution of these walls to the lateral resistant system of the buildings.

Table 3.6 – Modulus of elasticity, shear modulus and compressive strength of timber "tabique" walls

Variable X_k	$X_{k,low}$	$X_{k,up}$
E [GPa]	0.060	0.200
G [GPa]	0.001	0.003
f_c [MPa]	0.40	0.72

3.2.5. Classification of the connections between walls

In TREMURI program, the connection between walls is defined by default as good quality. However, it is known that one of the main vulnerabilities of these URM buildings are the connections between exterior walls and between exterior and interior walls. Due to the limited knowledge about the strength capacity of connections, in this thesis these are classified in a qualitative (expert judgement) way as follows:

1. Connection between rubble stone masonry façade wall and side clay brick masonry walls – Despite the use of different types of masonry (and the questionable interlocking of the units), it is expected that during the construction more attention was given to the connection between exterior walls. Due to these reasons, the connection between exterior walls may be classified as medium quality.

2. Connection between exterior walls and interior clay brick masonry walls – It is assumed that interior walls were constructed after exterior walls; thus, the interlocking between units is not effective, even when the same type of masonry is used (side and interior walls). Due to this, the connection between exterior and interior walls may be classified as weak quality.

In order to analyse the effect of the connections in the global seismic behaviour of the block of buildings, the interface between walls are modelled through link beams at the floor level, as exemplified in Figure

3.6. The properties of these link beams, namely the area (*A*) and inertia (*I*), are defined to simulate the medium and weak quality connections. These are set though an iterative procedure supported on the comparison of the global behaviour of the block of buildings in terms of pushover curves. This iterative procedure is presented in §3.3.1. The properties of the link beams representative of the weak quality connections are assumed as deterministic, whereas the ones representative of the medium quality connections are defined within a range of variation and treated as aleatory variables.

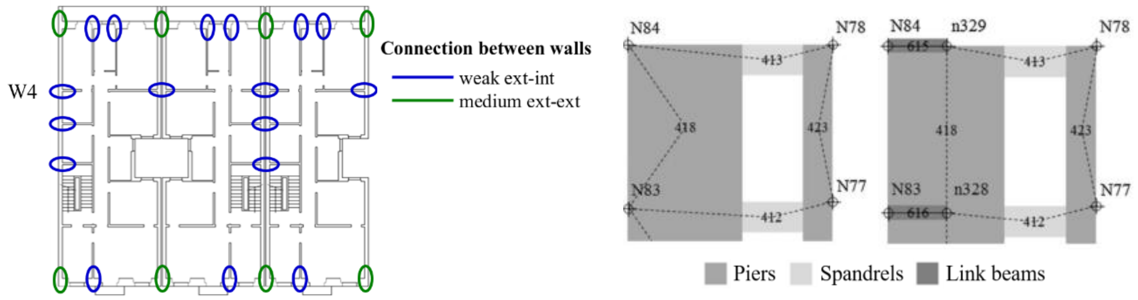

a) b) c)

Figure 3.6 – Connection between walls: a) identification of the connections in the plan view of the block, and example of the mesh of elements for the connection of the interior Wall-4 to the side wall b) before and c) after the introduction of the link beams

The behaviour of the connections between exterior and interior walls was also analysed in a previous work about these URM buildings in Lisbon (Simões et al., 2014b). The behaviour of the building was compared in terms of pushover curves showing that weak connections contributed to the reduction of the initial stiffness and strength of the building, as a consequence of the reduction of the flange effect induced by the exterior walls on the perpendicular walls.

3.2.6. Horizontal diaphragms: membrane elements

Horizontal diaphragms are modelled as membrane elements in order to consider the hypothesis of flexible diaphragms. These are defined as 3- or 4-nodes orthotropic membrane finite elements and characterized by the following equivalent parameters: thickness (t_{eq}), modulus of elasticity in the principal direction of the floor (spanning orientation) and in the perpendicular direction, respectively denoted as E_1 and E_2, and shear modulus (G_{12}). The modulus of elasticity represents the in-plane stiffness of the membrane along the two perpendicular directions and accounts, in addition, for the degree of connection between walls and horizontal diaphragms. The shear modulus influences the tangential stiffness of the diaphragm and the horizontal force distribution between walls. These equivalent parameters are computed directly in TREMURI program as a function of the material and geometry of the floors.

In these URM buildings, floors are made of timber joists set perpendicular to the façades and covered by one layer of timber boards (§2.6). It is considered that the loads are distributed only in the warping direction of the main timber joists. The modulus of elasticity of the material is assumed equal to

12 GPa, as indicated in (LNEC, 1997) for pine wood of structural class E. In TREMURI program, timber floors are modelled by membrane elements with 0.022 m of thickness, in correspondence to the thickness of the timber boards. The equivalent modulus of elasticity of the membrane are determined as a function of the material and geometry of the elements. In this case, E_1 takes into account the behaviour of the main joists, while E_2 takes into account the timber boards. As to the equivalent shear modulus (G_{12}), the quantification of this parameter is a difficult task. First, because it aims to characterize the flexible behaviour of the diaphragm and second, because there are few experimental tests regarding the mechanical characterization of timber diaphragms. The New Zealand Society for Earthquake Engineering, NZSEE Guidelines (2017) proposes reference values for the shear modulus of flexible timber diaphragms as a function of the floor system and state of conservation, based on the work from Giongo et al. (2013). Due to the uncertainties associated with the quantification of the shear modulus, this parameter is defined as an aleatory variable and it is assumed to vary within the values proposed by the NZSEE Guidelines.

The pitched timber roofs structure and the side gable walls that support the roof structure are accounted only by the corresponding self-weight and defined as linear loads on top of the exterior walls. The stone balconies in the street façade of the buildings are also defined by the corresponding self-weight, whereas the jack arch balconies with steel profiles in the rear façade walls are modelled as a membrane element following the geometric characteristics indicated in §2.6. In this case, the membrane element has an equivalent thickness of 0.040 m, in correspondence to the layer of mortar. It is considered that the loads on the balconies are distributed in the warping direction of the steel T section beams.

The equivalent properties of the membrane elements defining the horizontal diaphragms are presented in Table 3.7.

Table 3.7 – Equivalent properties of the membrane element defining the horizontal diaphragms

Equivalent properties	t_{eq} [m]	E_1 [GPa]	E_2 [GPa]	G_{12} [GPa]
Timber floor	0.022	29.18	12.00	6.14 – 15.01
Jack arch balcony	0.040	5.00	0	15.67

3.2.7. Load actions and combination

This section quantifies the load actions in the building: permanent loads (G_k), as a result of the self-weight of structural and non-structural elements, and variable loads (Q_k), as imposed loads arising from the occupancy of the building. The self-weight of the different elements are defined according to the reference values proposed by Ferreira and Farinha (1974), summarized in Table 3.8. The imposed loads are defined according to the provisions from Part 1-1 of Eurocode 1, EC1-1-1 (IPQ, 2009b) for domestic and residential activities (category A): 2.00 kN/m^2 for floors, 3.00 kN/m^2 for stairs and 2.50 kN/m^2 for balconies. The action loads are combined according to Eurocode 0 (IPQ, 2009a) considering a factor ψ_2 equal to 0.30.

Table 3.8 – Self-weight of structural and non-structural elements

Element	Self-weight
Rubble stone masonry	19.00 kN/m^3
Solid brick masonry	18.00 kN/m^3
Hollow brick masonry	15.00 kN/m^3
Timber "tabique" wall	13.50 kN/m^3
Timber floor	1.10 kN/m^2
Timber roof	1.30 kN/m^2
Limestone balcony	3.90 kN/m^2
Jack arch balcony	2.10 kN/m^2

3.2.8. Summary of aleatory variables and the Monte Carlo Method

The aleatory variables account for variations on the mechanical properties of masonry, strength and deformability characteristics of masonry piers and spandrels, mechanical properties of interior timber "tabique" walls, quality of connections between walls and in-plane stiffness of timber floors. In the previous sections, each aleatory variable was defined within a range of values. In this section, an appropriate continuous probability density function is attributed and characterized by median value ($X_{k,med}$) and dispersion (β) so that the 16% and 84% percentiles of the distribution correspond, respectively, to the lower ($X_{k,low}$) and upper ($X_{k,up}$) values of the range of variation. An alternative procedure to the 16% and 84% percentiles is to consider the coefficient of variation, as suggested in the Probabilistic Model Code (Joint Committee on Structural Safety, 2011). In regards to the continuous probability density function ($f_X(x)$), lognormal distributions are attributed to the aleatory variables varying between $]0,+\infty[$, while beta distributions are attributed for those varying between [0,1] or having, from a physical point of view, a range of variation equal to one.

Table 3.9 and Table 3.10 characterize the variables that follow, respectively, lognormal and beta distributions. A total of 50 aleatory variables are considered and divided in 17 groups.

Group 1 and 2 (rubble stone masonry), Group 3 and 4 (solid brick masonry) and Group 6 and 7 (hollow brick masonry) define the mechanical properties of masonry. The interval of values is defined from the application of the Bayesian update (§3.2.3).

Group 5, 8 and 11 refer to the modelling of the flexural behaviour of spandrels according to the criterion proposed by Cattari and Lagomarsino (2008) assuming an equivalent tensile strength on the elements (§3.2.2).

Table 3.9 – Characterization of aleatory variables following a lognormal distribution

Description	Group	X_k	$X_{k,low}$	$X_{k,up}$	$X_{k,med}$	β
Rubble stone masonry	1	E [GPa]	0.615	0.882	0.737	0.18
		G [GPa]	0.205	0.294	0.246	0.18
		f_c [MPa]	0.84	1.07	0.95	0.12
	2	τ_0 [MPa]	0.018	0.026	0.022	0.18
Solid clay brick masonry	3	E [GPa]	0.716	0.987	0.841	0.16
		G [GPa]	0.239	0.329	0.280	0.16
		f_c [MPa]	0.95	1.19	1.07	0.11
	4	τ_0 [MPa]	0.060	0.092	0.074	0.21
	5	μ_{loc}	0.40	0.70	0.53	0.28
Hollow clay brick masonry	6	E [GPa]	0.716	0.987	0.841	0.16
		G [GPa]	0.239	0.329	0.280	0.16
		f_c [MPa]	0.76	1.00	0.87	0.14
	7	τ_0 [MPa]	0.060	0.092	0.074	0.21
	8	μ_{loc}	0.40	0.70	0.53	0.28
Spandrels in façade walls	9	E [GPa]	0.615	0.987	0.779	0.24
	10	G [GPa]	0.205	0.329	0.260	0.24
		f_c [MPa]	0.84	1.19	1.00	0.17
		τ_0 [MPa]	0.018	0.092	0.041	0.82
	11	Int	0.50	2.00	1.00	0.69
		μ_{loc}	0.40	0.70	0.53	0.28
Drift thresholds for piers	12	δ_{F3}	0.0046	0.0074	0.0058	0.24
		δ_{F4}	0.0078	0.0122	0.0098	0.22
		δ_{F5}	0.0120	0.0180	0.0147	0.20
		δ_{S3}	0.0023	0.0037	0.0029	0.24
		δ_{S4}	0.0039	0.0061	0.0049	0.22
		δ_{S5}	0.0056	0.0084	0.0069	0.20
Drift thresholds for spandrels	13	δ_{F3}, δ_{S3}	0.0015	0.0025	0.0019	0.24
		δ_{F4}, δ_{S4}	0.0045	0.0075	0.0058	0.25
		δ_{F5}, δ_{S5}	0.0151	0.0249	0.0194	0.25
Timber "tabique" walls	16	E [GPa]	0.060	0.200	0.110	0.60
		G [GPa]	0.001	0.003	0.002	0.55
		f_c [MPa]	0.40	0.72	0.54	0.29
Connection between exterior walls	15	A [m^2]	0.0002	0.0006	0.0004	0.81
		I [m^4]	0.0001	0.0003	0.0002	0.81
Stiffness of timber floors	17	G [GPa]	0.006	0.016	0.099	0.48

E – modulus of elasticity, G – shear modulus, f_c – compressive strength, τ_0 – equivalent shear strength, μ_{loc} – coefficient of friction on the mortar joints in the end section of spandrels, Int – interlocking of the masonry units in the end section of spandrels, δ_{Si} – drift limit for the shear behaviour at damage level i, δ_{Fi} – drift limit for the flexural behaviour at damage level i, A – area of the link beams, I – inertia of the link beams

Table 3.10 – Characterization of aleatory variables following a beta distribution

Description	Group	X_k	$X_{k,low}$	$X_{k,up}$	X_{med}	β
Residual strength for piers	12	β_{F4}	0.80	0.90	0.85	0.05
		β_{S3}	0.60	0.80	0.70	0.10
		β_{S4}	0.25	0.55	0.40	0.15
Residual strength for spandrels (and ductility)	13	β_{F4}, β_{S3}, β_{S4}	0.40	0.70	0.55	0.15
		β_{F4}, β_{S3}, β_{S4} |faç	0.20	0.60	0.40	0.20
		μ |faç	3.21	5.19	4.20	0.99
Stiffness degradation of masonry panels	14	k_{in}	0.25	0.75	0.65	0.15
		k_0	0.50	0.80	0.50	0.25

β_{Si} – residual strength for the shear behaviour at damage level i, β_{Fi} – residual strength for the flexural behaviour at damage level i, μ – ductility of the brick arch for damage level 3, k_{in} – ratio between the initial and the secant stiffness, k_0 – ratio between the elastic strength and the ultimate strength

Group 9 and 10 characterize the mechanical properties of spandrels in the façade walls. Considering that these panels may be made of rubble stone masonry or clay brick masonry (§2.6), the properties attributed, range between the mechanical properties of the two types of materials.

Group 12, 13 and 14 are related to the formulation of the multi-linear constitutive law (Figure 3.3) associated with the initial stiffness degradation (k_{in} and k_0) and the progressive degradation of strength (δ_i and β_i) of the panels. In case of the clay brick arch architrave in the façade walls (faç), DL3 threshold is defined in terms of ductility (μ) instead of drift (δ). Due to the limited information available, the same intervals of values are adopted for the different types of masonry (§3.2.2).

Group 15 quantifies the mechanical properties of the interior timber “tabique” walls. These are determined based on the experimental results from compression and shear tests performed by Rebelo et al. (2015).

Group 16 defines the area (A) and inertia (I) of the link beams that set the connection between perpendicular exterior walls (§3.2.5). These connections are defined as medium quality connections justified by the use of different materials between façade walls (rubble stone masonry) and side walls (brick masonry), but supported on the idea that during the construction more attention was given to the connection between exterior walls.

Group 17 characterizes the flexible behaviour of timber floors, represented by the shear modulus (G) of an equivalent finite membrane element with 0.022 m of thickness, corresponding to the thickness of the timber boards (§3.2.6).

The aleatory variables identified are treated by the Monte Carlo Method. A total of 1000 samples are defined for each variable starting from the continuous probability density function attributed and considering additional correlations between variables, as described in the following. It is assumed that within the 17 groups, the aleatory variables are fully correlated in order to guarantee a positive linear relationship between the variables attributed to the same model (correlation coefficient, R = +1). A negative linear correlation (R = –1) is considered for Group 14 related to the initial stiffness degradation of the masonry panels. This aims to define two extreme behaviours for the transition between elastic and plastic phases. Thus, for higher initial stiffness degradation (higher value of k_{in}) a lower value of k_0 is expected, so to have a longer interval between the first cracks and the reaching of the ultimate strength capacity (the opposite relation is also valid). It is also proposed to assume a correlation coefficient of 0.5 between Group 1 and 2, Group 3 and 4, Group 6 and 7 and Group 9 and 10, taking into account that the modulus of elasticity (E), the shear modulus (G) and the compressive strength (f_c) are not fully correlated nor uncorrelated with the equivalent shear strength (τ_0).

Figure 3.7 a) compares the probability density function for the modulus of elasticity of rubble stone masonry, showing a good agreement between the function generated based on the 1000 Monte Carlo simulations and the target function defined by the median value and standard deviation of the reference interval of values. Figure 3.7 b) presents, as an example, the probability density function for the drift thresholds that characterize the flexural behaviour of piers at DL3, DL4 and DL5, putting in evidence the higher dispersion for higher damage levels.

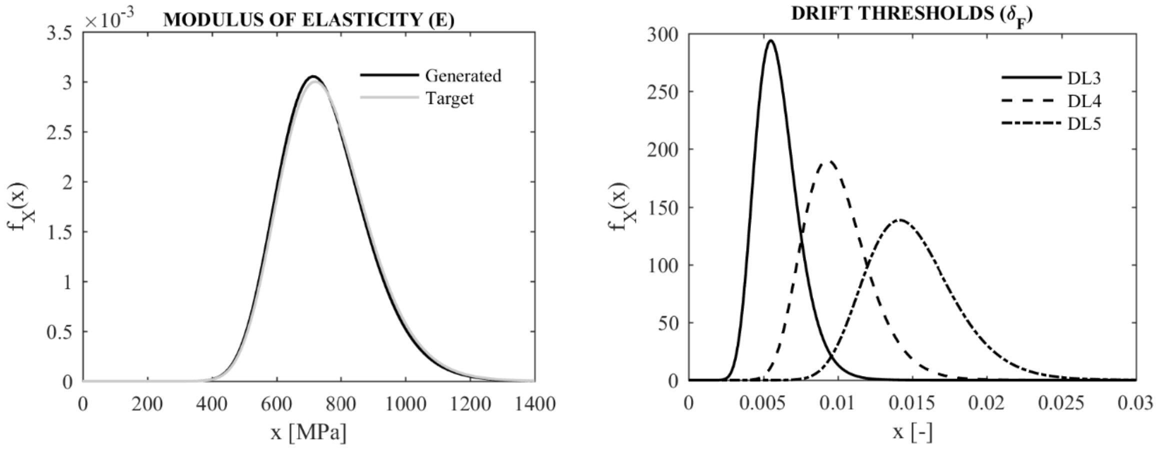

a) b)

Figure 3.7 – Probability density function for a) modulus of elasticity of rubble stone masonry, and b) drift thresholds for the flexural behaviour of masonry piers

The 1000 Monte Carlo simulations performed are used to define the input parameters for the different building models defined as cases of study (§2.6). These are attributed to the different models as a function of their reliability/weight. This allows to set a group of 1000 different models representative of the URM buildings of type I considering the main variations within the typology in terms of geometry, constructive details, materials and mechanical properties. These models are then considered for the analysis of the global seismic behaviour of the typology.

3.3. Non-linear static (pushover) analyses

Pushover is a non-linear static analysis method where the structure is subjected to constant gravity loads and monotonically increasing horizontal loads (CEN, 2004) aiming to simulate the effect of the seismic action on the structure. The behaviour of the structure is described by the pushover curve that relates the base shear force and the horizontal displacement of a control node, providing information about the stiffness, strength and displacement capacity. The EC8-1 (CEN, 2004) recommends to apply at least two distributions of horizontal loads: uniform – proportional to the mass, and modal – proportional to the fundamental mode shape. The modal distribution is not considered in this work because the mass participation involved in the first modes of vibration is, in all cases, lower than 70%; thus, the first mode may not be representative of the global seismic behaviour of the block of buildings. Annex A presents the results from the modal analysis of the different numerical models. In addition, several authors do not recommend the use of a modal distribution for the analysis of existing (irregular) URM buildings (Lourenço et al., 2011; Endo, Pelà and Roca, 2017). Other possible load patterns involve: 1) a pseudo-triangular distribution – proportional to the product between the mass and the height of the node, 2) the contribution of different modes combined by the SRSS (Square Root of Sum of Squares) or the CQC (Complete Quadratic Combination), 3) the contribution of different modes and the effects of their interaction (multi-modal pushover), 4) the update of the load distribution during the analysis as a function of the displacement shape of the structure (adaptive pushover).

In what concerns option 3) and 4), there are still few successful applications to the analysis of URM buildings with flexible diaphragms (Galasco, Lagomarsino and Penna, 2006; Lourenço et al., 2011; Endo, Pelà and Roca, 2017). As to option 1) and 2), Cattari et al. (2015) performed pushover analyses on 10 irregular URM buildings considering the following distributions: uniform, modal, pseudo-triangular, the contribution of different modes of vibration combined by the SRSS and CQC combinations. It was concluded that the analyses with a uniform and a SRSS combination provided more reliable results when compared with non-linear dynamic analyses; however, the pseudo-triangular distribution constitutes a reliable alternative to SRSS in most cases (particularly those characterized by a regular configuration). According to Lagomarsino and Cattari (2015b), if the building is regular in elevation, a simpler alternative is the use of a pseudo-triangular load distribution, because it assures that the seismic masses in all parts of the building are involved in the pushover analysis. Therefore, in this thesis, a uniform and a pseudo-triangular (herein called as triangular for simplicity) load distributions are considered to enable the analysis of a significant number of models with a reasonable computational burden.

3.3.1. Preliminary results and update of the cases of study

Pushover analyses are performed with the 32 numerical models, defined by the median properties of the aleatory variables, aiming to compare the global behaviour of the cases of study in terms of initial stiffness, strength and displacement capacity (Simões et al., 2018). Few simplifications are considered in this preliminary analysis: 1) the application only of the uniform load distribution on the positive X and Y directions of the building (indicated in Figure 3.1 b)), and 2) the connection between walls are defined as good quality (the default option from TREMURI program). The latter simplification is motivated by the fact that the introduction of the link beams (as proposed in §3.2.5), implies several modifications to the numerical models, and their consideration in this phase would not influence the main conclusions.

Figure 3.8 to Figure 3.11 plot the pushover curves defined as the ratio between the base shear force (V_b, from now on V) and the weight of the model (W), as a function of the average displacement of the roof weighted by the seismic modal mass of all nodes (d). The option for the average displacement of the roof represents a heuristic approach useful to define a curve representative of the whole structure in case of buildings with flexible diaphragms and/or in plan irregularities (Lagomarsino and Cattari, 2015b). For a matter of simplicity and interpretation of the results, the 32 models are divided in four groups as a function of the first two letters of the acronym: H-S, H-I, S-H and S-I (presented in the logic-tree from Figure 2.36).

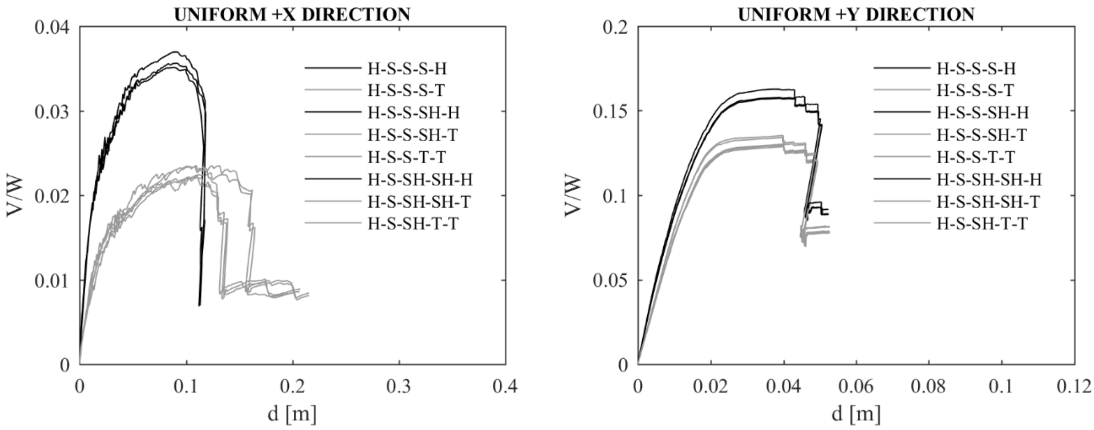

Figure 3.8 – Pushover curves for group of models H-S: +X direction (left) and +Y direction (right)

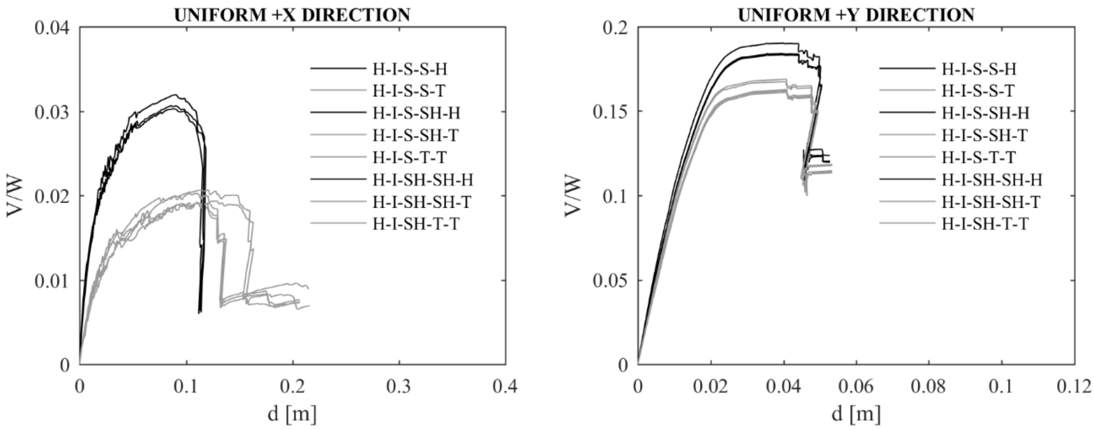

Figure 3.9 – Pushover curves for group of models H-I: +X direction (left) and +Y direction (right)

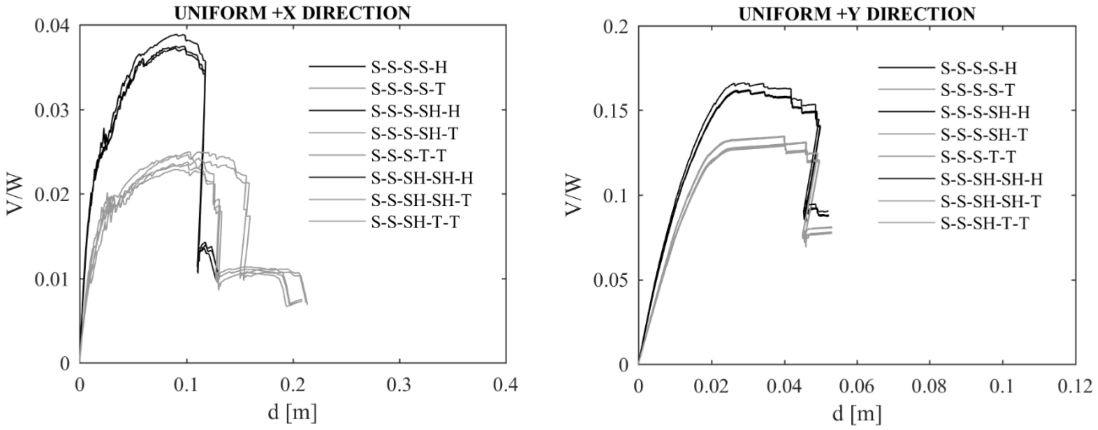

Figure 3.10 – Pushover curves for group of models S-S: +X direction (left) and +Y direction (right)

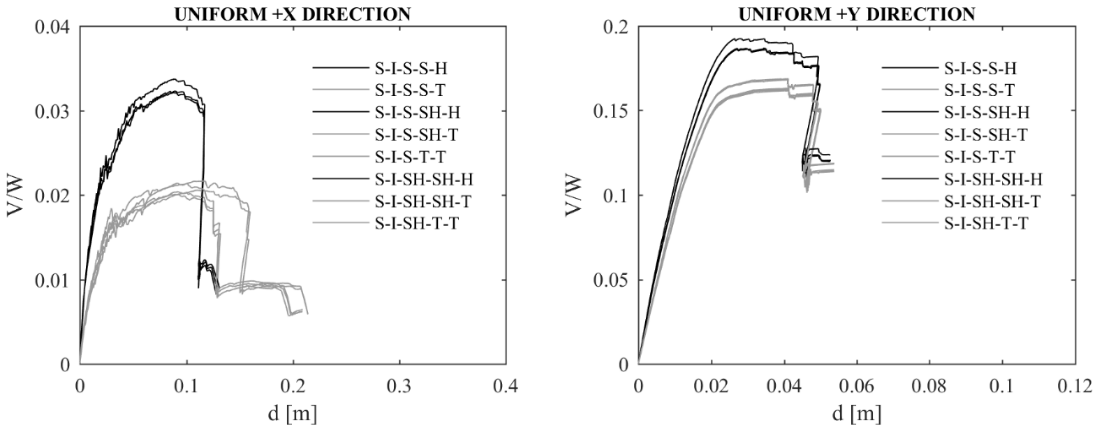

Figure 3.11 – Pushover curves for group of models S-I: +X direction (left) and +Y direction (right)

Within each group, it is observed a similar behaviour between models without and with interior timber "tabique" walls (black vs. grey lines) concerning the initial stiffness (K) and the ratio between maximum base shear force and weight (V_{max}/W). Table 3.11 provides the corresponding parameters in terms of the mean value (E[X]) and coefficient of variation (CoV). The initial stiffness (K) is defined as the ratio between the base shear force for 70% of V_{max} and the corresponding displacement.

Table 3.11 – Initial stiffness (K) and ratio between maximum base shear force and weight (V_{max}/W)

Group of Models	"Tabique" walls	X Direction				Y Direction			
		K [kN/m]		V_{max}/W		K [kN/m]		V_{max}/W	
		E[X]	CoV [%]	E[X]	CoV [%]	E[X]	CoV [%]	E[X]	CoV [%]
H-S	No	21616	3.2	0.036	2.2	166489	1.0	0.159	1.5
	Yes	10864	8.8	0.023	2.6	144606	1.7	0.132	2.0
H-I	No	15026	2.1	0.031	2.3	218482	1.1	0.186	1.7
	Yes	10574	9.0	0.020	3.4	200670	1.1	0.164	1.9
S-S	No	21766	7.8	0.038	1.9	172779	0.6	0.163	1.3
	Yes	15640	6.9	0.024	3.2	141745	1.2	0.132	1.9
S-I	No	24402	9.3	0.033	2.2	224471	0.9	0.189	1.5
	Yes	14628	9.2	0.021	3.0	194828	0.9	0.165	1.8

The variations are higher in the X direction than in the Y direction, but in all cases the coefficient of variation is lower than 10%. This shows that the global behaviour of the URM buildings of type I may be well represented by a lower number of models. Thus, it is proposed to adopt, for each of the four groups considered, a model without and a model with interior timber “tabique” walls, and reduce the number of models from 32 to 8. The final 8 building models are selected as a function of the ones with higher reliability/weight within the groups. For instance, group H-S composed by 8 models (Figure 3.8), is now represented by models H-S-S-S-H and H-S-SH-T-T, the first without and the second with interior timber “tabique” walls. The final 8 models selected are identified in the updated logic-tree from Figure 3.12 (in bold, in the right side). The probabilities associated with these models are updated by adding the contribution of the eliminated models, so that the final probability is equal to 1. For instance, the final probability of model H-S-S-S-H results from the sum between the initial probability of the model itself, plus the probability of the eliminated models H-S-S-SH-H and H-S-SH-SH-H.

The pushover curves of the final 8 models are presented in Figure 3.13. These 8 models are then modified in order to introduce the link beams on the connection between walls, as explained in §3.2.5. The properties of the equivalent beams (area, A, and moment of inertia, I) are set with an iterative procedure, basis on the comparison of the global behaviour of the models in terms pushover curves. The iterative procedure is described next:

1. Weak connection between exterior and interior walls – Reduction of the properties of the link beams until the verification of small variations on the pushover curves (in terms of initial stiffness and strength) in both directions. This defines the minimum properties of the link beams. This condition is exemplified in Figure 3.14 and Figure 3.15 as “weak ext-int”.

2. Medium connection between exterior walls – The properties of the link beams are defined in two steps: i) definition of the minimum properties of the link beams (“weak ext-ext”), and ii) definition of the average properties of the link beams (“medium ext-ext”) between the initial properties (“good”) and the minimum (“weak ext-ext”), as exemplified in Figure 3.14 and Figure 3.15. The properties of the link beams representative of the medium connections are defined within a range of values and treated as aleatory variables (§3.2.8).

The examples plotted in Figure 3.14 and Figure 3.15 show the variations in terms of pushover curve. The modification from good to weak connections between exterior and interior walls, results in the reduction of the initial stiffness and strength in both directions. For model H-I-S-S-H it is also verified the increase of the displacement capacity in the X direction. This can be explained by the reduction of the flange effect induced by the side walls on the perpendicular interior walls and the consequent reduction of the forces on the masonry piers from the interior walls, as testified also in a previous work (Simões et al., 2014b). The additional modification from good to medium connections between exterior walls also results in the reduction of the initial stiffness and strength mainly in the Y direction.

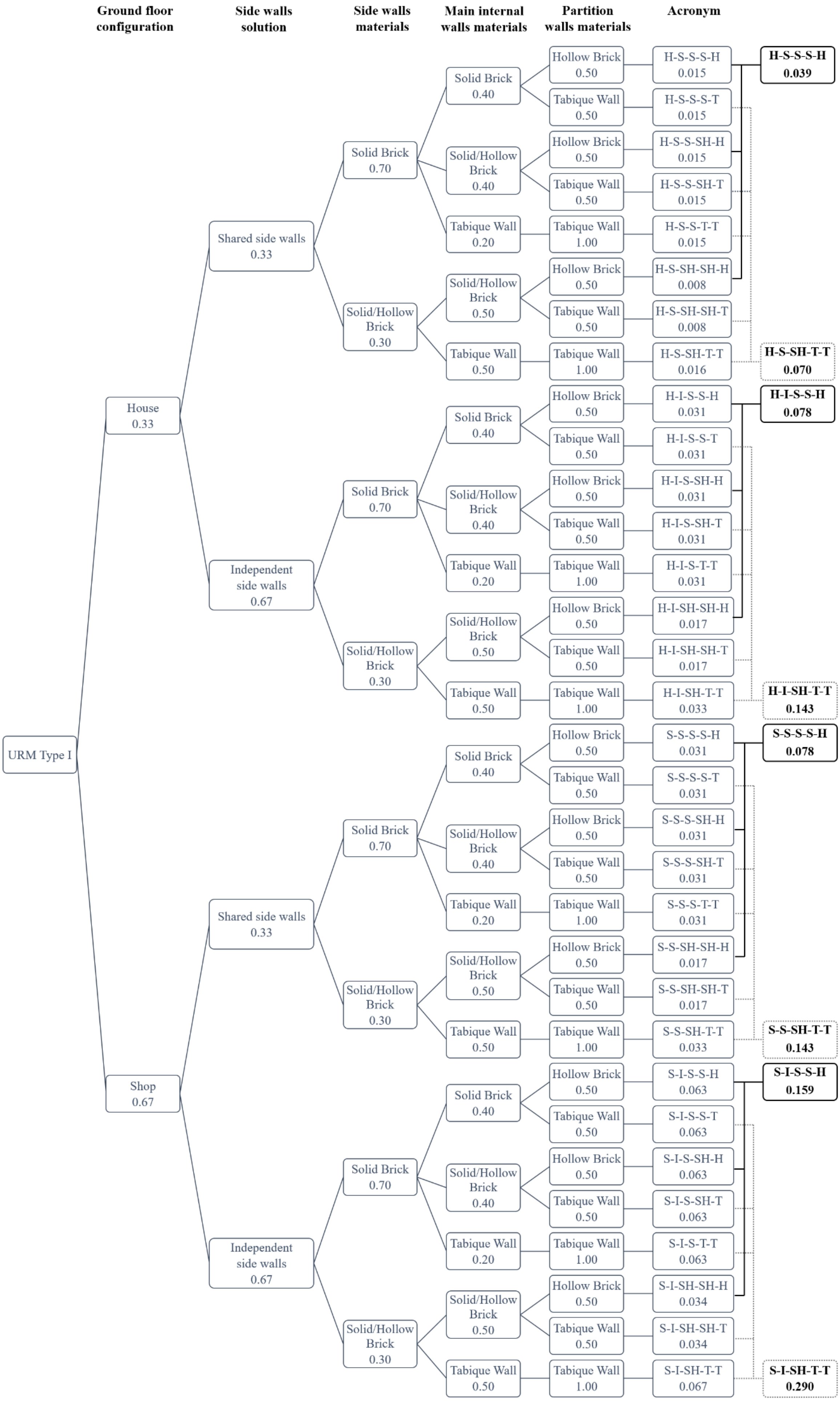

Figure 3.12 – Updated logic-tree with the reduction from 32 to 8 models

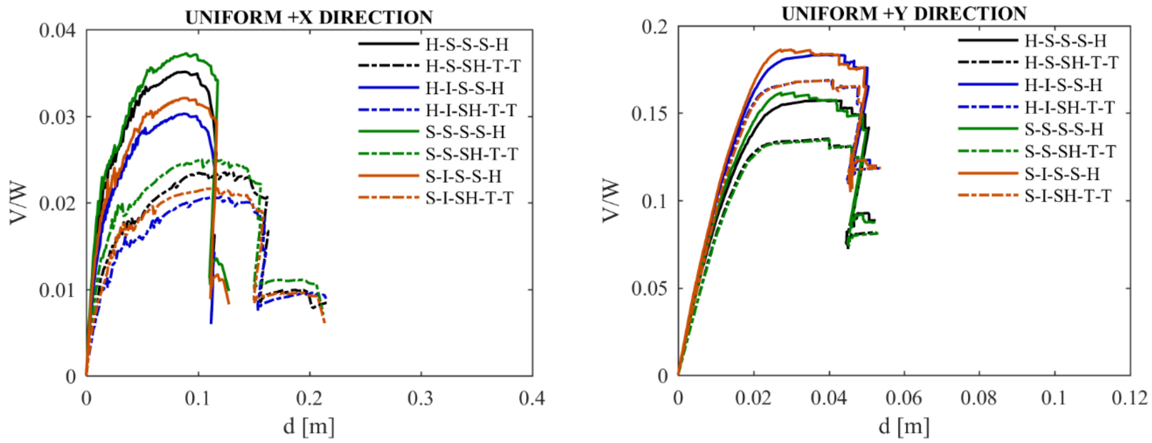

Figure 3.13 – Pushover curves for the final 8 models (defined by the median properties of part of the aleatory variables): X direction (left) and Y direction (right)

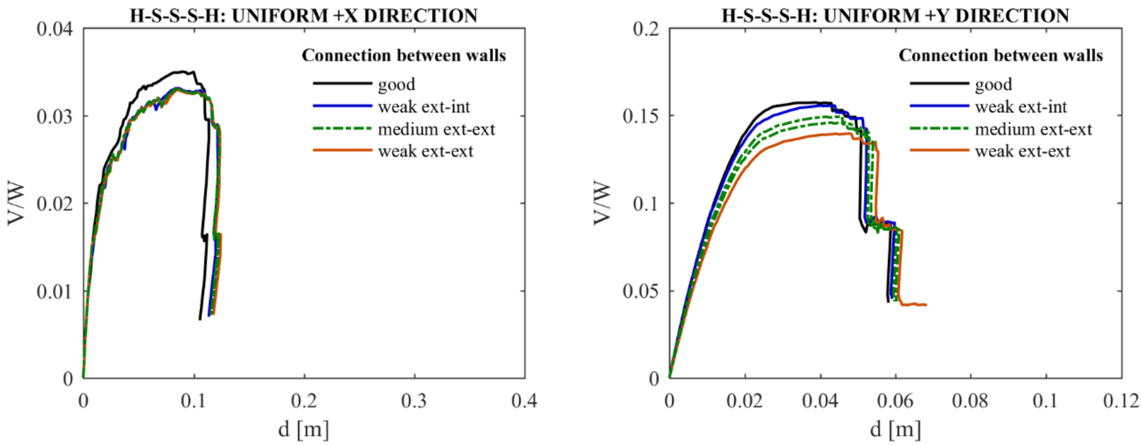

Figure 3.14 – Example of the definition of the connections for model H-S-S-S-H

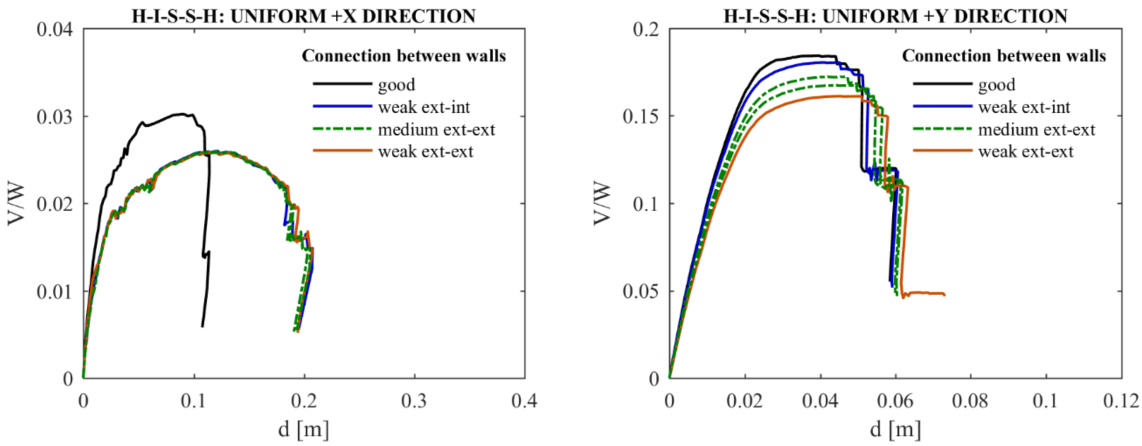

Figure 3.15 – Example of the definition of the connections for model H-I-S-S-H

3.3.2. Models defined by median properties

Figure 3.16 and Figure 3.17 present the pushover curves obtained with the 8 models, defined by the median properties of all aleatory variables, and considering the uniform and the triangular load distributions applied in the X and Y directions, including the negative and positive senses of direction.

Figure 3.18 compares the results obtained in the negative and positive direction for model H-S-S-S-H and model H-S-SH-T-T. For simplicity, Annex B presents the results obtained with all models in terms of initial stiffness (K) and ratio between maximum base shear force and weight (V_{max}/W), while Table 3.12 provides the corresponding mean value (E[X]) and coefficient of variation (CoV).

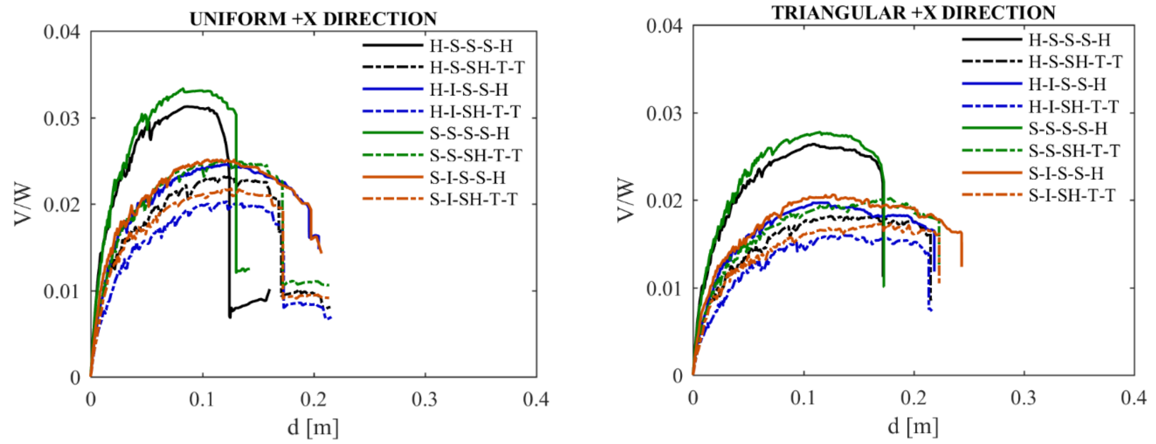

Figure 3.16 – Pushover curves for the final 8 models: Uniform +X direction (left) and Triangular +X direction (right)

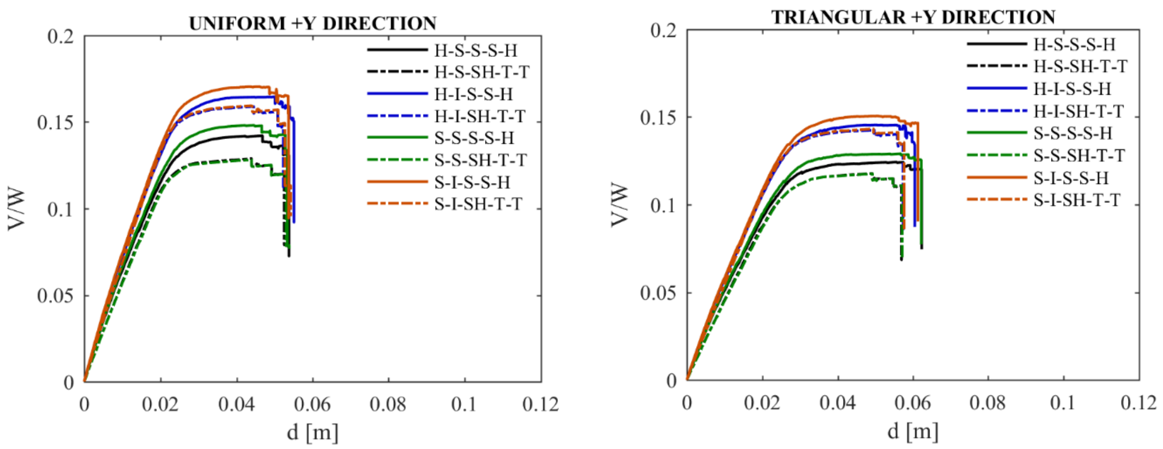

Figure 3.17 – Pushover curves for the final 8 models: Uniform +Y direction (left) and Triangular +Y direction (right)

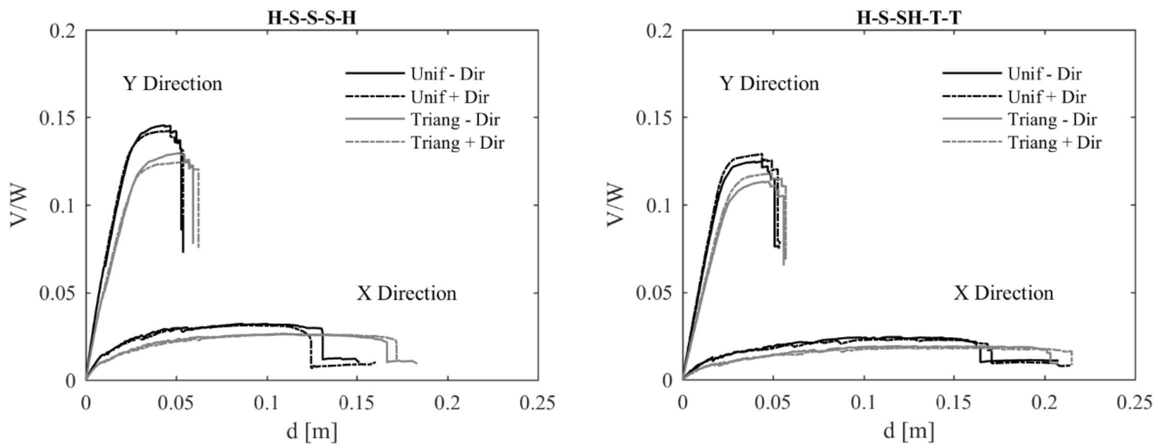

Figure 3.18 – Pushover curves for model H-S-S-S-H

Table 3.12 – Initial stiffness (K) and ratio between maximum base shear force and weight (V_{max}/W)

Model	X Direction				Y Direction			
	K [kN/m]		V_{max}/W		K [kN/m]		V_{max}/W	
	E[X]	CoV [%]	E[X]	CoV [%]	E[X]	CoV [%]	E[X]	CoV [%]
H-S-S-S-H	15547	23.1	0.029	9.3	106583	12.3	0.135	6.4
H-S-SH-T-T	7121	20.2	0.021	12.3	95059	12.2	0.121	5.1
H-I-S-S-H	13106	19.5	0.022	11.0	141319	11.8	0.158	6.3
H-I-SH-T-T	7378	20.3	0.018	12.2	133433	12.1	0.151	5.5
S-S-S-S-H	16360	19.5	0.031	9.7	108837	12.8	0.139	6.4
S-S-SH-T-T	9264	28.3	0.023	10.7	94793	12.1	0.121	4.9
S-I-S-S-H	13317	22.1	0.023	10.2	146438	11.0	0.162	6.1
S-I-SH-T-T	9367	25.5	0.020	11.4	134738	12.1	0.152	5.4

The response in the X direction is, in general, characterized by: 1) lower stiffness and strength for models with interior timber “tabique” walls (#-#-SH-T-T) in comparison with models without such walls (#-#-S-S-H), 2) lower stiffness and strength for models with independent side walls (#-I-#-#-#) in comparison with shared side walls (#-S-#-#-#), this being related to the reduction of the flange effect between the side and interior walls. In the Y direction, models with shared side walls (#-S-#-#-#) have lower stiffness and strength, due to the lower thickness of the side walls. The use of the ground floor as house (H-#-#-#-#) results on the lower value of the maximum base shear in both directions, as a consequence of the different layout of the prototype building (Figure 2.33 and Figure 2.34), despite the small differences in contrast with models with shop use (S-#-#-#-#).

The models have higher initial stiffness and strength in the Y direction than in the X: the ratio K_Y/K_X is between 6.7 and 18.1 and the ratio V_Y/V_X is between 4.5 and 8.2 (see Table B.1 to Table B.4 in Annex B). These differences are related to the presence of side blind walls in the Y direction, in contrast with the higher number of openings in the X direction. From Figure 3.19 it is visible that the side walls – Wall-22, Wall-25, Wall-26 and Wall-24 (see Figure 3.1 for the wall numbering) – have the major contribution to the total base shear in the Y direction, while in the X direction this contribution is distributed between the façade walls – Wall-2 (street) and Wall-1 (rear) – and the interior walls. This is also motivated by the orientation of the timber floors perpendicular to the façade walls, leading to the load distribution between walls.

There are small variations in the analysis in the negative and positive directions, as shown in Figure 3.18, and considering that in all cases the coefficient of variation is lower than 8.0% for the initial stiffness and lower than 2.7% for the maximum base shear force. In what concerns the load distributions (uniform vs. triangular), the variations are more significant, in particular in the X direction where the coefficient of variation for the initial stiffness is between 19.5% and 28.3%. In all cases, the triangular distribution provides a pushover curve with lower initial stiffness and strength, but higher displacement capacity, in comparison with the uniform distribution. In §3.3.3 a comparison with results from non-linear dynamic analyses is performed to take some conclusions on the reliability of the load distributions considered for the non-linear static (pushover) analyses.

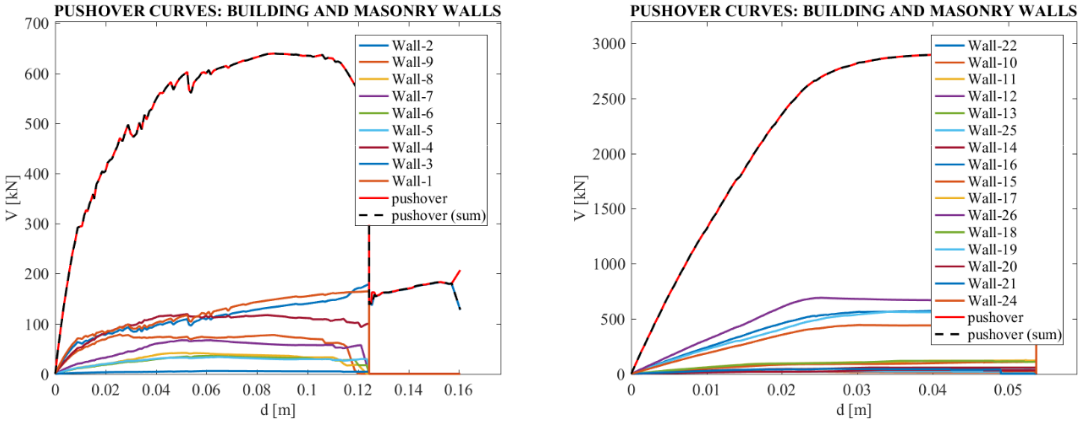

Figure 3.19 – Pushover curves for model H-S-S-S-H: Uniform +X direction (left) and +Y direction (right) (see Figure 3.1 a) for wall numbering)

The plan deformation and damage pattern for the maximum displacement capacity is shown in Figure 3.20 and Figure 3.21 for model H-S-S-S-H. The legend displays the failure mode and damage level in the element (according to the multi-linear constitute law, Figure 3.3).

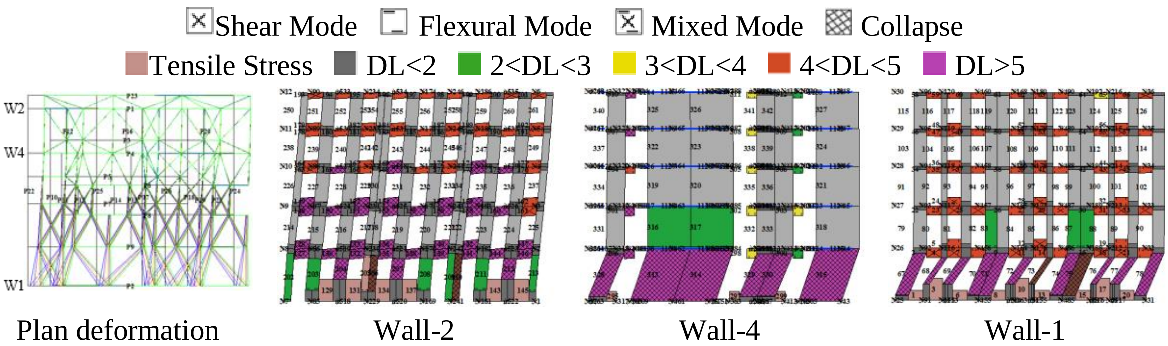

Figure 3.20 – Damage in model H-S-S-S-H for the maximum displacement: Uniform +X direction

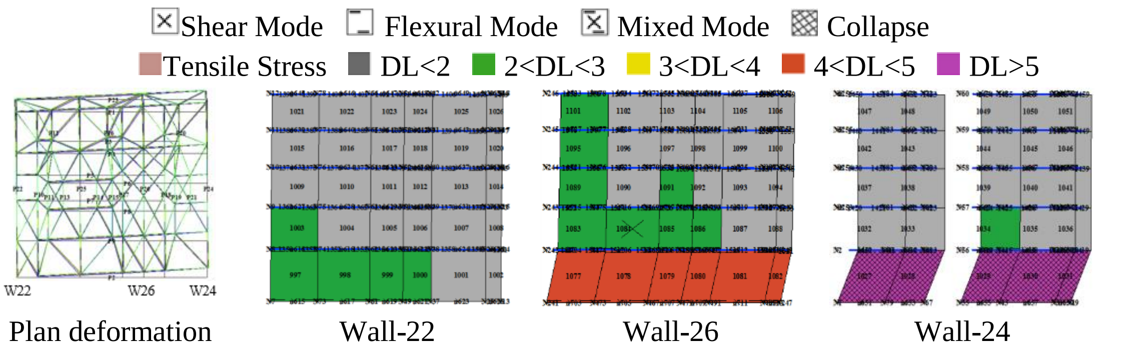

Figure 3.21 – Damage in model H-S-S-S-H for the maximum displacement: Uniform +Y direction

The plan deformation of the block of buildings is irregular. In the X direction, Wall-2 (street façade) has a uniform deformation, while the remaining walls have a soft-storey mechanism. In the Y direction, the structure has a torsional deformation causing a soft-storey mechanism between Wall-26 and Wall-24 (building C on the right – Figure 3.1). This is associated with the asymmetry of the group and with the position of vertical airshaft on the side of the buildings. Failure in the elements occurs mainly due to the flexural behaviour in both directions. Damage in piers is mainly concentrated on the elements on the ground floor, while all spandrels reached their maximum strength (≥DL3). In fact, spandrels show a quite weak behaviour since the beginning of the pushover analyses. This is due to the presence of weak lintels and flexible timber floors. The analysis with both load distribution provide similar distribution of damage in the buildings.

3.3.3. Reliability of the load distributions

Non-linear dynamic analyses with time integration are performed with the objective of verifying if the load distributions considered in the non-linear static analyses are able to capture the global behaviour of the buildings. These analyses are carried out by subjecting the structure to ground-motion acceleration time-histories records compatible with the code elastic seismic action in Lisbon (zone 3) and soil type B (IPQ, 2010). Two types of elastic response spectra are considered with a return period of 475 years and equivalent viscous damping (ξ) of 5%: type 1 – inter-plate earthquake – with PGA equal to 1.50 m/s^2 and soil factor (S) equal to 1.29, and type 2 – intra-plate earthquake – with PGA equal to 1.70 m/s^2 and S equal to 1.27.

A set of 30 real ground-motion records are selected with SelEQ tool (Macedo and Castro, 2017), a software application for record selection that features a wide variety of filtering criteria. A preliminary code-based record selection is carried out considering geophysical data (expected magnitude, source-to-site distance, rupture mechanism and soil type) consistent with the two seismic scenarios (Araújo et al., 2016). The records are afterwards scaled in order that the median of the 30 spectra matches the target response spectrum in the range of periods $0.2T_1$ and $2T_1$, as established in EC8-1 (CEN, 2004), where T_1 is the fundamental period of the structure in the direction where the record is applied. The average fundamental periods of the 8 building models, defined by the median properties of the aleatory variables, are considered in order to comprise the period content of all models (T_{1X}=1.22 s and T_{1Y}=0.52 s, Annex A). Figure 3.22 and Figure 3.23 compare the 30 scaled response spectra with the code response spectrum for seismic action type 1 and type 2, respectively. Each of the 30 response spectra is defined by the acceleration spectra associated with the geometric mean of the two horizontal components affected by a scale factor.

The non-linear dynamic analyses are performed in TREMURI program. The time-dependent response of the structure is obtained through direct numerical integration of the differential equations of motion of the system, considering both horizontal components of the records acting simultaneously. The effects of the viscous damping are considered by adopting the Rayleigh damping formulation for the definition of the structure damping matrix (D) given by Equation (3.12):

$$D = \alpha \cdot M + \beta \cdot K \tag{3.12}$$

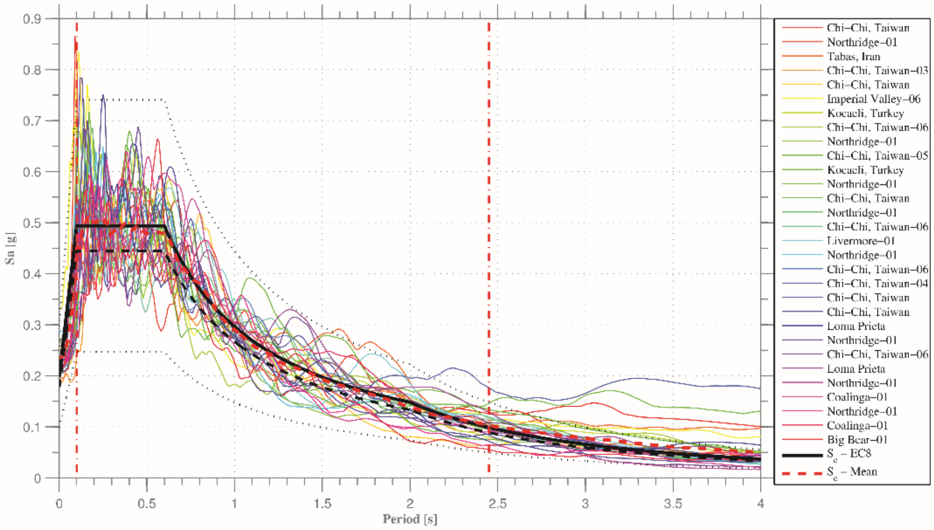

Figure 3.22 – Comparison between the 30 scaled response spectra (S_e – Mean, in dashed red line) with the code response spectrum for action type 1 (S_e – EC8, in black line)

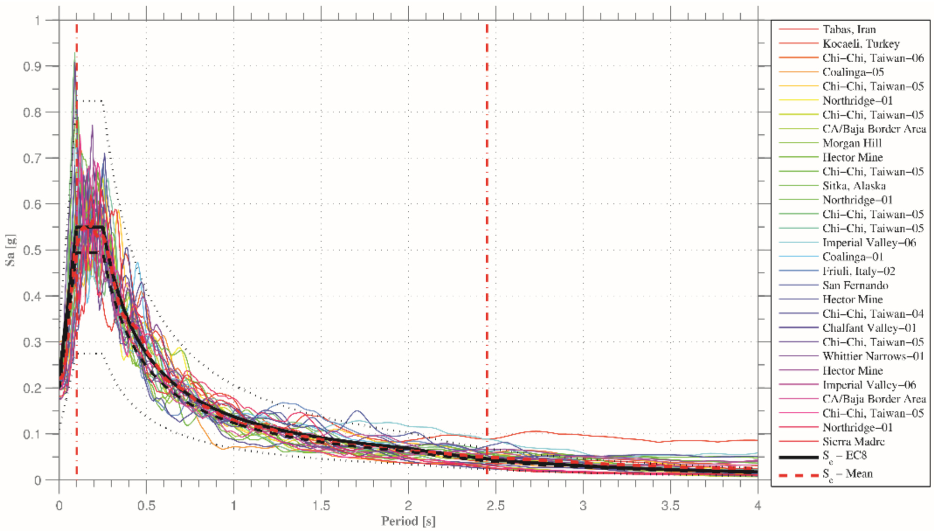

Figure 3.23 – Comparison between the 30 scaled response spectra (S_e – Mean, in dashed red line) with the code response spectrum for action type 2 (S_e – EC8, in black line)

In Equation (3.12) *M* and *K* are the mass and stiffness matrixes of the structure. The coefficients α and β are defined by approximating the structure (Multiple-Degree-Of-Freedom, MDOF) to an equivalent SDOF system and by imposing that in the pulse range [ω_1, ω_2], the equivalent viscous damping (ξ) is constant and equal to 3% (Cattari et al., 2005). The two pulses correspond to two stiffness values of the structure: ω_1 the initial elastic stiffness and ω_2 the secant stiffness corresponding to the ultimate limit state assumed for the structure. Pulse ω_1 is assumed equal to the pulse of the structure (Equation (3.13)).

Pulse ω_2 is estimated in a simplified way (Equation (3.14)) starting from ω_1 and assuming a suitable value of ductility (μ). In this case, the value of ductility is assumed equal to 4, defined by the average ratio between d_{PL4} and d_{PL2}, determined after the definition of the displacement performance limit states thresholds discussed in §3.4 (here in terms of Performance Levels, PLk with k=1,…,4). Coefficients α and β are determined by solving the system of Equations (3.15). The corresponding values are presented in Table 3.13.

$$\omega_1 = 2\pi / T_1 \tag{3.13}$$

$$\omega_2 = \omega_1 / \sqrt{\mu} \tag{3.14}$$

$$\begin{cases} \xi = 0.03 = \dfrac{\alpha}{2\omega_1} + \dfrac{\beta\omega_1}{2} \\ \xi = 0.03 = \dfrac{\alpha}{2\omega_2} + \dfrac{\beta\omega_2}{2} \end{cases} \tag{3.15}$$

Table 3.13 – Results for the coefficients α and β

Model	T_1 [s]	ω_1 [rad/s]	ω_2 [rad/s]	α	β
H-S-S-S-H	1.00	6.31	3.16	0.1263	0.0063
H-S-SH-T-T	1.25	5.01	2.50	0.1003	0.0080
H-I-S-S-H	1.26	4.97	2.49	0.0995	0.0080
H-I-SH-T-T	1.37	4.60	2.30	0.0921	0.0087
S-S-S-S-H	0.98	6.40	3.20	0.1280	0.0063
S-S-SH-T-T	1.24	5.05	2.53	0.1010	0.0079
S-I-S-S-H	1.28	4.93	2.46	0.0986	0.0081
S-I-SH-T-T	1.36	4.64	2.32	0.0927	0.0086

Non-linear dynamic analyses (NLDA) are performed with the 8 models, defined by the median properties of the aleatory variables, considering all records compatible with seismic action type 1 and type 2, applied in the X and Y directions of the structure. The results obtained are compared to the results obtained from the non-linear static analyses (NLSA) with the uniform and triangular load distribution, as exemplified for model H-S-S-S-H in Figure 3.24 (Annex C compiles the results obtained for all models). The curves plot the ratio between the base shear force and the weight of the structure (*V/W*) as a function of the average displacement of the roof (*d*).

The cloud of curves puts in evidence some uncertainties in the definition of the most representative load distribution. Since the 30 records are scaled in the range of periods of the structure and not to the same value of PGA, some records highlight the quite linear response of the structure; in particular in the X direction, which corresponds to the first mode of vibration of the structure. On the other hand, some records highlight the strong non-linear response until the collapse of the structure. The curves from the NLDA obtained in the Y direction are less scatter and in fact, these are closer to the pushover curves obtained with the triangular distribution. The different outcome from NDLA is also motivated by the characteristic global behaviour of these URM buildings: Y direction is mainly governed by the response of the side walls, while the X direction is divided between the façade and interior walls and has some interactions with the Y direction (flange effect).

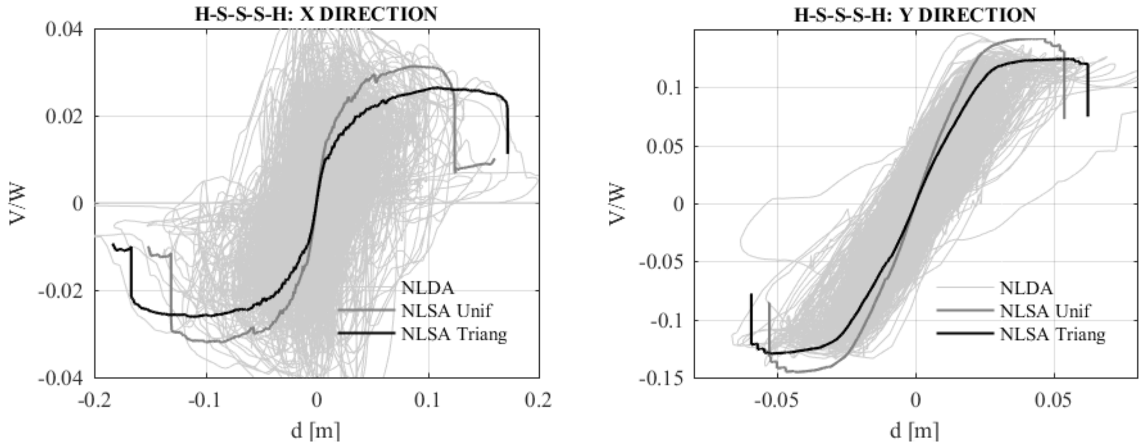

Figure 3.24 – Model H-S-S-S-H: comparison between NLDA by using a seismic input compatible with the code action type 1 (all records) and NLSA with uniform and triangular distributions: X direction (left) and Y direction (right)

Despite this general outcome, the analyses of the results record-by-record, as exemplified in Figure 3.25, reveals that, in general, the non-linear behaviour of the structure may be better characterized by the uniform distribution in the X direction and by the triangular distribution in the Y direction. Thus, in order to have a reliable seismic assessment of the global behaviour of these URM buildings, it is recommended to perform the NLSA with both load distributions and confront the results in terms of the seismic intensity measure compatible with the performance limit states.

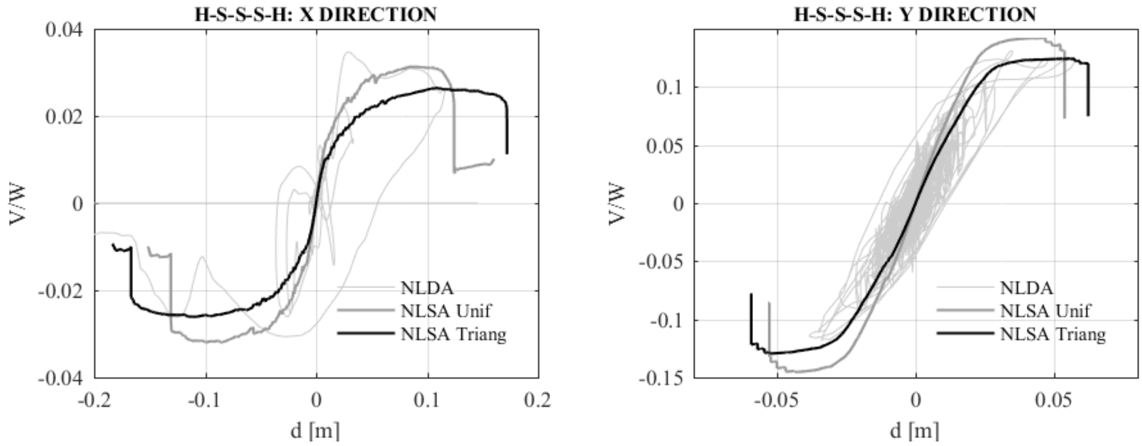

Figure 3.25 – Comparison between NLDA by using a seismic input compatible with the code action type 1 and the NLSA: X direction (left) and Y direction (right)

3.3.4. Models defined by aleatory properties

After analysing the behaviour of the 8 building models, defined by the median properties of the aleatory variables (§3.3.2), and after confirming the reliability of both the load distributions (§3.3.3), non-linear static (pushover) analyses are performed with the 8 building models combined with the aleatory variables defined by the Monte Carlo Method. As referred in §3.2.8, 1000 Monte Carlo simulations were considered to sample the 50 aleatory variables and define the input variables for the numerical models (now reduced to 8) as a function of the probability attributed. For instance, model H-S-S-S-H with a probability of 3.9% is represented by 39 models defined by the 39 simulations, whereas model H-S-SH-T-T with a probability of 7.0% is represented by 70 models and so forth. This defines a group of 1000 models that combine the main variations within the typology in terms of geometry, constructive details, materials and mechanical properties. The number of Monte Carlo simulations was defined in order to have from a statistical point of view: 1) a sufficient number of models able to describe the behaviour of the 8 groups of models, and 2) a sufficient number of results to reach a good convergence in the estimation of the parameters that define fragility functions, which is the final aim of this thesis.

The analyses are performed considering the uniform and the triangular load distributions applied in the X and Y directions, including negative and positive senses of direction, resulting in a total of 8000 pushover analyses. Figure 3.26 to Figure 3.29 show, as an example, the pushover curves obtained with group H-S-SH-T-T defined by 70 models and with group S-S-S-S-H defined by 78 models. The pushover curves obtained with the models, defined by the median properties of the aleatory variables, are also included for comparison. As expected, these are not positioned in the middle of the cloud of curves. First, because the median properties are associated with the interval of values of the variable and not to the interval of values attributed to each group of models with the Monte Carlo simulations, and second, because it is a non-linear analysis i.e. the use of the median properties of the aleatory variables provides a good estimate of the median curve, but not in a complete rigorous way. The results obtained for all models and combinations are presented in Figure D.1 to Figure D.32 in Annex D.

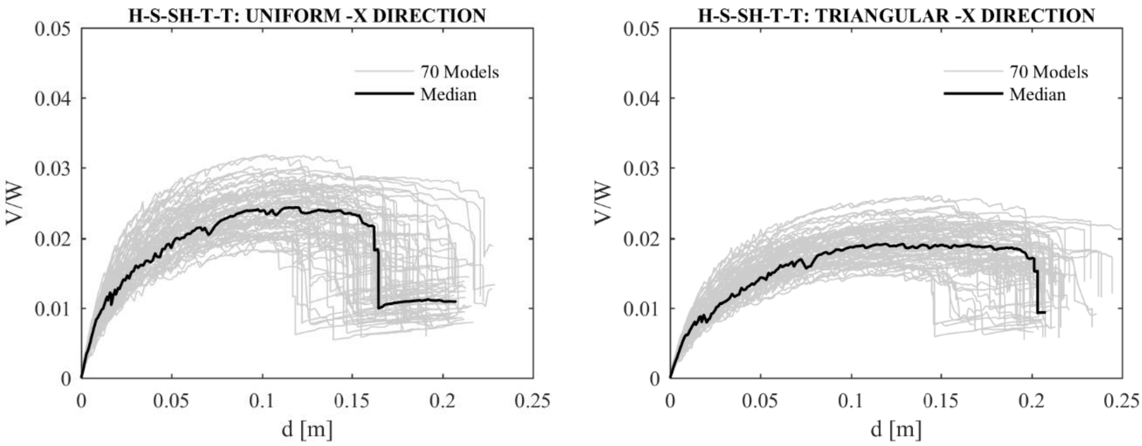

Figure 3.26 – Pushover curves for H-S-SH-T-T: Uniform –X direction (left) and Triangular –X direction (right)

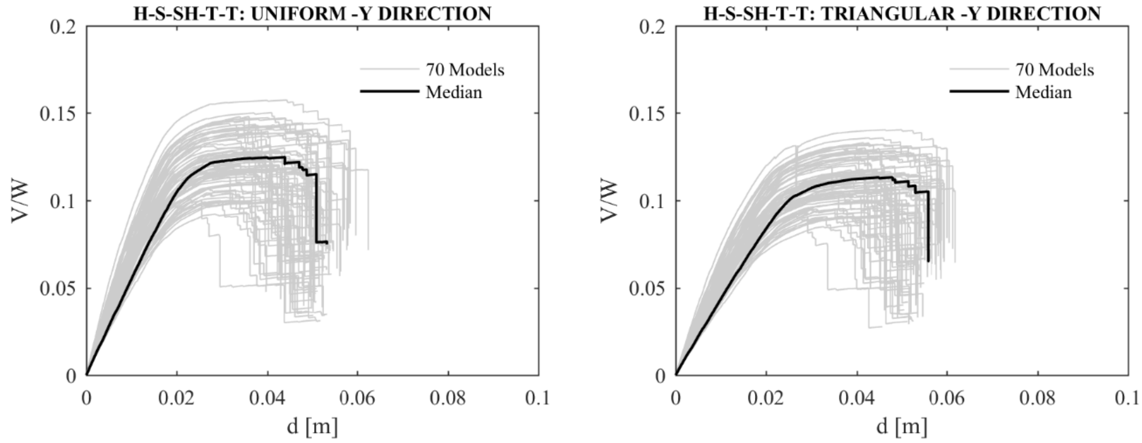

Figure 3.27 – Pushover curves for H-S-SH-T-T: Uniform –Y direction (left) and Triangular –Y direction (right)

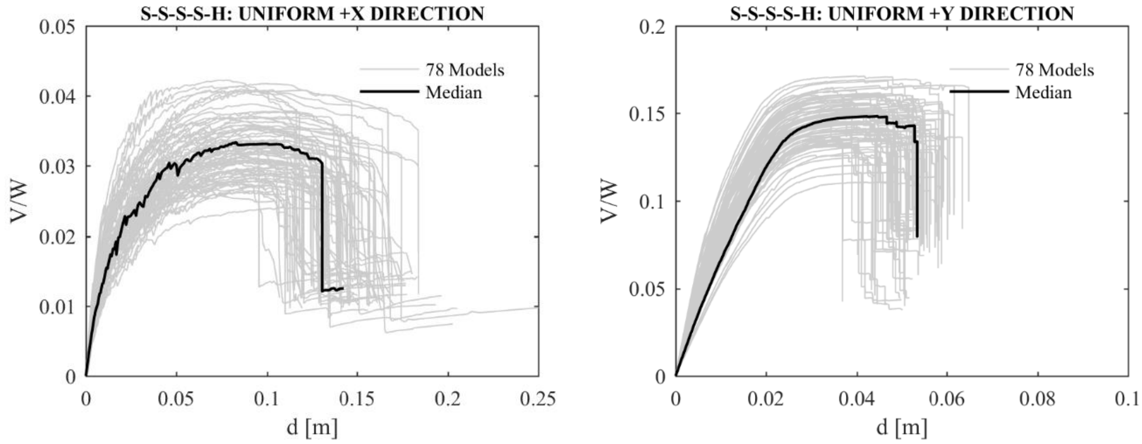

Figure 3.28 – Pushover curves for S-S-S-S-H: Uniform +X direction (left) and +Y direction (right)

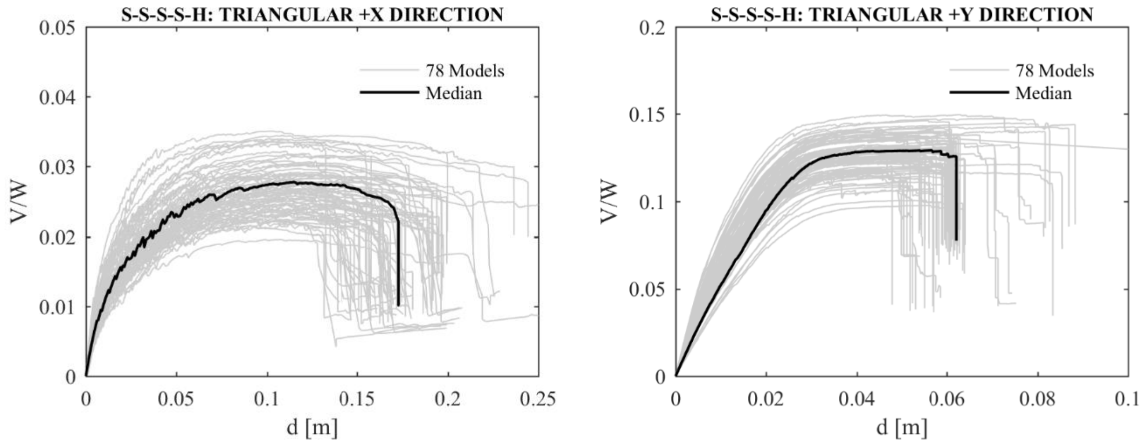

Figure 3.29 – Pushover curves for S-S-S-S-H: Triangular +X direction (left) and +Y direction (right)

3.4. Definition of performance limit states

The EC8-3 (IPQ, 2017) recommends the consideration of three performance limit states as a function of the level of damage in the structure: damage limitation, significant damage and near collapse. These limits are directly defined on the pushover curve based on conventional displacement limits corresponding to: 1) the yielding displacement (d_y) of the idealized elasto-perfectly plastic force–displacement relationship of the equivalent SDOF system, for damage limitation limit state, 2) the ultimate displacement capacity (d_u) corresponding to the point of 20% decay of the maximum base shear force, for near collapse limit state, and 3) ¾ of d_u, for significant damage limit state.

Lagomarsino and Cattari (2013) proposed, in alternative, to define performance limit states based on a multi-scale approach that correlates the behaviour of the structure at three scales: 1) structural elements (piers and spandrels), 2) macro-elements (walls and horizontal diaphragms) and 3) global (represented by the pushover curve). The multi-scale approach is a heuristic procedure that aims to monitor the occurrence of significant damage in parts of the structure that may not be evident in the pushover curve in terms of strength degradation. This is particular important for URM buildings with flexible diaphragms considering that in this case, the limited load transfer between vertical elements leads to a more independent behaviour of the walls. As a consequence, the reaching of serious damage in a wall may not appear evident on the pushover curve, when this wall offers a small contribution to the total base shear force. In addition, the attainment of a certain limit state should also consider the lack of homogeneity on damage distribution in the building and its possible premature concentration in some walls.

A comparison between the criterion proposed by the EC8-3 (IPQ, 2017) and the criterion proposed by Lagomarsino and Cattari (2013) for the definition of performance limit states was carried out in a previous work about these URM buildings in Lisbon (Simões et al., 2014b). It was verified that the definition of the performance limit states was conditioned by the multi-scale approach (Cattari and Lagomarsino, 2013). The difference between both criteria was particularly evident on the verification of the near collapse limit state in the direction parallel to the façade walls, as the displacement threshold was reduced in 58% with the application of the multi-scale approach. Based on this, in the present work, the definition of the performance limit states in the pushover curve is based only on the multi-scale approach (Cattari and Lagomarsino, 2013).

For a matter of consistence with the original formulation, the performance limit states are defined in terms of performance levels (PLk, with k=1,…,4). The three limit states recommended by the EC8-3 (IPQ, 2017) are assumed to correspond to the performance levels PL2, PL3 and PL4, while PL1 is assumed to correspond to the operational limit state. In addition, a direct correspondence between performance levels (PLk, with k=1,…,4) and damage levels in the structure (DLk, with k=1,…,4) is considered. According to the multi-scale approach, the position of the DLk in the pushover curve is defined by the minimum displacement threshold obtained from the verification of conventional limits at the three scales, as explained in the following:

1. Element Scale – comprehends the assessment of the cumulative rate of damage in piers that reach DLi in accordance to the element multi-linear constitutive law (§3.2.1).

The cumulative rate of damage ($\Lambda_{P,DLk}$) is defined as the percentage of piers that reached or exceeded DLi, weighted on the corresponding cross section (A_p), as defined in Equation (3.16):

$$\Lambda_{P,DLk} = \frac{\sum_p A_p H\left(\frac{\delta_p}{\delta_{DLi}} - 1\right)}{\sum_p A_p} \qquad \text{with } i = k + 1 \tag{3.16}$$

where the sum $\sum_P$ is extended to the total number of piers in the building, N_p ($p = 1,\ldots,N_p$) and H is the Heaviside function (equal to 0 until the demand δ_p in the s-th pier does not reach the capacity δ_i and equal to 1 after). The final threshold (Λ_P) is defined by Equation (3.17), in order to allow the attainment of DLi in a limited percentage of elements and to avoid that the threshold DLk at the element scale is reached just due to one element. This equation was calibrated through an extensive application of the multi-scale approach to several buildings, by considering various irregularities and diaphragms of different in-plane stiffness (Cattari and Lagomarsino, 2013). In particular, the proposed threshold takes into account the damage induced by the application of the gravity loads ($\Lambda_{P,DLk,0}$) and the number of piers in the given building.

$$\Lambda_P = 0.04 + \Lambda_{P,DLk,0} + \frac{2}{N_P} \tag{3.17}$$

The verification at the level of spandrels was neglected since these elements show very weak behaviour since the beginning of the non-linear static (pushover) analysis, as referred in §3.3.2, in addition to the fact that these are secondary elements.

2. Macro-Element Scale – comprehends the verification of inter-storey drift limits in each wall and level (θ_{DLk}).

In this work, the inter-storey drift thresholds are defined according to the proposal from Calvi (1999): 0.2% for DL1, 0.3% for DL2, 0.6% for DL3 and 0.9% for DL4. However, a preliminary analyse of the results of the buildings under study, indicated that in some cases the position of DL3 and DL4 occur much before the descending part of the pushover curve, in particular in the X direction, due to higher displacement capacity of the buildings (exemplified in Figure 3.30 a)). It was concluded that this conventional criterion was not suitable for this type of URM buildings, as it provides an over conservative assessment of the response, with all DLk in the hardening part of the pushover curve.

A new formulation for the macro-element scale is adopted in this work, as proposed by Lagomarsino (2018). It comprehends the assessment of the cumulative damage of piers in a given wall and level ($\Lambda_{P,WL,DLk}$). This criterion comprises the verification of the maximum value of the minimum DLi attained in piers located in a given wall and level, as exemplified in Figure 3.31 for DL3 threshold. This is useful to detect when piers from a given level reached a DLi equal or greater than that assumed as reference for checking the occurrence of a soft-storey mechanism.

Figure 3.30 compares the position of the DLk in the pushover curve defined from both criteria: inter-storey drift limits (θ_{DLk}) and cumulative damage of piers in a given wall and level ($\Lambda_{P,WL,DLk}$), putting in evidence a more uniform distribution of the DLk with the later criterion. Due to this, the cumulative damage of piers in a given wall and level ($\Lambda_{P,WL,DLk}$) is adopted in this work for the verification at the macro-element scale.

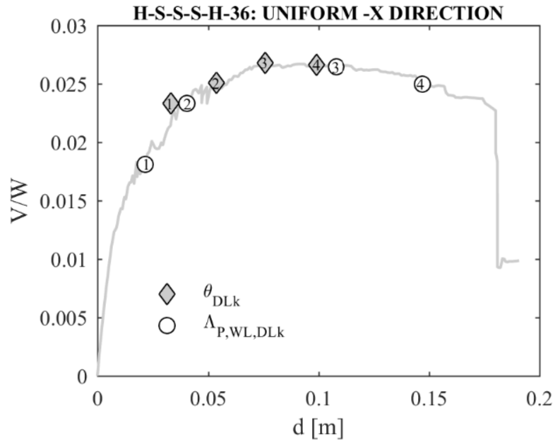

Figure 3.30 – Comparison of the position of DLk in the pushover curve from the application of the macro-element scale defined by inter-storey drift limits (θ_{DLk}) and cumulative damage of piers in a given wall and level ($\Lambda_{P,WL,DLk}$)

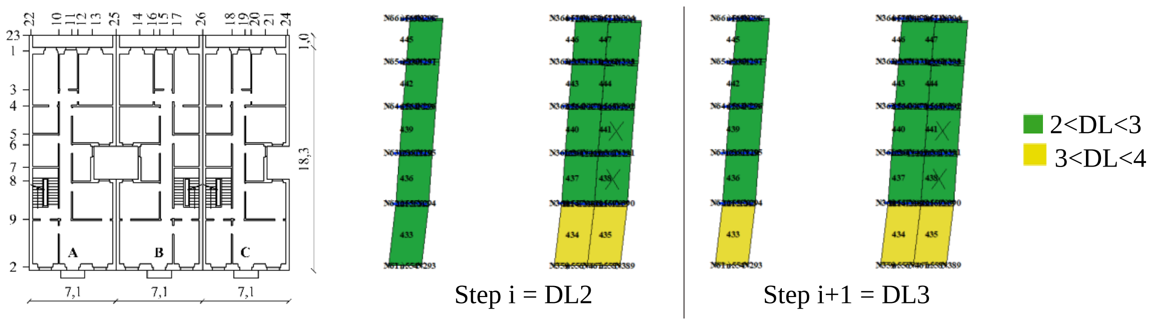

Figure 3.31 – Example of the attainment of the cumulative damage ($\Lambda_{P,W7\_L1,DL3}$) in piers from Wall-7 Level 1 for DL3 with step i+1 of the pushover analysis (indication of the damage level at the scale of the element in the right side)

In the original formulation of the macro-element scale, an additional verification in terms of the angular deformation of horizontal diaphragms is proposed. This verification is not considered in this work.

3. Global Scale – defined as a function of a rate (k_G) of the maximum base shear force (V/V_{max}). The following limits are considered: 1.0 for DL2, 0.8 for DL3 and 0.6 for DL4.

After setting the minimum displacement threshold between the three scales, an additional verification is set in order to avoid the positioning of DL1 and DL2 in the very beginning of the pushover curve. Here, it is assumed that k_G should not be lower than 0.50 and 0.75, respectively. Figure 3.32 exemplifies the final position of the DLk in the pushover curve in the X and Y directions for one of the models analysed.

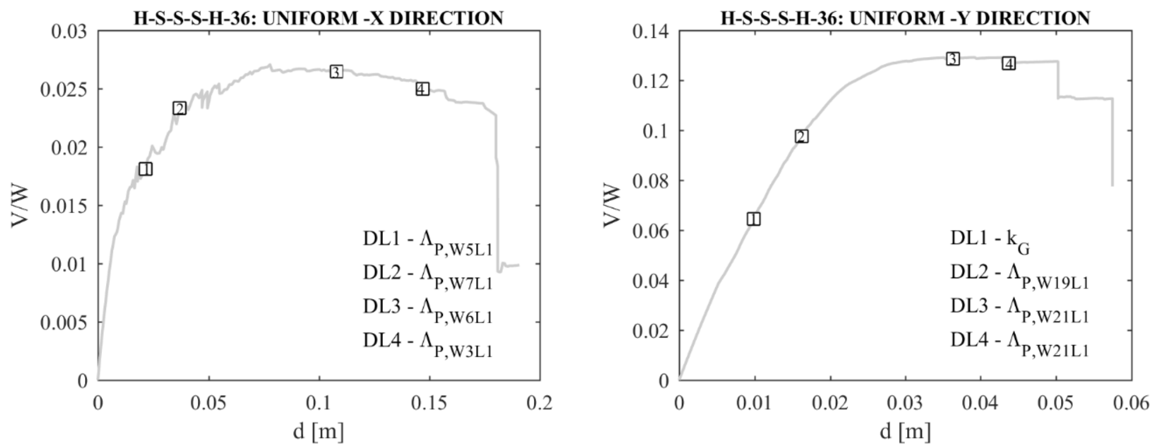

Figure 3.32 – Example of the final position of DLk in the pushover curve obtained in the X direction (left) and in the Y direction (right)

Considering the 1000 building models under study and the 8000 pushover curves obtained, the criterion that in average defines the position of the DLk is, in the X direction, the verification at the macro-element scale, and in the Y direction, the global scale for DL1 and DL2 and the macro-element scale for DL3 and DL4. The verification at the element scale is less frequent, but still important for the definition of DL1. Figure 3.33 identifies, as an example, the criterion that in average defines the position of the DLk in the X and Y directions for the group of models H-S-S-S-H and H-S-SH-T-T.

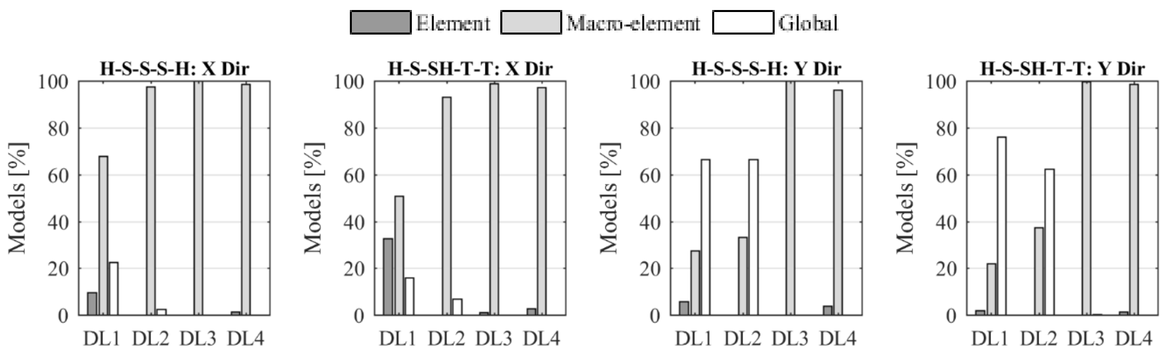

Figure 3.33 – Percentage of models as a function of the criteria for the definition of each DLk

In what concerns the displacement compatible with the DLk, it was observed that there are small variations between negative and positive directions (the coefficient of variation is lower than 8%). In average, higher displacements are obtained with the triangular load distribution, in comparison with the uniform distribution, and in the X direction, in comparison with the Y direction of the block of buildings.

Figure 3.34 and Figure 3.35 present the median values of the displacement compatible with the DLk, respectively, in the X and Y directions. As stated above, a direct correspondence between performance levels (PLk, with k=1,…,4) and damage levels (DLk, with k=1,…,4) is considered in this work, the former term is used as reference in the next sections.

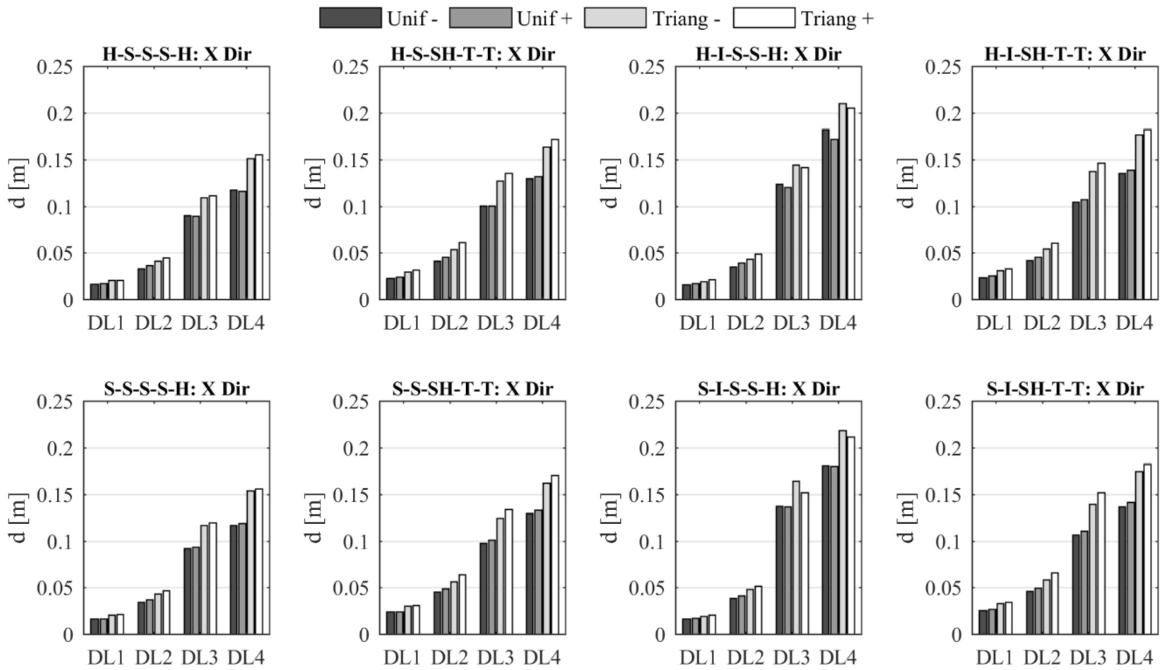

Figure 3.34 – Median values of displacement for each DLk: X direction

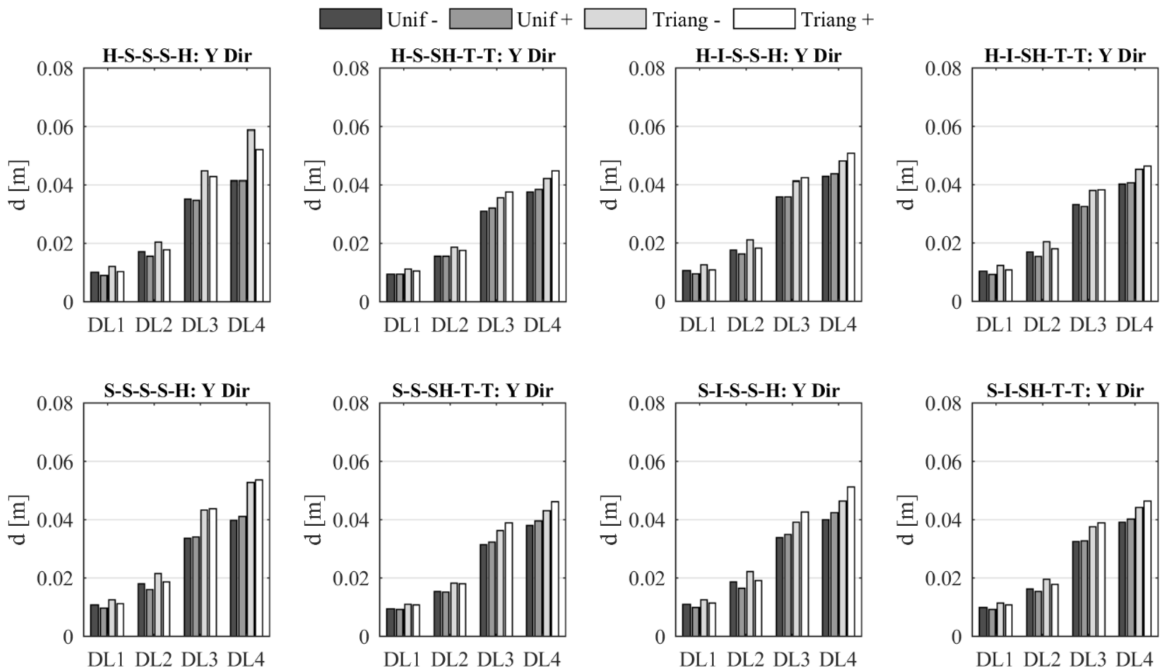

Figure 3.35 – Median values of displacement for each DLk: Y direction

3.5. Definition of the seismic intensity measure and dispersion

3.5.1. Procedure for the computation of the seismic intensity measure

In this thesis, the seismic intensity measure is represented by the peak ground acceleration (PGA) that produces the attainment of specified performance limit states (here referred as performance levels, PLk). As stated in §1.2, the PGA is the most frequently adopted seismic intensity measure.

Nevertheless, the option for the PGA is also justified by the direct relation between the characteristics of the structure and the spectral characteristics of the seismic input.

The procedure for the computation of the PGA values comprehends the comparison between the capacity of the structure and the seismic demand. The capacity is described by the displacement thresholds identified in the previous section for the PLk. The next step consists on the conversion of the pushover curve to the capacity curve of an equivalent SDOF system to establish the comparison with the seismic demand, obtained by a properly reduced ADRS. As referred in §1.2, different methods are available for the evaluation of the displacement demand on the capacity curve. Cattari et al. (2015) compared the application of the N2-Method (Fajfar, 2000) and the Capacity-Spectrum Method (Freeman, 1998; Fajfar, 1999), concluding that the latter provides more reliable and conservative results for the assessment of plan irregular URM buildings with flexible diaphragms. In addition, the Capacity-Spectrum Method does not require transforming the pushover curve into an equivalent bilinear relationship, which is influenced by the definition of the equivalent period of the structure (T*) associated with the elastic response, inducing therefore more uncertainties.

The Capacity-Spectrum Method with over-damped spectrum is adopted in this work without any iterative procedure, as proposed by Lagomarsino and Cattari (2015b), being addressed to compute the maximum PGA for specific target displacement. The procedure is based on the following steps:

1. Definition of the capacity curve by converting the pushover curve (MDOF system) into an equivalent SDOF system. The conversion is based on a transformation factor computed as a function of a displacement shape vector, assumed to be consistent with the fundamental mode shape of the system, as proposed by Fajfar (2000). The transformation factor (Γ) is calculated according to Equation (3.18), where m_i and Φ_i are, respectively, the mass and modal displacement (normalized to the roof level) in each node i of the structure and m^* is the mass of the equivalent SDOF system. The base shear force (V^*) and the displacement (d^*) of the equivalent SDOF system are computed according to Equation (3.19). The capacity curve is plotted in spectral coordinates, i.e. spectral acceleration (S_a) as a function of spectral displacement (S_d), assuming the equivalences presented in Equation (3.20).

$$\Gamma = \frac{\sum m_i \Phi_i}{\sum m_i \Phi_i^2} = \frac{m^*}{\sum m_i \Phi_i^2} \tag{3.18}$$

$$V^* = V/\Gamma \quad \text{and} \quad d^* = d/\Gamma \tag{3.19}$$

$$S_a = V^*/m^* \quad \text{and} \quad S_d = d^* \tag{3.20}$$

2. Determination of the equivalent viscous damping for each performance level (ξ_{PLk}), as the sum between the initial elastic viscous damping (ξ_{el}) and the hysteretic damping (ξ_{hyst}). The initial

elastic viscous damping (ξ_{el}) is assumed equal to 5%. The hysteretic damping (ξ_{hyst}) is determined after performing cyclic pushover analyses, assuming as target displacement of the cycle the displacement threshold for each performance level (d_{PLk}), considering that damping increases with the damage in the building. The hysteretic damping (ξ_{hyst}) is related to the area enclosed by full hysteresis loops as defined in Figure 3.36, where E_D is the energy dissipated by the structure during the cyclic response and E_0 is the total strain energy (with $E_0 = E_{S0+} + E_{S0-}$).

3. Definition of the seismic demand in the ADRS format, i.e. spectral acceleration (S_a) as a function of spectral displacement (S_d), for an equivalent viscous damping (ξ) of 5%. Normalization of the response spectrum (S_{d1}), so that $S_a(S_d=0)=1$.

4. Reduction of the normalized elastic response spectrum by a damping correction factor (η), given by Equation (3.21):

$$\eta = \sqrt{\frac{10}{5+\xi_{PLk}}} \leq 0.55 \tag{3.21}$$

5. Computation of the PGA for which the seismic displacement demand (S_d) is equal to the displacement capacity of the equivalent SDOF (d^*) for a specified PLk, according to Equation (3.22), where T^* is the period of the equivalent SDOF given by Equation (3.23).

$$PGA_{PLk} = \frac{d^*_{PLk}}{S_{d1}(T^*)\eta(T^*)} \tag{3.22}$$

$$T^* = 2\pi\sqrt{\frac{S_d}{S_a}} \tag{3.23}$$

Figure 3.37 exemplifies the capacity curve and the over-damped response spectra, in spectral coordinates, used for the computation of the PGA values compatible with the four performance levels.

In what concerns the option for the computation of the equivalent viscous damping, this approximated estimation based on cyclic pushover analyses, allows to take into account the specific seismic behaviour of the structure, which is a better estimation with respect to the adoption of analytical expressions proposed in literature for similar structures (Calvi, 1999; Blandon and Priestley, 2005). Nevertheless, for simplification, the cyclic pushover analyses are carried out only with the 8 building models, defined by the median properties of the aleatory variables, and used to compute the seismic intensity measure of each group of models, defined by the aleatory properties. Table 3.14 summarizes the corresponding values of the equivalent viscous damping.

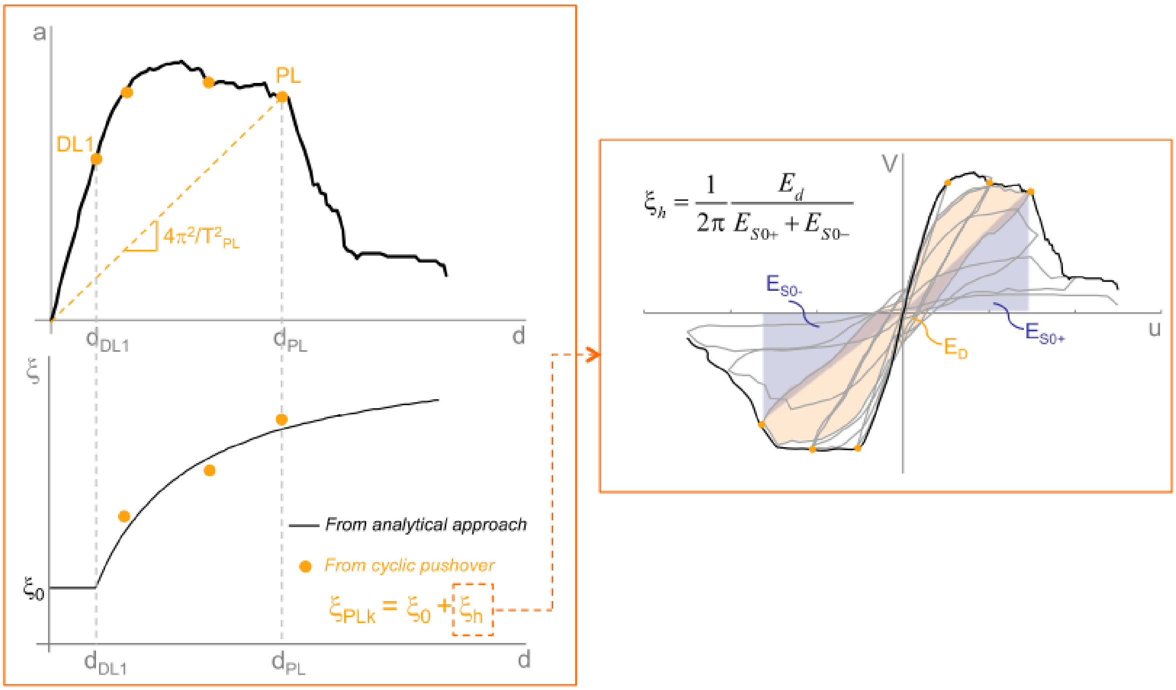

Figure 3.36 – Evaluation of the equivalent viscous damping (Cattari and Lagomarsino, 2013)

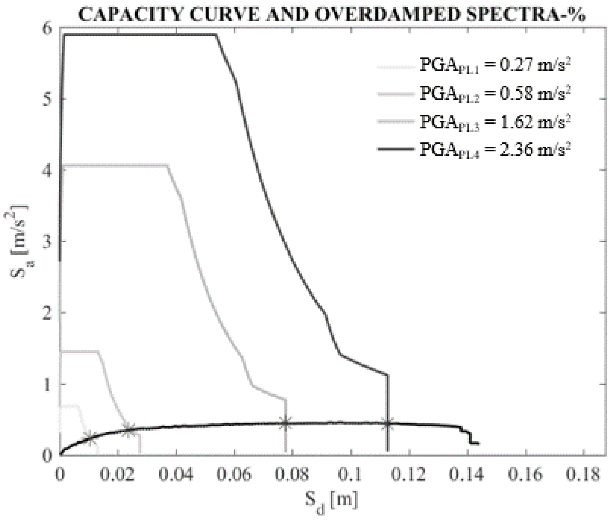

Figure 3.37 – Computation of the PGA values compatible with the four performance levels

In Table 3.14, it is observed that the equivalent viscous damping is higher in the X direction when compared with the Y direction. This is mainly related to the spread of damage in the structure and the higher displacement capacity of the structure in the X direction, in contrast with the concentration of damage in the side walls in the Y direction. In addition, PL1 and PL2 have the same equivalent viscous damping in the Y direction because both displacements are located in the first almost-linear branch of the pushover curve (see for example Figure 3.32), leading to the low dissipation of the cycle. Models with interior timber "tabique" walls exhibit higher equivalent viscous damping in comparison with the models only with interior clay brick walls.

Table 3.14 – Results of the equivalent viscous damping

Model	X Direction				Y Direction			
	PL1	PL2	PL3	PL4	PL1	PL2	PL3	PL4
H-S-S-S-H	12.6	13.0	13.0	13.8	7.1	7.1	9.0	10.0
H-S-SH-T-T	15.1	15.6	15.6	15.6	7.1	7.1	7.9	9.1
H-I-S-S-H	13.5	13.9	13.9	15.1	6.8	6.8	8.2	9.0
H-I-SH-T-T	15.6	16.1	16.1	16.1	6.9	6.9	8.1	9.0
S-S-S-S-H	12.3	12.7	12.7	13.5	6.8	6.8	8.3	9.0
S-S-SH-T-T	14.6	15.0	15.0	15.4	7.3	7.3	7.9	9.4
S-I-S-S-H	13.6	14.3	14.5	15.5	6.6	6.6	8.4	8.8
S-I-SH-T-T	15.4	15.8	15.8	16.0	7.1	7.1	8.7	9.1

Final reference to the fact that while performing the non-linear dynamic analyses (§3.3.3) a lower value of equivalent viscous damping was adopted (ξ= 3%), in contrast with the 5% now considered for the initial elastic viscous damping. This is justified since the hysteretic contribution is estimated in a more accurate way with the non-linear dynamic analyses than with the cyclic pushover analyses.

3.5.2. Determination of the median intensity measure and dispersion in the capacity

The procedure for the computation of the PGA values that produces the attainment of the PLk, is applied with the 8000 pushover curves, considering the seismic demand defined by the code elastic response spectrum for Lisbon (zone 3) and soil type B (IPQ, 2010): action type 1 (PGA=1.50 m/s^2 and S=1.29) and type 2 (PGA=1.70 m/s^2 and S=1.27). The corresponding PGA values are treated with the final objective of determining the parameters for the derivation of the fragility functions. The following steps are considered:

1. The PGA values obtained for the PLk are sorted in ascending order for the 8 groups of models.

2. An equal probability is attributed to each PGA value (p=1/N, where N is the number of models associated with each group).

3. Calculation of the median value (50% percentile, $PGA_{50\%}$) and corresponding dispersion (β_C) assuming that the PGA values are lognormal distributed. The dispersion β_C represents the uncertainty in the definition of the capacity of each group of models.

Figure 3.38 and Figure 3.39 plot, as an example, the $PGA_{50\%}$ values obtained with the group of models H-S-S-S-H and H-S-SH-T-T determined with seismic action type 1 and type 2, respectively. The results for all groups are presented in Annex E. It is observed that, within each group, there are small variations between the $PGA_{50\%}$ values obtained with the negative and positive directions (the coefficient of variation is lower than 5.7%) and between the uniform and triangular distributions (the coefficient of variation is lower than 10.4%) even though, the uniform distribution provides, in general, lower $PGA_{50\%}$

values. It is also observed that action type 1 is the most demanding seismic scenario as it provides lower $PGA_{50\%}$ values in both directions of the structure. In what concerns the different performance levels, lower $PGA_{50\%}$ values are obtained for PL1 and PL2 in the X direction and for PL3 and PL4 in the Y direction.

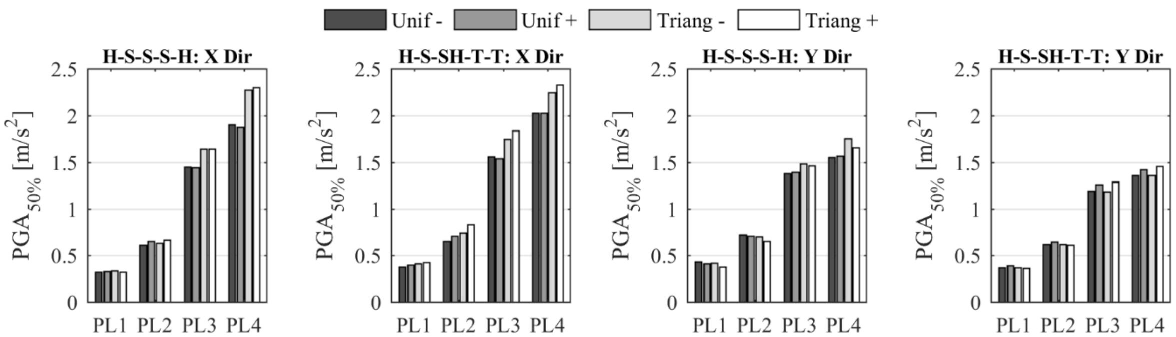

Figure 3.38 – Median values of PGA obtained in the X and Y directions for the group of models H-S-S-S-H and H-S-SH-T-T: seismic action type 1

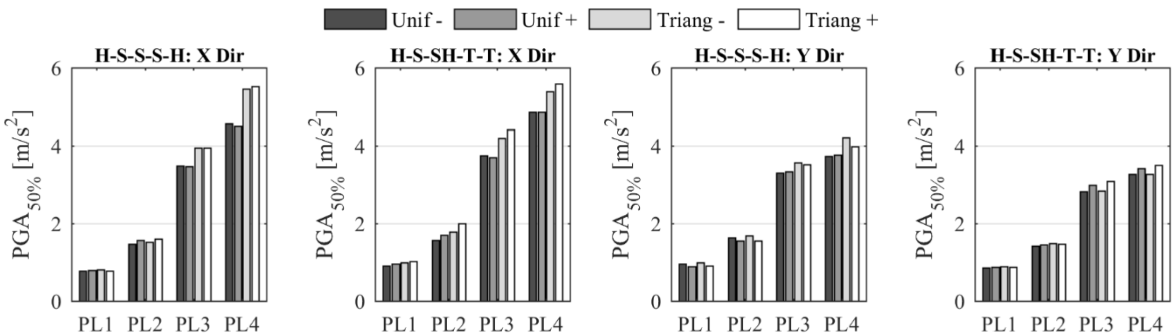

Figure 3.39 – Median values of PGA obtained in the X and Y directions for the group of models H-S-S-S-H and H-S-SH-T-T: seismic action type 2

Figure 3.40 and Figure 3.41 plot the dispersion in the capacity (β_C) for the same group of models. The results for all groups are presented in Annex E. The dispersion in the capacity (β_C) is lower in the Y direction than in the X direction. The behaviour of the block of buildings in the Y direction is mainly governed by the response of the side blind walls, and consequently, mainly affected by the variations of the mechanical properties of masonry and by the deformability and strength characteristics of piers. This direction is also influenced by the connection between exterior walls, as shown in §3.3.1. On the other hand, the behaviour in the X direction is affected by the full set of aleatory variables considered: the mechanical properties of masonry, the deformability and strength characteristics of piers and spandrels, the properties of the interior timber “tabique” walls, the in-plane stiffness of timber floors and the quality of connections between walls (including some interactions with the Y direction in regards to the flange effect).

From Figure 3.40 and Figure 3.41, it is visible that the dispersion in the capacity (β_C) has the highest value for PL1 in the X direction. Although the macro-element scale is the criterion that defines, in general, the position of the DLk in the pushover curves obtained for the X direction, as exemplified in

Figure 3.33, it is also observed that for DL1 it is divided between the three criteria, increasing therefore the dispersion in the capacity (β_C) for PL1. Moreover, the determination of DL1 is in general a difficult task because it is associated with a state of slight damage in the structure. Comparing the outcome from seismic action type 1 and type 2, the dispersion in the capacity is practically the same in the X direction. This is related to the shape of the response spectra and to the dynamic characteristics of the structure. First, the corner period (T_C) is equal to 0.60 s for action type 1 and 0.25 s for type 2. Second, the fundamental period of the structures is, in average, 1.22 s in the X direction and 0.52 s in the Y direction (Annex A). The spectral acceleration (S_a) corresponding to the attainment of the PLk in the X direction is characterized by a period content $T>T_C$ (range of constant velocity of the spectrum), while in the Y direction it varies between $T_B<T<T_D$ (here T_B=0.1 s and T_D=2 s) increasing therefore the uncertainties in the outcome of the PGA values in the Y direction.

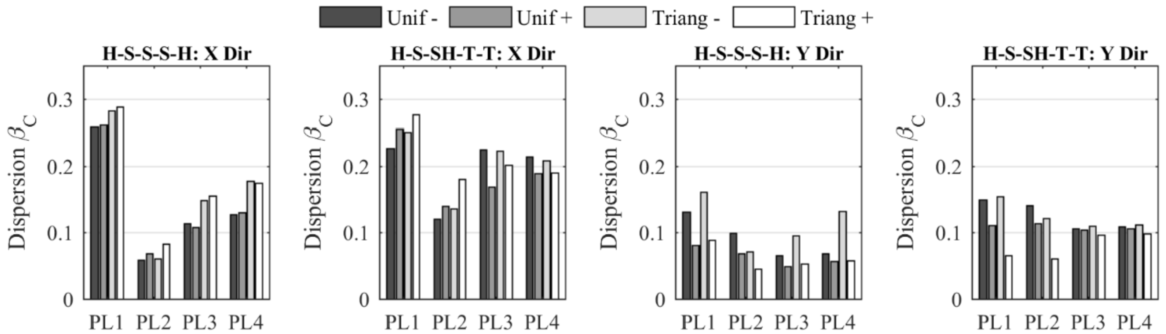

Figure 3.40 – Dispersion in the capacity (β_C) for the group of models H-S-S-S-H and H-S-SH-T-T: seismic action type 1

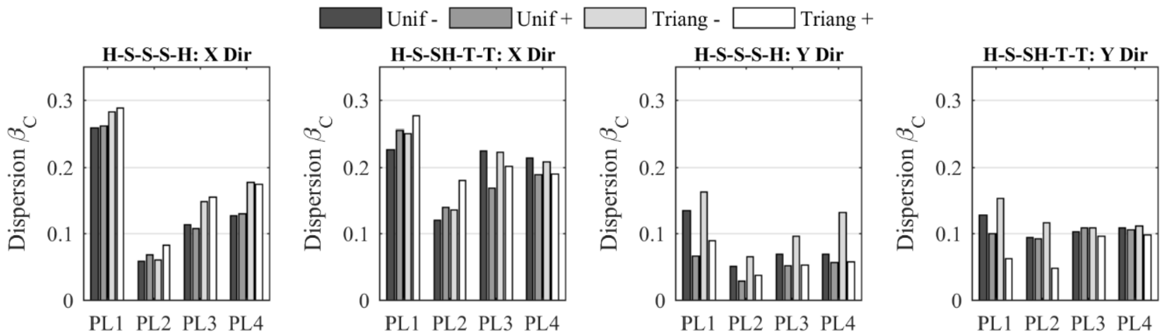

Figure 3.41 – Dispersion in the capacity (β_C) for the group of models H-S-S-S-H and H-S-SH-T-T: seismic action type 2

Taking into account the small variations between the $PGA_{50\%}$ values obtained in the negative and positive directions of the models and between the $PGA_{50\%}$ values obtained with the application of the uniform and triangular load distributions, it is proposed to set for each model the minimum PGA value between these results, as this leads to the most demanding condition for the block of buildings. Figure 3.42 and Figure 3.43 plot the corresponding $PGA_{50\%}$ values and dispersion in the capacity (β_C) for all the groups of models determined with seismic action type 1 and type 2.

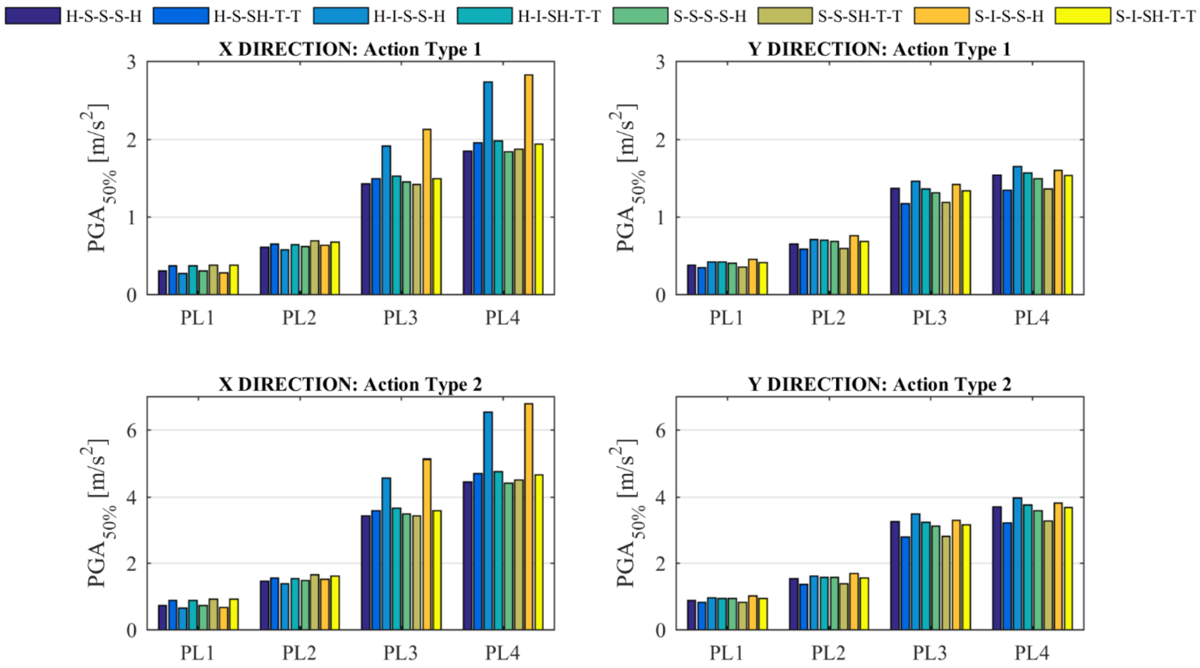

Figure 3.42 – Median values of PGA for all groups of models: seismic action type 1 and type 2

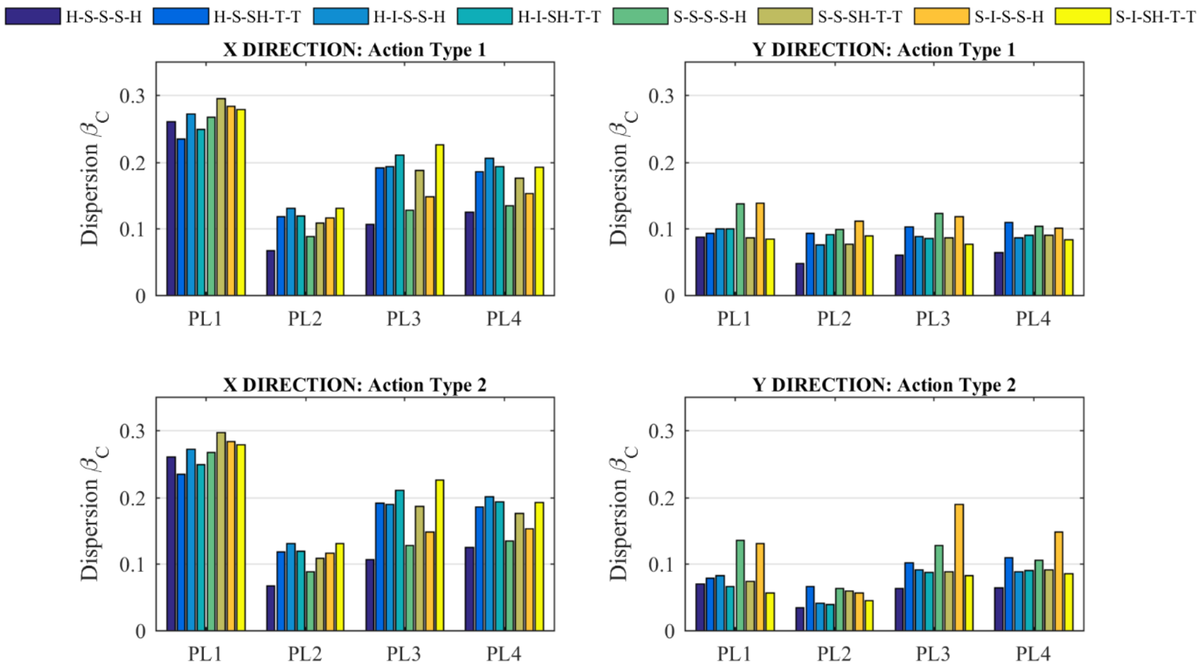

Figure 3.43 – Dispersion in the capacity (β_C) for all groups of models: seismic action type 1 and type 2

Comparing the behaviour of each group, it is observed that the $PGA_{50\%}$ values are similar for PL1 and PL2 (coefficient of variation lower than 13.1%) and are in general lower in the X direction. For PL3 and PL4, lower values are obtained in the Y direction, in particular for models with interior timber “tabique” walls. In the X direction, it is visible that the $PGA_{50\%}$ values obtained for PL3 and PL4 with models H-I-S-S-H and S-I-S-S-H are approximately 1.5 times higher than with the other models. Results from the non-linear static analyses have also shown that these models have higher displacement capacity in comparison with models H-S-S-S-H and S-S-S-S-H (see §3.3.1, Figure 3.14 and Figure 3.15). This can be explained by the reduction of the flange effect in the first case. In what regards the dispersion in the capacity (β_C), in the X direction usually higher values are obtained for models with interior timber "tabique" walls, whereas in the Y direction similar results are obtained between PLk, with some variations for the group of models S-S-S-S-H and S-I-S-S-H.

3.5.3. Determination of the dispersion in the seismic demand

As stated in §1.2, the uncertainties in the definition of the seismic demand may include: i) epistemic uncertainties (β_H) related to the derivation of the hazard curve, and ii) intrinsic/aleatory uncertainties (β_D) related to the variability of the seismic input (spectral shape), as the seismic response of the structure is described only by the PGA value. This section is addressed to the determination of the dispersion in the seismic demand (β_D) as given by Equation (3.24):

$$\beta_D = \frac{1}{2} \times \left| \log PGA_{84\%} - \log PGA_{16\%} \right| \tag{3.24}$$

where $PGA_{84\%}$ and $PGA_{16\%}$ represent the PGA values that produces the attainment of the different performance levels by considering as seismic input, the response spectra corresponding to the 84% and 16% percentiles. The set of 30 records compatible with the code seismic action type 1 and type 2, used to perform the non-linear dynamic analyses (§3.3.3), are adopted to compute these response spectra percentiles. Figure 3.44 compares the response spectrum for the 50% percentile ($S_{a,50\%}$) with the code response spectrum ($S_{a,Code}$) and plots the response spectra associated with the 84% and 16% percentiles, $S_{a,84\%}$ and $S_{a,16\%}$, respectively, for seismic action type 1 and type 2.

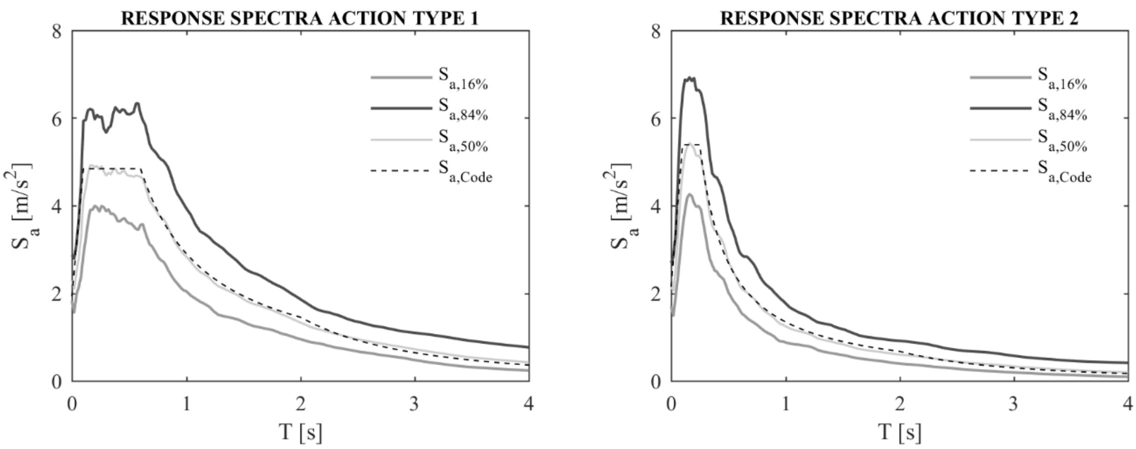

Figure 3.44 – Response spectra for seismic action type 1 (left) and type 2 (right)

The $PGA_{84\%}$ and $PGA_{16\%}$ values are computed for each PLk considering the 8 building models, defined by the median properties of the aleatory variables. Figure 3.45 presents the dispersion in the seismic demand (β_D) considering the seismic action type 1 and type 2, respectively, defined as the maximum value between the all results obtained (negative and positive directions with the uniform and triangular distributions). The dispersion in the seismic demand varies between 0.27 and 0.51 for the seismic action type 1 and between 0.33 and 0.65 for type 2.

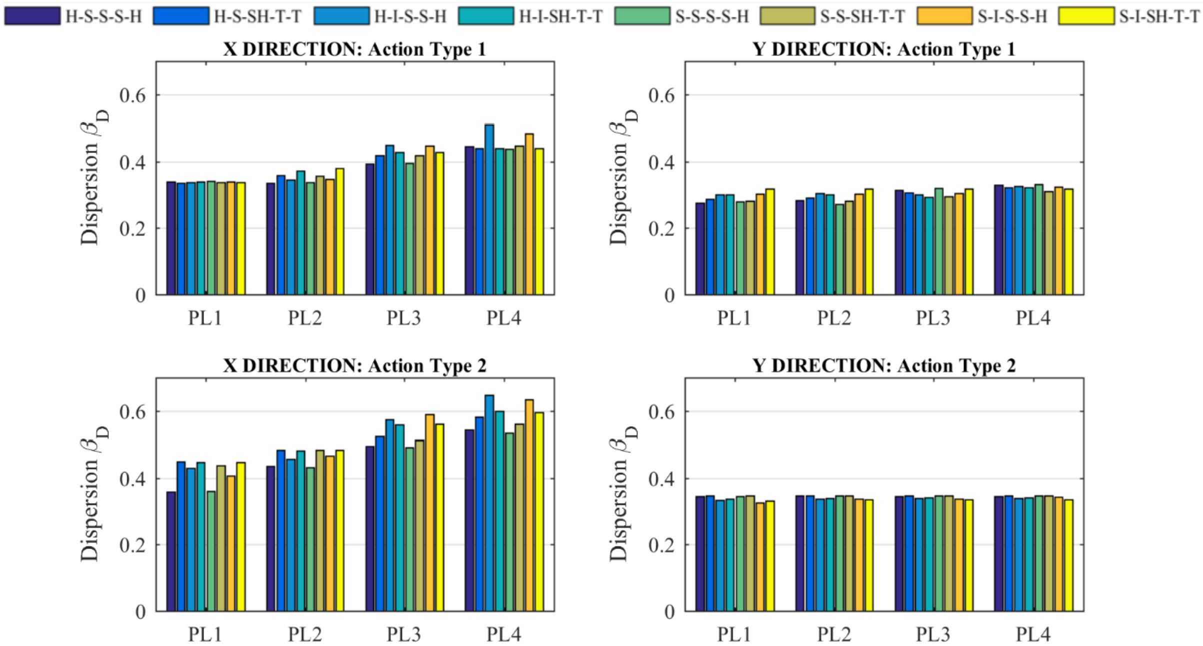

Figure 3.45 – Dispersion in the seismic demand (β_D) for all groups of models: seismic action type 1 and type 2

3.5.4. Summary of results and derivation of fragility functions

Table 3.15 to Table 3.22 summarize the results obtained in terms of the median value of PGA ($PGA_{50\%}$), dispersion in the determination of capacity of the block of buildings (β_C), dispersion in the determination of the seismic demand (β_D) and the final dispersion related to the global seismic behaviour (β_G), for the different performance levels, direction of the structure (X and Y) and considering seismic action type 1 and type 2.

The dispersion related to the global seismic behaviour (β_G) is defined according to Equation (3.25). The reliability/weight (w) of each group of models are also indicated in the tables. As expected, the dispersion in the seismic demand (β_D) has an important contribution to the dispersion of the global seismic behaviour (β_G). In this work, the uncertainties in the definition of the performance limit states (β_T) are indirectly taken into account by the definition of the dispersion in the capacity (β_C) and in the seismic demand (β_D). Moreover, the dispersion (β_T) is assumed to be reduced by the application of the multi-scale approach for the definition of the different performance levels (§3.4).

$$\beta_G = \sqrt{\beta_C^2 + \beta_D^2} \tag{3.25}$$

Table 3.15 – Parameters obtained for all groups of models in the X direction for PL1

PL1		Action Type 1				Action Type 2			
Model	w	$PGA_{50\%}$ [m/s^2]	β_C	β_D	β_G	$PGA_{50\%}$ [m/s^2]	β_C	β_D	β_G
H-S-S-S-H	0.039	0.303	0.260	0.340	0.428	0.727	0.260	0.358	0.443
H-S-SH-T-T	0.070	0.373	0.235	0.336	0.410	0.894	0.235	0.449	0.506
H-I-S-S-H	0.078	0.275	0.272	0.337	0.433	0.659	0.272	0.430	0.509
H-I-SH-T-T	0.143	0.368	0.250	0.340	0.422	0.884	0.250	0.448	0.513
S-S-S-S-H	0.078	0.305	0.267	0.341	0.433	0.732	0.267	0.360	0.448
S-S-SH-T-T	0.143	0.380	0.295	0.337	0.448	0.918	0.297	0.438	0.529
S-I-S-S-H	0.159	0.283	0.283	0.339	0.442	0.680	0.283	0.406	0.495
S-I-SH-T-T	0.290	0.383	0.278	0.338	0.438	0.921	0.278	0.448	0.528

Table 3.16 – Parameters obtained for all groups of models in the X direction for PL2

PL2		Action Type 1				Action Type 2			
Model	w	$PGA_{50\%}$ [m/s^2]	β_C	β_D	β_G	$PGA_{50\%}$ [m/s^2]	β_C	β_D	β_G
H-S-S-S-H	0.039	0.608	0.068	0.336	0.343	1.460	0.068	0.437	0.442
H-S-SH-T-T	0.070	0.652	0.119	0.358	0.378	1.566	0.119	0.484	0.499
H-I-S-S-H	0.078	0.578	0.132	0.344	0.369	1.388	0.132	0.457	0.475
H-I-SH-T-T	0.143	0.643	0.120	0.372	0.391	1.543	0.120	0.483	0.498
S-S-S-S-H	0.078	0.620	0.089	0.337	0.349	1.489	0.089	0.433	0.442
S-S-SH-T-T	0.143	0.690	0.109	0.357	0.374	1.657	0.109	0.484	0.496
S-I-S-S-H	0.159	0.633	0.117	0.347	0.367	1.520	0.117	0.467	0.481
S-I-SH-T-T	0.290	0.674	0.131	0.380	0.402	1.618	0.131	0.483	0.501

Table 3.17 – Parameters obtained for all groups of models in the X direction for PL3

PL3		Action Type 1				Action Type 2			
Model	w	$PGA_{50\%}$ [m/s^2]	β_C	β_D	β_G	$PGA_{50\%}$ [m/s^2]	β_C	β_D	β_G
H-S-S-S-H	0.039	1.434	0.107	0.394	0.408	3.441	0.107	0.496	0.507
H-S-SH-T-T	0.070	1.496	0.192	0.418	0.460	3.590	0.192	0.524	0.559
H-I-S-S-H	0.078	1.916	0.194	0.449	0.489	4.576	0.190	0.575	0.606
H-I-SH-T-T	0.143	1.527	0.211	0.427	0.476	3.665	0.211	0.559	0.597
S-S-S-S-H	0.078	1.454	0.128	0.395	0.416	3.490	0.128	0.492	0.508
S-S-SH-T-T	0.143	1.424	0.188	0.418	0.458	3.425	0.187	0.513	0.546
S-I-S-S-H	0.159	2.134	0.148	0.446	0.471	5.121	0.148	0.591	0.609
S-I-SH-T-T	0.290	1.498	0.226	0.428	0.484	3.596	0.226	0.561	0.605

Table 3.18 – Parameters obtained for all groups of models in the X direction for PL4

PL4		Action Type 1				Action Type 2			
Model	w	$PGA_{50\%}$ [m/s^2]	β_C	β_D	β_G	$PGA_{50\%}$ [m/s^2]	β_C	β_D	β_G
H-S-S-S-H	0.039	1.855	0.125	0.446	0.464	4.452	0.125	0.545	0.559
H-S-SH-T-T	0.070	1.960	0.186	0.441	0.478	4.705	0.186	0.582	0.611
H-I-S-S-H	0.078	2.735	0.207	0.511	0.551	6.529	0.202	0.647	0.678
H-I-SH-T-T	0.143	1.988	0.193	0.439	0.480	4.770	0.193	0.600	0.631
S-S-S-S-H	0.078	1.843	0.135	0.438	0.458	4.423	0.135	0.535	0.551
S-S-SH-T-T	0.143	1.875	0.177	0.447	0.481	4.503	0.177	0.561	0.588
S-I-S-S-H	0.159	2.825	0.154	0.484	0.508	6.780	0.154	0.635	0.653
S-I-SH-T-T	0.290	1.945	0.193	0.440	0.481	4.668	0.193	0.597	0.627

Table 3.19 – Parameters obtained for all groups of models in the Y direction for PL1

PL1		Action Type 1				Action Type 2			
Model	w	$PGA_{50\%}$ [m/s^2]	β_C	β_D	β_G	$PGA_{50\%}$ [m/s^2]	β_C	β_D	β_G
H-S-S-S-H	0.039	0.379	0.087	0.275	0.289	0.889	0.070	0.346	0.353
H-S-SH-T-T	0.070	0.350	0.093	0.288	0.303	0.826	0.079	0.347	0.356
H-I-S-S-H	0.078	0.420	0.101	0.301	0.317	0.959	0.082	0.333	0.343
H-I-SH-T-T	0.143	0.419	0.100	0.301	0.317	0.946	0.067	0.338	0.344
S-S-S-S-H	0.078	0.407	0.138	0.279	0.311	0.942	0.136	0.346	0.371
S-S-SH-T-T	0.143	0.354	0.087	0.282	0.295	0.836	0.075	0.347	0.355
S-I-S-S-H	0.159	0.452	0.139	0.303	0.333	1.011	0.131	0.327	0.352
S-I-SH-T-T	0.290	0.410	0.085	0.319	0.330	0.938	0.057	0.331	0.336

Table 3.20 – Parameters obtained for all groups of models in the Y direction for PL2

PL2		Action Type 1				Action Type 2			
Model	w	$PGA_{50\%}$ [m/s^2]	β_C	β_D	β_G	$PGA_{50\%}$ [m/s^2]	β_C	β_D	β_G
H-S-S-S-H	0.039	0.650	0.048	0.284	0.288	1.533	0.034	0.347	0.348
H-S-SH-T-T	0.070	0.589	0.093	0.292	0.306	1.375	0.066	0.347	0.353
H-I-S-S-H	0.078	0.707	0.076	0.304	0.313	1.626	0.042	0.337	0.340
H-I-SH-T-T	0.143	0.701	0.092	0.301	0.314	1.570	0.039	0.339	0.341
S-S-S-S-H	0.078	0.683	0.099	0.273	0.290	1.574	0.063	0.347	0.353
S-S-SH-T-T	0.143	0.592	0.077	0.282	0.292	1.389	0.060	0.347	0.352
S-I-S-S-H	0.159	0.757	0.112	0.303	0.323	1.688	0.057	0.337	0.342
S-I-SH-T-T	0.290	0.687	0.090	0.319	0.331	1.560	0.045	0.335	0.338

Table 3.21 – Parameters obtained for all groups of models in the Y direction for PL3

PL3		Action Type 1				Action Type 2			
Model	w	$PGA_{50\%}$ [m/s^2]	β_C	β_D	β_G	$PGA_{50\%}$ [m/s^2]	β_C	β_D	β_G
H-S-S-S-H	0.039	1.371	0.061	0.314	0.320	3.267	0.064	0.346	0.352
H-S-SH-T-T	0.070	1.173	0.103	0.306	0.323	2.794	0.102	0.347	0.362
H-I-S-S-H	0.078	1.463	0.088	0.301	0.314	3.489	0.092	0.340	0.352
H-I-SH-T-T	0.143	1.363	0.085	0.292	0.305	3.230	0.088	0.341	0.353
S-S-S-S-H	0.078	1.317	0.124	0.320	0.343	3.128	0.128	0.347	0.370
S-S-SH-T-T	0.143	1.187	0.087	0.295	0.307	2.823	0.088	0.347	0.358
S-I-S-S-H	0.159	1.421	0.119	0.304	0.326	3.301	0.190	0.337	0.387
S-I-SH-T-T	0.290	1.342	0.077	0.319	0.328	3.157	0.083	0.335	0.346

Table 3.22 – Parameters obtained for all groups of models in the Y direction for PL4

PL4		Action Type 1				Action Type 2			
Model	w	$PGA_{50\%}$ [m/s^2]	β_C	β_D	β_G	$PGA_{50\%}$ [m/s^2]	β_C	β_D	β_G
H-S-S-S-H	0.039	1.544	0.064	0.329	0.336	3.706	0.065	0.346	0.352
H-S-SH-T-T	0.070	1.345	0.110	0.323	0.341	3.228	0.110	0.347	0.364
H-I-S-S-H	0.078	1.655	0.087	0.325	0.336	3.967	0.088	0.340	0.351
H-I-SH-T-T	0.143	1.569	0.090	0.322	0.335	3.766	0.090	0.341	0.353
S-S-S-S-H	0.078	1.495	0.104	0.331	0.347	3.585	0.106	0.347	0.363
S-S-SH-T-T	0.143	1.364	0.091	0.311	0.324	3.272	0.092	0.347	0.359
S-I-S-S-H	0.159	1.605	0.101	0.324	0.339	3.810	0.149	0.343	0.373
S-I-SH-T-T	0.290	1.535	0.084	0.319	0.330	3.678	0.086	0.335	0.346

Based on the values of $PGA_{50\%}$ and dispersion β_G, it is possible to derive the fragility functions considering only the global seismic behaviour. For this, it is proposed to define the minimum between the results obtained in the X and Y directions, as this leads to the most demanding condition for the block of buildings. Figure 3.46 exemplifies the fragility functions obtained for model H-S-S-S-H in the X and Y direction and the minimum combination between both (represented by the solid lines).

It is important to highlight that the resulting fragility functions are not a lognormal cumulative distribution function. The parameters that characterize the fragility functions are presented in Table 3.23 and Table 3.24, respectively for seismic action type 1 and type 2. Here, the dispersion β_G is determined in an approximated way according to Equation (3.26), taking into account the values of PGA corresponding to the 84% and 16% percentile of the distribution.

$$\beta_G = \frac{1}{2} \times \left| \log PGA_{84\%} - \log PGA_{16\%} \right| \tag{3.26}$$

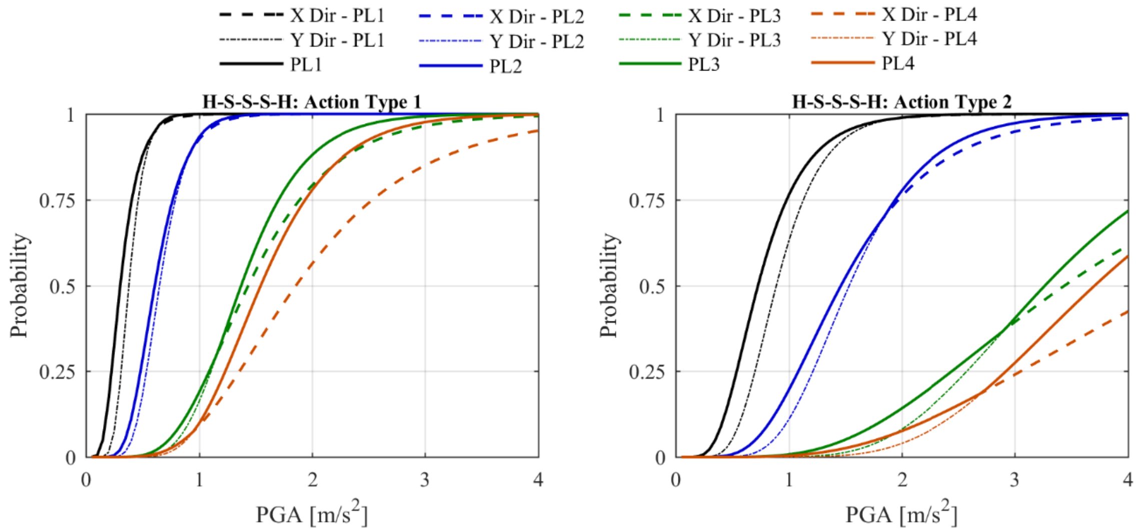

Figure 3.46 – Combination of the fragility functions obtained in the X and Y directions for the group of models H-S-S-S-H: seismic action type 1 (left) and type 2 (right)

Table 3.23 – Approximated parameters obtained for all groups of models from the combination of the fragility functions obtained in the X and Y directions: seismic action type 1

Action Type 1		PL1		PL2		PL3		PL4	
Model	w	$PGA_{50\%}$ [m/s^2]	β_G	$PGA_{50\%}$ [m/s^2]	β_G	$PGA_{50\%}$ [m/s^2]	β_G	$PGA_{50\%}$ [m/s^2]	β_G
H-S-S-S-H	0.039	0.303	0.426	0.608	0.342	1.371	0.340	1.544	0.334
H-S-SH-T-T	0.070	0.350	0.324	0.589	0.305	1.173	0.322	1.345	0.339
H-I-S-S-H	0.078	0.275	0.430	0.578	0.367	1.463	0.312	1.655	0.335
H-I-SH-T-T	0.143	0.368	0.419	0.643	0.389	1.363	0.332	1.569	0.333
S-S-S-S-H	0.078	0.305	0.431	0.620	0.347	1.317	0.341	1.495	0.345
S-S-SH-T-T	0.143	0.354	0.333	0.592	0.290	1.187	0.306	1.364	0.323
S-I-S-S-H	0.159	0.283	0.440	0.633	0.364	1.421	0.325	1.605	0.337
S-I-SH-T-T	0.290	0.383	0.415	0.674	0.374	1.342	0.349	1.535	0.328

Table 3.24 – Approximated parameters obtained for all groups of models from the combination of the fragility functions obtained in the X and Y directions: seismic action type 2

Action Type 2		PL1		PL2		PL3		PL4	
Model	w	$PGA_{50\%}$ [m/s^2]	β_G	$PGA_{50\%}$ [m/s^2]	β_G	$PGA_{50\%}$ [m/s^2]	β_G	$PGA_{50\%}$ [m/s^2]	β_G
H-S-S-S-H	0.039	0.727	0.441	1.460	0.418	3.267	0.401	3.706	0.361
H-S-SH-T-T	0.070	0.826	0.390	1.375	0.359	2.794	0.360	3.228	0.362
H-I-S-S-H	0.078	0.659	0.506	1.388	0.472	3.489	0.350	3.967	0.350
H-I-SH-T-T	0.143	0.884	0.460	1.543	0.426	3.230	0.410	3.766	0.373
S-S-S-S-H	0.078	0.732	0.445	1.489	0.421	3.128	0.383	3.585	0.360
S-S-SH-T-T	0.143	0.836	0.392	1.389	0.349	2.823	0.355	3.272	0.357
S-I-S-S-H	0.159	0.680	0.493	1.520	0.462	3.301	0.385	3.810	0.371
S-I-SH-T-T	0.290	0.921	0.438	1.560	0.399	3.157	0.407	3.678	0.365

Figure 3.47 compares, for the group of models H-S-S-S-H, the fragility functions resulting from the combination between X and Y direction and the approximated lognormal curve fitting in grey colour, putting in evidence the rough estimate in case of PL3 and PL4 with seismic action type 2.

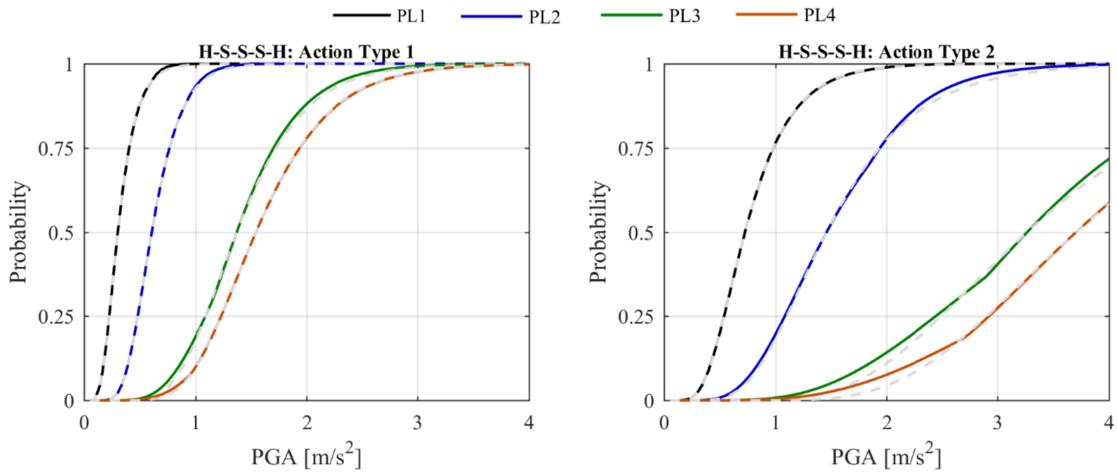

Figure 3.47 – Comparison of the fragility functions with the lognormal curve fitting in grey colour for model H-S-S-S-H: seismic action type 1 (left) and type 2 (right)

Based on the data from Table 3.23 and Table 3.24, it is possible to derive the fragility functions considering the global seismic behaviour of the URM buildings of type I by adding the contribution of the different groups of models as a function of their reliability/weight (w_j with j=1,…,8), according to Equation (3.27) and Equation (3.28). It is worth noting once more that these equations are approximated, in particular Equation (3.28). Table 3.25 summarizes the parameters for the fragility functions considering the global seismic behaviour of the typology and Figure 3.48 plot the corresponding functions for seismic action type 1 and type 2. It is clear that seismic action type 1 is the most demand case for this typology of URM buildings.

$$PGA_{50\%} = \sum_{j=1}^{8} w_j PGA_{50\%,j} \tag{3.27}$$

$$\beta_G = \sqrt{\sum_{j=1}^{8} w_j \beta_{G,j}^2} \tag{3.28}$$

Table 3.25 – Approximated parameters for the fragility functions considering the global seismic behaviour of the typology of buildings

Global Behaviour	Action Type 1		Action Type 2	
	$PGA_{50\%}$ [m/s^2]	β_G	$PGA_{50\%}$ [m/s^2]	β_G
PL1	0.341	0.406	0.816	0.447
PL2	0.631	0.356	1.491	0.413
PL3	1.332	0.331	3.145	0.387
PL4	1.520	0.332	3.638	0.364

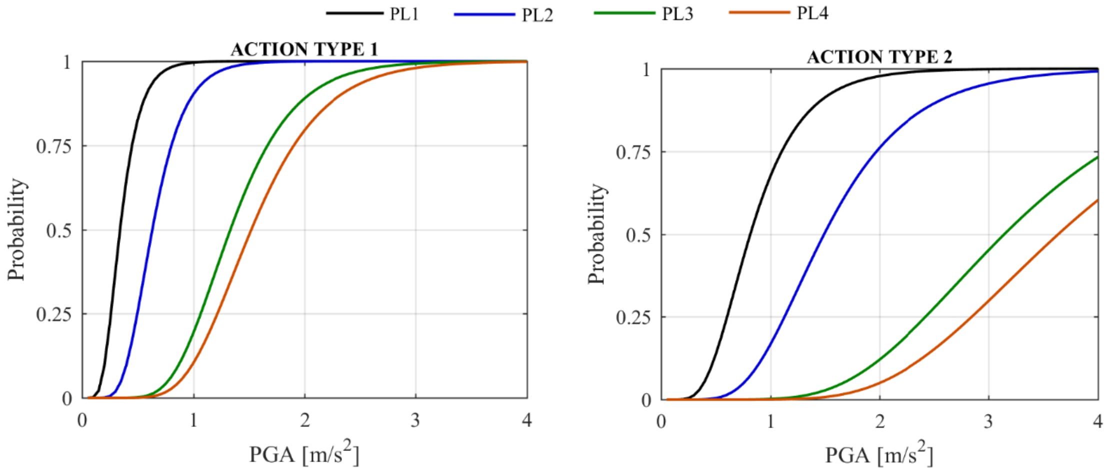

Figure 3.48 – Fragility functions considering the global seismic behaviour of the typology of buildings: seismic action type 1 (left) and type 2 (right)

Finally, the discrete probability associated with different damage state (P_{DSk}) is determined according to Equation (3.29) and Equation (3.30) for k=1,2 and 3 and considering a given value of PGA (pga):

$$P_{DSk}(pga) = P_{PLk}(pga) - P_{PLk+1}(pga) \tag{3.29}$$

$$P_{PLk}(pga) = \Phi\left(\frac{1}{\beta_{PLk}}\log\left(\frac{pga}{PGA_{50\%,PLk}}\right)\right) \tag{3.30}$$

In what concerns P_{DS4}, it is generically named as “complete” damage, including both DS4 – very heavy damage and DS5 – collapse according to the EMS-98 (Grünthal, 1998), resulting that P_{DS4}=P_{PL4}. This occurs because PL5 cannot be correctly captured by numerical analysis. However, by assuming that the discrete probability distribution (P_{DSk}) is well represented by the binomial distribution, as proposed by Lagomarsino and Cattari (2014), it is possible to divide P_{PL4} and define P_{DS5} and P_{DS4} according to Equation (3.31) and Equation (3.32), respectively.

$$P_{DS5}(pga) = 0.8\left[1-(1-0.14\mu_{DS}^{1.4})^{0.35}\right]P_{PL4}(pga) \tag{3.31}$$

$$P_{DS4}(pga) = P_{PL4}(pga) - P_{DS5}(pga) \tag{3.32}$$

In Equation (3.31), μ_{DS} is given by Equation (3.33):

$$\mu_{DS} = \sum_{k=1}^{4} P_{PLk} \tag{3.33}$$

The probability associated to the no damage state, P_{DS0}, is calculated according to Equation (3.34):

$$P_{DS0}(pga) = 1 - P_{PL1}(pga) = \Phi\left(\frac{1}{\beta_{PL1}}\log\left(\frac{pga}{PGA_{50\%,PL1}}\right)\right) \tag{3.34}$$

Based on the above mentioned, Figure 3.49 presents the probability damage distribution for the code seismic action for Lisbon (IPQ, 2017): type 1 (PGA = 1.94 m/s^2) and type 2 (PGA = 2.16 m/s^2). The results put in evidence the high seismic vulnerability of these URM buildings, particularly for seismic action type 1 – inter-plate earthquake. In this case, it is estimated that buildings of type I have about 50% probability of having very heavy damage (DS4) and more than 30% probability of collapse (DS5).

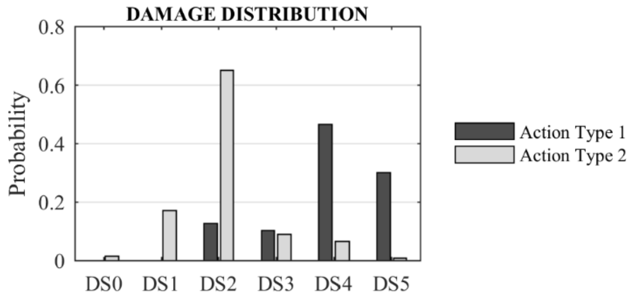

Damage Distribution	DS0	DS1	DS2	DS3	DS4	DS5
Action Type 1 PGA=1.94 m/s^2	0.000	0.001	0.128	0.104	0.467	0.301
Action Type 2 PGA=2.16 m/s^2	0.015	0.171	0.649	0.089	0.066	0.009

Figure 3.49 – Probability damage distribution considering the global seismic behaviour of the typology of buildings for seismic action type 1 (PGA=1.94 m/s^2) and type 2 (PGA=2.16 m/s^2)

3.6. Conclusion

The chapter is focused on the definition of a methodology for the analysis of the global seismic behaviour aiming to estimate the parameters for the derivation of the corresponding fragility functions. The seismic analysis was supported on non-linear static (pushover) analyses of different building models representative of the URM buildings of type I. The reference model is composed by three buildings in order to simulate the condition of the buildings constructed in aggregates.

The performance of preliminary non-linear static (pushover) analyses indicated that some building models present a similar response in terms of initial stiffness, strength and maximum displacement. Therefore, it was proposed to reduce the number of cases of study, identified by the logic-tree approach in the previous chapter, from 32 to 8 building models. Non-linear static (pushover) analyses were after carried out with a group of 1000 building models that combine the 8 building models with the various parameters assumed as aleatory variables.

The interval of values considered in this work for the different aleatory variables may be used for future studies regarding the assessment/retrofitting of URM buildings in Lisbon. Nevertheless, additional studies should be addressed for the characterization of the mechanical properties of masonry, deformability characteristics of masonry piers and spandrels, connection between walls and in-plane stiffness of timber floors. In what concerns the application of the Bayesian approach for the definition of the mechanical properties of masonry, one of the advantages is that in presence of new tests results, the interval of values proposed in this thesis are easily updated.

The selection of the load distributions to perform non-linear static (pushover) analyses is a critical issue. In this work two load distributions were considered: uniform and pseudo-triangular. In all cases, the pseudo-triangular distribution provided a pushover curve with lower initial stiffness and strength, and higher displacement capacity. It was also verified that the block of buildings has higher initial stiffness and strength in the direction of the side walls (Y direction) than in the direction of the façade walls (X direction). The comparison between non-linear static (pushover) analyses and non-linear dynamic analyses with time integration pointed that the behaviour of the block of buildings is better characterized by a pseudo-triangular distribution in the Y direction and by a uniform distribution in the X direction (however, this was less conclusive).

In contrast, the computation of the seismic intensity measure (here in terms of PGA) compatible with the different performance limit states, indicated that in general lower PGA values were obtained with the uniform distribution and that the Y direction is the most vulnerable direction of the structure. Thus, for the analysis of the global seismic behaviour of the URM buildings of type I it is important to consider at least both load distributions to perform non-linear static (pushover) analyses and determine the worst condition for the structure from the seismic performance-based assessment. Nevertheless, this is not a general result and thus, in other cases, it could be useful to assign a weight to PGA values obtained with the different load distributions and not to directly consider the worst case.

The variation of the PGA values, i.e. the dispersion in the determination of capacity of the block of buildings, is lower in the Y direction than in the X direction. In one hand, the seismic behaviour in the Y direction is mainly governed by the response of the side blind walls, while in the X direction the response is more influenced by the by the full set of aleatory variables considered: the mechanical properties of masonry, the deformability and strength characteristics of piers and spandrels, the properties of the interior timber “tabique” walls, the in-plane stiffness of timber floors and the quality of connections between walls (including some interactions with the Y direction in regards to the flange effect).

Moreover, the higher dispersion in the capacity obtained in the X direction may also be related to the criteria adopted for the definition of the performance limit states. Here, the multi-scale approach was considered in order to correlate the damage in the structure at different scales (element, macro-element and global). In this work, a new formulation for the macro-element scale verification was applied for the first time in an extensive way aiming to detect the occurrence of soft-storey mechanisms, but avoiding the drawback of defining conventional inter-storey drift thresholds. Such criterion revealed to be more effective in providing more accurate results for this typology of buildings.

Finally, the fragility functions associated with the global seismic behaviour of buildings of type I were derived considering the contribution of the dispersion in the capacity of the block of buildings and the dispersion in the determination of the seismic demand. The fragility functions and the probability distribution of damage put in evidence the high seismic vulnerability of the URM buildings of type I. Results for a seismic event, as defined in the earthquake-resistant code for Lisbon, indicate that these buildings have about 50% probability of having very heavy damage and about 30% probability of collapse. This highlights the need for the urgent structural intervention and for the design of retrofitting measures.

4. ANALYSIS OF THE LOCAL SEISMIC BEHAVIOUR

4.1. Introduction

URM buildings under seismic actions are particular prone to local failure modes related to the out-of-plane mechanism of façade walls insufficiently connected to the rest of the structure and standing out elements, such as gable walls, parapets and chimneys. Due to the negligible tensile strength of masonry and the slenderness of the elements, these can lose static equilibrium for very low values of PGA. The out-of-plane behaviour is mainly related to the geometric stability of the part of the structure involved in the mechanism rather than to the strength of materials. Damage observation after strong seismic events or shaking table tests, have also proved that the dynamic equilibrium is still possible after the activation of rocking (even for displacements close to the quasi-static limit equilibrium), suggesting the adoption of displacement-based approaches for the assessment of the out-of-plane behaviour instead of the traditional force-based approaches. On this, reference to the methodology proposed in the NTC (2008), latter developed and calibrated by Lagomarsino (2015) and Degli Abbati and Lagomarsino (2017), and the methodology proposed by the NZSEE Guidelines (2017), based on the work from Doherty et al. (2002). In Cattari et al. (2015) a comparison between these methodologies is presented.

In this work, the local seismic behaviour is analysed according to the displacement-based approach proposed by Lagomarsino (2015) aiming to define the seismic intensity measure compatible with specific performance limit states. The first step for the analysis comprehends the identification of the possible out-of-plane mechanisms in the URM buildings of type I. These are defined based on the geometry of the building, layout of openings, constructive details and restrains given by the structure. In this case, it is reasonable to consider the collapse involving only the upper level of the façade walls (Simões et al., 2014b). This hypothesis is also supported by experimental results from shaking table tests on reduced scale building models representative of the buildings under study, referred in §2.5. The reliability of each mechanisms is analysed as an epistemic uncertainty and treated through the logic-tree approach. In addition, as the out-of-plane behaviour is mainly related to the geometric stability rather than to the strength of materials, the geometry of the elements and the actions involved in the mechanisms are assumed as aleatory variables. These variables are treated by a full factorial combination in order to define the input parameters for the set of mechanisms.

The mechanisms are modelled according to the macro-block approach making use of MB-PERPETUATE program (Lagomarsino and Ottonelli, 2012). Non-linear kinematic analyses are performed to define the capacity of the mechanisms. The performance-based assessment comprehends the comparison between the displacement capacity of the mechanisms, identified for different performance limit states, and the seismic demand, expressed by a properly reduced acceleration-displacement response spectrum (ADRS). As the mechanisms under study are located in the upper level of the buildings, the seismic input is defined through a floor response spectrum that takes into account the dynamic filtering effect of the buildings. Moreover, in this work, the floor response spectrum is computed for each performance limit state based on an iterative procedure in order to consider the progressive damage in the building determined with the analysis of the global seismic behaviour (§3).

The values of the seismic intensity measure compatible with the attainment of the performance limit states are treated in order to derive the parameters for the definition of the fragility functions. This includes the determination of the dispersion related to the definition of the capacity of the mechanisms based on the Response Surface Method (Liel et al., 2009; Lagomarsino and Cattari, 2014), the dispersion related to the definition of the seismic demand and the dispersion related to the definition of the floor response spectrum. Finally, the fragility functions associated with the local seismic behaviour of the typology of buildings are presented and the damage distribution is estimated for different seismic scenarios.

4.2. Identification of local mechanisms and variations

The identification of possible local mechanisms is supported on the systematic damage observation in URM buildings after past earthquakes (D'Ayala and Paganoni, 2011; Penna et al., 2014) and from experimental tests on reduced scale models (Candeias, 2008; Lourenço et al., 2011). These vary as a function of the quality and strength of the connection between the façade walls and other elements of the structure, such as side walls, partition walls, floors and roof structure. In case specific measures have been implemented to prevent the simple overturning of the façade walls, for example with the introduction of tie-rods or ring beams at the floor level, out-of-plane mechanisms relying on arch effect (flexural mechanisms) may also occur. In addition, standing out elements (e.g. gable walls, parapets and chimneys) are very vulnerable to overturning even for low intensity seismic actions.

In what concerns the block of three buildings under study, it is reasonable to consider the collapse involving only the upper level of the façade walls, as proposed in a previous study about these buildings (Simões et al., 2014b). Although it is evident the whole façade is very slender (17 m height with decreasing thickness), there are many restrains that prevent the global overturning of the street façade wall, namely the connection to the side walls and the orientation of the timber floors perpendicular to the façade walls. The first restrain is also consistent with what was assumed for the analysis of the global seismic behaviour of the buildings, as these connections were modelled through link beams representing medium quality connections (§3.2.5). Concerning the second restrain, even if there are no specific connections between the timber floor joists and the façade wall, the friction originated in the contact surface is sufficient to prevent the global overturning of the façade. The hypothesis of limiting the out-of-plane behaviour to the last floor of the buildings is also supported by experimental evidence from shaking table tests on reduced scale models representing the buildings under study (Candeias, 2008; Mendes, Lourenço and Campos-Costa, 2014). On the other hand, these local mechanisms are more likely to occur on the street façade than on the rear façade due to the presence of the jack arch balconies with steel profiles.

After analysing the constructive details of the last floor (Figure 4.1), three out-of-plane mechanisms may be considered (Figure 4.2): the overturning of the central pier, with a plastic hinge at the base (Mech. 1), the flexural mechanism of the central pier, with a plastic hinge at the base and a plastic hinge separating the pier in two blocks (Mech. 2), and the overturning of the parapet, with a plastic hinge at the base (Mech. 3). The selection of these mechanisms is supported by the following motivations.

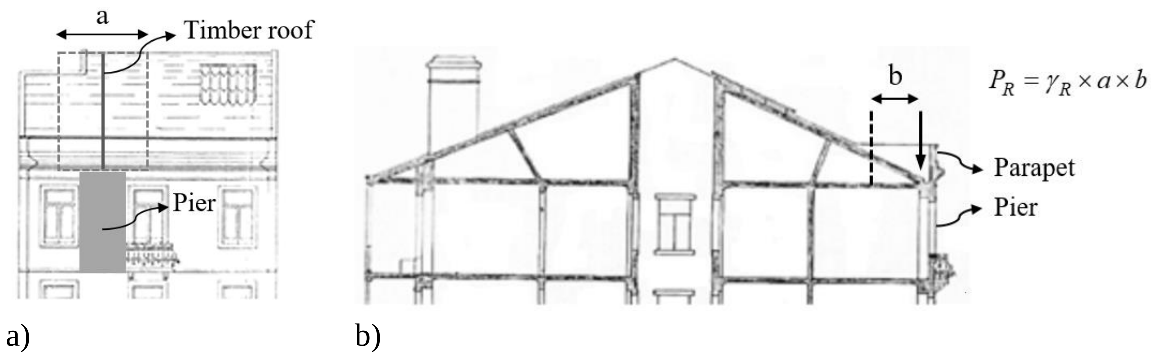

Figure 4.1 – View from the last floor of the buildings: a) street façade wall and b) section cut

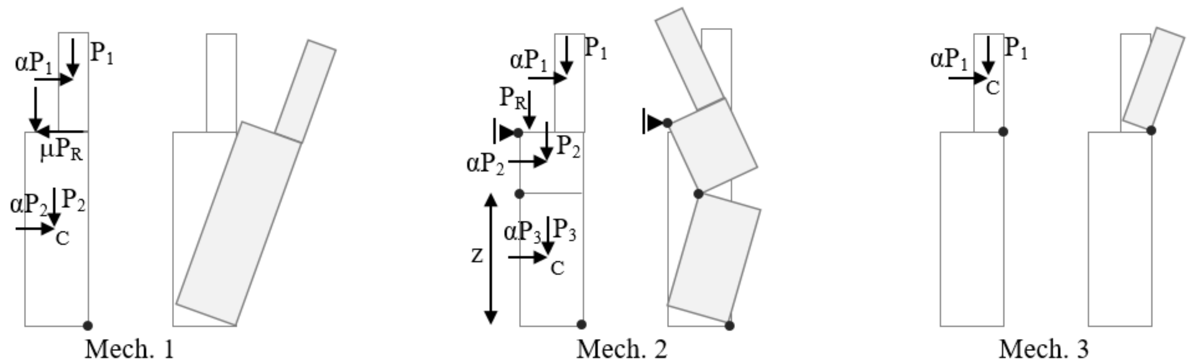

Figure 4.2 – Configuration and actions involved on the out-of-plane mechanisms: Mech. 1 – overturning of the central pier, Mech. 2 – flexural mechanism of the central pier and Mech. 3 – overturning of the parapet

Concerning Mech. 1, the two central piers (1.00 m length x 2.97 m height) are more vulnerable to overturning than the lateral piers (0.70 m length x 2.97 m height) as they are connected to the side walls. The lintels that link lateral and central piers are very slender elements and prone to rotate around a vertical axis with torsional sliding on the masonry joints (the friction contribution is close to zero because the vertical loads are low at this level). From the configuration of the street façade wall (Figure 4.1 a), the central piers have a door on one side and a window on the other; the possible restraint provided by the masonry panel below the window is neglected due to its lower thickness (0.27 m). Although one of the central piers has a perpendicular interior wall (Wall-10, Wall-17 and Wall-18 identified in Figure 3.1 a)), it is considered that the interlocking between interior and exterior walls is not effective. This assumption is also coherent with what was assumed in the analysis of the global seismic behaviour of the buildings, where these connections were modelled as weak (§3.2.5). The roof timber structure is placed perpendicular to the façade walls and aligned with the central piers (Figure 4.1). Assuming that the timber roof structure is connected to the interior walls and simply supported on the façade walls, in case of the overturning of the central piers, the timber elements will slide and unthread, transmitting a stabilizing horizontal force to the piers due to the friction originated in the contact surface. This force is equivalent to the vertical load transmitted by the roof to the piers (P_R) multiplied by the coefficient of friction (μ).

The development of Mech. 2 is supported on the hypothesis that the horizontal displacement on top of the central piers is restrained due to the effect of some strengthening solutions, such as the insertion of tie-rods connecting the central piers to the interior walls or the introduction of a light beam at the top of the wall (in order to provide flexural stiffness). In this scenario, the most likely mechanism is the flexural mechanism of the central piers (Mech. 2), as discussed by Griffith et al. (2004) and confirmed by the experimental results in Mendes et al. (2014).

Concerning Mech. 3, the overturning of the parapet may also occur, unless these elements are restrained, for example by the insertion of tie-rods connecting the parapets at the base or to the roof structure.

Figure 4.2 identifies the actions involved on the three mechanisms: P_1, P_2 and P_3 are, respectively, the parapet and central pier self-weight; P_R is the weight of the roof transmitted to the pier (determined according to Figure 4.1), this is applied at 1/3 of the support length of the timber structure on top of the pier; α is the coefficient proportional to the vertical loads (P_1, P_2 and P_3) that induces the loss of equilibrium of the system and activates the kinematism, denominated as the static seismic multiplier. The static seismic multiplier is determined by evaluating the work done by equilibrated forces on a set of compatible generalized virtual displacements by the application of the Principle of Virtual Works.

The occurrence of one or more mechanisms depends on the actual condition of the buildings, considering the possibility that they have been subjected or not to some strengthening intervention to prevent the simple overturning of the central piers and parapets. In this regards, the local behaviour of the buildings may be analysed by considering two different scenarios related to the out-of-plane mechanisms involving:

1. The last floor of the buildings, with the hypothesis of: i) simple overturning of the central piers (Mech. 1) or ii) flexural mechanism of the central piers (Mech. 2).

2. The parapet, with the hypothesis of: i) simple overturning (Mech. 3) or ii) no problem, in case some strengthening solution has been implemented to restrain the overturning or in case the building has no parapet.

Each scenario is assumed as an epistemic uncertainty and treated by the logic-tree approach, as presented in Figure 4.3. An expert judgement probability is attributed to each branch of the tree to quantify the reliability of the different options. In what concerns the first scenario, a lower probability is defined for Mech. 2 considering that the flexural mechanism only occurs in case some strengthening solution has been implemented. Thus, it is assumed that in 70% of the cases Mech. 1 may occur, while only in 30% of the cases Mech. 2 may occur. In what concerns the second scenario, also a lower probability is attributed to the case of having no problem. It is assumed that in 60% of the cases Mech. 3 may occur, while in 40% there is no problem. In this point, it is important to note that the overturning of the parapet to the street is relevant from the point of view of life safety, however from the point of view of the performance limit state of the main building, it represents the possible damage of a non-structural element.

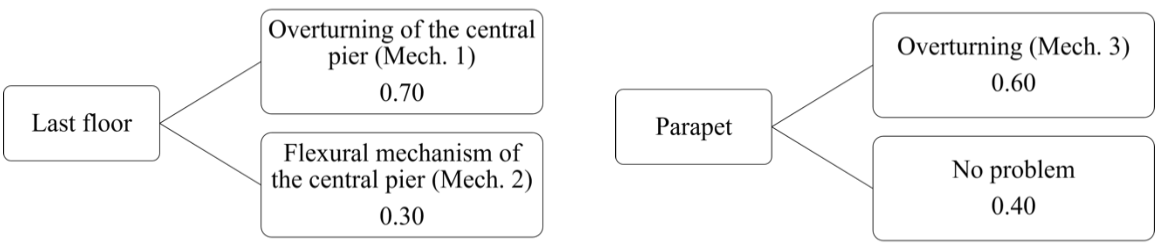

a) b)

Figure 4.3 – Local seismic behaviour of a) last floor of the building and b) parapet

In parallel to what was defined for the analysis of the global seismic behaviour, different parameters are considered as aleatory variables in order to take into account both the fact that some of these parameters are not well known and the intrinsic variability between buildings belonging to the same typology. In this case, the geometry of the blocks involved in the mechanisms and the value of the external forces applied define the aleatory variables. Although the geometry of the buildings was considered deterministic (§2.6), for the analysis of the local seismic behaviour, the thickness of the parapet ($t_{parapet}$) and the thickness of the central pier (t_{pier}) are considered aleatory variables as the behaviour of the mechanisms is mainly influenced by the geometry of the blocks. The external forces applied comprehend the weight of the roof transmitted to the pier (P_R) and the equivalent horizontal force (μP_R), i.e. the self-weight of the roof (γ_R) and the coefficient of friction (μ) are considered as aleatory variables. The lower, median and upper values of the four aleatory variables ($X_{k,low}$, $X_{k,med}$ and $X_{k,up}$, respectively) are summarized in Table 4.1. Next the main assumptions for the definition of these values are presented.

Table 4.1 – Characterization of the aleatory variables

Variables X_k	$X_{k,low}$	$X_{k,med}$	$X_{k,up}$
$t_{parapet}$ [m]	0.10	0.13	0.15
t_{pier} [m]	0.35	0.38	0.40
γ_R [kN/m2]	0.88	1.09	1.30
μ [-]	0.40	0.50	0.60

In the global model of the buildings, the street façade in the last floor was defined with 0.40 m of thickness (§2.6). Considering that the thickness of the façade walls decreases along the height, approximately 0.05 m in each floor, the same variation is now assumed for the thickness of the central pier (t_{pier}). In addition, in the global model of the buildings, the parapet was defined with 0.15 m of thickness and 0.80 m of height. In this case, the thickness of the parapet ($t_{parapet}$) is considered between 0.10 m and 0.15 m.

The self-weight of the roof (γ_R) is defined by the interval of values proposed by Ferreira and Farinha (1974). In the global model of the buildings, this was defined equal to 1.30 kN/m^2. The dimensions *a* and *b*, defining the area of influence of the timber roof structure supported on the central pier (Figure 4.1 a)), are assumed deterministic (a = 2.27 m and b = 3.90 m). The coefficient of friction (μ) between timber and masonry is defined from reference values in the literature. For instance, Farinha and Reis (1993) suggest between timber and masonry a coefficient of friction of 0.50 if the fibres are parallel to the motion, and 0.60 if perpendicular. Another reference is the coefficient of friction between timber and stone: equal to 0.40 according to Farinha and Reis (1993) and 0.50 determined from experimental works carried out by Zhang et al. (2008). The minimum and maximum of these values is adopted for the definition of the coefficient of friction.

The aleatory variables are treated by a full factorial combination at two levels. This option is linked to the subsequent application of the Response Surface Method for the definition of the dispersion in the determination of the capacity of the mechanism, discussed in §4.5.2. In this case, M=2^N models are defined, where N is the number of aleatory variables. In each model, the aleatory variables assume the values correspondent to the lower ($X_{k,low}$) and upper ($X_{k,up}$) values of the interval, in association to the 16% and 84% percentiles of the distribution, as defined for the analysis of the global seismic behaviour of the buildings.

Table 4.2 identifies the variables involved in the three out-of-plane mechanisms and the number of combinations/models considered for the analysis of the local seismic behaviour. A model in which all aleatory variables take the median values is also defined for each mechanism.

Table 4.2 – Combination of aleatory variables for each mechanism

Mech.	Variables X_k	N	2^N
1	$t_{parapet}$, t_{pier}, γ_R, μ	4	16
2	$t_{parapet}$, t_{pier}, γ_R	3	8
3	$t_{parapet}$	1	2

4.3. Non-linear incremental kinematic analyses and definition of the equivalent SDOF system

Non-linear incremental kinematic analysis is based on the assessment of the work done by equilibrated forces applied to the kinematism on a set of compatible generalized virtual displacements (Principle of Virtual Works) which are increased step-by-step in order to account for the geometric non-linearity of the system (Lagomarsino, 2015). Along this incremental kinematic analysis, the contribution of the restrains (e.g. the stabilizing contribution of the roof structure, the presence of tie-rods) is taken into account, till to the ultimate equilibrium condition.

The response of the mechanism is described by a curve that relates the static seismic multiplier (α) with the incremental horizontal displacement of a control node (d_C). This curve may be regarded as equivalent to the pushover curve obtained for the analysis of the global seismic behaviour of the buildings. This curve is then converted into the capacity curve of an equivalent SDOF system in analogy to the procedure described in §3.5.1, and assuming that each block is defined by lumped masses at their barycentre. Equation (4.1) and Equation (4.2) provide the definition of the capacity curve, respectively, in spectral acceleration (S_a) and displacement (S_d) coordinates.

$$S_a = \frac{g\alpha(d*)}{e*} \tag{4.1}$$

$$S_d = d* = d_C / \Gamma \tag{4.2}$$

In Equation (4.1), $e*$ is the rate of total mass that participates in the mechanism, defined as in Equation (4.3). The transformation factor (Γ) from Equation (4.2) is given by Equation (4.4).

$$e* = \frac{\left[\sum_{k=1}^{n_b}(W_k + Q_k)\delta_{Qx,k}\right]^2}{\left[\sum_{k=1}^{n_b}(W_k + Q_k)\right]\left[\sum_{k=1}^{n_b}(W_k + Q_k)\delta_{Qx,k}^2\right]} \tag{4.3}$$

$$\Gamma = \frac{\delta_{Cx}\sum_{k=1}^{n_b}(W_k + Q_k)\delta_{Qx,k}}{\sum_{k=1}^{n_b}(W_k + Q_k)\delta_{Qx,k}^2} \tag{4.4}$$

In the previous equations, n_b is the number of blocks (with k=1,…,n_b), W_k is the weight of block k plus the masses it carries during the activation of the kinematism, Q_k is the total weight of masses that are not carried by block k but are connected to it during the activation of the kinematism (e.g. the weight of the roof), $\delta_{Qx,k}$ is the virtual horizontal displacement of the barycenter of weights W_k and Q_k, assumed positive in the direction of the seismic action that activates the kinematism and δ_{Cx} is the horizontal component of the virtual displacement of the control node. In the examined mechanisms, the curve obtained with Mech. 3 corresponds directly to the capacity curve.

According to Doherty et al. (2002) and Lagomarsino (2015), an initial pseudo-elastic branch must be added to the capacity curve to describe the dynamic response of the considered part of the structure before the activation of the kinematism. This is based on the formulation of the bi-linear model in opposition to the model proposed by Housner (1963). The Housner model assumes that the dynamic behaviour of a single block under seismic excitation is supported on the hypothesis of rigid blocks and infinite compressive strength. It considers that horizontal displacements occur only after the activation of rocking. However, recent experimental tests on masonry panels clearly show small deformations before rocking as a result of the elastic deformability and the progressive formation of the hinge (Griffith et al., 2004; Candela et al., 2013). It has also been verified that after rocking activation, the behaviour is similar to that of the rigid block, with a linear descending branch due to the geometric non-linearity of the system (Doherty et al., 2002; de Felice, 2011; Candela et al., 2013).

The bi-linear model is assumed as reference because it is closer to the actual behaviour before rocking and produces overturning conditions similar to those obtained by the Housner model. The bi-linear model is defined by two distinct periods: the elastic period of the equivalent SDOF (T_e) and the secant period (T_s). In this case, the capacity curve is expressed according to Equation (4.5):

$$S_a(d^*)=\begin{cases} \dfrac{4\pi^2}{T_e^2}d^* & d^*\le d_e \\ \dfrac{4\pi^2}{T_e^2\left(1-d_e/d_s\right)}d_e\left[1-\dfrac{d}{d_s}-\dfrac{T_e^2}{T_s^2}\left(1-\dfrac{d^*}{d_s}\right)\right] & d_e<d^*<d_s \\ \dfrac{g\cdot\alpha(d^*)}{e^*} & d^*\ge d_s \end{cases} \tag{4.5}$$

where, d_e and d_s are, respectively, the displacements corresponding to T_e and T_s. In this work, the elastic period (T_e) is calculated by approximation to the period of a cantilever beam (first mode for Mech. 1 and Mech. 3 and second mode for Mech. 2). The secant period (T_s) is estimated assuming that the secant stiffness is 50% of the elastic stiffness. The secant displacement is obtained by the intersection with the descending branch of the capacity curve, defining the point of rocking activation.

MB-PERPETUATE program is adopted in this work to perform the non-linear incremental kinematic analysis of the three mechanisms and variations considered, taking into account the dynamic behaviour of the system and the contribution of the restrains (internal and external). The program provides an accurate evaluation of all masses involved in the mechanism, particularly important in presence of multiple blocks (as the case of Mech. 1 and Mech. 2), and verifies further compatibility conditions in order to prevent not admissible kinematic configurations. The control node (C) considered for each mechanism is identified in Figure 4.2. Table 4.3 presents the static seismic multiplier (α) for the initial configuration of the mechanism, in terms of median value (α_{med}) and coefficient of variation (CoV) of the models defined by the full factorial analyses.

Table 4.3 – Static seismic multiplier

Mech.	α_{med}	CoV [%]
1	0.551	22.0
2	0.751	8.1
3	0.156	20.0

In what concerns Mech. 2, the height of the hinge (z) that divides the central pier in two blocks (Figure 4.2), was calculated in order to minimize the static seismic multiplier for each of the models considered. Mech. 3 involving the overturning of the parapet has the lowest static load multiplier as it is the mechanisms with lower gravity loads involved. Figure 4.4 plots the capacity curves for the three mechanisms considered, including the models defined by the full factorial analyses and the model defined by the median properties of the aleatory variables.

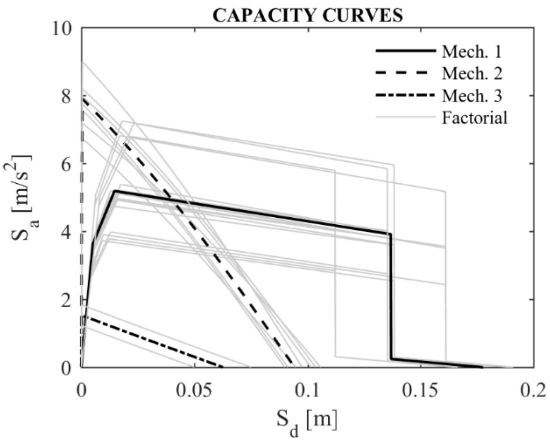

Figure 4.4 – Capacity curves for the three mechanisms

In Mech. 1, the sudden decay of strength after 0.11 m displacement is consequence of the complete unthreading of the roof timber structure. The strength variation obtained with the different models is related to the variation of the coefficient of friction, while the variation of the displacement corresponding to the unthreading of the roof timber structure is related to the variation of the thickness of the pier, and consequently to the support length of the roof on top of the pier. It is also verified that the strength of Mech. 2 is higher than that of Mech. 1, but it is characterized by a lower displacement capacity. Mech. 3, which only involves the parapet, is the most critical mechanism as it exhibits the lowest strength and displacement capacity due to the reduced thickness of the element.

The equivalent SDOF system is defined in addition by the equivalent viscous damping (ξ). This is determined according to Equation (4.6) by taking the contribution of both the initial elastic viscous damping (ξ_{el}) and the hysteretic damping (ξ_{hyst}), considering that damping increases as the mechanism develops due to local non-linear effects in masonry (elasto-plastic and/or friction connections).

$$\xi(d^*) = \begin{cases} \xi_{el} & d^* \leq d_e \\ \xi_{el} + \xi_{hyst}\left(1 - \dfrac{d_e}{d^*}\right) & d^* > d_e \end{cases} \tag{4.6}$$

The initial elastic viscous damping (ξ_{el}) is assumed equal to 5% and the hysteretic damping (ξ_{hyst}) equal to 7% following experimental results (Lagomarsino, 2015; Degli Abbati and Lagomarsino, 2017).

4.4. Definition of performance limit states

Four performance levels are defined in correspondence to the limits considered for the analysis of the global seismic behaviour of the buildings (PLk, with k=1,…,4) and assuming a direct relation to damage levels (DLk, with k=1,…,4). The evaluation of damage levels for rocking structures is not an easy task due to the progressive increase of damage. The displacement thresholds proposed by Lagomarsino (2015) based on a wide parametric incremental dynamic analysis on rigid blocks are adopted in this work and defined directly on the capacity curve of the mechanism. The displacement thresholds associated with DL1 and DL2 are coincident, respectively, with the limit of the elastic behaviour ($d_{DL1} = d_e$) and the point of rocking activation ($d_{DL2} = d_s$). DL3 and DL4 are defined as a function of displacement where the capacity curve is zero (d_0), point in which overturning occurs. The displacement associated with DL4 (d_{DL4}) is assumed equal to $0.4d_0$, in order to be coherent with the definition of near collapse limit state. As to DL3, it is assumed before DL4 ($d_{DL3} = 0.25d_0$) and after checking that no failure of important connections occurs (e.g. unthreading of rafters or beams). Figure 4.5 presents the position of the DLk in the capacity curves for the mechanisms defined by the median properties of the aleatory variables. Table 4.4 provides the corresponding spectral acceleration (S_a – Equation (4.1)), spectral displacement (S_d – Equation (4.2)) and period (T^* – Equation (3.24)).

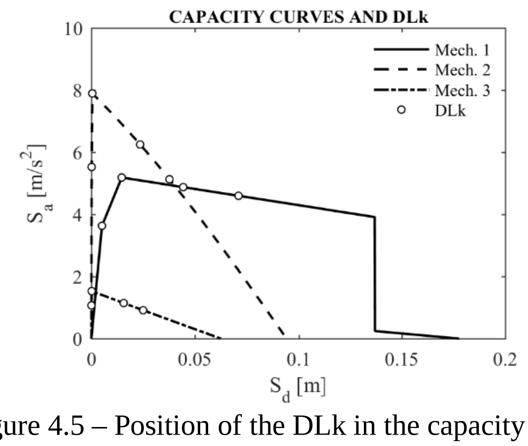

Figure 4.5 – Position of the DLk in the capacity curves

Table 4.4 – Position of the DLk in the capacity curves: spectral displacement (S_d), spectral acceleration (S_a) and period (T^*)

Capacity Curve	Mech. 1			Mech. 2			Mech. 3		
	S_d [m]	S_a [m/s^2]	T^* [s]	S_d [m]	S_a [m/s^2]	T^* [s]	S_d [m]	S_a [m/s^2]	T^* [s]
DL1	0.0051	3.630	0.236	0.0002	5.526	0.034	0.0001	1.070	0.047
DL2	0.0146	5.186	0.334	0.0005	7.894	0.048	0.0002	1.529	0.066
DL3	0.0443	4.876	0.599	0.0235	6.250	0.385	0.0156	1.144	0.734
DL4	0.0710	4.598	0.781	0.0377	5.130	0.538	0.0250	0.913	1.039

4.5. Definition of the seismic intensity measure and dispersion

4.5.1. Procedure for the computation of the seismic intensity measure

As referred for the analysis of the global seismic behaviour, in this thesis, the seismic intensity measure is represented by the PGA values that produces the attainment of specified performance limit states defined in terms of displacement thresholds. The procedure presented in §3.5.1 based on the Capacity-Spectrum Method with over-damped spectrum is also adopted in this case. Step 1 and Step 2 regarding the definition of the equivalent non-linear SDOF system were already discussed in §4.3. In what concerns Step 3, regarding the definition of the seismic demand, as the local mechanisms under study are located in the upper part of the buildings, the seismic input should be defined through a floor response spectrum that takes into account the dynamic filtering effect of the building.

There are different formulations available in literature and codes for the evaluation of the floor response spectrum. However, these are usually related to the seismic verification or design of secondary systems in terms of forces. The Commentary to the NTC (MIT, 2009) proposes the definition of a floor response spectrum specifically addressed to the verification, in terms of displacements, of local mechanisms located in the upper part of the buildings. This formulation has been improved by Degli Abbati et al. (2017) in order to take into account the input response spectrum at the base of the structure and the dynamic parameters of all the relevant modes of the main structure. This improved formulation is adopted in this work, as presented in the following.

The computation of the acceleration response spectrum at position Z of the main structure, where the mechanism of period T and equivalent viscous damping ξ is located, is given by Equation (4.7):

$$S_{aZ}(T,\xi) = \max\left[S_a(T,\xi)\cdot\eta(\xi) \quad ; \quad \sqrt{\sum_{k=1}^{N} S_{aZ,k}^2(T,\xi)} \right] \tag{4.7}$$

where $S_a(T,\xi)$ is the ground motion response spectrum, η is the damping correction factor defined by Equation (3.21), $S_{aZ,k}(T,\xi)$ is the acceleration response spectrum at position Z due to kth mode of the N modes of the main structure considered, defined according to Equation (4.8):

$$S_{aZ,k}(T,\xi)=\begin{cases}\dfrac{f_k\cdot\eta(\xi)\cdot PFA_{Z,k}}{1+\left[f_k\cdot\eta(\xi)-1\right]\cdot\left(1-\dfrac{T}{T_k}\right)^{1.6}} & T\le T_k\\ \dfrac{f_k\cdot\eta(\xi)\cdot PFA_{Z,k}}{1+\left[f_k\cdot\eta(\xi)-1\right]\cdot\left(\dfrac{T}{T_k}-1\right)^{1.2}} & T>T_k\end{cases} \tag{4.8}$$

where $PFA_{Z,k}$ is the peak floor acceleration defined by Equation (4.9), f_k is the factor of amplification of $PFA_{Z,k}$ that gives the peak of the floor acceleration response spectrum at the period T_k of the main structure defined by Equation (4.10).

$$PFA_{Z,k}=S_a(T_k)\cdot\eta(\xi_k)\cdot\left|\gamma_k\cdot\psi(x,y,z)\right|\cdot\sqrt{1+4\xi_k^2} \tag{4.9}$$

$$f_k=\xi_k^{-0.6} \tag{4.10}$$

In Equation (4.9), $S_a(T_k)$ is the acceleration of the ground motion at period T_k of the main structure, ξ_k is the equivalent viscous damping of the main structure, γ_k and $\psi_k(x,y,z)$ are the modal participation coefficient and the modal shape of mode *k*.

In this work, different floor response spectra are evaluated in order to consider the dynamic properties of the 8 building models defining the final cases of study (here the models defined by the median properties of the aleatory variables, §3.3.2, are considered) and the contribution of the first modes corresponding to the translation of the structure in the Y direction (Annex A). The modal participation coefficient (γ_k) is calculated according to Equation (4.11), taking into account the modal mass (m_i) and displacement (Φ_i) mobilized in the k^{th} mode in each node *i* of the main structure. The modal shape ($\psi_k(x,y,z)$) of mode *k* is evaluated after the normalization to the maximum horizontal displacement of the main structure.

$$\gamma_k=\frac{\sum m_i\Phi_i}{\sum m_i\Phi_i^2} \tag{4.11}$$

In addition, different floor response spectra are evaluated for Mech. 1 and Mech. 2, located at the base of the last floor of the building (Z=14 m), and for Mech. 3, located at the top of the last floor (Z=17 m). Figure 4.6 exemplifies the evaluation of the floor response spectra taking into account the filtering effect of model H-S-S-S-H. The floor response spectra are defined taking the contribution of mode 5 (T=0.522 s, M_Y=66.6%) and mode 6 (T=0.472 s, M_Y=16.3%). Figure 4.6 a) compares the ground response spectrum for seismic action type 1 (S_a) with the floor response spectrum (S_{aZ}) at the base of the last floor (Z=14 m) due to the contribution of mode 5 ($S_{aZ,5}$) and mode 6 ($S_{aZ,6}$), as defined in Equation (4.7). It is visible that, in this case, mode 5 has the main contribution to the floor response spectrum.

Figure 4.6 b) compares the ground response spectrum for seismic action type 1 (S_a) with the floor response spectrum (S_{aZ}) defined at the base (Z=14 m) and at the top of the last floor (Z=17 m).

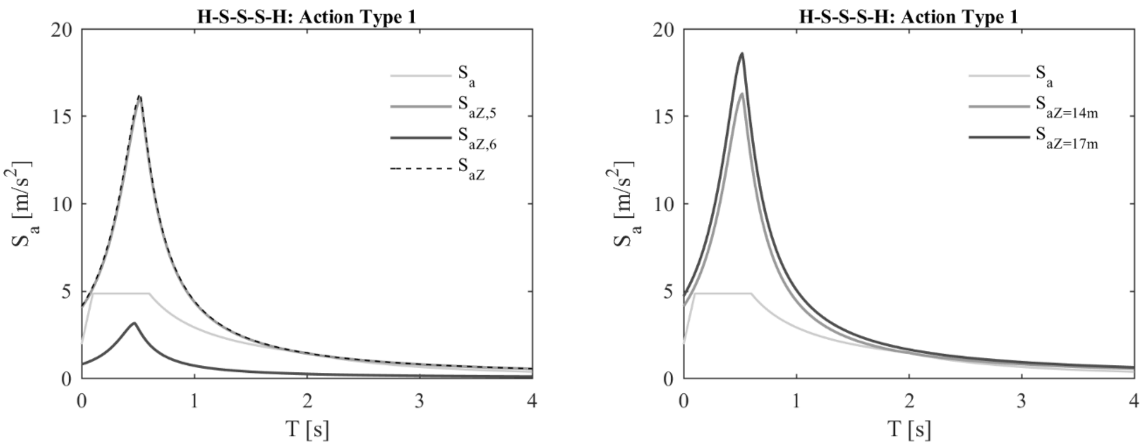

a) b)

Figure 4.6 – Evaluation of the floor response spectra for model H-S-S-S-H: a) comparison between the ground response spectrum for seismic action type 1 and the floor response spectrum at the base of the last floor (Z=14 m), and b) comparison between the ground response spectrum and the floor response spectrum at the base of the last floor (Z=14 m) and at the top of the last floor (Z=17 m)

In the previous example, the modified response spectra are defined starting from the period T_k of the main structure, obtained from the modal analysis, and by considering: 1) the equivalent viscous damping of the main structure (ξ_k) equal to 10%, to account the expected damage in the building, and 2) the equivalent viscous damping of the mechanism (ξ) equal to 5% (i.e. by excluding the hysteric contribution). This sets the initial parameters to define the over-damped floor response spectra. Indeed, the over-damped floor response spectrum has to be updated through an iterative procedure in order to consider the interaction effects between the non-linear behaviour of the main structure and the non-linear behaviour of the mechanism.

This iterative procedure aims to guarantee coherence between the damping properties at the global and local scales and to establish a limit for the seismic verification at the local scale taking into account the progression of damage at the global scale. A similar verification procedure has been applied for the seismic out-of-plane assessment of Podestà Palace in Mantua (Italy) carried out by Degli Abbati et al. (2014). To this end, an over-damped floor response spectrum has been computed for each PLk according to the following steps: 1) definition of the period of the main structure ($T_{k,PLk}$) based on the results from the non-linear static (pushover) analyses of the building on the negative Y direction (§3.3.2) and corresponding equivalent viscous damping ($\xi_{k,PLk}$) in order to account for the progressing non-linear response of the building, 2) definition of the floor response spectrum, 3) determination of the maximum PGA compatible with each PLk from the comparison between the capacity curve of the mechanism and the floor response spectrum, 4) comparison of the maximum PGA compatible with each PLk at the local scale with the corresponding PGA at the global scale: a) if $PGA_{PLk,Local} > PGA_{PLk,Global}$, then the seismic verification at the global scale prevails (i.e. the building is no longer usable, even if the mechanism is verified), b) if $PGA_{PLk,Local} \leq PGA_{PLk,Global}$, then update $T_{k,PLk}$ and $\xi_{k,PLk}$ and repeat points 2) to 4) until the process converges. This iterative procedure to compute the over-damped floor response spectrum associated with each PLk is computed for the 8 building models, defined by the median properties of the aleatory variables.

4.5.2. Determination of the median intensity measure and dispersion in the capacity

The procedure for the computation of the PGA values that produces the attainment of the PLk, is applied with the different mechanisms defined from the full factorial combinations (Mech. 1 – 16 models, Mech. 2 – 8 models and Mech. 3 – 2 models), considering seismic demand defined by the code elastic response spectrum for Lisbon (zone 3) and soil type B (IPQ, 2010): action type 1 (PGA=1.50 m/s^2 and S=1.29) and type 2 (PGA=1.70 m/s^2 and S=1.27). A total of 32 groups of floor response spectra are defined in order to analyse the seismic behaviour of Mech. 1 and Mech. 2, located at the base of the last floor (Z=14 m), and Mech. 3, located at the top of the last floor (Z=17 m), and to consider the seismic input compatible with seismic action type 1 and type 2, in addition to the filtering effect of the 8 building models defined by the median properties of the aleatory variables. The corresponding PGA values are treated with the final objective of determining the parameters for the derivation of the fragility functions. The following steps are considered:

1. Calculation of the median value of the PGA ($PGA_{50\%}$) obtained for the PLk for each of the three groups of mechanisms and for the 8 building models.
2. Calculation of the dispersion (β_C) in the definition of the capacity of each mechanism by the application of the Response Surface Method (Liel et al., 2009; Lagomarsino and Cattari, 2014).

The option for the full factorial combination of the aleatory variables and the subsequent application of the Response Surface Method for the evaluation of the dispersion in the capacity (β_C), in contrast with the Monte Carlo Method considered for the analysis of the global seismic behaviour (§3.5.2), is justified by the simplicity of the analysis of the local mechanisms and by the lower number of aleatory variables considered. The Response Surface Method is based on the approximation of the hyperplane that fits the response surface of the variable log($PGA_{50\%}$) in the hyperspace of the normalized variables representing the aleatory variables considered. The angular coefficients (β_{Ci}) defining the hyperplane are determined according to Equation (4.12):

$$\beta_{Ci} = \left(Z^T Z\right)^{-1} Z^T Y \tag{4.12}$$

where, Z is a matrix, with M rows x N columns (where M=2^N is the number of models defined by the full factorial combination (§4.2) and N is the number of aleatory variables), which collects in each row the corresponding normalized variables (equal to -1 for $X_{k,low}$ and +1 for $X_{k,up}$) and Y is a vector, with M rows, which collects in each row the corresponding log($PGA_{50\%}$) values. The dispersion (β_C) in the definition of the capacity of each mechanism is given by Equation (4.13):

$$\beta_C = \sqrt{\beta_{Ci}^T \cdot \beta_{Ci}} \tag{4.13}$$

Figure 4.7 plots the corresponding $PGA_{50\%}$ values for Mech. 1, Mech. 2 and Mech. 3 obtained with the 8 building models by considering seismic action type 1 and type 2. Mech. 3 is the most vulnerable case, followed by Mech. 1 and Mech. 2. Here, only the results concerning the attainment of PL1 and PL2 are presented provided that PL3 and PL4 are coincident with PL2 (i.e. the PGA values compatible with PL2, PL3 and PL4 are the same). This is justified because the attainment of PL2 corresponds to the final equilibrium condition of the mechanisms. In addition, it is observed that the same values of PGA are obtained for Mech. 2 with seismic action type 1 and type 2, and practically the same for Mech. 3. This is related to the fact that the secant periods associated with the attainment of PL1 and PL2 are very short (see Table 4.4).

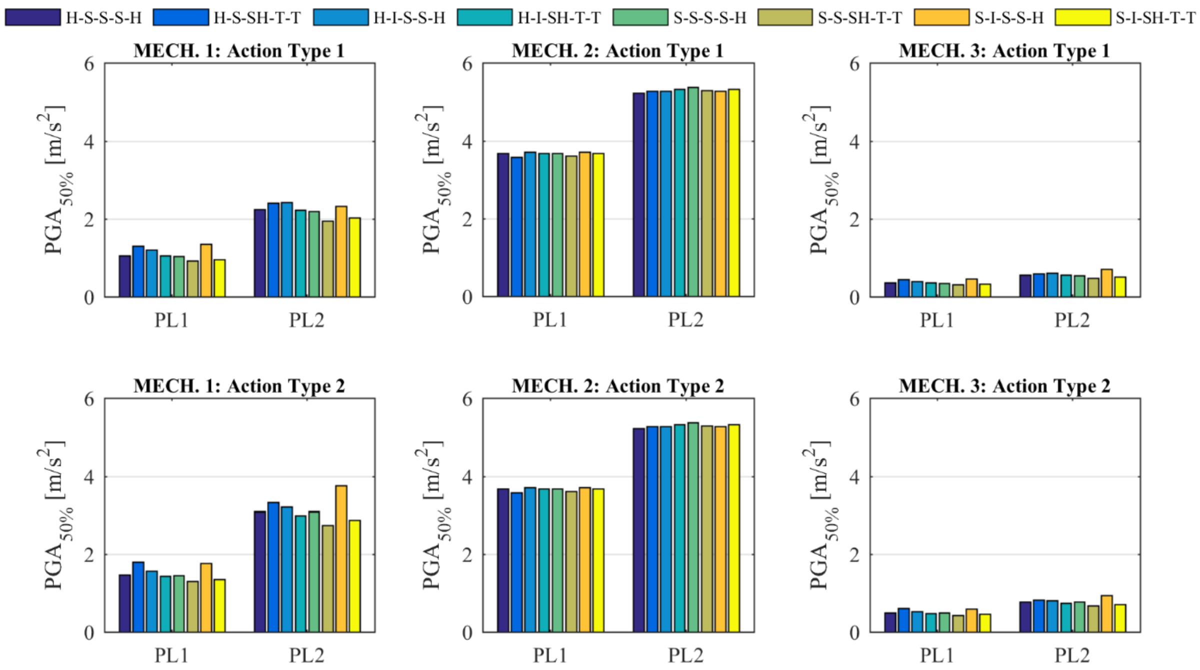

Figure 4.7 – Median values of PGA for Mech. 1, Mech. 2 and Mech. 3 obtained with the 8 building models: seismic action type 1 and type 2

Figure 4.8 presents the contribution of each aleatory variable for the dispersion in the capacity, meaning the angular coefficients (β_{Ci}) or partial dispersion, exemplified for model H-S-S-S-H. It is visible that the self-weight of the roof (γ_R) and the coefficient of friction (μ) are the parameters that have higher contribution to the variability of Mech. 1. For Mech. 2 the contribution of the three aleatory variables is similar. In case of Mech. 3, the partial dispersion (β_{Ci}) coincides with the dispersion in the capacity (β_C). In §4.1, it was referred that the out-of-plane behaviour is mainly related to the geometric stability of the part of the structure involved in the mechanism rather than to the strength of materials. From these results, it is also visible that the actions involved in the mechanisms also have an important role. Figure 4.9 plot the dispersion in the capacity (β_C) for Mech. 1, Mech. 2 and Mech. 3 obtained with the 8 building models by considering seismic action type 1 and type 2. It is observed that Mech. 2 presents the lowest dispersion from all. This is also related to the fact that the secant periods associated with the attainment of PL1 and PL2 are very short.

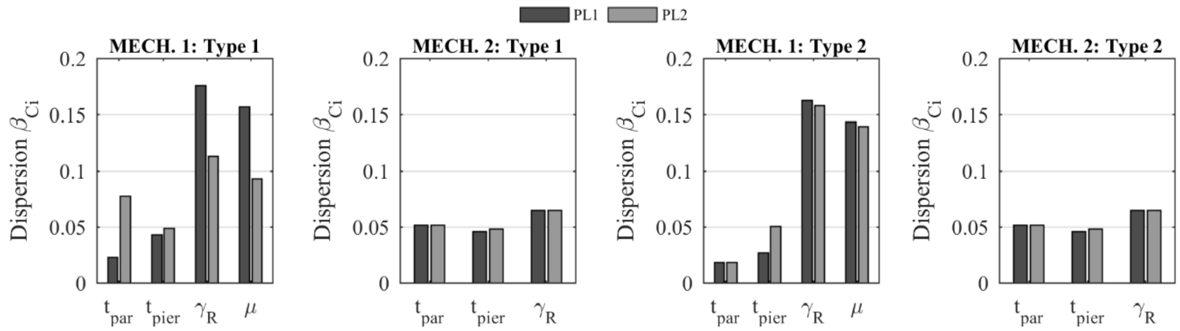

Figure 4.8 – Partial dispersion (β_{Ci}) for Mech. 1 and Mech. 2 obtained with model H-S-S-S-H: seismic action type 1 and type 2

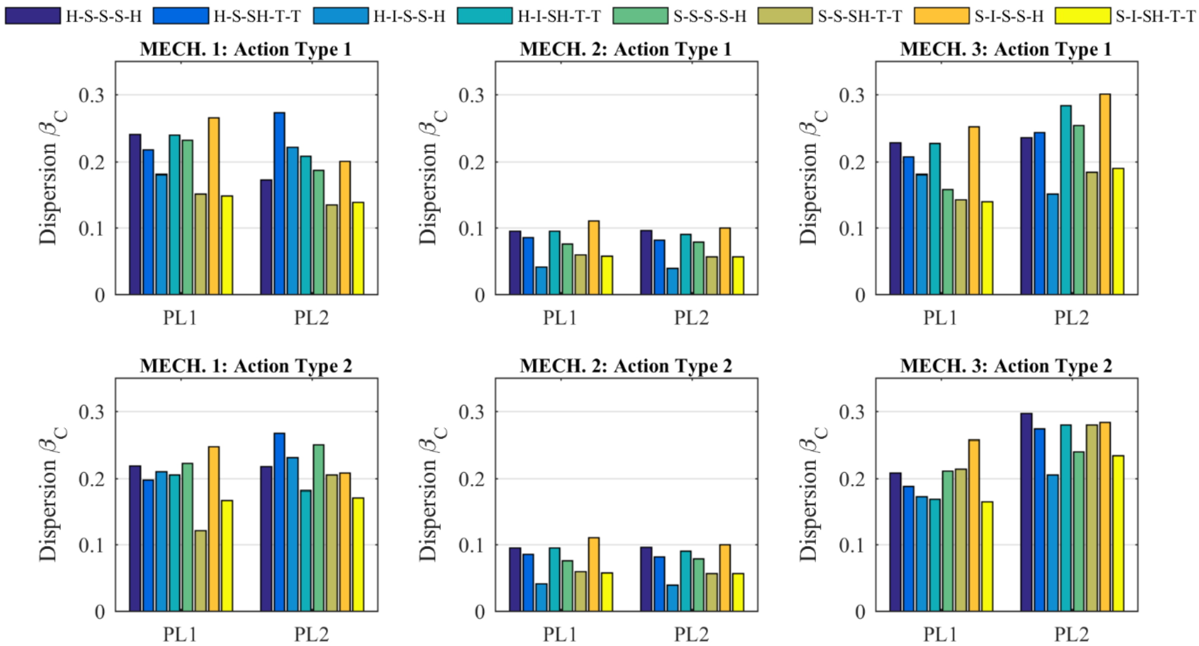

Figure 4.9 – Dispersion in the capacity (β_C) for Mech. 1, Mech. 2 and Mech. 3 obtained with the 8 building models: seismic action type 1 and type 2

4.5.3. Determination of the dispersion in the seismic demand

The dispersion in the seismic demand (β_D) is related to the variability of the seismic input. This is estimated according to Equation (3.24), as presented for the analysis of the global seismic behaviour, by considering as seismic input, the response spectra corresponding to the 84% and 16% percentiles of the set of 30 records compatible with the code seismic action type 1 and type 2. The $PGA_{84\%}$ and $PGA_{16\%}$ values that produces the attainment of the PLk are determined with each mechanism, defined by the median properties of the aleatory variables, and by applying the iterative procedure to define the modified floor response spectrum, as referred in §4.5.1. Figure 4.10 presents the dispersion in the seismic demand (β_D) obtained with the 8 building models by considering seismic action type 1 and type 2. These results are in general higher than the ones obtained with the analysis of the global seismic behaviour for PL1 and PL2 because they also take into account the filtering effect of the building.

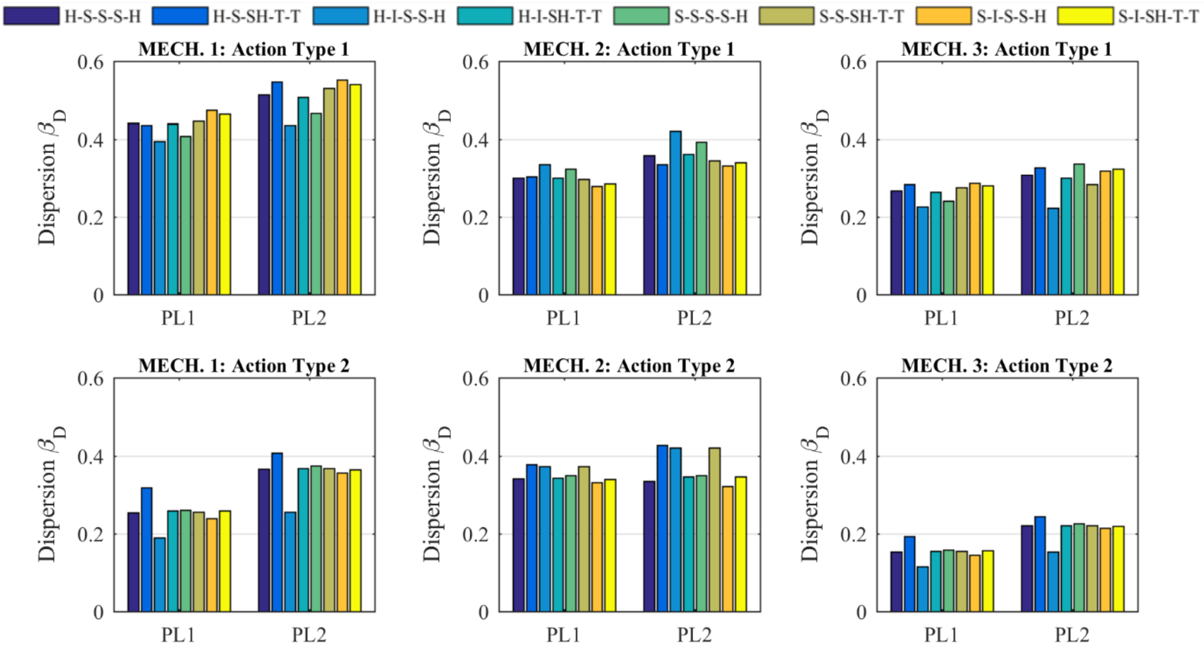

Figure 4.10 – Dispersion in the seismic demand (β_D) for Mech. 1, Mech. 2 and Mech. 3 obtained with the 8 building models: seismic action type 1 and type 2

For the definition of the fragility functions, an additional contribution to the dispersion needs to be considered to take into account the uncertainties in the determination of the dynamic characteristics of the main structure that influence the filtering effect and the determination of the floor response spectrum. This additional contribution is referred here as the dispersion in the floor response spectrum (β_{FS}). This dispersion is also estimated according to Equation (3.24). The $PGA_{84\%}$ and $PGA_{16\%}$ values that produces the attainment of the PLk are determined by considering each mechanism, defined by the median properties of the aleatory variables, and by applying the iterative procedure to define the floor response spectrum, as referred in §4.5.1. However, in this case, the period of the main structure ($T_{k,PLk}$) and the PGA value compatible with the PLk at the global scale ($PGA_{PLk,Global}$), are defined as the values corresponding to the 84% and 16% percentiles of the 8 groups of building models.

Figure 4.11 shows the dispersion in the floor spectrum (β_{FS}) obtained by considering seismic action type 1 and type 2. In case of Mech. 1, the dispersion for PL2 is higher than the dispersion for PL1 because to activate the mechanism a higher value of PGA was necessary (Figure 4.7). On the other hand, the dispersion in the floor spectrum associated with Mech. 2 is zero and for Mech. 3 is close to zero, because the computation of the PGA is almost not affected by the filtering effect of the building.

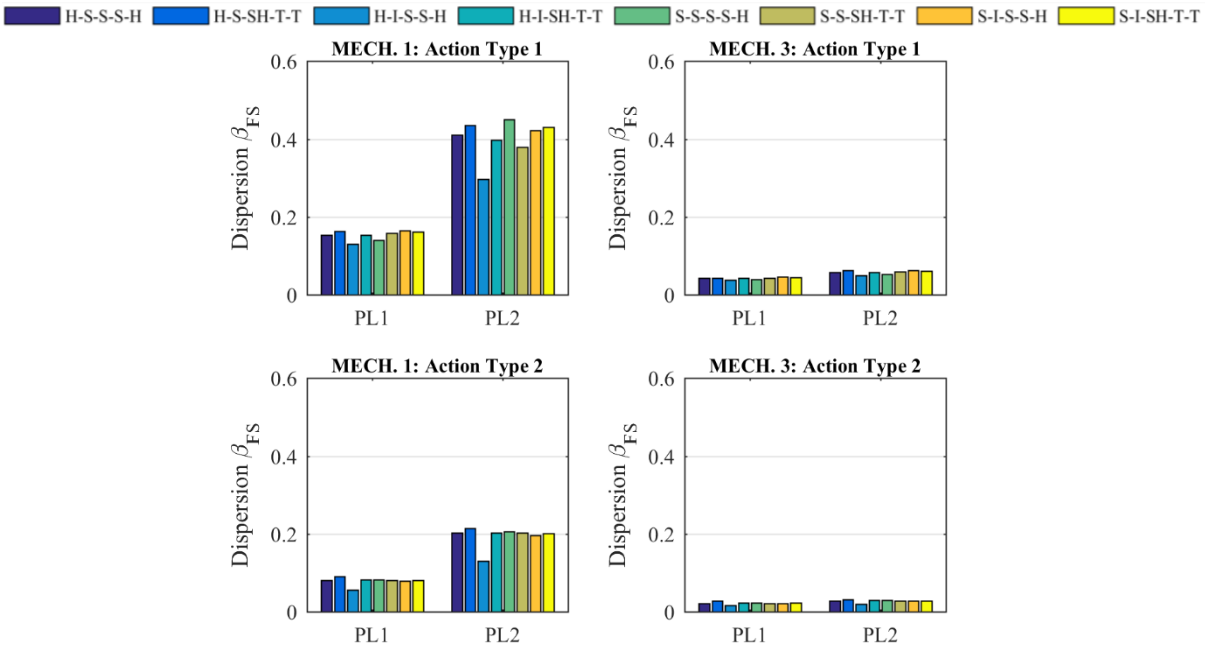

Figure 4.11 – Dispersion in the floor spectra (β_{FS}) for Mech. 1 and Mech. 3 obtained with the 8 building models: seismic action type 1 and type 2

4.5.4. Summary of results and fragility functions

Table 4.5 to Table 4.10 summarize the results obtained in terms of the median value of PGA ($PGA_{50\%}$), dispersion in the determination of capacity of the mechanisms (β_C), dispersion in the determination of the seismic demand (β_D), dispersion in the determination of the floor response spectrum (β_{FS}) and the final dispersion related to the local seismic behaviour (β_L), for the different performance levels and considering seismic action type 1 and type 2. The dispersion related to the local seismic behaviour (β_L) is defined according to Equation (4.14). The uncertainties in the definition of the performance limit states (β_T) are not directly accounted, as in the case of the analysis of the global behaviour (§3.5.4).

$$\beta_L = \sqrt{\beta_C^2 + \beta_D^2 + \beta_{FS}^2} \tag{4.14}$$

Table 4.5 – Parameters obtained with the 8 building models with Mech. 1 for PL1

PL1	Action Type 1					Action Type 2				
Model	$PGA_{50\%}$ [m/s^2]	β_C	β_D	β_{FS}	β_L	$PGA_{50\%}$ [m/s^2]	β_C	β_D	β_{FS}	β_L
H-S-S-S-H	1.063	0.241	0.441	0.154	0.526	1.464	0.219	0.255	0.081	0.346
H-S-SH-T-T	1.307	0.218	0.437	0.164	0.515	1.800	0.198	0.319	0.090	0.387
H-I-S-S-H	1.199	0.181	0.395	0.131	0.454	1.572	0.210	0.190	0.056	0.288
H-I-SH-T-T	1.061	0.240	0.440	0.153	0.524	1.443	0.205	0.259	0.082	0.340
S-S-S-S-H	1.032	0.232	0.409	0.140	0.491	1.458	0.223	0.261	0.083	0.353
S-S-SH-T-T	0.924	0.151	0.446	0.159	0.497	1.300	0.121	0.256	0.081	0.295
S-I-S-S-H	1.359	0.265	0.474	0.166	0.568	1.771	0.248	0.240	0.079	0.354
S-I-SH-T-T	0.964	0.148	0.465	0.162	0.514	1.358	0.167	0.259	0.081	0.318

Table 4.6 – Parameters obtained with the 8 building models with Mech. 1 for PL2

PL2	Action Type 1					Action Type 2				
Model	$PGA_{50\%}$ [m/s^2]	β_C	β_D	β_{FS}	β_L	$PGA_{50\%}$ [m/s^2]	β_C	β_D	β_{FS}	β_L
H-S-S-S-H	2.248	0.173	0.514	0.412	0.681	3.106	0.218	0.367	0.203	0.473
H-S-SH-T-T	2.411	0.273	0.548	0.437	0.752	3.331	0.267	0.408	0.214	0.533
H-I-S-S-H	2.436	0.222	0.436	0.297	0.572	3.226	0.231	0.256	0.131	0.369
H-I-SH-T-T	2.230	0.208	0.508	0.399	0.679	2.999	0.182	0.369	0.203	0.459
S-S-S-S-H	2.190	0.187	0.467	0.450	0.675	3.112	0.251	0.376	0.206	0.497
S-S-SH-T-T	1.948	0.135	0.531	0.380	0.667	2.740	0.205	0.368	0.203	0.467
S-I-S-S-H	2.329	0.201	0.553	0.424	0.726	3.774	0.208	0.357	0.197	0.457
S-I-SH-T-T	2.039	0.139	0.540	0.432	0.705	2.870	0.171	0.366	0.202	0.451

Table 4.7 – Parameters obtained with the 8 building models with Mech. 2 for PL1

PL1	Action Type 1					Action Type 2				
Model	$PGA_{50\%}$ [m/s^2]	β_C	β_D	β_{FS}	β_L	$PGA_{50\%}$ [m/s^2]	β_C	β_D	β_{FS}	β_L
H-S-S-S-H	3.683	0.095	0.301	0	0.315	3.683	0.095	0.342	0	0.355
H-S-SH-T-T	3.595	0.086	0.304	0	0.316	3.595	0.086	0.379	0	0.437
H-I-S-S-H	3.723	0.041	0.336	0	0.338	3.723	0.041	0.374	0	0.424
H-I-SH-T-T	3.691	0.095	0.301	0	0.316	3.691	0.095	0.344	0	0.359
S-S-S-S-H	3.680	0.076	0.324	0	0.333	3.680	0.076	0.350	0	0.358
S-S-SH-T-T	3.624	0.060	0.297	0	0.303	3.624	0.060	0.374	0	0.426
S-I-S-S-H	3.722	0.111	0.280	0	0.301	3.722	0.111	0.332	0	0.340
S-I-SH-T-T	3.691	0.058	0.286	0	0.291	3.691	0.058	0.340	0	0.352

Table 4.8 – Parameters obtained with the 8 building models with Mech. 2 for PL2

PL2	Action Type 1					Action Type 2				
Model	$PGA_{50\%}$ [m/s^2]	β_C	β_D	β_{FS}	β_L	$PGA_{50\%}$ [m/s^2]	β_C	β_D	β_{FS}	β_L
H-S-S-S-H	5.231	0.096	0.358	0	0.370	5.231	0.096	0.336	0	0.349
H-S-SH-T-T	5.278	0.082	0.336	0	0.346	5.278	0.082	0.428	0	0.388
H-I-S-S-H	5.278	0.039	0.422	0	0.424	5.278	0.039	0.422	0	0.376
H-I-SH-T-T	5.331	0.091	0.362	0	0.373	5.331	0.091	0.347	0	0.356
S-S-S-S-H	5.381	0.079	0.394	0	0.402	5.381	0.079	0.350	0	0.359
S-S-SH-T-T	5.291	0.057	0.346	0	0.351	5.291	0.057	0.422	0	0.379
S-I-S-S-H	5.270	0.100	0.332	0	0.347	5.270	0.100	0.322	0	0.347
S-I-SH-T-T	5.328	0.057	0.340	0	0.345	5.328	0.057	0.347	0	0.345

Table 4.9 – Parameters obtained with the 8 building models with Mech. 3 for PL1

PL1	Action Type 1					Action Type 2				
Model	$PGA_{50\%}$ [m/s^2]	β_C	β_D	β_{FS}	β_L	$PGA_{50\%}$ [m/s^2]	β_C	β_D	β_{FS}	β_L
H-S-S-S-H	0.356	0.229	0.267	0.042	0.354	0.490	0.208	0.154	0.022	0.260
H-S-SH-T-T	0.437	0.207	0.285	0.042	0.354	0.602	0.188	0.193	0.028	0.271
H-I-S-S-H	0.401	0.181	0.226	0.038	0.292	0.526	0.173	0.115	0.017	0.208
H-I-SH-T-T	0.355	0.228	0.264	0.042	0.351	0.483	0.169	0.156	0.023	0.231
S-S-S-S-H	0.345	0.158	0.242	0.039	0.292	0.488	0.211	0.158	0.023	0.265
S-S-SH-T-T	0.309	0.143	0.276	0.043	0.314	0.435	0.214	0.155	0.022	0.265
S-I-S-S-H	0.454	0.253	0.287	0.046	0.386	0.592	0.257	0.145	0.021	0.296
S-I-SH-T-T	0.323	0.140	0.281	0.045	0.317	0.454	0.165	0.157	0.023	0.229

Table 4.10 – Parameters obtained with the 8 building models with Mech. 3 for PL2

PL2	Action Type 1					Action Type 2				
Model	$PGA_{50\%}$ [m/s^2]	β_C	β_D	β_{FS}	β_L	$PGA_{50\%}$ [m/s^2]	β_C	β_D	β_{FS}	β_L
H-S-S-S-H	0.558	0.236	0.309	0.058	0.393	0.771	0.297	0.221	0.028	0.371
H-S-SH-T-T	0.599	0.244	0.328	0.062	0.413	0.827	0.274	0.245	0.032	0.369
H-I-S-S-H	0.605	0.151	0.223	0.049	0.273	0.801	0.205	0.154	0.020	0.257
H-I-SH-T-T	0.554	0.284	0.300	0.057	0.417	0.745	0.280	0.222	0.029	0.358
S-S-S-S-H	0.544	0.255	0.338	0.052	0.427	0.773	0.240	0.226	0.029	0.331
S-S-SH-T-T	0.484	0.184	0.285	0.060	0.344	0.681	0.280	0.221	0.028	0.358
S-I-S-S-H	0.714	0.301	0.319	0.062	0.443	0.938	0.284	0.214	0.028	0.357
S-I-SH-T-T	0.507	0.190	0.324	0.061	0.380	0.713	0.234	0.220	0.028	0.322

In reference to §4.2, two possible scenarios were identified for the local seismic behaviour of the buildings related to: 1) the mechanisms involving the last floor of the buildings and 2) the mechanisms involving the parapet or the case of having no problem. These were assumed as epistemic uncertainties and treated by the logic-tree approach, presented in Figure 4.3. It is now proposed to define the $PGA_{50\%}$ and the dispersion (β_L) associated with each scenario taking into account the reliability/weight attributed to the different options. For the first scenario, the parameters are determined according to Equation (4.15) and Equation (4.16):

$$PGA_{50\%,LastFloor} = 0.70PGA_{50\%,Mech1} + 0.30PGA_{50\%,Mech2} \tag{4.15}$$

$$\beta_{LastFloor} = \sqrt{0.70\beta^2_{L,Mech1} + 0.30\beta^2_{L,Mech2}} \tag{4.16}$$

As referred for the analysis of the global seismic behaviour (§3.5.4), the previous equations are an approximation (in particular Equation (4.16)), as the fragility curves obtained from the combination of the two possible scenarios are not a lognormal cumulative distribution. Table 4.11 summarizes the parameters obtained with the 8 building models. Figure 4.12 exemplifies with model H-S-S-S-H, the resulting fragility functions (solid lines represent the fragility functions for this scenario).

For the second scenario, the “no problem” hypothesis is characterized by a PGA that tends to infinity. Thus, the parameters that define the fragility functions associated with this scenario are obtained directly from the ones determined for Mech. 3 (Table 4.9 and Table 4.10), but imposing that the probability associated with the different performance levels cannot exceed 0.60, which corresponds to the reliability/weight of this hypothesis (Figure 4.3 b)). Figure 4.13 exemplifies for model H-S-S-S-H the fragility functions obtained for the local mechanism involving the parapet of the buildings.

Table 4.11 – Parameters obtained with the 8 building models considering the local mechanism involving the last floor of the buildings

Last Floor		Action Type 1				Action Type 2			
		PL1		PL2		PL1		PL2	
Model	w	$PGA_{50\%}$ [m/s^2]	β_L	$PGA_{50\%}$ [m/s^2]	β_L	$PGA_{50\%}$ [m/s^2]	β_L	$PGA_{50\%}$ [m/s^2]	β_L
H-S-S-S-H	0.039	1.849	0.473	3.143	0.605	2.130	0.349	3.743	0.439
H-S-SH-T-T	0.070	1.993	0.464	3.271	0.657	2.338	0.402	3.915	0.494
H-I-S-S-H	0.078	1.956	0.422	3.289	0.532	2.217	0.335	3.841	0.371
H-I-SH-T-T	0.143	1.850	0.471	3.160	0.604	2.118	0.346	3.699	0.431
S-S-S-S-H	0.078	1.827	0.449	3.148	0.606	2.125	0.355	3.793	0.460
S-S-SH-T-T	0.143	1.734	0.448	2.951	0.590	1.997	0.339	3.506	0.442
S-I-S-S-H	0.159	2.068	0.503	3.211	0.636	2.356	0.350	4.223	0.427
S-I-SH-T-T	0.290	1.782	0.459	3.026	0.620	2.058	0.329	3.608	0.422

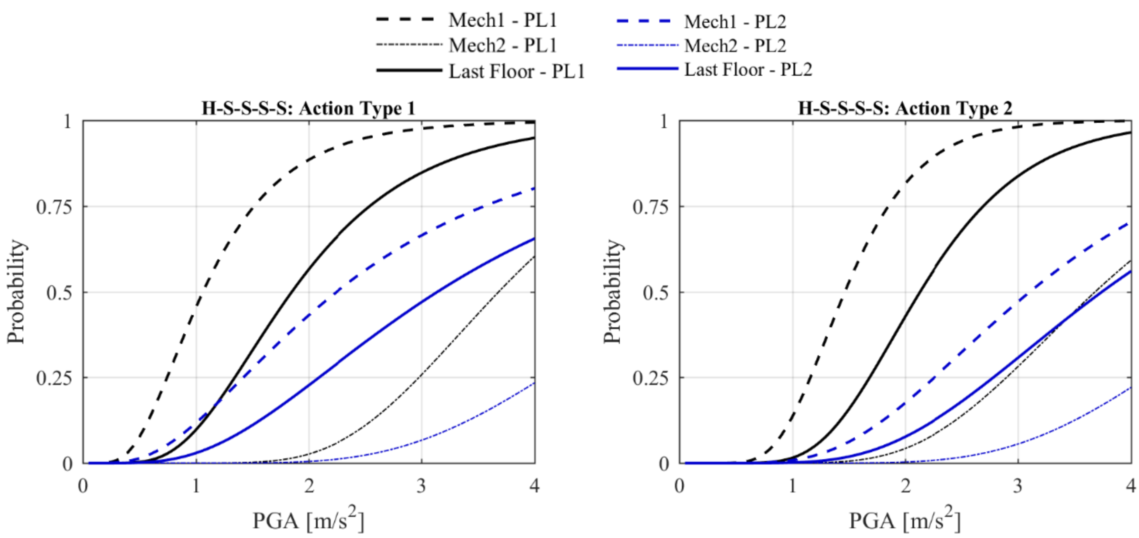

Figure 4.12 – Fragility functions for model H-S-S-S-H with the local mechanism involving the last floor of the buildings: seismic action type 1 (left) and type 2 (right)

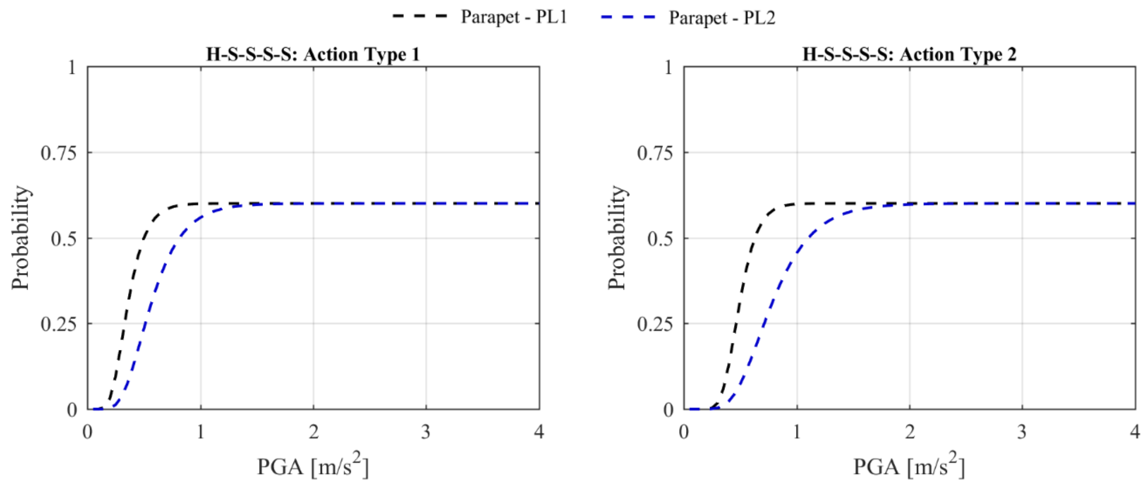

Figure 4.13 – Fragility functions for model H-S-S-S-H with the local mechanism involving the parapet of the buildings: seismic action type 1 (left) and type 2 (right)

Based on this data, it is possible to derive the fragility functions for the URM buildings of type I considering only the local seismic behaviour. These are defined taking into account the weight of the each group of models by applying Equation (3.27) and Equation (3.28) presented for the analysis of the global seismic behaviour (§3.5.4). The approximated parameters defining the fragility functions are provided in Table 4.12 for the local mechanism involving the last floor of the buildings and the parapet. In the second case, the probability of the fragility functions varies between 0 and 0.60. The resulting fragility functions are presented in Figure 4.14 for seismic action type 1 and type 2.

The discrete probability associated with the different damage states is determined following the procedure presented in §3.5.4 for the analysis of the global seismic behaviour. The code seismic action for Lisbon: type 1 (PGA = 1.94 m/s^2) and type 2 (PGA = 2.16 m/s^2) is also considered for the estimation of the damage distribution considering the local seismic behaviour of the typology. Figure 4.15 shows the corresponding probability damage distribution. It is important to refer that the probability of DS2 also includes the probability of DS3, DS4 and DS5, as the activation of the mechanisms corresponds, at the same time, to the out-of-plane collapse (as referred in §4.5.2). In this context, the results indicate the sure collapse of the parapets for both types of seismic action, while it is estimated that the local mechanisms involving the last floor of the buildings have a probability of collapse (DS5) of about 22% for seismic action type 1 and 10% for type 2.

Table 4.12 – Approximated parameters for the fragility functions considering the local mechanisms

Local Behaviour	Last Floor				Parapet			
	Action Type 1		Action Type 2		Action Type 1	Action Type 2	Action Type 1	Action Type 2
	$PGA_{50\%}$ [m/s^2]	β_L	$PGA_{50\%}$ [m/s^2]	β_L	$PGA_{50\%}$ [m/s^2]	β_L	$PGA_{50\%}$ [m/s^2]	β_L
PL1	1.865	0.464	2.145	0.345	0.363	0.334	0.497	0.252
PL2	3.116	0.611	3.763	0.433	0.562	0.391	0.771	0.340

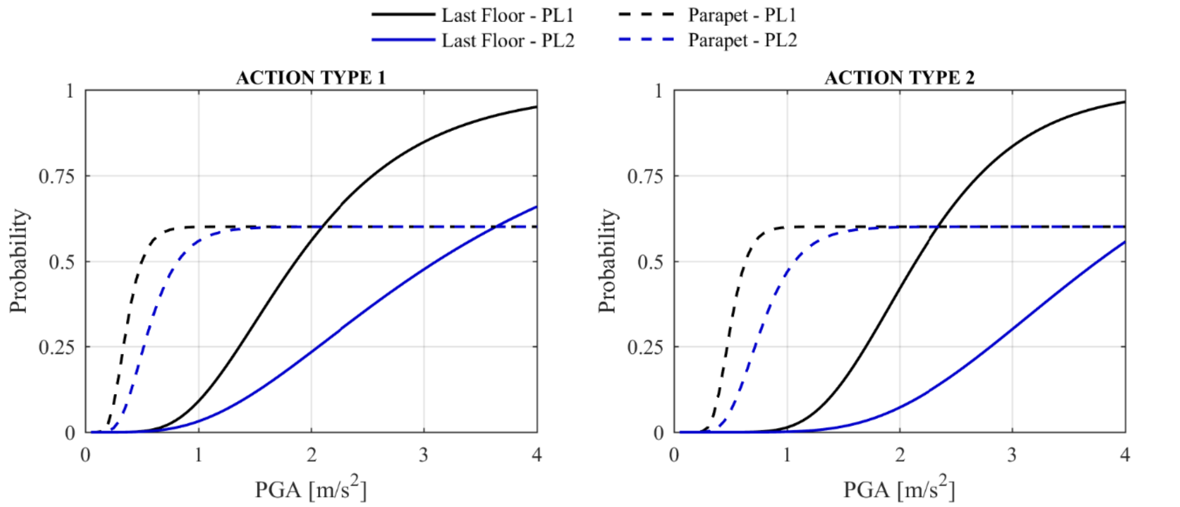

Figure 4.14 – Fragility functions considering the local seismic behaviour of the typology: seismic action type 1 (left) and type 2 (right)

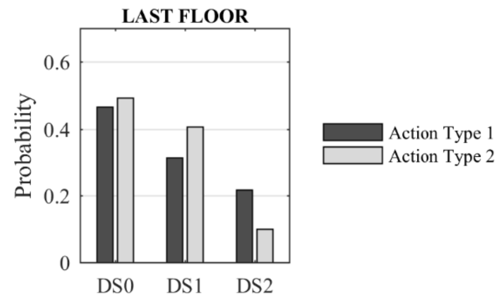

Distribution of damage	Scenario	DS0	DS1	DS2
Action Type 1 PGA = 1.94 m/s^2	Last Floor	0.467	0.314	0.218
	Parapet	0	0	1.000
Action Type 2 PGA = 2.16 m/s^2	Last Floor	0.494	0.407	0.099
	Parapet	0	0	1.000

Figure 4.15 – Distribution of damage considering the local mechanism involving the last floor of the buildings for seismic action type 1 (PGA=1.94 m/s^2) and type 2 (PGA=2.16 m/s^2)

4.6. Conclusion

The chapter presents a methodology for the analysis of the local seismic behaviour aiming to estimate the parameters for the derivation of the corresponding fragility functions. The seismic analysis was supported on the non-linear kinematic analyses of different mechanisms involving the upper level of the façade walls of the URM buildings of type I. In this case, two possible scenarios were identified: 1) the mechanisms involving the last floor of the buildings and 2) the mechanisms involving the parapet or the case of having no problem.

The reliability of each mechanisms was analysed as an epistemic uncertainty, while the geometry of the elements and the actions involved in each mechanism were assumed as aleatory uncertainties. The aleatory variables were treated by a full factorial combination aiming the subsequent application of the

Response Surface Method for the evaluation of the dispersion in the capacity (β_C). The quantification of the uncertainties associated with the local seismic behaviour constitutes a novelty in comparison with previous works. Moreover, the computation of the PGA values compatible with the different performance limit states was determined through an iterative procedure in order to consider the interaction effects between the non-linear behaviour of the main structure and the non-linear behaviour of the mechanism and to establish a limit for the seismic verification at the local scale.

In this study, it was verified that in all cases the attainment of PL2 corresponds both to the activation of the mechanism and to the out-of-plane collapse (the PGA values compatible with PL2, PL3 and PL4 are the same). It was concluded that the overturning of the parapet is the most critical mechanism as it exhibits the lowest strength and displacement capacity due to the reduced thickness of the element. In fact, the probability distribution of damage for the code seismic action for Lisbon indicates the sure collapse of the parapets for both types of action. In what concerns the mechanisms involving the last floor of the buildings, it was estimated that these have a probability of collapse of about 22% for seismic action type 1 and 10% for type 2. Therefore, strengthening solutions aiming to solve the vulnerability associated with the out-of-plane response of the upper level of the façade walls are needed and particular attention should be given to the buildings with parapets. A possible intervention is to fix this non-structural element at its base or to the roof structure by the application of steel tie-rods.

5. DERIVATION OF FRAGILITY FUNCTIONS

5.1. Introduction

The previous chapters addressed the analysis of the global and local behaviour of the URM buildings of type I taking into account the various parameters that influence the seismic response until the definition of the corresponding fragility functions. The purpose of this chapter is to derive the fragility functions for the typology of buildings by considering the contribution of both global and local seismic behaviour. The fragility functions proposed in this thesis are then compared with fragility functions obtained from different methods. In what concerns traditional masonry buildings, it is recognised that the fragility functions derived for buildings located in different regions is questionable as the seismic vulnerability depends on the local materials and on the local seismic culture. Therefore, the comparison of fragility functions is based mainly on the results from previous works addressed to the URM buildings in Lisbon.

5.2. Proposed fragility functions

The global seismic behaviour of the block of buildings was analysed in §3 considering the two main directions – parallel to the façade walls (X direction) and parallel to the side walls (Y direction). The local seismic behaviour was analysed in §4 considering the two possible scenarios related to: 1) the mechanisms involving the last floor of the buildings and 2) the mechanisms involving the parapet or the case of having no problem; both scenarios affect the seismic response of the main structure in the Y direction. In order to derive the final fragility functions, it is first necessary to combine the global and the local seismic behaviour in the Y direction for the different performance limit states. Notwithstanding the relevance of the second scenario for the life safety, the simple overturning of the parapets is secondary for the verification of the main structure at a global scale. Therefore, the contribution of the local seismic response is limited to the mechanisms involving the last floor of the buildings.

In what concerns the contribution of the global behaviour, the different performance limit states are directly correlated to the behaviour of the main structure in the Y direction. In what concerns the contribution of the local behaviour, it is worth noting that in one hand, PL1 at the local scale is not relevant at a global scale; on the other hand, in this work, the occurrence of PL2 at the local scale is related both to the activation of the mechanism and to the out-of-plane collapse (i.e. the PGA values compatible with PL2, PL3 and PL4 are the same). Thus, it is proposed to add the contribution of PLk greater than PL1 at the local scale to the corresponding PLk at the global scale.

The combination of the fragility functions is exemplified in the following for model H-S-S-S-H. Table 5.1 summarizes the parameters that characterize the fragility functions defined from the analysis of the global seismic behaviour of the buildings in the Y direction and from the analysis of the local mechanisms involving the last floor of the buildings (these values were obtained directly from the tables presented in §3.5.4 and §4.5.4). The resulting fragility functions are defined by the application of Equation (5.1). Figure 5.1 to Figure 5.3 present the corresponding curves and the final result for PL2, PL3 and PL4. In this case, PL1 is determined directly from Table 5.1. It is observed that the local behaviour has a negligible contribution for the definition of PL2, but an important contribution for the other PLk, in particular considering seismic action type 2.

$$P_{PLk} = P_{G,PLk} + (1 - P_{G,PLk})P_{L,PLk} \tag{5.1}$$

Table 5.1 – Parameters for model H-S-S-S-H: seismic action type 1 and type 2

Model H-S-S-S-H	Action Type 1				Action Type 2			
	Global Behaviour		Local Behaviour		Global Behaviour		Local Behaviour	
	Y Direction		Last Floor		Y Direction		Last Floor	
w=0.039	$PGA_{50\%}$ [m/s^2]	β_G	$PGA_{50\%}$ [m/s^2]	β_L	$PGA_{50\%}$ [m/s^2]	β_G	$PGA_{50\%}$ [m/s^2]	β_L
PL1	0.379	0.289	--	--	0.889	0.353	--	--
PL2	0.650	0.288	3.143	0.605	1.533	0.348	3.743	0.349
PL3	1.371	0.320	3.143	0.605	3.267	0.352	3.743	0.349
PL4	1.544	0.336	3.143	0.605	3.706	0.352	3.743	0.349

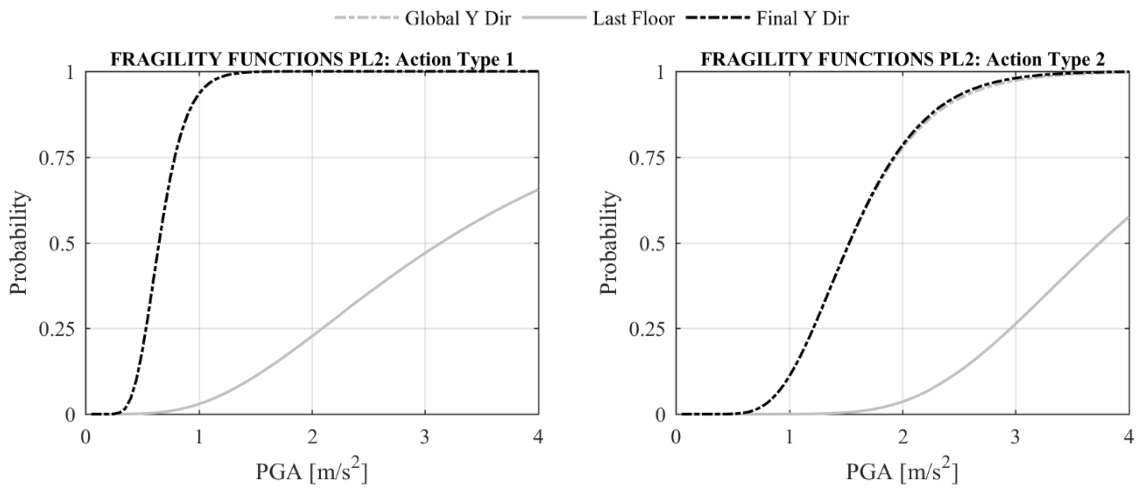

Figure 5.1 – Combination of the fragility functions in the Y direction for model H-S-S-S-H for PL2: seismic action type 1 (left) and type 2 (right)

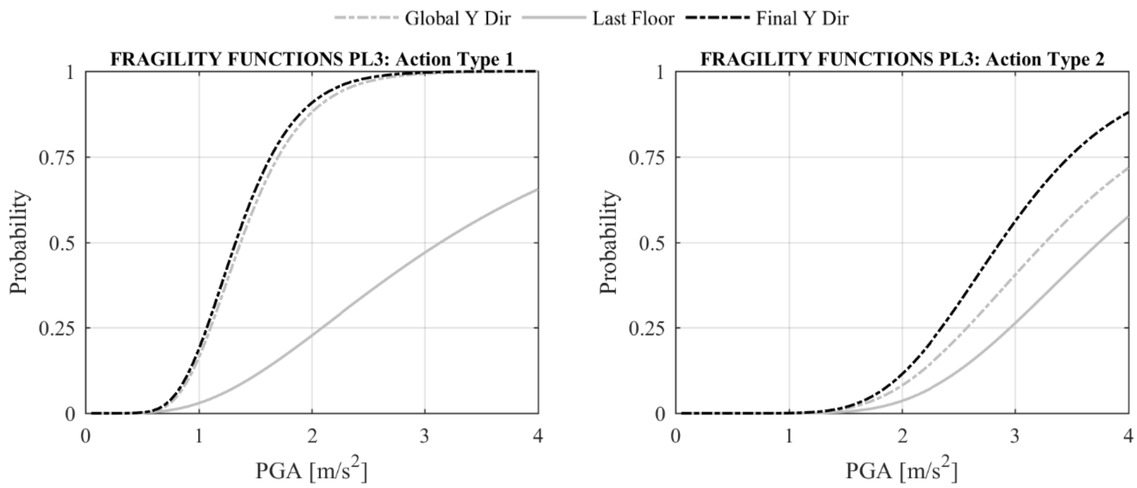

Figure 5.2 – Combination of the fragility functions in the Y direction for model H-S-S-S-H for PL3: seismic action type 1 (left) and type 2 (right)

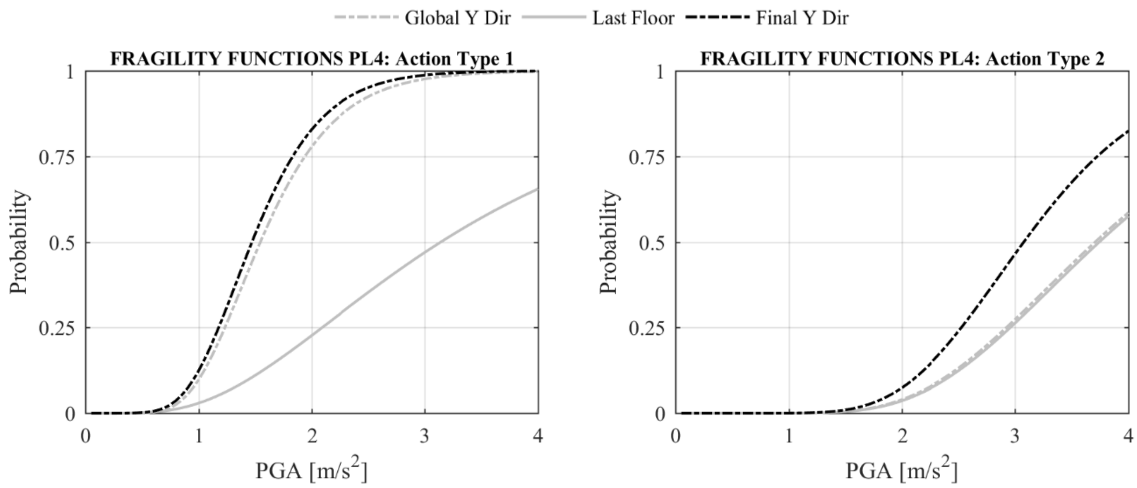

Figure 5.3 – Combination of the fragility functions in the Y direction for model H-S-S-S-H for PL4: seismic action type 1 (left) and type 2 (right)

Finally, it is proposed to consider the minimum between the results obtained in the X and Y directions, the later including the local behaviour, as this leads to the most demanding condition for the block of buildings. Figure 5.4 exemplifies the fragility functions obtained with model H-S-S-S-H in the X and Y direction and the minimum combination between both. The parameters that characterize the fragility functions for the different building models are presented in Table 5.2 and Table 5.3, respectively for seismic action type 1 and type 2. Here, the final dispersion β is determined in an approximated way according to Equation (3.26), taking into account that the resulting fragility functions are not a lognormal cumulative distribution function.

Based on the data from Table 5.2 and Table 5.3, it is possible to derive the final fragility functions for the typology of buildings by adding the contribution of the different models as a function of their reliability/weight (w), according to Equation (3.27) and Equation (3.28). Table 5.4 presents the parameters while Figure 5.5 plots the final fragility functions for the URM buildings of type I (solid lines) considering the contribution of the global and local seismic behaviour.

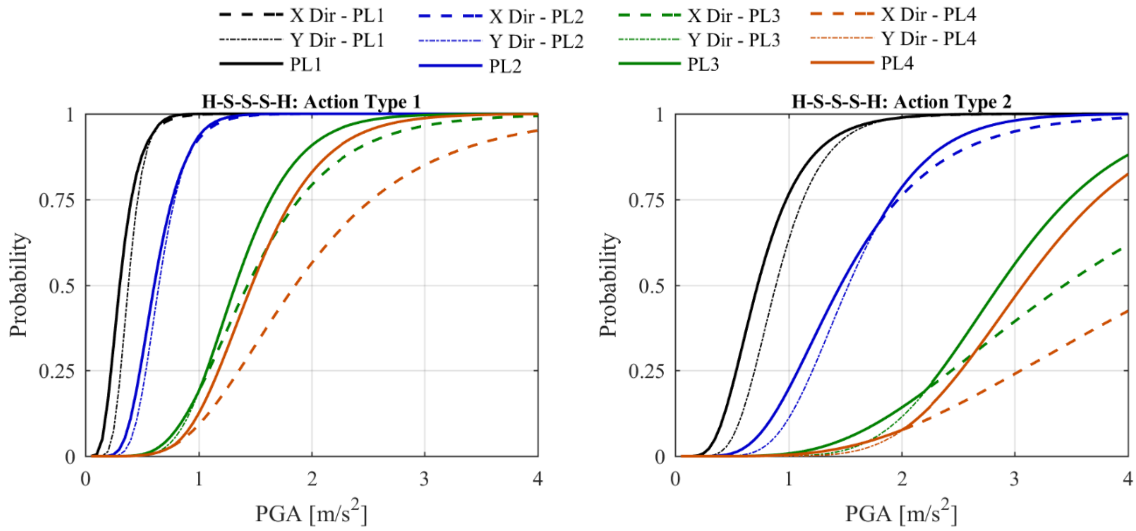

Figure 5.4 – Combination of the fragility functions in the X and Y directions for model H-S-S-S-H: seismic action type 1 (left) and type 2 (right)

Table 5.2 – Approximated parameters obtained for all groups of models from the combination of the fragility functions obtained in the X and Y directions: seismic action type 1

Action Type 1		PL1		PL2		PL3		PL4	
Model	w	$PGA_{50\%}$ [m/s^2]	β	$PGA_{50\%}$ [m/s^2]	β	$PGA_{50\%}$ [m/s^2]	β	$PGA_{50\%}$ [m/s^2]	β
H-S-S-S-H	0.039	0.303	0.426	0.608	0.341	1.326	0.318	1.470	0.326
H-S-SH-T-T	0.070	0.350	0.324	0.588	0.304	1.145	0.317	1.296	0.333
H-I-S-S-H	0.078	0.275	0.430	0.579	0.367	1.428	0.303	1.590	0.320
H-I-SH-T-T	0.143	0.368	0.419	0.643	0.389	1.321	0.313	1.492	0.325
S-S-S-S-H	0.078	0.305	0.431	0.621	0.347	1.276	0.332	1.428	0.335
S-S-SH-T-T	0.143	0.354	0.333	0.592	0.290	1.160	0.300	1.314	0.315
S-I-S-S-H	0.159	0.283	0.440	0.634	0.364	1.365	0.319	1.515	0.332
S-I-SH-T-T	0.290	0.383	0.415	0.674	0.371	1.291	0.324	1.452	0.323

Table 5.3 – Approximated parameters obtained for all groups of models from the combination of the fragility functions obtained in the X and Y directions: seismic action type 2

Action Type 2		PL1		PL2		PL3		PL4	
Model	w	$PGA_{50\%}$ [m/s^2]	β	$PGA_{50\%}$ [m/s^2]	β	$PGA_{50\%}$ [m/s^2]	β	$PGA_{50\%}$ [m/s^2]	β
H-S-S-S-H	0.039	0.727	0.441	1.460	0.411	2.870	0.302	3.078	0.286
H-S-SH-T-T	0.070	0.826	0.390	1.372	0.354	1.071	0.693	2.845	0.315
H-I-S-S-H	0.078	0.659	0.506	1.388	0.472	3.028	0.284	3.236	0.280
H-I-SH-T-T	0.143	0.884	0.460	1.542	0.419	2.840	0.310	3.085	0.287
S-S-S-S-H	0.078	0.732	0.445	1.489	0.415	2.793	0.304	3.030	0.295
S-S-SH-T-T	0.143	0.836	0.392	1.387	0.345	2.560	0.302	2.796	0.288
S-I-S-S-H	0.159	0.680	0.493	1.520	0.456	1.240	0.713	3.285	0.299
S-I-SH-T-T	0.290	0.921	0.438	1.556	0.392	2.792	0.310	3.030	0.276

Table 5.4 – Approximated parameters for the fragility functions considering the global and local seismic behaviour of the typology of buildings

Final Parameters	Action Type 1		Action Type 2	
	$PGA_{50\%}$ [m/s^2]	β	$PGA_{50\%}$ [m/s^2]	β
PL1	0.341	0.406	0.816	0.447
PL2	0.631	0.354	1.489	0.407
PL3	1.289	0.317	2.420	0.431
PL4	1.447	0.325	3.050	0.288

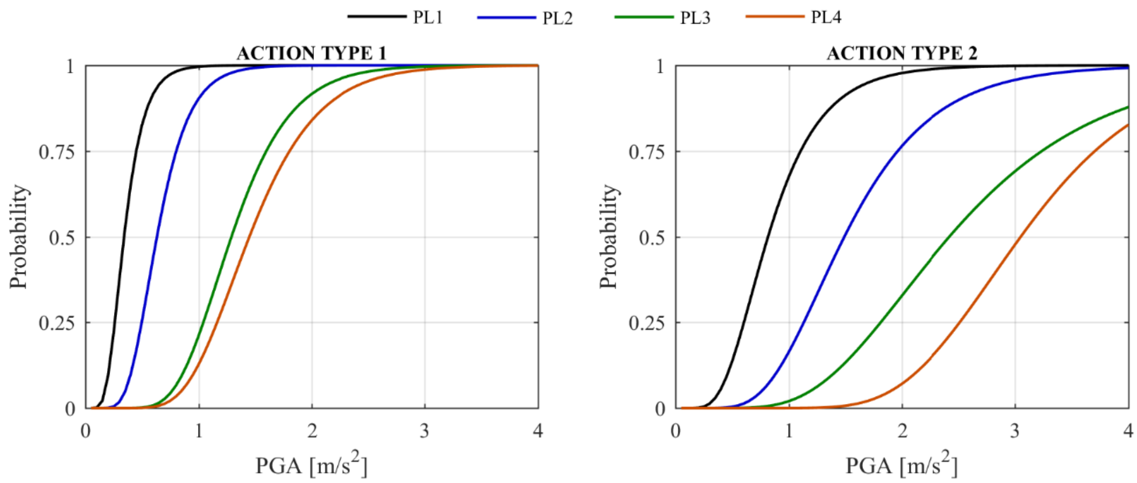

Figure 5.5 – Fragility functions considering the global seismic behaviour of the URM buildings of type I: seismic action type 1 (left) and type 2 (right)

The discrete probability associated with the different damage states is determined following the procedure presented in §3.5.4 for the analysis of the global seismic behaviour. The code seismic action for Lisbon: type 1 (PGA = 1.94 m/s^2) and type 2 (PGA = 2.16 m/s^2) is considered for the estimation of the damage distribution for the typology of buildings. Figure 5.6 shows the corresponding probability damage distribution. The probability damage distribution obtained considering only the global seismic behaviour of the buildings is also included for comparison.

As expected, the contribution of the local seismic behaviour increased the final vulnerability. In terms of the overall assessment of the URM buildings of type I, the fragility functions derived highlight the high seismic vulnerability of the buildings, particularly for seismic action type 1. It is estimated that there is about 46% probability of having very heavy damage (DS4) and about 34% probability of collapse (DS5). Nevertheless, for the lower damage states, seismic action type 2 is the most demanding case and mainly due to the contribution of the out-of-plane mechanisms involving the last floor of the buildings, considering that the probability of having heavy damage (DS3) increased from 8.9% to 28%. Moreover, it is expected the sure collapse of the parapets for both types of seismic action in Lisbon, as referred in §4.5.4. These outcomes, put in evidence the high seismic vulnerability of these URM buildings and the urgent need to reduce potential losses due to future earthquakes.

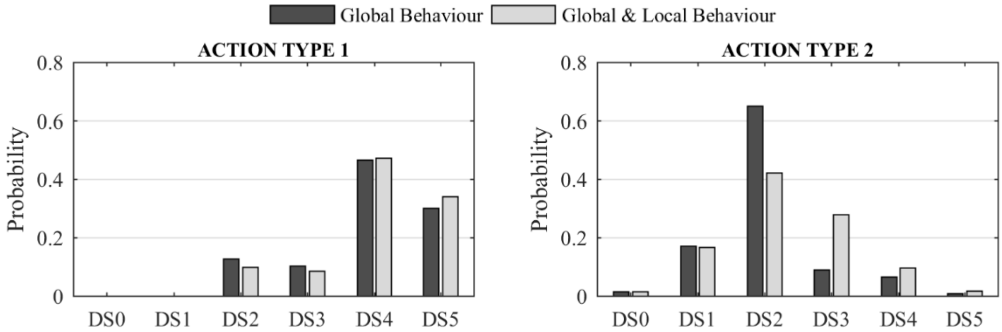

Distribution of damage		DS0	DS1	DS2	DS3	DS4	DS5
Action Type 1 PGA = 1.94 m/s^2	Global Behaviour	0.000	0.001	0.128	0.104	0.467	0.301
	Global & Local Behaviour	0.000	0.001	0.099	0.085	0.474	0.341
Action Type 2 PGA = 2.16 m/s^2	Global Behaviour	0.015	0.171	0.649	0.089	0.066	0.009
	Global & Local Behaviour	0.015	0.167	0.424	0.280	0.097	0.017

Figure 5.6 – Distribution of damage for the URM buildings of type I for seismic action type 1 (PGA=1.94 m/s^2) and type 2 (PGA=2.16 m/s^2)

5.3. Comparison with other fragility functions

As discussed in §1.2, fragility functions may be derived based on empirical, expert elicitation/judgement, analytical and hybrid methods. Empirical methods are based on the observation of actual damage after the occurrence of an earthquake. This data is valuable since it is directly correlated to the actual seismic behaviour of buildings and is useful for calibration/validation of fragility functions obtained with the other methods. Expert elicitation/judgement methods are used to assess the vulnerability of building typologies, if no data is available and structural analysis is not feasible. In this case, one or more experts can offer an opinion on the seismic intensity level at which damage is likely to occur. Analytical methods comprehend the prediction of the seismic behaviour using simplified or detailed models and non-linear analysis procedures. Hybrid methods result from the combination of any of the abovementioned methods.

In one hand, the number of fragility functions available in the literature addressed to the URM buildings in Lisbon is scarce. On the other hand, the comparison of fragility functions defined for traditional masonry located in different regions is questionable as the seismic vulnerability depends on the local materials and on the local seismic culture, as highlighted in §5.1. Therefore, in this section, the fragility functions proposed for the URM buildings of type I are compared with the fragility functions derived in previous studies about these buildings (Simões et al., 2014a, 2015). In addition, the method proposed by Vicente et al. (2011) for the vulnerability assessment of masonry buildings is applied to the present cases of study in order to derive the corresponding fragility functions and compare with the fragility functions proposed. A final comparison is made with the fragility functions proposed by D’Ayala et al. (1997) for the URM buildings located in Alfama, one of the oldest districts in Lisbon. These buildings may be classified as belonging to the first masonry typology of buildings referred in §1.1: buildings that resisted to the 1755 earthquake, fire and tsunami. Despite the different period of construction and the fact that these buildings have been severely damaged after the 1755 earthquake, these results are considered as both building typologies were constructed in Lisbon.

In Simões et al. (2014a, 2015) the fragility functions for a URM building of type I were determined based on non-linear static (pushover) analyses and considering only the global seismic behaviour. The fragility functions were defined by assuming a lognormal cumulative distribution and some conventional values for the dispersion (β) of the different performance limit states (also in terms of PLk, with k=1,…,4). In this case, the dispersion accounted for the uncertainties in the definition of the capacity (β_C) of buildings, seismic demand (β_D), limit states (β_T) and the error associated with the model used for the analysis (β_ε).

In what concerns the dispersion in the capacity (β_C), in Simões et al. (2014a) different values were considered for each PLk, namely 0.35, 0.35, 0.37 and 0.38, following the suggestion from Pagnini et al. (2011), while in Simões et al. (2015) this was set equal to 0.40. These values are much higher when compared to the values evaluated in the present work. For instance, for the analysis of the global seismic behaviour, the dispersion in the capacity is in average 0.14, with a coefficient of variation of about 50%, and takes as maximum value 0.30 (§3.5.2).

In what concerns the dispersion in the seismic demand (β_D), in the previous works referred, this was assumed equal to 0.25, while in the present work it is in average 0.39, with a coefficient of variation of about 23%, and takes as minimum value 0.27 (§3.5.3). In terms of the total dispersion (β), in the previous works, it varies between 0.52 and 0.58, while in the present work, it varies between 0.33 and 0.45 in case only the global behaviour of the buildings is considered (Table 3.25).

In Simões et al. (2014a, 2015), the fragility functions obtained in the direction of the façade walls and in the direction of the side walls were not combined. Therefore, in order to establish a comparison with the fragility functions derived in this thesis, the fragility functions with lower values of PGA, for each of the performance limit states, are considered. Figure 5.7 compares the fragility functions in question and considering only the results for seismic action type 1 (the most demanding case).

It is observed that the fragility functions previously defined are closer to each, whereas the fragility functions now proposed for PL2 to PL4 are shifted to the right side of the plot. Figure 5.8 compares the probability damage distribution for the code seismic action for Lisbon. The probabilities associated with the lower damage states increased with the fragility functions proposed in this thesis, in particular when the contribution of the local seismic behaviour is considered, whereas the probability of collapse (DS5) decreased from 54% to 30% in the present work.

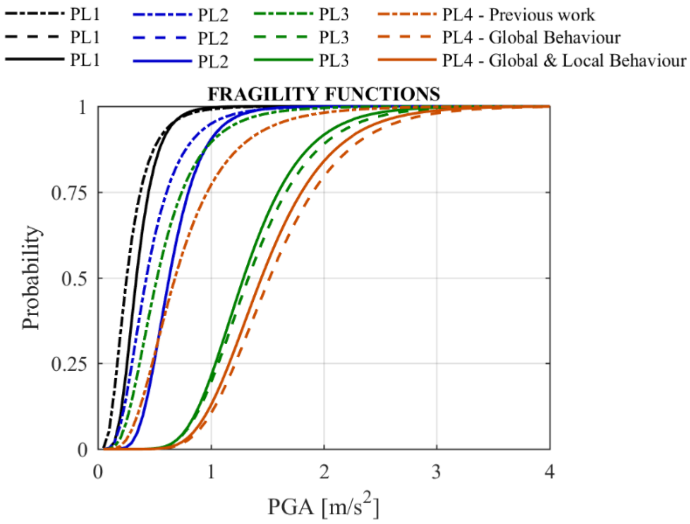

Figure 5.7 – Comparison of the fragility functions obtained in previous work (Simões et al., 2015) and in the present work considering the global behaviour and the combination between global and local

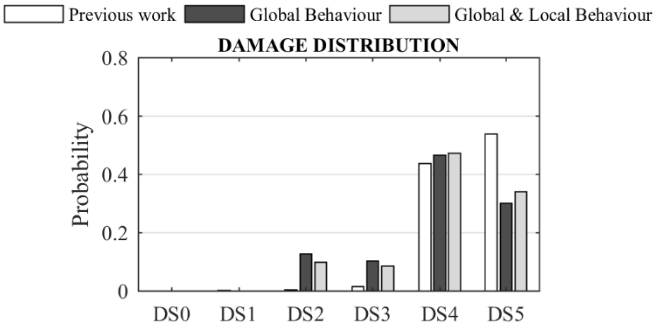

Figure 5.8 – Distribution of damage considering for seismic action type 1 (PGA=1.94 m/s^2)

The method developed by Vicente et al. (2011) is now applied to the 8 building models considered in this work (defined by the median properties of the aleatory variables §3.3.2). The method combines the empirical vulnerability index formulation suggested by the GNDT II level approach (GNDT, 1994), including some modifications proposed by Vicente (2008), with the Macroseismic Vulnerability Model defined by Lagomarsino and Giovinazzi (2006). This method has been applied to different city centres in Portugal, including Coimbra (Vicente et al., 2011), Seixal (Ferreira et al., 2013) and Faro (Maio et al., 2016). It was also applied for the assessment of a block of URM buildings in the area of "Avenidas Novas" in Lisbon (Simões et al. (2016a)), as referred in §2.5.

The procedure comprehends the determination of a vulnerability index (I_V) based on the weight sum of 14 parameters that evaluate the building in what concerns the: 1) structural system, 2) irregularities and interactions, 3) floor slabs and roof and 4) conservation status and other elements. The vulnerability index (I_V) is then related to the vulnerability (V) as proposed in the Macroseismic Vulnerability Model (Lagomarsino and Giovinazzi, 2006). The Macroseismic Vulnerability Model proposes to define the vulnerability (V) of a class/typology of buildings through a vulnerability function, which gives the mean damage (μ_D) as a function of the macroseismic intensity (I) according to Equation (5.2):

$$\mu_D = 2.5 + 3\tanh\left(\frac{I + 6.25V - 12.7}{Q}\right) \qquad 0 \le \mu_D \le 5 \tag{5.2}$$

where Q is the ductility index for that class/typology of buildings. Vulnerability (V) has been defined to vary between 0 and 1 for the six vulnerability classes suggested by the EMS-98 (Grünthal, 1998). Finally, the fragility functions for different performance limit states (LS) are evaluated by the binomial probability distribution, as presented in Equation (5.3) and Equation (5.4).

$$P_{LSk} = \sum_{i=k}^{5} P_{DSi} \qquad k = 1,\ldots,5 \tag{5.3}$$

$$P_{DSk} = \frac{5!}{k!(5-k)!}\left(\frac{\mu_D}{5}\right)^k \left(1 - \frac{\mu_D}{5}\right)^{5-k} \qquad k = 0,\ldots,5 \tag{5.4}$$

It is estimated that the Vulnerability Index (I_V) for the 8 building models, defined by the median properties of the aleatory variables (§3.3.2), is equal to 49.6 and 50.2, respectively, for buildings without and with interior timber "tabique" walls. Thus, an average value of 49.9 for the Vulnerability Index (I_V) is considered, which corresponds to a Vulnerability (V) of 0.86. In reference to the work developed for the assessment of the block of URM buildings in "Avenidas Novas" (Simões et al. (2016a)), it was estimated an average vulnerability of 0.88. Considering the ranges of maximum plausibility of the six vulnerability classes proposed for the EMS-98 (Lagomarsino and Cattari, 2014), this value of vulnerability is consistent with vulnerability class A (V between 0.84 and 0.92).

The fragility functions are derived as a function of the mean damage (μ_D), which in turn depends on the ductility index (Q). This factor was assumed equal to 2.3 as in the original formulation of the Macroseismic Vulnerability Model. Finally, in order to compare the fragility functions, it is necessary to use the same seismic intensity measure, and so to convert the macroseismic intensity I in PGA. The relationship proposed by Lagomarsino (2006) is adopted to this end.

Figure 5.9 compares the fragility functions obtained from the application of the hybrid method proposed by Vicente et al. (2011), dashed lines, and the fragility functions proposed in this work, considering both the global and local behaviour, solid lines. This option is consistent with the hybrid method and the parameters analysed for the definition of the Vulnerability Index (I_V) of the buildings which also take into account the local seismic behaviour. In addition, in this case, a direct correspondence between the performance limit states is considered, i.e. between LSk and PLk.

Figure 5.10 compares the results in terms of the probability damage distribution for PGA = 1.94 m/s^2, showing that the probability of having heavy damage (DS4) and the probability of collapse (DS5) estimated by the hybrid method are lower than the proposed in this work: 38% in contrast with 47% for DS4, and 19% in contrast with 34% for DS5.

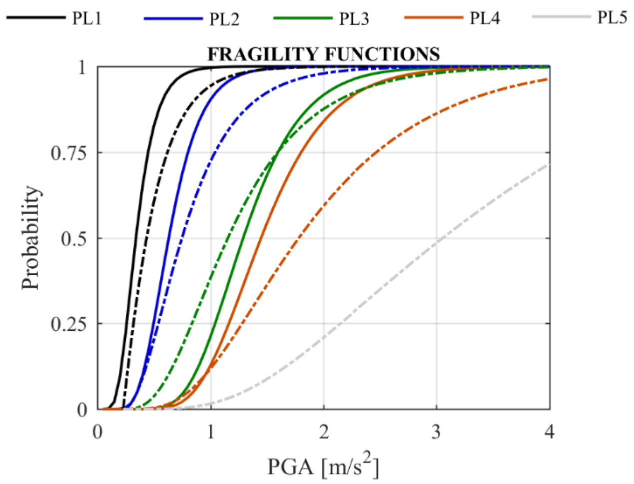

Figure 5.9 – Comparison of the fragility functions: discontinuous lines refer to results from the hybrid method (Vicente et al., 2011) while solid lines refer to the results from the present work

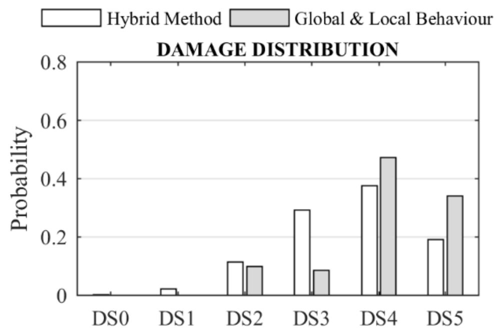

Figure 5.10 – Distribution of damage considering for seismic action type 1 (PGA=1.94 m/s^2)

D'Ayala et al. (1997) analysed 200 URM buildings in Alfama district, in Lisbon, with 2 to 6 storeys. The vulnerability assessment was supported on the application of a simplified limit-state approach (analytical method). The fragility functions proposed by D'Ayala et al. (1997) consider as performance limit states the damage scale from the European Macroseismic Scale (EMS-92): DS1 – negligible, DS2 – moderate, DS3 – substantial, DS4 – very heavy, and DS5 – destruction. Here a direct correspondence between PLk and the DSk is considered. Figure 5.11 compares the fragility functions proposed by D'Ayala et al. (1997), dashed lines, and the fragility functions proposed in this thesis. The curves are quite diverse and indicate that the URM buildings constructed in the 15th century are less vulnerable than the URM buildings of type I constructed in the transition between the 19th and 20th centuries in Lisbon. Figure 5.12 compares the results in terms of the probability damage distribution for PGA = 1.94 m/s^2.

In summary, the comparison of the fragility functions and the corresponding distribution of damage for the code seismic action type 1 for Lisbon (PGA = 1.94 m/s^2) indicated that the vulnerability estimated in the present work is between the results obtained from previous works, supported on a simplified approach (only one building was analysed) and conventional parameters, and the results obtained from the application of the hybrid method proposed by Vicente et al. (2011). The fragility functions proposed by D'Ayala et al. (1997) indicated that these older URM buildings are less vulnerable than the URM buildings under study. However, this is not a general conclusion and it is likely that the simplified analytical method adopted requires further calibration.

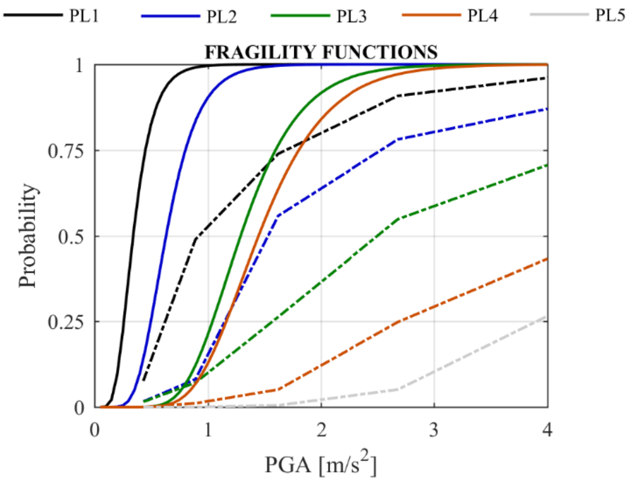

Figure 5.11 – Comparison of the fragility functions: discontinuous lines refer to the results proposed by D'Ayala et al. (1997) while solid lines refer to the results from the present work

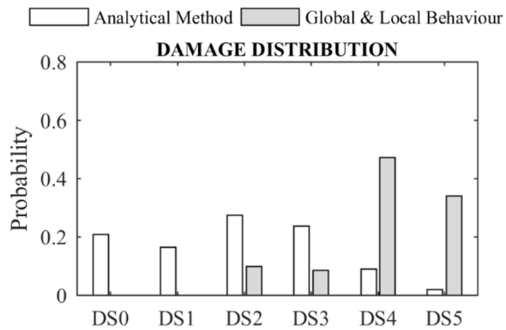

Figure 5.12 – Distribution of damage considering for seismic action type 1 (PGA=1.94 m/s^2)

5.4. Conclusion

In this chapter, a procedure for the combination of fragility functions considering the contribution of both global and local seismic behaviour is proposed, aiming to derive the final fragility functions for the URM buildings of type I. In this work, as expected, the contribution of the local seismic behaviour increased the final vulnerability of the buildings. For the lower damage states, seismic action type 2 – intra-plate earthquake, is the most demanding scenario considering that the probability of having heavy damage (DS3) increased from 8.9% to 28% due to the contribution of the out-of-plane mechanisms involving the last floor of the buildings. Nevertheless, with seismic action type 1 – inter-plate earthquake, it is estimated that there is about 50% probability of having very heavy damage (DS4) and 34% probability of collapse (DS5). This puts in evidence the high seismic vulnerability of these URM buildings and the urgent need to reduce potential losses due to future earthquakes. The proposed fragility functions were compared with other functions obtained based on more simplified approaches.

It may be stated that the parameters estimated in this thesis related to the dispersion in the capacity of the buildings and to the dispersion in the definition of the seismic demand may be considered for the conduction of other works related to the seismic vulnerability assessment of URM buildings.

6. FINAL REMARKS AND FUTURE WORK

This thesis focuses on the evaluation of the seismic vulnerability of unreinforced masonry buildings and addresses the buildings constructed between the 19th and 20th centuries in Lisbon, Portugal. It was proposed to define the seismic vulnerability based on the derivation of fragility functions supported on non-linear static procedures and performance/displacement-based approaches. The following objectives were proposed: 1) characterization of the building typology, 2) definition of cases of study, 3) analysis of the seismic behaviour considering the global and local seismic response, and 4) definition of fragility functions considering different uncertainties that influence the seismic behaviour of the buildings. All these objectives were accomplished.

The characterization of the buildings was based on a multidisciplinary approach aiming to increase the knowledge about the architectural and structural features of the buildings and to identify the main variations within the typology. These buildings may be sub-divided into four types (from I to IV) as a function of the plan geometry and configuration of the structure. In this thesis, it was proposed to evaluate the seismic behaviour of buildings of type I – buildings with small size façades and one flat per floor – supported by the higher probability of collapse in comparison with the other types, estimated in previous studies, and by their representativeness in the existing building stock.

The geometry of a prototype building was defined based on a survey conducted to a block of buildings in Lisbon. The prototype building has five storeys (which is the average of the typology) and is characterized by unreinforced masonry walls and timber floors and roof structure. This prototype building was replicated in order to set a block of three buildings aiming to take into account the interaction of buildings constructed in aggregates and the possibility that the side walls are shared or independent between buildings. The analysis of the pounding effect was not in the scope of this thesis.

The main variations identified for the building typology in terms of geometry, constructive details and materials were assumed as epistemic uncertainties. These were treated through the logic-tree approach, resulting in the definition of different building models. In future works, the logic-tree may be extended to the analysis of buildings with different number of floors (e.g. it was referred that these buildings have between four and six storeys high) or to the study of the effect of the common structural alterations induced from human activities (e.g. the removal of interior walls).

The analysis of the seismic behaviour of the buildings of type I was addressed to the global response, mainly governed by the in-plane capacity of the walls, and the local response, related to the activation of out-of-plane mechanisms, considering different methodologies, models and verification procedures. This is justified considering the different failure modes involved in the seismic response. The global seismic behaviour of masonry buildings depends on the capability of the structure to redistribute the horizontal loads between the elements in order to explore the maximum in-plane strength of masonry walls. The in-plane strength of masonry walls may be dominated by flexural or shear failure modes, which in turn depends on the geometry of the elements and on the mechanical properties of the material. The local seismic behaviour is typically consisting on the out-of-plane failure of parts of the building insufficiently connected to the rest of the structure. In this case, the response is mainly related to the geometric stability of the part of the structure involved in the mechanism rather than to the strength of materials. Therefore, in this thesis, the overall seismic behaviour of the buildings was determined by the combination between the global and local seismic behaviour in terms of fragility functions. To this end, different sources of uncertainties affecting the seismic response were considered in the analysis of the global and local behaviour aiming to estimate the parameters for the derivation of the corresponding fragility functions. In this point, reference to the fact that the quantification of the uncertainties associated with the local seismic behaviour constitutes a novelty in comparison with previous works.

The methodology proposed for the analysis of the global seismic behaviour is supported on the non-linear static (pushover) analyses of a group of 1000 blocks of buildings representative of the typology. The group of buildings resulted from the combination between the models identified based on the logic-tree approach (epistemic uncertainties) and the parameters assumed as aleatory variables aiming to account both the uncertainties in the quantification of the values and the intrinsic variations between buildings belonging to the same typology. In this case, the Monte Carlo Method was considered to sample the 50 aleatory variables and define the input variables for the set of building models as a function of the probability/reliability attributed.

The interval of values considered for the aleatory variables may be used as reference for future studies regarding the analysis of URM buildings in Lisbon. Nevertheless, additional works should be carried out for the characterization of the mechanical properties of masonry, deformability characteristics of masonry piers and spandrels, connection between walls and in-plane stiffness of timber floors. In this work, the Bayesian update approach was applied to define the mechanical properties of the different types of masonry present in the buildings taking into account the experimental results from tests performed in masonry walls in Lisbon. One advantage of the Bayesian approach is that in presence of new tests results, the interval of values proposed in this thesis, may be simply updated.

Non-linear dynamic time-history analyses were also performed in order to confirm the reliability of the load distributions considered on the non-linear static (pushover) analyses. It was verified that, for this building type, the non-linear static (pushover) analyses should be performed by considering at least the uniform load distribution (proportional to the mass) and the pseudo-triangular load distributions (proportional to the product between the mass and the height of the node) and determine the worst case from the seismic performance-based assessment. Despite the fact that the pseudo-triangular distribution provided a pushover curve with lower initial stiffness and strength, and higher displacement capacity, the computation of the seismic intensity measure (here in terms of PGA) compatible with the different performance limit states, indicated that in general lower PGA values were obtained with the uniform distribution. In what concerns the performance limit states, these were defined based on the multi-scale approach, which correlates damage in the structure at different scales, namely single elements, macro-elements and global. In this work, a new formulation for the macro-element scale verification was applied for the first time in an extensive way, aiming to detect the occurrence of soft-storey mechanisms, but avoiding the drawback of defining conventional inter-storey drift thresholds. This criterion revealed to be more effective in providing accurate results for this typology of buildings.

The methodology proposed for the analysis of the local seismic behaviour was defined based on non-linear kinematic analyses to define the capacity of different out-of-plane collapse mechanisms involving the upper level of the façade walls. This hypothesis was supported by experimental results from shaking table tests on reduced scale models of these masonry buildings performed in previous works. The reliability of each mechanisms was analysed as an epistemic uncertainty and treated through the logic-tree approach. The geometry of the elements and the actions involved in the mechanisms were assumed as aleatory variables. These aleatory variables were combined through a complete factorial analysis in order to define the input parameters for the set of mechanisms. Considering that the mechanisms are located in the upper level of the buildings, the seismic input was defined through a floor response spectrum that takes into account the dynamic filtering effect of the buildings and progressive damage in the building. This was quantified based on an iterative procedure that aimed to guarantee coherence between the damping properties at the global and local level and to establish a limit for the seismic verification of the mechanisms.

The fragility functions associated with the global and the local seismic behaviour were derived considering the contribution of the uncertainties in the capacity and the uncertainties in the determination of the seismic demand. The dispersion in the capacity was supported on the application of the Monte Carlo Method in case of the global seismic behaviour and of the Response Surface Method in case of the local seismic behaviour for the treatment of the aleatory variables considered. The first method requires a larger number of analyses to obtain a reliable outcome, while the second method needs only a few points to define the hyperplane that fits the response surface of the variables. Notwithstanding the lower computational burden, the application of the Response Surface Method to the analysis of the global seismic behaviour would not be feasible for the comprehensive analyses of the variations within a typology of buildings. In what concerns the dispersion in the seismic demand, this was quantified by considering a set of 30 records compatible with the code seismic action type 1 and type 2 for Lisbon. For the analysis of the local seismic behaviour of the façade walls, an additional contribution to the dispersion was considered to take into account the uncertainties associated with the definition of the floor response spectrum and the dynamic filtering effect provided by the building.

The final fragility functions for the unreinforced masonry buildings of type I were derived from the combination between the global and the local seismic behaviour. Considering the earthquake-resistant code for Lisbon (action type 1 with a return period of 475 years), the results indicated that these buildings of type I have about 50% probability of having very heavy damage and more than 30% probability of collapse. Here, it is important to refer that these results represent the upper line of the expected distribution of damage, taking into account that: 1) the worst case scenario was considered in the main steps of the methodology and, 2) the recommendation given by the Portuguese National Annex to the EC8-3 (IPQ, 2017) to reduce of the reference peak ground acceleration for the assessment of existing buildings was disregarded. Nevertheless, these results put in evidence the high seismic vulnerability of these buildings and the urgent need for the structural intervention and for the design of retrofitting measures in order to reduce potential losses due to future earthquakes. In this regards, it was verified that concerning the local out-of-plane response, the buildings are particularly vulnerable to the overturning of the central piers from the last floor and of the parapets. In fact, the probability distribution of damage for the code seismic action for Lisbon indicates the sure collapse of the parapets for both types of action. A possible intervention is to fix this non-structural element at its base or to the roof structure by the application of steel tie-rods. Concerning the global response, the main criticality of the buildings in the direction of the side walls, is related to the insufficient capacity in terms of ductility more than overall strength, while in the direction of the façade walls the opposite occurs. Thus, the improvement of the connection between perpendicular walls and between walls and horizontal diaphragms, as well as the increase of the in-plane stiffness of the later ones, should be considered in a first approach to improve the global and local response and reduce the seismic vulnerability of the buildings. A second approach would be to increase the in-plane capacity of the masonry walls through reinforced plasters or by the introduction of new shear walls.

In future work, it is suggested to take the next step and design different strengthening solutions to improve the seismic performance of these buildings supported on cost-benefit analyses. The fragility functions proposed in this thesis are useful for comparison with the fragility functions obtained with the reinforced models. It is also suggested to adopt an equivalent methodology for the analyses of buildings of type II, III and IV and perform the overall seismic vulnerability assessment of the unreinforced masonry buildings constructed in Lisbon in this period. Finally, the methodology adopted for the evaluation of the seismic vulnerability may be considered for the analysis of other masonry building typologies.

REFERENCES

Appleton, J. (2003) *Reabilitação de Edifícios Antigos. Patologias e tecnologias de intervenção*. 1st edn. Amadora: Edições Orion (In Portuguese).

Appleton, J. G. (2005) *Reabilitação de Edifícios 'Gaioleiros'*. 1st edn. Lisboa: Edições Orion (In Portuguese).

Araújo, M., Macedo, L., Marques, M. and Castro, J. M. (2016) 'Code-based record selection methods for seismic performance assessment of buildings', *Earthquake Engineering & Structural Dynamics*, 45, pp. 129–148. doi: 10.1002/eqe.2620.

ASCE (2014) *ASCE/SEI 41-13 - Seismic Evaluation and Retrofit of Existing Buildings*. American Socity of Civil Engineers (ASCE), Reston, Virginia, USA.

ASTM (2002) *ASTM E 519-02: Standard test method for diagonal (shear) in masonry assemblages*. American Society for Testing and Materials (ASTM) International, West Conshohocken, USA.

ASTM (2004) *ASTM C 1197-04: Standard Test ASTM C1197-04a, Standard test method for in situ measurement of masonry deformability properties using the flatjack method*. American Society for Testing and Materials (ASTM) International, West Conshohocken, USA.

Beyer, K. (2012) 'Peak and residual strengths of brick masonry spandrels', *Engineering Structures*. Elsevier Ltd, 41, pp. 533–547. doi: 10.1016/j.engstruct.2012.03.015.

Beyer, K. and Dazio, A. (2012) 'Quasi-static cyclic tests on masonry spandrels', *Earthquake Spectra*, 28(3), pp. 907–929. doi: 10.1193/1.4000063.

Beyer, K. and Mangalathu, S. (2014) 'Numerical Study on the Peak Strength of Masonry Spandrels with Arches', *Journal of Earthquake Engineering*, 18, pp. 169–186. doi: 10.1080/13632469.2013.851047.

Blandon, C. A. and Priestley, M. J. N. (2005) 'Equivalent Viscous Damping Equations for Direct Displacement Based Design', *Journal of Earthquake Engineering*, 9(2), pp. 257–278. doi: 10.1142/S1363246905002390.

Bracchi, S., Rota, M., Magenes, G. and Penna, A. (2016) 'Seismic assessment of masonry buildings accounting for limited knowledge on materials by Bayesian updating', *Bulletin of Earthquake Engineering*, 14(8), pp. 2273–2297. doi: 10.1007/s10518-016-9905-8.

Branco, F. and Correia, J. (2003) *Ensaios à compressão de elementos de parede de alvenaria da Praça de Touros do Campo Pequeno*. Relatório ICIST EP Nº 82/03, Instituto Superior Técnico, Universidade de Lisboa (In Portuguese).

Branco, M. and Guerreiro, L. (2011) ‘Seismic rehabilitation of historical masonry buildings’, *Engineering Structures*. Elsevier Ltd, 33(5), pp. 1626–1634. doi: 10.1016/j.engstruct.2011.01.033.

Calderini, C., Cattari, S. and Lagomarsino, S. (2009) ‘In-plane strength of unreinforced masonry piers’, *Earthquake Engineering and Structural Dynamics*, 38, pp. 243–267. doi: 10.1002/eqe.

Calvi, G. M. (1999) ‘A displacement-based approach for vulnerability evaluation of classes of buildings’, *Journal of Earthquake Engineering*, 3(3), pp. 411–438. doi: 10.1080/13632469909350353.

Calvi, G. M. and Pinho, R. (2004) *LESSLOSS: a European integrated project on risk mitigation for earthquakes and landslides. Research Report Rose 2004/02*. Pavia: IUSS Press.

Calvi, G. M. and Pinho, R. (2006) ‘Development of seismic vulnerability assessment methodologies over the past 30 years’, *ISET Journal of Earthquake Technology*, 43(3), pp. 75–104.

Candeias, P. (2008) *Avaliação da vulnerabilidade sísmica de edifícios de alvenaria*. PhD Thesis. Universidade do Minho. Guimarães (In Portuguese).

Candela, M., Cattari, S., Lagomarsino, S. and Fonti, R. (2013) ‘Prove in situ per la caratterizzazione della muratura in pietrame grezzo alle azioni nel piano e fuori dal piano’, in *Proceedings of the XV Convegno ANIDIS ‘l’Ingegneria Sismica in Italia"*. Padova (In Italian).

Carvalho, E. C., Coelho, E., Campos Costa, A., Sousa, M. L. and Candeias, P. (2002) ‘Vulnerability evaluation of residential buildings in Portugal’, in *Proceedings of the 12th European Conference on Earthquake Engineering*. London.

Carvalho, J. (2008) *Caracterização mecânica de paredes resistentes em alvenaria de pedra através de ensaios não destrutivos*. MSc Thesis. Instituto Superio Técnico, Universidade de Lisboa. Lisboa (In Portuguese).

Cattari, S. (2007) *Modelling of existing masonry and mixed-masonry concrete buildings by the equivalent frame approach: formulation of synthetic models*. PhD Thesis, University of Genoa. Genova.

Cattari, S. and Beyer, K. (2015) ‘Influence of spandrel modelling on the seismic assessment of existing masonry buildings’, in *Proceedings of the 10th Pacific Conference on Earthquake Engineering Building an Earthquake-Resilient Pacific*. Sydney.

Cattari, S., Curti, E., Galasco, A. and Resemini, S. (2005) *Analisi sismica lineare e non lineare di edifici in muratura. Teoria ed esempi di applicazione second OPCM 3274/2003 e 3431/2005*. 1st edn. Napoli: Gruppo Editoriale Esselibri - Simone (In Italian).

Cattari, S. and Lagomarsino, S. (2008) ‘A strength criterion for the flexural behaviour of spandrels in un-reinforced masonry walls’, in *Proceedings of the 14th Earthquake Conference on Earthquake Engineerring*. Beijing.

Cattari, S. and Lagomarsino, S. (2009) ‘Modelling the seismic response of unreinforced existing masonry buildings: a critical review of some models proposed by codes’, in *Proceedings of the 11th Canadian Masonry Symposium*. Toronto.

Cattari, S. and Lagomarsino, S. (2013) ‘Masonry Structures’, in Sullivan, T. and Calvi, G. M. (eds) *Developments in the field of displacement based seismic assessment*. IUSS Press, pp. 151–200. doi: 10.1002/ejoc.201200111.

Cattari, S., Lagomarsino, S., Bazzurro, A. and Porta, F. (2015) ‘Critical review of analytical models for the in-plane and out-of-plane assessment of URM buildings’, in *Proceedings of the New Zealand Society for Earthquake Engineering (NZSEE) Annual Technical Conference*. Rotorua.

Cattari, S., Lagomarsino, S., Bosiljkov, V. and D’Ayala, D. (2015) ‘Sensitivity analysis for setting up the investigation protocol and defining proper confidence factors for masonry buildings’, *Bulletin of Earthquake Engineering*, 13(1), pp. 129–151. doi: 10.1007/s10518-014-9648-3.

Cattari, S., Marino, S. and Lagomarsino, S. (2015) ‘Seismic assessment of plan irregular masonry buildings with flexible diaphragms’, in *Proceedings of the 10th Pacific Conference on Earthquake Engineering Building an Earthquake-Resilient Pacific*. Sydney.

CEN (2004) *Eurocode 8: Design of structures for earthquake resistance. Part 1: General rules, seismic actions and rules for buildings Eurocode, EN 1998-1*. European Committee for Standardization (CEN), Brussels.

CEN (2005) *Eurocode 6: Design of masonry structures. Part 1-1: Genral rules for reinforced and unreinforced masonry structures, EN 1996-1-1:2005*. European Committee for Standardization (CEN). Brussels.

CNR (2014) *Istruzioni per la valutazione affidabilistica della sicurezza sismica di edifici esistenti. CNR-DT 212/2013*.

Cóias e Silva, V. (2007) *Reabilitação Estrutural de Edifícios Antigos. Alvenaria e Madeira. Técnicas Pouco Intrusivas*. 2nd edn. Lisboa: Argumentum and GECoRPA (In Portuguese).

Cornell, C. A., Jalayer, F., Hamburger, R. O. and Foutch, D. A. (2002) ‘Probabilistic Basis for 2000 SAC Federal Emergency Management Agency Steel Moment Frame Guidelines’, *Journal of Structural Engineering*, 128, pp. 526–533. doi: 10.1061/(ASCE)0733-9445(2002)128:4(526).

Correia, J. (2011) *Análise experimental de um murete de alvenaria de pedra tradicional de grandes dimensões*. MSc Thesis. Universidade Nova de Lisboa. Lisboa (In Portuguese).

D’Ayala, D. and Lagomarsino, S. (2015) ‘Performance-based assessment of cultural heritage assets: outcomes of the European FP7 PERPETUATE project’, *Bulletin of Earthquake Engineering*, 13(1), pp. 5–12. doi: 10.1007/s10518-014-9710-1.

D’Ayala, D. and Paganoni, S. (2011) ‘Assessment and analysis of damage in L’Aquila historic city centre after 6th April 2009’, *Bulletin of Earthquake Engineering*, 9(1), pp. 81–104. doi: 10.1007/s10518-010-9224-4.

D’Ayala, D., Spence, R., Oliveira, C. S. and Pomonis, A. (1997) ‘Earthquake Loss Estimation for Europe’s Historic Town Centres’, *Earthquake Spectra*, 13(4), pp. 773–793.

D’Ayala, D. and Speranza, E. (2003) ‘Definition of Collapse Mechanisms and Seismic Vulnerability of Historic Masonry Buildings’, *Earthquake Spectra*, 19(3), pp. 479–509. doi: 10.1193/1.1599896.

Degli Abbati, S., Cattari, S. and Lagomarsino, S. (2017) ‘Proposta di spettri di piano per la verifica di elementi non strutturali e meccanismi locali negli edifici in muratura’, in *Proceedings of the XVII Convegno ANIDIS ‘l’Ingegneria Sismica in Italia"*. Pistoia (In Italian).

Degli Abbati, S., Cattari, S., Marassi, I. and Lagomarsino, S. (2014) ‘Seismic Out-of-Plane Assessment of Podestà Palace in Mantua (Italy)’, *Key Engineering Materials*, 624, pp. 88–96. doi: 10.4028/www.scientific.net/KEM.624.88.

Degli Abbati, S. and Lagomarsino, S. (2017) ‘Out-of-plane static and dynamic response of masonry panels’, *Engineering Structures*, 150, pp. 803–820. doi: 10.1016/j.engstruct.2017.07.070.

Doherty, K., Griffith, M. C., Lam, N. and Wilson, J. (2002) ‘Displacement-based seismic analysis for out-of-plane bending of unreinforced masonry walls’, *Earthquake Engineering and Structural Dynamics*, 31(4), pp. 833–850. doi: 10.1002/eqe.126.

Endo, Y., Pelà, L. and Roca, P. (2017) ‘Review of Different Pushover Analysis Methods Applied to Masonry Buildings and Comparison with Nonlinear Dynamic Analysis’, *Journal of Earthquake Engineering*, 21(8), pp. 1234–1255. doi: 10.1080/13632469.2016.1210055.

Erberik, M. A. (2008) ‘Generation of fragility curves for Turkish masonry buildings considering in-plane failure modes’, *Earthquake Engineering & Structural Dynamics*, 37(3), pp. 387–405. doi: 10.1002/eqe.760.

Fajfar, P. (1999) ‘Capacity spectrum method based on inelastic demand spectra’, *Earthquake Engineering and Structural Dynamics*, 28(9), pp. 979–993. doi: 10.1002/(SICI)1096-9845(199909)28:9<979::AID-EQE850>3.0.CO;2-1.

Fajfar, P. (2000) ‘A Nonlinear Analysis Method for Performance-Based Seismic Design’, *Earthquake Engineering and Structural Dynamics*, 16(3), pp. 573–592. doi: 10.1193/1.1586128.

Farinha, J. and Reis, A. (1993) *Tabelas Técnicas*. 2nd edn. Setúbal: Edição P.O.B. (In Potuguese).

de Felice, G. (2011) 'Out-of-plane seismic capacity of masonry depending on wall section morphology', *International Journal of Architectural Heritage*, 5, pp. 466–482. doi: 10.1080/15583058.2010.530339.

FEMA (2005) *FEMA 440 - Improvement of Nonlinear Static Seismic Analysis Procedures*. Federal Emergency Management Agency (FEMA). Washington, D.C., USA.

Fernandes, J. M. (1993) *Arquitectura Modernista em Portugal*. 1st edn. Lisboa (In Portuguese): Gradiva.

Ferreira, T. M., Costa, A. A. and Costa, A. (2015) 'Analysis of the out-of-plane seismic behavior of unreinforced masonry: a literature review', *International Journal of Architectural Heritage*, 9(8), pp. 949–972. doi: 10.1080/15583058.2014.885996.

Ferreira, T. M., Vicente, R., Mendes da Silva, J. A. R., Varum, H. and Costa, A. (2013) 'Seismic vulnerability assessment of historical urban centres: case study of the old city centre in Seixal, Portugal', *Bulletin of Earthquake Engineering*, 11, pp. 1753–1773. doi: 10.1007/s10518-013-9447-2.

Ferreira, V. and Farinha, J. (1974) *Tabelas Técnicas para Engenharia Civil*. 7th edn. Lisboa: Técnica. Associação de Estudantes do Instituto Superior Técnico (In Portuguese).

França, J. A. (1977) *Lisboa Pombalina e o Iluminismo*. 2nd edn. Lisboa: Livraria Bertrand (In Portuguese).

França, J. A. (2009) *Lisboa, História Física e Moral*. 2nd edn. Lisboa: Livros Horizonte (In Portuguese).

Franchin, P., Pinto, P. E. and Rajeev, P. (2010) 'Confidence factor?', *Journal of Earthquake Engineering*, 14(7), pp. 989–1007. doi: 10.1080/13632460903527948.

Frazão, M. (2013) *Modelação de um edifício 'Gaioleiro' para Avaliação e Reforço Sísmico*. MSc Thesis. Instituto Superior Técnico, Universidade de Lisboa. Lisboa (In Portuguese).

Freeman, S. A. (1998) 'Development and use of capacity spectrum method', in *Proceedings of the 6th US NCEE Conference on Earthquake Engineering/EERI*. Seattle, Washington, p. 269.

Galasco, A., Lagomarsino, S. and Penna, A. (2006) 'On the use of pushover analysis for existing masonry buildings', in *Proceedings of the 1st European Conference on Earthquake Engineering and Seismology*. Geneva.

Gattesco, N., Clemente, I., Macorini, L. and Noè, S. (2008) 'Experimental investigation on the behavior of spandrels in ancient masonry buildings', in *Proceedings of the 14th World Conference on Earthquake Engineering*. Beijing.

Giongo, I., Dizhur, D., Tomasi, R. and Ingham, J. M. (2013) ‘In-plane assessment of existing timber diaphragms in URM buildings via quasi-static and dynamic in situ tests’, *Advanced Materials Research*, 778, pp. 495–502. doi: 10.4028/www.scientific.net/AMR.778.495.

GNDT (1994) *Scheda di esposizione e vulnerabilità e di rilevamento danni di primo livello e secondo livello (muratura e cemento armato)*. Gruppo Nazionale per la Difesa dai Terremoti (GNDT). Roma (In Italian).

Gomes, R. (2011) *Sistema Estrutural de Edifícios Antigos de Lisboa - Os Edifícios ‘Pombalinos’ e os Edifícios ‘Gaioleiros’*. MSc Thesis. Instituto Superior Técnico, Universidade de Lisboa. Lisboa (In Portuguese).

Graziotti, F., Magenes, G. and Penna, A. (2012) ‘Experimental cyclic behaviour of stone masonry spandrels’, in *Proceedings of the 15th World Conference on Earthquake Engineering*. Lisboa.

Griffith, M. C., Lam, N. T. K., Wilson, J. L. and Doherty, K. (2004) ‘Experimental investigation of unreinforced brick masonry walls in flexure’, *Journal of Structural Engineering*, 130(3), pp. 423–432. doi: 10.1061/(ASCE)0733-9445(2004)130:3(423).

Grünthal, G. (1998) *European Macroseismic Scale 1998: EMS-98*. Chaiers du Centre Européen de Géodynamique et de Séismologie. Luzembourg.

Haddad, J., Cattari, S. and Lagomarsino, S. (2017) ‘The use of sensitivity analysis for the probabilistic-based seismic assessment of existing buildings’, in *16th World Conference on Earthquake Engineering*. Santiago Chile.

Housner, G. W. (1963) ‘The behavior of inverted pendulum structures during earthquakes’, *Bulletin of the Seismological Society of America*, 53(2), pp. 403–417.

Ilustração Portugueza (1921) *A Manifestação Operária de protesto contra os gaioleiros. O desastre de Campo de Ourique*. Ilustração Portugueza. Edição Semanal do Jornal ‘O Século’. Lisboa (In Portuguese).

INE (2012) *Censos 2011 Resultados Definitivos - Portugal*. Instituto Nacional de Estatística (INE), I.P.. Lisboa (In Portuguese).

IPQ (2009a) *Eurocódigo - Bases para o projeto de estruturas, NP EN 1990:2009*. Instituto Português da Qualidade (IPQ). Caparica (In Portuguese).

IPQ (2009b) *Eurocódigo 1 - Bases para o projeto de estruturas. Parte 1-1: Acções Gerais. Pesos volúmicos, pesos próprios, sobrecargas em edifícios, NP EN 1991-1-1:2009*. Instituto Português da Qualidade (IPQ). Caparica (In Portuguese).

IPQ (2010) *Eurocódigo 8 - Projecto de estruturas para resistência aos sismos. Parte 1: Regras gerais,* *acções sísmicas e regras para edifícios, NP EN 1998-1:2010*. Instituto Português da Qualidade (IPQ). Caparica (In Portuguese).

IPQ (2017) *Eurocódigo 8 – Projeto de estruturas para resistência aos sismos Parte 3: Avaliação e reabilitação de edifícios, NP EN 1998-3:2017*. Instituto Português da Qualidade (IPQ). Caparica (In Portuguese).

IREBA (1918) *Instruções Regulamentares para o Emprego do Beton Armado (IREBA)*. Decreto N.º 4036 de 28/03/1918. Lisboa (In Portuguese).

Jalayer, F. and Cornell, C. A. (2003) *A Technical Framework for Probability-Based Demand and Capacity Factor Design (DCFD)*. PEER Report 2003/08. Pacific Earthquake Engineering Center (PEER). Richmond, California.

Jalayer, F. and Cornell, C. A. (2009) 'Alternative non-linear demand estimation methods for probability-based seismic assessments', *Earthquake Engineering and Structural Dynamics*, 38, pp. 951–972. doi: 10.1002/eqe.

Jalayer, F., Elefante, L., Iervolino, I. and Manfredi, G. (2011) 'Knowledge-Based Performance Assessment of Existing RC Buildings', *Journal of Earthquake Engineering*, 15(3), pp. 362–389. doi: 10.1080/13632469.2010.501193.

Joint Committee on Structural Safety (2011) *Probabilistic Model Code. Part 3: Resistance Models. 3.2. Masonry Properties*. Available at: http://www.jcss.byg.dtu.dk/Publications.

Kržan, M., Gostič, S., Cattari, S. and Bosiljkov, V. (2015) 'Acquiring reference parameters of masonry for the structural performance analysis of historical buildings', *Bulletin of Earthquake Engineering*, 13(1), pp. 203–236. doi: 10.1007/s10518-014-9686-x.

Lagomarsino, S. (2006) 'Vulnerability assessment of historical buildings', in Oliveira, C. S., Roca, A., and Goula, X. (eds) *Assessing and Managing Earthquake Risk*. Springer Netherlands, pp. 135–158. doi: 10.1007/978-1-4020-3608-8.

Lagomarsino, S. (2015) 'Seismic assessment of rocking masonry structures', *Bulletin of Earthquake Engineering*, 13(1), pp. 97–128. doi: 10.1007/s10518-014-9609-x.

Lagomarsino, S. (2018) 'Seismic assessment of existing masonry buildings: modelling, analysis and verification procedures', in *Proceedings of the 16th European Conference on Earthquake Engineering*. Thessaloniki (to be published).

Lagomarsino, S. and Cattari, S. (2014) 'Fragility functions of masonry buildings', in Pitilakis, K., Crowley, H., and Kaynia, A. (eds) *SYNER-G: Typology Definition and Fragility Functions for Physical Elements at Seismic Risk, Buildings, Lifelines, Transportation Networks and Critical Facilities,* *Geotechnical, Geological and Earthquake Engineering, 27*. Springer, pp. 111–156. doi: 10.1007/978-94-007-7872-6_5.

Lagomarsino, S. and Cattari, S. (2015a) 'PERPETUATE guidelines for seismic performance-based assessment of cultural heritage masonry structures', *Bulletin of Earthquake Engineering*, 13(1), pp. 13–47. doi: 10.1007/s10518-014-9674-1.

Lagomarsino, S. and Cattari, S. (2015b) 'Seismic Performance of Historical Masonry Structures Through Pushover and Nonlinear Dynamic Analyses', in Ansal, A. (ed.) *Perspectives on European Earthquake Engineering and Seismology, Geotechnical, Geological and Earthquake Engineering, 39*. Springer International Publishing, pp. 265–292. doi: 10.1007/978-3-319-16964-4.

Lagomarsino, S. and Giovinazzi, S. (2006) 'Macroseismic and mechanical models for the vulnerability and damage assessment of current buildings', *Bulletin of Earthquake Engineering*, 4, pp. 415–443. doi: 10.1007/s10518-006-9024-z.

Lagomarsino, S. and Ottonelli, D. (2012) *MB_PERPETUATE A Macro-Block program for the seismic assessment (Freeware software for the safety verification of seismic local mechanisms)*. PERPETUATE (EC- FP7 Project), Deliverable D29. Available at: http://www.perpetuate.eu/final-results/deliverables/.

Lagomarsino, S., Penna, A., Galasco, A. and Cattari, S. (2012) 'TREMURI program: seismic analyses of 3D masonry buildings'. Release 2.0. University of Genoa (e-mail to: tremuri@gmail.com).

Lagomarsino, S., Penna, A., Galasco, A. and Cattari, S. (2013) 'TREMURI program: An equivalent frame model for the nonlinear seismic analysis of masonry buildings', *Engineering Structures*, 56, pp. 1787–1799. doi: 10.1016/j.engstruct.2013.08.002.

Lamego, P., Lourenço, P. B., Sousa, M. L. and Marques, R. (2017) 'Seismic vulnerability and risk analysis of the old building stock at urban scale: application to a neighbourhood in Lisbon', *Bulletin of Earthquake Engineering*, 15(7), pp. 2901–2937. doi: 10.1007/s10518-016-0072-8.

Liel, A. B., Haselton, C. B., Deierlein, G. G. and Baker, J. W. (2009) 'Incorporating modeling uncertainties in the assessment of seismic collapse risk of buildings', *Structural Safety*, 31, pp. 197–211. doi: 10.1016/j.strusafe.2008.06.002.

LNEC (1997) *Pinho bravo para estruturas. Madeira para construção*. Laboratório Nacional de Engenharia Civil (LNEC). Lisboa (In Portuguese).

Lopes, M. (1996) 'Evaluation of the seismic performance of an old masonry building', in *Proceedings of the 11th World Conference on Earthquake Engineering*. Acapulco, p. 1484.

Lopes, M., Meireles, H., Cattari, S., Bento, R. and Lagomarsino, S. (2014) 'Pombalino Constructions: Description and Seismic Assessment', in Costa, A., Guedes, J. M., and Varum, H. (eds) *Structural*

Rehabilitation of Old Buildings, Building Pathology and Rehabilitation, 2. 1st edn. Springer Berlin Heidelberg, pp. 187–233. doi: 10.1007/978-3-642-39686-1.

López, J. (2013) *Edificio de estilo 'gaioleiro' en Lisboa (Portugal)*. Final Report. Universidad Politécnica de Cartagena. Cartagena (In Spanish).

Lourenço, P. B. (2002) 'Computations on historic masonry structures', *Progress in Structural Engineering and Materials*, 4(3), pp. 301–319. doi: 10.1002/pse.120.

Lourenço, P. B., Mendes, N., Ramos, L. F. and Oliveira, D. V (2011) 'Analysis of Masonry Structures Without Box Behavior', *International Journal of Architectural Heritage*, 5, pp. 369–382. doi: 10.1080/15583058.2010.528824.

Macedo, L. and Castro, J. M. (2017) 'SelEQ: An advanced ground motion record selection and scaling framework', *Advances in Engineering Software*, 114, pp. 32–47. doi: 10.1016/j.advengsoft.2017.05.005.

Magenes, G. and Calvi, G. M. (1997) 'In-Plane Seismic Response of Brick Masonry Walls', *Earthquake Engineering and Structural Dynamics*, 26, pp. 1091–1112. doi: 10.1002/(SICI)1096-9845(199711)26:11<1091::AID-EQE693>3.0.CO;2-6.

Magenes, G. and Penna, A. (2009) 'Existing masonry buildings: general code issues and methods of analysis and assessment', in Cosenza, E. (ed.) *Eurocode 8 perspectives from the Italian Standpoint Workshop*. Napoli, pp. 185–198.

Magenes, G. and Penna, A. (2011) 'Seismic design and assessment of masonry buildings in Europe: recent research and code development issues', in *Proceedings of the 9th Australasian Masonry Conference*. Queenstown.

Maio, R., Ferreira, T. M., Vicente, R. and Estêvão, J. (2016) 'Seismic vulnerability assessment of historical urban centres: case study of the old city centre of Faro, Portugal', *Journal of Risk Research*, 19(5), pp. 551–580. doi: 10.1080/13669877.2014.988285.

Martins, S. (2014) *Ligação pavimento/parede com pregagens para reabilitação de edifícios antigos*. MSc Thesis. Universidade Nova de Lisboa. Lisboa (In Portuguese).

McGuire, R. K. (2004) *Seismic hazard and risk analysis*. 1st edn, *Seismic Hazard and Risk Analysis*. 1st edn. Oakland, CA: Earthquake Engineering Research Institute.

Meireles, H., Bento, R., Cattari, S. and Lagomarsino, S. (2014) 'Seismic assessment and retrofitting of Pombalino buildings by pushover analyses', *Earthquake and Structures*, 7(1), pp. 57–82. doi: 10.12989/eas.2014.7.1.057.

Mendes, N., Costa, A. A., Lourenço, P. B., Bento, R., Beyer, K., de Felice, G., Gams, M., Griffith, M.

C., Ingham, J. M., Lagomarsino, S., Lemos, J. V, Liberatore, D., Modena, C., Oliveira, D. V, Penna, A. and Sorrentino, L. (2017) ‘Methods and Approaches for Blind Test Predictions of Out-of-Plane Behavior of Masonry Walls: A Numerical Comparative Study’, *International Journal of Architectural Heritage*, 11(1), pp. 59–71. doi: 10.1080/15583058.2016.1238974.

Mendes, N. and Lourenço, P. B. (2014) ‘Sensitivity analysis of the seismic performance of existing masonry buildings’, *Engineering Structures*, 80, pp. 137–146. doi: 10.1016/j.engstruct.2014.09.005.

Mendes, N., Lourenço, P. B. and Campos-Costa, A. (2014) ‘Shaking table testing of an existing masonry building: assessment and improvement of the seismic performance’, *Earthquake Engineering & Structural Dynamics*, 43(2), pp. 247–266. doi: 10.1002/eqe.2342.

Milošević, J., Cattari, S. and Bento, R. (2018) ‘Sensitivity analyses of seismic performance of ancient mixed masonry-RC buildings in Lisbon’, *International Journal of Masonry Research and Innovation*, (in press).

Milošević, J., Gago, A. S., Lopes, M. and Bento, R. (2013) ‘Experimental assessment of shear strength parameters on rubble stone masonry specimens’, *Construction and Building Materials*, 47, pp. 1372–1380. doi: 10.1016/j.conbuildmat.2013.06.036.

Milošević, J., Lopes, M., Bento, R. and Gago, A. S. (2014) ‘Experimental Study of Rubble Stone Masonry Specimens’, in *Proceedings of the 9th International Masonry Conference*. Guimarães.

MIT (2009) *Istruzioni per l’applicazione delle ‘Norme tecniche per le costruzioni’ di cui al Decreto Ministeriale 14/01/2008*. Ministero delle Infrastrutture e dei Trasporti (MIT). Roma (In Italian).

Monteiro, J. (2012) *Análise Sísmica de Edifícios ‘Gaioleiros’*. MSc Thesis. Instituto Superior Técnico, Universidade de Lisboa. Lisboa (In Portuguese).

Morais, H. (2011) *Análise experimental de um murete de alvenaria de pedra tradicional*. MSc Thesis. Universidade Nova de Lisboa. Lisboa (In Portuguese).

Moreira, S. (2015) *Seismic retrofit of masonry-to-timber connections in historical constructions*. PhD Thesis. Universidade do Minho. Guimarães.

Mouroux, P. and Le Brun, B. (2006) ‘Presentation of RISK-UE project’, *Bulletin of Earthquake Engineering*, 4(4), pp. 323–339. doi: 10.1007/s10518-006-9020-3.

NTC (2008) *Norme tecniche per le costruzioni (NTC). Decreto Ministeriale 14/01/2008*. Roma (In Italian).

NZSEE (2017) *The Seismic Assessment of Existing Buildings. Technical Guidelines for Engineering Assessments. Part C - Detailed Seismic Assessment. Part C8 - Unreinforced Masonry Buildings*. New Zealand Society for Earthquake Engineering (NZSEE) Inc.. Wellington.

Oliveira, M. (2009) *Avaliação sísmica de um quarteirão Pombalina*. MSc Thesis. Instituto Superior Técnico, Universidade de Lisboa. Lisboa (In Portuguese).

Pagnini, L., Vicente, R., Lagomarsino, S. and Varum, H. (2011) ‘A mechanical model for the seismic vulnerability assessment of old masonry buildings’, *Earthquakes and Structures*, 2(1), pp. 25–42. doi: 10.12989/eas.2011.2.1.025.

Penna, A. (2014) ‘Seismic assessment of existing and strengthened stone-masonry buildings: critical issues and possible strategies’, *Bulletin of Earthquake Engineering*, 13(4), pp. 1051–1071. doi: 10.1007/s10518-014-9659-0.

Penna, A., Morandi, P., Rota, M., Manzini, C. F., da Porto, F. and Magenes, G. (2014) ‘Performance of masonry buildings during the Emilia 2012 earthquake’, *Bulletin of Earthquake Engineering*, 12(5), pp. 2255–2273. doi: 10.1007/s10518-013-9496-6.

Pinho, F., Lúcio, V. and Baião, M. (2012) ‘Rubble stone masonry walls in Portugal strengthened with reinforced micro-concrete layers’, *Bulletin of Earthquake Engineering*, 10, pp. 161–180. doi: 10.1007/s10518-011-9280-4.

Pinho, R. (2012) ‘GEM: a participatory framework for open, state-of-the-art models and tools for earthquake risk assessment’, in *Proceedings of the 15th World Conference on Earthquake Engineering*. Lisboa.

Pinto, P. E. and Franchin, P. (2014) ‘Existing Buildings: The New Italian Provisions for Probabilistic Seismic Assessment’, in Ansal, A. (ed.) *Perspectives on European Earthquake Engineering and Seismology, Geotechnical, Geological and Earthquake Engineering, 34*. Springer, pp. 97–130. doi: 10.1007/978-3-319-07118-3.

Pires, A. (2013) *Análise de Paredes de Tabique e de Medidas de Reforço Estrutural; Estudo Numérico*. MSc Thesis. Faculdade de Engenharia, Universidade do Porto. Porto (In Portuguese).

Pitilakis, K., Crowley, H. and Kaynia, A. M. (2014) *SYNER-G: Typology Definition and Fragility Functions for Physical Elements at Seismic Risk*. Springer. doi: 10.1007/978-94-007-7872-6.

Populi, F. (1946) *Os Construtores Civis Tomarenses e o Desenvolvimento da Construção Urbana em Lisboa*. 1st edn. Imprensa Portugal - Brasil. Lisboa (In Portuguese).

Portas, N. (1980) ‘Cerdà e os Traçados’, *Revista de Arquitectura*.

Porter, K., Kennedy, R. and Bachman, R. (2007) ‘Creating fragility functions for performance-based earthquake engineering’, *Earthquake Spectra*, 23(2), pp. 471–489. doi: 10.1193/1.2720892.

Priestley, M. J. N., Calvi, G. M. and Kowalsky, M. J. (2007) *Displacement-based seismic design of structures*. 1st edn. Pavia: IUSS Press.

Ramos, L. F. (2002) *Análise experimental e numérica de estruturas históricas de alvenaria*. MSc Thesis. Universiade do Minho. Guimarães (In Portuguese).

Ramos, L. F. and Lourenço, P. B. (2004) 'Modeling and vulnerability of historical city centers in seismic areas: a case study in Lisbon', *Engineering Structures*, 26(9), pp. 1295–1310. doi: 10.1016/j.engstruct.2004.04.008.

Rebelo, A., Guedes, J. M., Quelhas, B. and Ilharco, T. (2015) 'Assessment of the mechanical behaviour of tabique walls through experimental tests', in *Proceedings of the 2nd International Conference on Historic Earthquake-Resistant Timber Frames in the Mediterranean Region*. Lisboa.

Reboredo, F. and Pais, J. (2012) 'A construção naval e a destruição do coberto florestal em Portugal - Do Século XII ao Século XX', *Ecologia*, 4, p. 31–42 (In Portuguese).

RGEUL (1930) *Regulamento Geral das Edificações Urbanas em Lisboa (RGEUL)*. Postura da Câmara Municipal de Lisboa de 28/08/1930. Lisboa (In Portuguese).

RILEM (1994) 'LUM B6 Diagonal tensile strength tests of small wall specimens, 1991', in *RILEM Recommendations for the Testing and Use of Constructions Materials*. International Union of Laboratories and Experts in Construction Materials, Systems and Structures (RILEM), pp. 488–489. doi: 10.1617/2351580117.152.

RILEM (2004) 'RILEM Recommendation MDT. D.5: In-situ stress-strain behaviour tests based on the flat jack. RILEM TC 177-MDT: "Masonry Durability and on-site Testing"', *Materials and Structures*, 37, pp. 497–501. doi: 10.1007/BF02481589.

Rodrigues, T. F. and Ferreira, O. A. V (1993) 'As cidades de Lisboa e Porto na viragem do século XIX - Caracerísticas da sua evolução demográfica: 1864-1930', *Revista de História*, 12, p. 297–324 (In Portuguese).

Rota, M., Penna, A. and Magenes, G. (2010) 'A methodology for deriving analytical fragility curves for masonry buildings based on stochastic nonlinear analyses', *Engineering Structures*, 32(5), pp. 1312–1323. doi: 10.1016/j.engstruct.2010.01.009.

Rota, M., Penna, A. and Magenes, G. (2014) 'A framework for the seismic assessment of existing masonry buildings accounting for different sources of uncertainty', *Earthquake Engineering and Structural Dynamics*, 43(7), pp. 1045–1066. doi: 10.1002/eqe.2386.

RSCCS (1958) *Regulamento de Segurança das Construções Contra os Sismos (RSCCS). Decreto-Lei nº 41658 de 31/05/1958*. Lisboa (In Portuguese).

RSEP (1961) *Regulamento de Solicitações em Edifícios e Pontes (RSEP). Decreto-Lei n.º 44041 de 18/11/1961*. Lisbon (In Portuguese).

RSEU (1903) *Regulamento de Salubridade das Edificações Urbanas (RSEU), Decreto de 14/02/1903 (In Portuguese)*.

Rubinstein, R. Y. (2011) *Simulation and the Monte Carlo Method*. John Wiley & Sons, Inc.

Santos, M. H. R. (2005) *A Baixa Pombalina. Passado e Futuro*. 2nd edn. Lisboa: Livros Horizonte (In Portuguese).

Segurado, J. E. S. (1903) *Carpintaria Civil*. 1st edn. Lisboa: Biblioteca de Instrução Profissional. Livraria Bertrand, Lisboa (In Portuguese).

Segurado, J. E. S. (1908) *Alvenaria e cantaria*. 1st edn. Lisboa: Biblioteca de Instrução Profissional. Livraria Bertrand. Lisboa (In Portuguese).

Silva, R. H. (1989) *Lisboa de Frederico Ressano Garcia 1874-1909*. 1st edn. Lisboa: Câmara Municipal de Lisboa, Fundação Calouste Gulbenkian (In Portuguese).

Silva, V., Crowley, H., Pagani, M., Monelli, D. and Pinho, R. (2014) 'Development of the OpenQuake engine, the Global Earthquake Model's open-source software for seismic risk assessment', *Natural Hazards*, 72(3), pp. 1409–1427. doi: 10.1007/s11069-013-0618-x.

Silva, V., Crowley, H., Varum, H. and Pinho, R. (2015) 'Seismic risk assessment for mainland Portugal', *Bulletin of Earthquake Engineering*, 13, pp. 429–457. doi: 10.1007/s10518-014-9630-0.

Silva, V., Crowley, H., Varum, H., Pinho, R. and Sousa, L. (2015) 'Investigation of the characteristics of Portuguese regular moment-frame RC buildings and development of a vulnerability model', *Bulletin of Earthquake Engineering*, 13(5), pp. 1455–1490. doi: 10.1007/s10518-014-9669-y.

Simões, A. (2010) *Comportamento sísmico de um quarteirão Pombalino*. MSc Thesis. Instituto Superior Técnico, Universidade de Lisboa. Lisboa (In Portuguese).

Simões, A., Appleton, J. G., Bento, R., Caldas, J. V, Lourenço, P. B. and Lagomarsino, S. (2017) 'Architectural and Structural Characteristics of Masonry Buildings between the 19th and 20th Centuries in Lisbon, Portugal', *International Journal of Architectural Heritage*. Taylor & Francis, 11(4), pp. 457–474. doi: 10.1080/15583058.2016.1246624.

Simões, A., Bento, R., Cattari, S. and Lagomarsino, S. (2014a) 'Seismic Assessment of "Gaioleiro" buildings in Lisbon', in *Proceedings of the 9th International Masonry Conference*. Guimarães.

Simões, A., Bento, R., Cattari, S. and Lagomarsino, S. (2014b) 'Seismic performance-based assessment of "Gaioleiro" buildings', *Engineering Structures*, 80, pp. 486–500. doi: 10.1016/j.engstruct.2014.09.025.

Simões, A., Bento, R., Gago, A. and Lopes, M. (2016) 'Mechanical Characterization of Masonry Walls

With Flat-Jack Tests', *Experimental Techniques*, 40(3), pp. 1163–1178. doi: 10.1007/s40799-016-0114-9.

Simões, A., Bento, R., Lagomarsino, S. and Lourenço, P. B. (2016) 'Simplified evaluation of seismic vulnerability of early 20th century masonry buildings in Lisbon', in *Proceedings of the 10th International Conference on Structural Analysis of Historical Constructions*. Leuven.

Simões, A. G., Bento, R., Lagomarsino, S. and Lourenço, P. B. (2018) 'The seismic assessment of masonry buildings between the 19th and 20th centuries in Lisbon - Evaluation of uncertainties', in *Proceedings of the 10th International Masonry Conference*. Milan.

Simões, A., Milošević, J., Meireles, H., Bento, R., Cattari, S. and Lagomarsino, S. (2015) 'Fragility curves for old masonry building types in Lisbon', *Bulletin of Earthquake Engineering*, 13(10), pp. 3083–3105. doi: 10.1007/s10518-015-9750-1.

Simões, L. (2015) *Ligação pavimentos/paredes de edifícios antigos. Ensaios e verificações de projeto*. MSc Thesis. Universidade Nova de Lisboa. Lisboa (In Portuguese).

Soares, M. (2013) 'Ruiu mais uma parte de um prédio devoluto em Lisboa', *Público*, 28 March. Available at: https://www.publico.pt/2013/03/28/jornal/ruiu-mais-uma-parte-de-um-predio-devoluto-em-lisboa-26295186.

Sorrentino, L., D'Ayala, D., de Felice, G., Griffith, M. C., Lagomarsino, S. and Magenes, G. (2017) 'Review of Out-of-Plane Seismic Assessment Techniques Applied To Existing Masonry Buildings', *International Journal of Architectural Heritage*, 11(1), pp. 2–21. doi: 10.1080/15583058.2016.1237586.

Tondelli, M., Rota, M., Penna, A. and Magenes, G. (2012) 'Evaluation of uncertainties in the seismic assessment of existing masonry buildings', *Journal of Earthquake Engineering*, 16(S1), pp. 36–64. doi: 10.1080/13632469.2012.670578.

Turnšek, V. and Čačovič, F. (1970) 'Some experimental results on the strength of brick masonry walls', in *Proceedings of the 2nd International Brick Masonry Conference*. Stoke-on-Trent.

Turnšek, V. and Sheppard, P. (1980) 'The shear and flexural resistance of masonry walls', in *Proceedings of the International Research Conference on Earthquake Engineering*. Skopje.

Vamvatsikos, D. and Cornell, C. A. (2002) 'Incremental dynamic analysis', *Earthquake Engineering and Structural Dynamics*, 31(3), pp. 491–514. doi: 10.1002/eqe.141.

Vanin, F., Zaganelli, D., Penna, A. and Beyer, K. (2017) 'Estimates for the stiffness, strength and drift capacity of stone masonry walls based on 123 quasi-static cyclic tests reported in the literature', *Bulletin of Earthquake Engineering*, pp. 1–45. doi: 10.1007/s10518-017-0188-5.

Vicente, R. (2008) *Estratégias e metodologias para intervenções de reabilitação urbana Avaliação da vulnerabilidade e do risco sísmico do edificado da Baixa de Coimbra*. PhD Thesis. Universidade de Aveiro. Aveiro (In Portuguese).

Vicente, R., Ferreira, T. M., Mendes da Silva, J. A. R. and Varum, H. (2015) 'In Situ Flat-Jack Testing of Traditional Masonry Walls: Case Study of the Old City Center of Coimbra, Portugal', *International Journal of Architectural Heritage*, 9, pp. 794–810. doi: 10.1080/15583058.2013.855840.

Vicente, R., Parodi, S., Lagomarsino, S., Varum, H. and Mendes da Silva, J. (2011) 'Seismic vulnerability and risk assessment: case study of the historic city centre of Coimbra, Portugal', *Bulletin of Earthquake Engineering*, 9, pp. 1067–1096. doi: 10.1007/s10518-010-9233-3.

Zhang, P., Nagae, T., McCormick, J., Ikenaga, M., Katsuo, M. and Nakashima, M. (2008) 'Friction-based sliding between steel and steel, steel and concrete, and wood and stone', in *Proceedings of the 14th World Conference on Earthquake Engineering*. Beijing.

This page was intentionally left blank

ANNEX A

Modal analyses were performed with the 32 models, defined by the median properties of the aleatory variables. Table A.1 to Table A.8 present the results for the first 10 modes of vibration, the corresponding period (*T*), frequency (*f*) and the dynamic mass participation in the X and Y directions of the structure (M_X and M_Y), for the 8 final models (in reference to §3.3.1). Figure A.1 exemplifies the plan deformation of model H-S-S-S-H for different modes.

Table A.1 – Modal properties of model H-S-S-S-H

Mode	1	2	3	4	5	6	7	8	9	10
T [s]	0.995	0.795	0.690	0.605	0.522	0.472	0.329	0.298	0.293	0.285
f [Hz]	1.005	1.258	1.448	1.654	1.915	2.119	3.037	3.360	3.410	3.508
M_X [%]	67.9	0.1	9.5	3.1	0.0	0.0	10.1	0.9	0.4	0.9
M_Y [%]	0.0	0.0	0.0	0.5	66.6	16.3	0.0	0.0	0.1	0.0

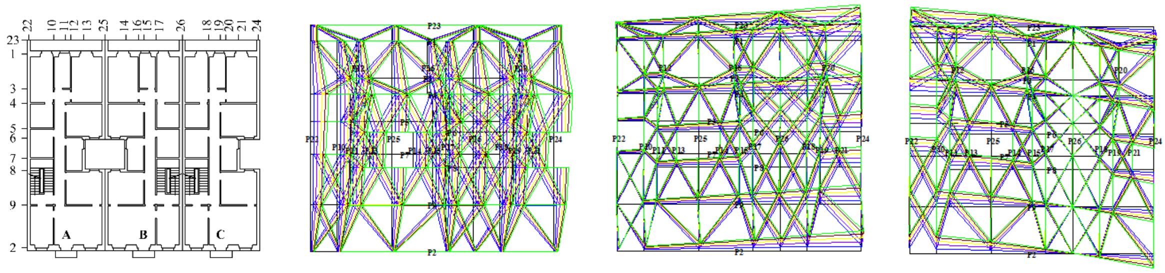

a) b) c) d)

Figure A.1 – Model H-S-S-S-H: a) plan view, and plan deformation corresponding to the b) first translation in the X direction (mode 1), c) first translation in the Y direction (mode 5) and d) second translation in the Y direction (mode 6)

Table A.2 – Modal properties of model H-S-SH-T-T

Mode	1	2	3	4	5	6	7	8	9	10
T [s]	1.253	0.911	0.716	0.640	0.614	0.574	0.563	0.490	0.451	0.451
f [Hz]	0.798	1.097	1.397	1.562	1.627	1.741	1.776	2.041	2.218	2.219
M_X [%]	53.2	0.7	10.4	1.6	15.9	0.8	0.7	0.0	0.0	0.0
M_Y [%]	0.0	0.0	0.0	0.0	1.2	58.7	10.3	14.1	0.0	0.0

Table A.3 – Modal properties of model H-I-S-S-H

Mode	1	2	3	4	5	6	7	8	9	10
T [s]	1.263	0.887	0.764	0.648	0.490	0.468	0.408	0.342	0.310	0.299
f [Hz]	0.791	1.128	1.309	1.543	2.040	2.138	2.450	2.927	3.229	3.340
M_X [%]	57.7	4.0	14.0	3.9	0.003	0.0	8.8	1.2	2.8	0.0
M_Y [%]	0.0	0.0	0.0	0.1	53.8	28.7	0.0	0.0	0.0	0.0

Table A.4 – Modal properties of model H-I-SH-T-T

Mode	1	2	3	4	5	6	7	8	9	10
T [s]	1.365	1.009	0.771	0.694	0.657	0.607	0.515	0.481	0.451	0.451
f [Hz]	0.733	0.991	1.298	1.44	1.522	1.648	1.941	2.078	2.218	2.22
M_X [%]	52.5	1.3	10.0	0.8	18.4	0.6	0.0	0.0	0.0	0.0
M_Y [%]	0.0	0.0	0.0	0.0	0.1	0.1	56.5	26.4	0.0	0.0

Table A.5 – Modal properties of model S-S-S-S-H

Mode	1	2	3	4	5	6	7	8	9	10
T [s]	0.982	0.803	0.711	0.631	0.520	0.471	0.322	0.295	0.292	0.289
f [Hz]	1.019	1.245	1.406	1.586	1.923	2.124	3.109	3.385	3.42	3.464
M_X [%]	69.7	2.0	9.8	0.0	0.0	0.0	11.1	0.2	0.0	2.8
M_Y [%]	0.0	0.0	0.0	0.2	65.6	17.0	0.0	0.1	0.0	0.0

Table A.6 – Modal properties of model S-S-SH-T-T

Mode	1	2	3	4	5	6	7	8	9	10
T [s]	1.244	0.921	0.715	0.692	0.629	0.573	0.532	0.49	0.451	0.451
f [Hz]	0.804	1.086	1.398	1.445	1.589	1.744	1.879	2.039	2.218	2.219
M_X [%]	53.4	1.5	11.8	9.0	3.5	0.1	4.9	0.0	0.0	0.0
M_Y [%]	0.0	0.0	0.0	0.1	0.2	69.5	0.0	14.2	0.0	0.0

Table A.7 – Modal properties of model S-I-S-S-H

Mode	1	2	3	4	5	6	7	8	9	10
T [s]	1.275	0.886	0.773	0.696	0.489	0.467	0.412	0.318	0.309	0.304
f [Hz]	0.785	1.128	1.294	1.437	2.047	2.143	2.426	3.146	3.233	3.285
M_X [%]	55.9	9.0	15.2	0.1	0.0	0.0	8.6	1.6	4.7	0.1
M_Y [%]	0.0	0.0	0.0	0.1	52.3	29.7	0.0	0.0	0.0	0.0

Table A.8 – Modal properties of model S-I-SH-T-T

Mode	1	2	3	4	5	6	7	8	9	10
T [s]	1.355	1.016	0.770	0.738	0.684	0.573	0.516	0.482	0.451	0.451
f [Hz]	0.738	0.984	1.299	1.355	1.463	1.746	1.939	2.076	2.218	2.220
M_X [%]	52.5	2.1	8.9	12.0	3.8	4.9	0.0	0.0	0.0	0.0
M_Y [%]	0.0	0.0	0.0	0.0	0.0	0.1	56.0	26.8	0.0	0.0

ANNEX B

In reference to §3.3.2, non-linear static (pushover) analyses were performed with the 8 models, defined by the median properties of the aleatory variables, considering the uniform and the triangular load distributions applied in the two main directions of the structure (X and Y) and in the two senses of direction (negative and positive). Table B.1 to Table B.4 present the initial stiffness (*K*) and the ratio between maximum base shear force and weight (V_{max}/W). These tables plot: 1) the mean value (E[X]) and Coefficient of Variation (CoV) of the values obtained in the negative and positive directions, 2) E[X] and CoV of the values obtained with the uniform and triangular distributions, 3) the ratio between the Y and X directions and 4) the ratio between models without and with timber "tabique" walls. Table B.5 provides the weight of the models.

Table B.1 – Models with median properties: initial stiffness (*K*, kN/m)

Model | Direction Distribution			Negative and Positive		Uniform and Triangular		Ratio	
			E[X]	CoV [%]	E[X]	CoV [%]		
H-S-S-S-H	X	Unif	19092	2.4	15547	23.1	$\frac{K_Y}{K_X}=6.9$	$\frac{K_{X(H-S-S-S-H)}}{K_{X(H-S-SH-T-T)}}=2.2$
		Trian	12001	5.0				
	Y	Unif	119495	2.3	106583	12.3		
		Trian	93670	2.0				
H-S-SH-T-T	X	Unif	8544	3.3	7121	20.2	$\frac{K_Y}{K_X}=13.3$	$\frac{K_{Y(H-S-S-S-H)}}{K_{Y(H-S-SH-T-T)}}=1.1$
		Trian	5697	1.1				
	Y	Unif	106444	2.1	95059	12.2		
		Trian	83675	2.5				
H-I-S-S-H	X	Unif	15578	3.1	13106	19.5	$\frac{K_Y}{K_X}=10.8$	$\frac{K_{X(H-I-S-S-H)}}{K_{X(H-I-SH-T-T)}}=1.8$
		Trian	10633	7.4				
	Y	Unif	157882	1.0	141319	11.8		
		Trian	124757	0.8				
H-I-SH-T-T	X	Unif	8862	2.3	7378	20.3	$\frac{K_Y}{K_X}=18.1$	$\frac{K_{Y(H-I-S-S-H)}}{K_{Y(H-I-SH-T-T)}}=1.1$
		Trian	5894	3.1				
	Y	Unif	149451	1.7	133433	12.1		
		Trian	117416	1.8				
S-S-S-S-H	X	Unif	19434	5.7	16360	19.5	$\frac{K_Y}{K_X}=6.7$	$\frac{K_{X(S-S-S-S-H)}}{K_{X(S-S-SH-T-T)}}=1.8$
		Trian	13285	3.4				
	Y	Unif	122501	2.5	108837	12.8		
		Trian	95173	2.3				
S-S-SH-T-T	X	Unif	11868	1.4	9264	28.3	$\frac{K_Y}{K_X}=10.2$	$\frac{K_{Y(S-S-S-S-H)}}{K_{Y(S-S-SH-T-T)}}=1.1$
		Trian	6660	4.9				
	Y	Unif	106218	0.5	94793	12.1		
		Trian	83368	0.8				

Table B.2 – Models with median properties: initial stiffness (K, kN/m)

Model | Direction Distribution			Negative and Positive		Uniform and Triangular		Ratio	
			E[X]	CoV [%]	E[X]	CoV [%]		
S-I-S-S-H	X	Unif	16197	0.0	13317	22.1	$\frac{K_Y}{K_X}=11.0$	$\frac{K_{X(S-I-S-S-H)}}{K_{X(S-I-SH-T-T)}}=1.4$
		Trian	10437	8.0				
	Y	Unif	162224	1.1	146438	11.0		
		Trian	130652	3.3				
S-I-SH-T-T	X	Unif	11732	4.2	9367	25.5	$\frac{K_Y}{K_X}=14.4$	$\frac{K_{Y(S-I-S-S-H)}}{K_{Y(S-I-SH-T-T)}}=1.1$
		Trian	7003	0.8				
	Y	Unif	150968	0.3	134738	12.1		
		Trian	118508	0.5				

Table B.3 – Models with median properties: ratio between maximum base shear force and weight (V_{max}/W)

Model | Direction Distribution			Negative and Positive		Uniform and Triangular		Ratio	
			E[X]	CoV [%]	E[X]	CoV [%]		
H-S-S-S-H	X	Unif	0.032	1.1	0.029	9.3	$\frac{V_Y}{V_X}=4.7$	$\frac{(V_X/W)_{H-S-S-S-H}}{(V_X/W)_{H-S-SH-T-T}}=1.4$
		Trian	0.026	0.5				
	Y	Unif	0.144	1.1	0.135	6.4		
		Trian	0.127	2.0				
H-S-SH-T-T	X	Unif	0.024	2.5	0.021	12.3	$\frac{V_Y}{V_X}=5.7$	$\frac{(V_Y/W)_{H-S-S-S-H}}{(V_Y/W)_{H-S-SH-T-T}}=1.1$
		Trian	0.019	2.7				
	Y	Unif	0.127	1.7	0.121	5.1		
		Trian	0.116	2.1				
H-I-S-S-H	X	Unif	0.025	0.3	0.022	11.0	$\frac{V_Y}{V_X}=7.2$	$\frac{(V_X/W)_{H-I-S-S-H}}{(V_X/W)_{H-I-SH-T-T}}=1.2$
		Trian	0.020	0.1				
	Y	Unif	0.168	1.8	0.158	6.3		
		Trian	0.149	2.0				
H-I-SH-T-T	X	Unif	0.021	2.1	0.018	12.2	$\frac{V_Y}{V_X}=8.2$	$\frac{(V_Y/W)_{H-I-S-S-H}}{(V_Y/W)_{H-I-SH-T-T}}=1.0$
		Trian	0.016	1.8				
	Y	Unif	0.160	0.3	0.151	5.5		
		Trian	0.143	0.2				
S-S-S-S-H	X	Unif	0.034	1.4	0.031	9.7	$\frac{V_Y}{V_X}=4.5$	$\frac{(V_X/W)_{S-S-S-S-H}}{(V_X/W)_{S-S-SH-T-T}}=1.4$
		Trian	0.028	0.5				
	Y	Unif	0.148	0.4	0.139	6.4		
		Trian	0.130	0.6				
S-S-SH-T-T	X	Unif	0.025	0.8	0.023	10.7	$\frac{V_Y}{V_X}=5.3$	$\frac{(V_Y/W)_{S-S-S-S-H}}{(V_Y/W)_{S-S-SH-T-T}}=1.1$
		Trian	0.020	0.6				
	Y	Unif	0.127	1.0	0.121	4.9		
		Trian	0.116	1.7				

Table B.4 – Models with median properties: ratio between maximum base shear force and weight (V_{max}/W)

Model | Direction Distribution			Negative and Positive		Uniform and Triangular		Ratio	
			E[X]	CoV [%]	E[X]	CoV [%]		
S-I-S-S-H	X	Unif	0.025	0.2	0.023	10.2	$\frac{V_Y}{V_X}=7.1$	$\frac{(V_X/W)_{S-I-S-S-H}}{(V_X/W)_{S-I-SH-T-T}}=1.2$
		Trian	0.021	0.5				
	Y	Unif	0.171	0.4	0.162	6.1		
		Trian	0.152	0.5				
S-I-SH-T-T	X	Unif	0.022	0.4	0.020	11.4	$\frac{V_Y}{V_X}=7.7$	$\frac{(V_Y/W)_{S-I-S-S-H}}{(V_Y/W)_{S-I-SH-T-T}}=1.1$
		Trian	0.017	0.8				
	Y	Unif	0.160	0.2	0.152	5.4		
		Trian	0.144	0.1				

Table B.5 – Weight of the models

Model	W [ton]
H-S-S-S-H	2081.22
H-S-SH-T-T	1967.78
H-I-S-S-H	2412.41
H-I-SH-T-T	2277.17
S-S-S-S-H	2077.42
S-S-SH-T-T	1963.87
S-I-S-S-H	2408.61
S-I-SH-T-T	1963.87

ANNEX C

In reference to §3.3.3, non-linear dynamic analyses (NLDA) with time integration were performed with the 8 building models, defined by the median properties of the aleatory variables, with the objective of verifying if the load distributions considered in the non-linear static (pushover) analysis (NLSA) were able to capture the global behaviour of these URM buildings. Figure C.1 to Figure C.16 compare the results obtained from the NLDA, considering all records compatible with seismic action type 1 and 2, were compared to the results from the NLSA with the uniform and triangular load distribution. The curves plot the ratio between the base shear force and the weight of the structure (V/W) as a function of the average displacement of the roof (d).

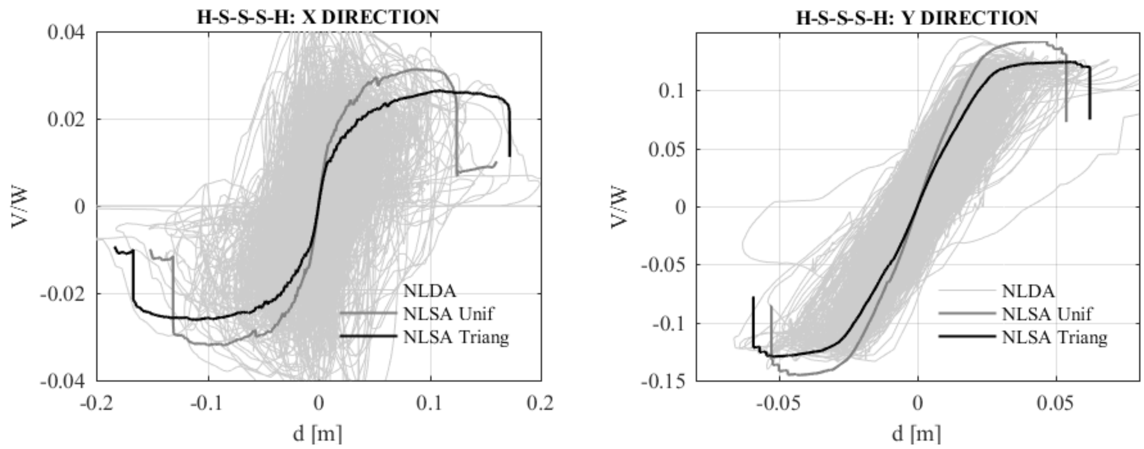

Figure C.1 – Model H-S-S-S-H: comparison between NLDA by using a seismic input compatible with the code seismic action type 1 (all records) and the NLSA: X direction (left) and Y direction (right)

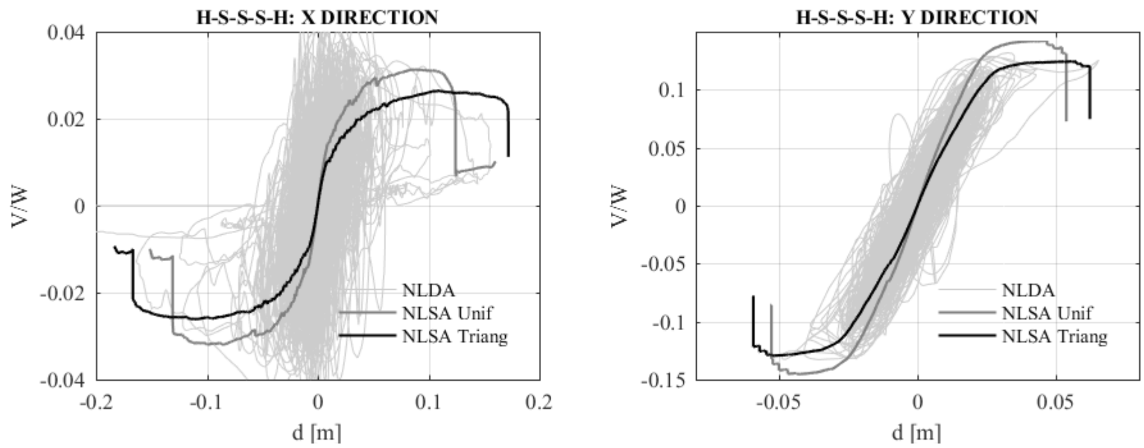

Figure C.2 – Model H-S-S-S-H: comparison between NLDA by using a seismic input compatible with the code seismic action type 2 (all records) and the NLSA: X direction (left) and Y direction (right)

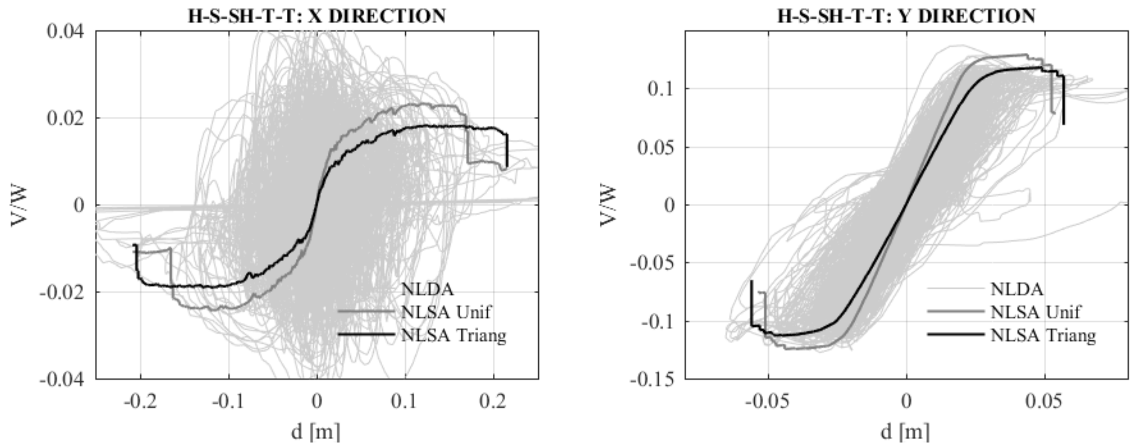

Figure C.3 – Model H-S-SH-T-T: comparison between NLDA by using a seismic input compatible with the code seismic action type 1 (all records) and the NLSA: X direction (left) and Y direction (right)

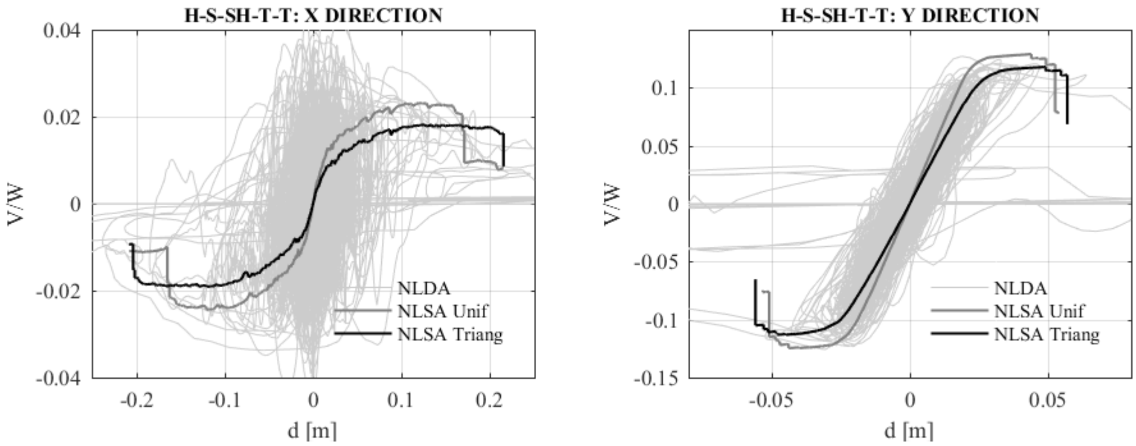

Figure C.4 – Model H-S-SH-T-T: comparison between NLDA by using a seismic input compatible with the code seismic action type 2 (all records) and the NLSA: X direction (left) and Y direction (right)

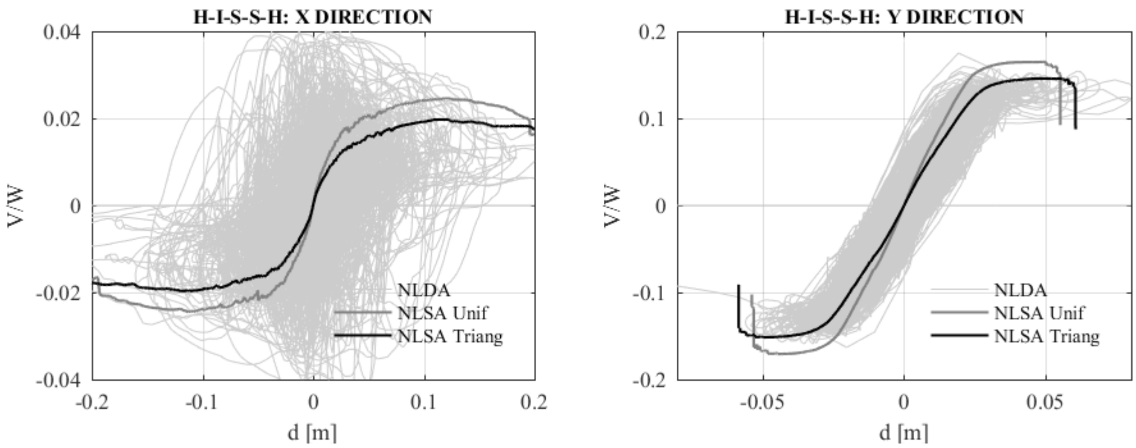

Figure C.5 – Model H-I-S-S-H: comparison between NLDA by using a seismic input compatible with the code seismic action type 1 (all records) and the NLSA: X direction (left) and Y direction (right)

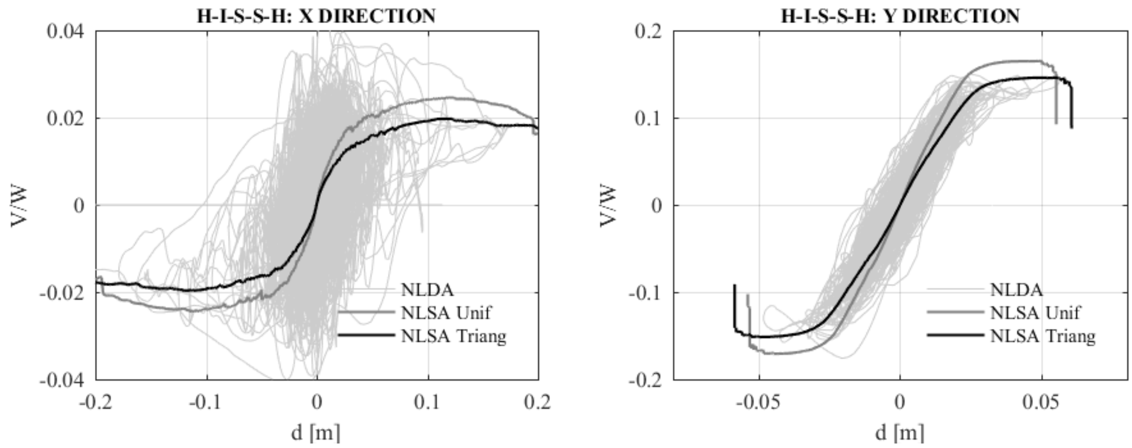

Figure C.6 – Model H-I-S-S-H: comparison between NLDA by using a seismic input compatible with the code seismic action type 2 (all records) and the NLSA: X direction (left) and Y direction (right)

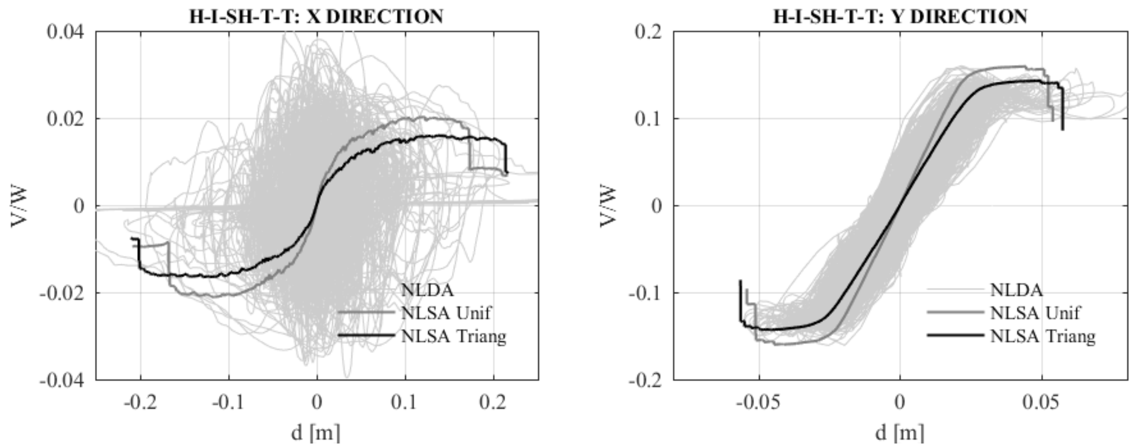

Figure C.7 – Model H-I-SH-T-T: comparison between NLDA by using a seismic input compatible with the code seismic action type 1 (all records) and the NLSA: X direction (left) and Y direction (right)

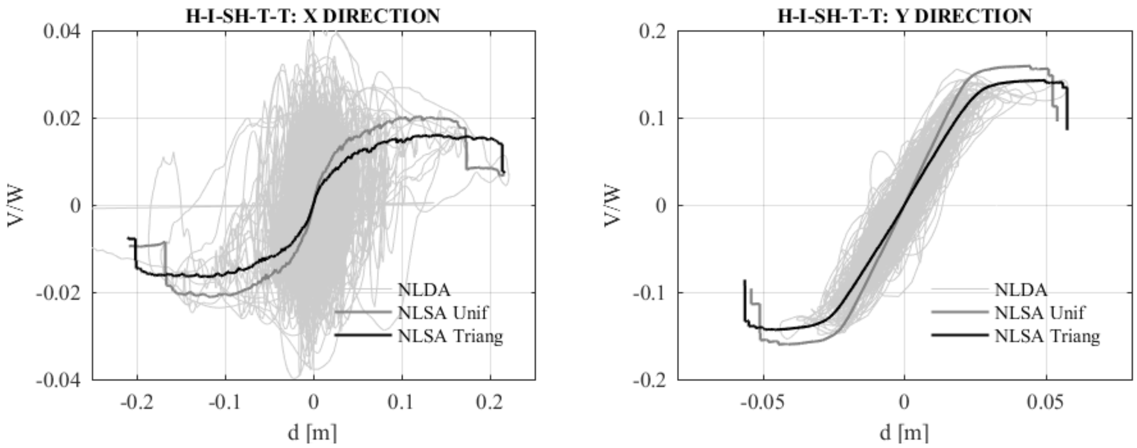

Figure C.8 – Model H-I-SH-T-T: comparison between NLDA by using a seismic input compatible with the code seismic action type 2 (all records) and the NLSA: X direction (left) and Y direction (right)

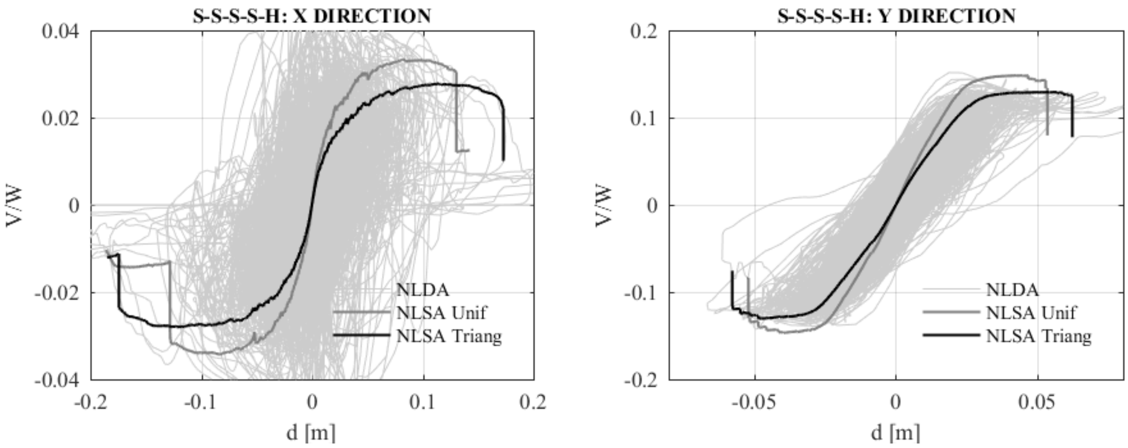

Figure C.9 – Model S-S-S-S-H: comparison between NLDA by using a seismic input compatible with the code seismic action type 1 (all records) and the NLSA: X direction (left) and Y direction (right)

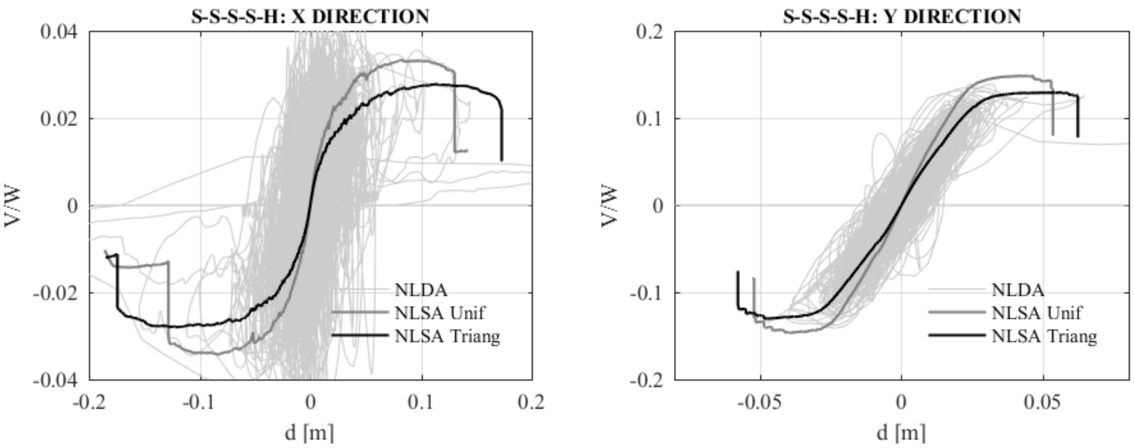

Figure C.10 – Model S-S-S-S-H: comparison between NLDA by using a seismic input compatible with the code seismic action type 2 (all records) and the NLSA: X direction (left) and Y direction (right)

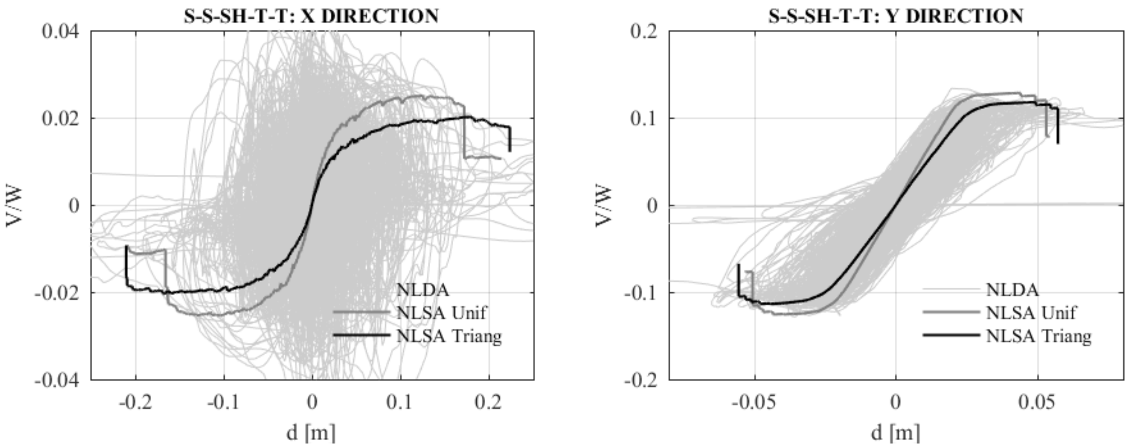

Figure C.11 – Model S-S-SH-T-T: comparison between NLDA by using a seismic input compatible with the code seismic action type 1 (all records) and the NLSA: X direction (left) and Y direction (right)

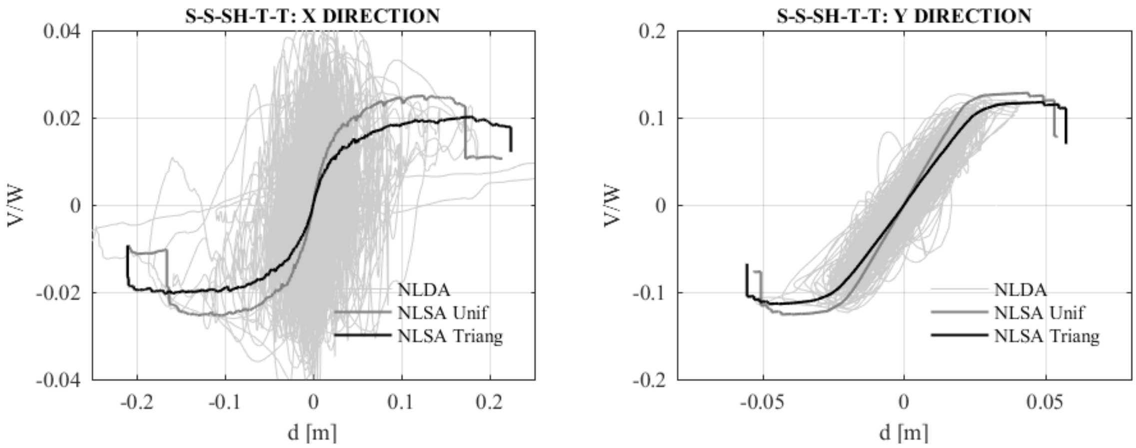

Figure C.12 – Model S-S-SH-T-T: comparison between NLDA by using a seismic input compatible with the code seismic action type 2 (all records) and the NLSA: X direction (left) and Y direction (right)

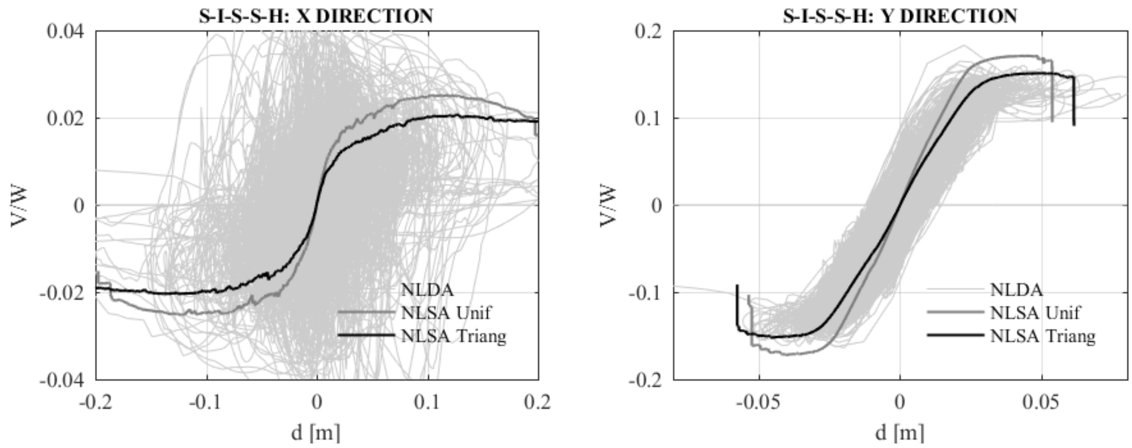

Figure C.13 – Model S-I-S-S-H: comparison between NLDA by using a seismic input compatible with the code seismic action type 1 (all records) and the NLSA: X direction (left) and Y direction (right)

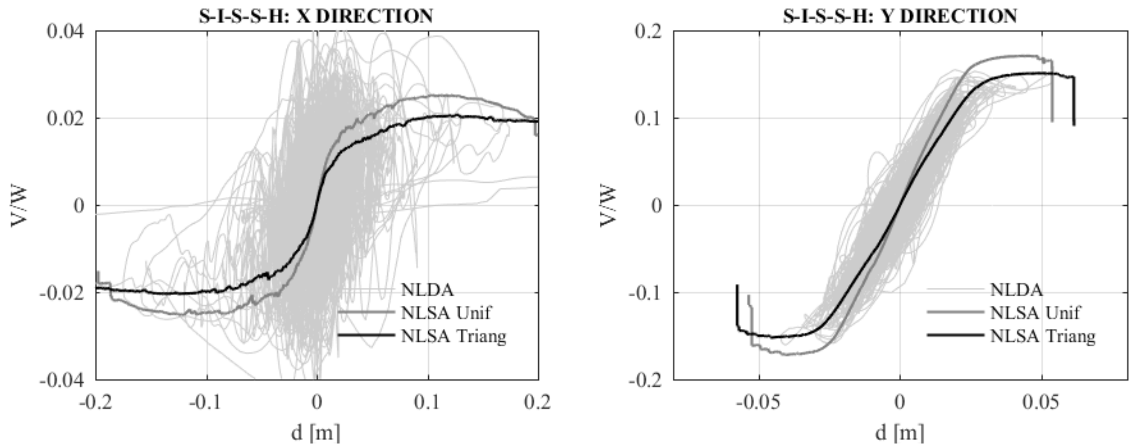

Figure C.14 – Model S-I-S-S-H: comparison between NLDA by using a seismic input compatible with the code seismic action type 2 (all records) and the NLSA: X direction (left) and Y direction (right)

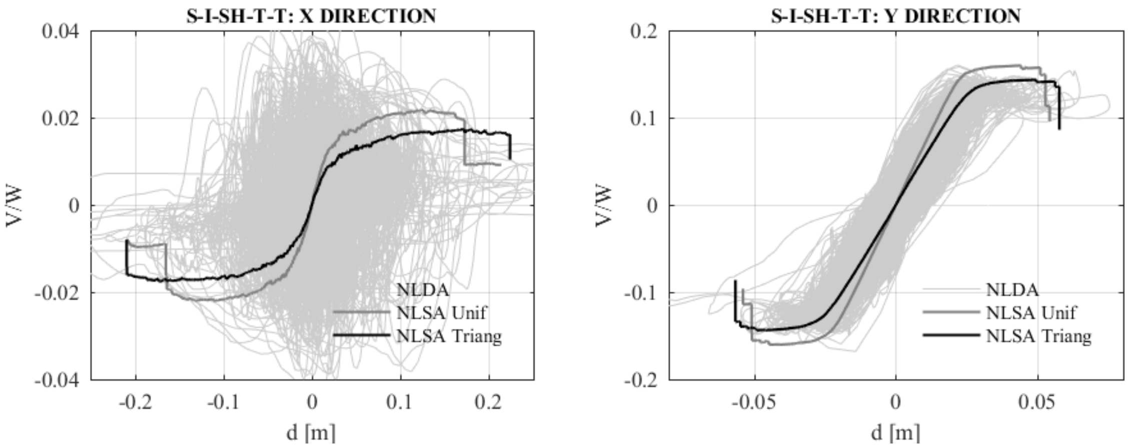

Figure C.15 – Model S-I-SH-T-T: comparison between NLDA by using a seismic input compatible with the code seismic action type 1 (all records) and the NLSA: X direction (left) and Y direction (right)

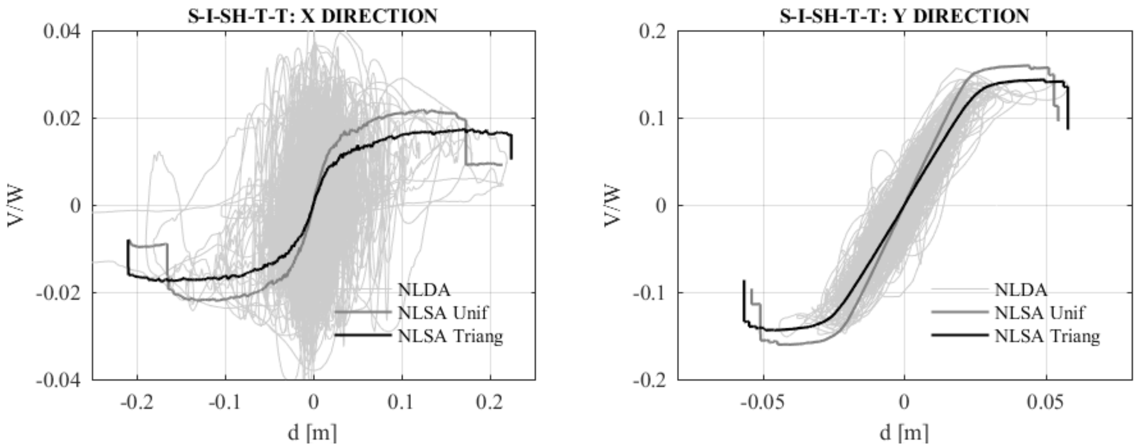

Figure C.16 – Model S-I-SH-T-T: comparison between NLDA by using a seismic input compatible with the code seismic action type 2 (all records) and the NLSA: X direction (left) and Y direction (right)

ANNEX D

In reference to §3.3.4, non-linear static (pushover) analyses were performed with the 1000 building models, defined by the aleatory properties set by the Monte Carlo simulations, considering the uniform and the triangular load distributions applied in the two main directions of the structure (X and Y) and in the two senses of direction (negative and positive). Figure D.1 to Figure D.32 plot the pushover curves for the 8 groups of models, including the pushover curves defined by the median properties of the aleatory variables.

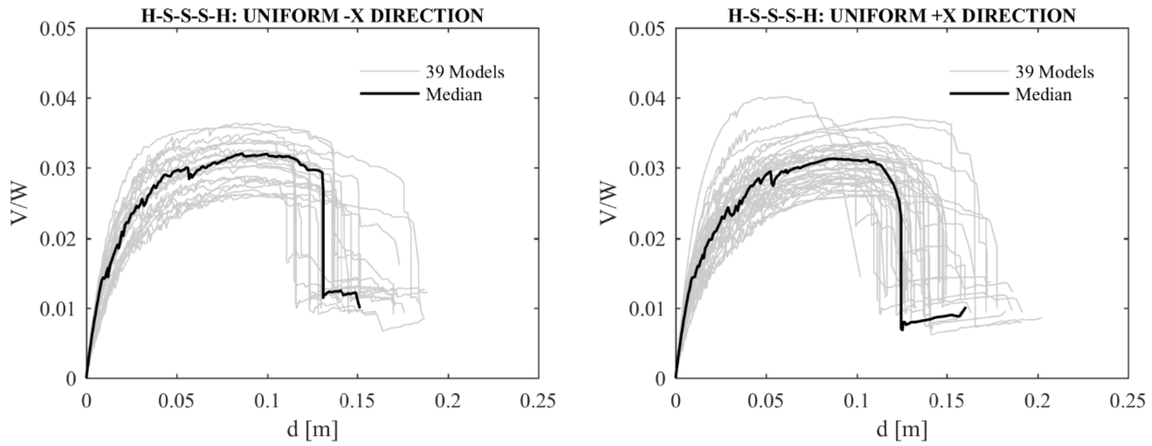

Figure D.1 – Pushover curves for H-S-S-S-H: Uniform –X direction (left) and +X direction (right)

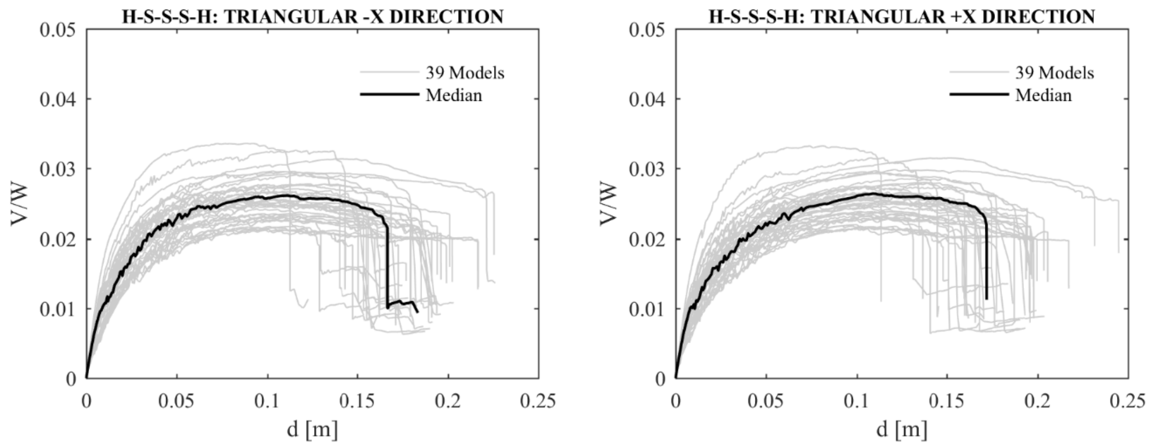

Figure D.2 – Pushover curves for H-S-S-S-H: Triangular –X direction (left) and +X direction (right)

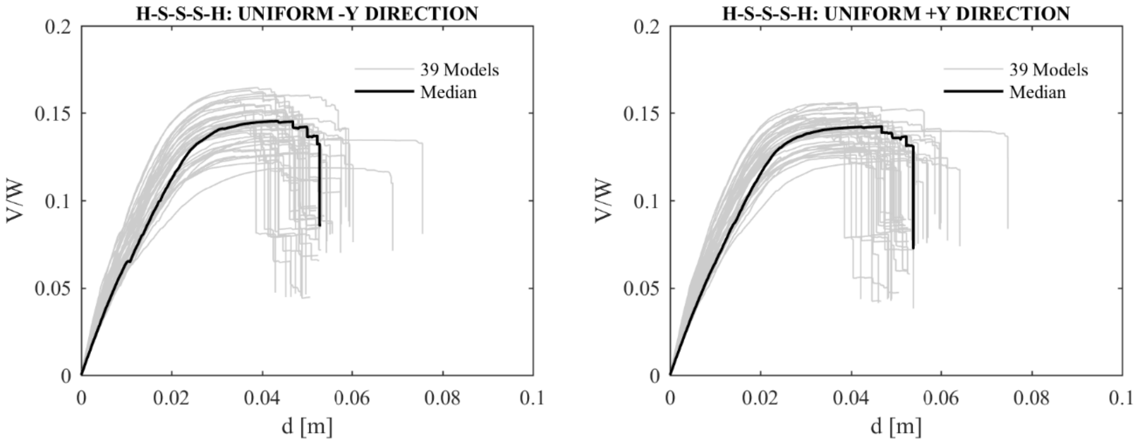

Figure D.3 – Pushover curves for H-S-S-S-H: Uniform –Y direction (left) and +Y direction (right)

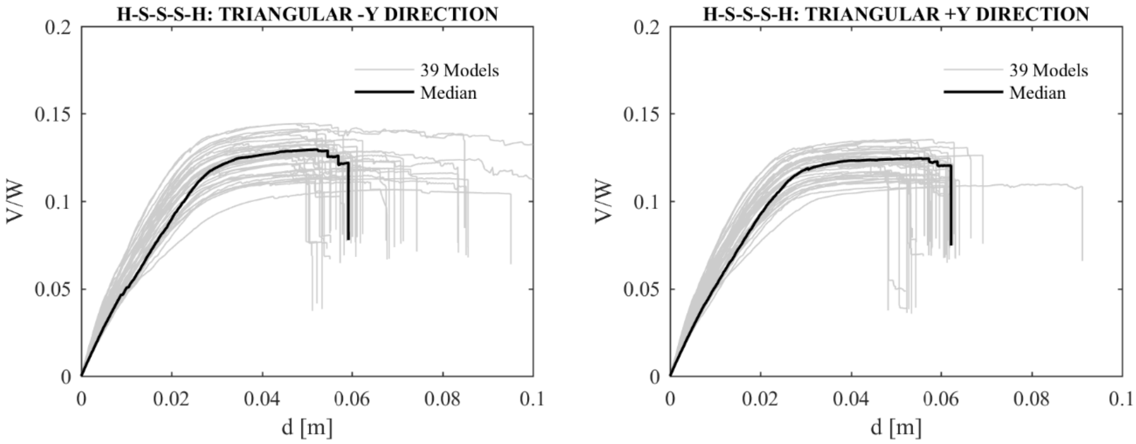

Figure D.4 – Pushover curves for H-S-S-S-H: Triangular –Y direction (left) and +Y direction (right)

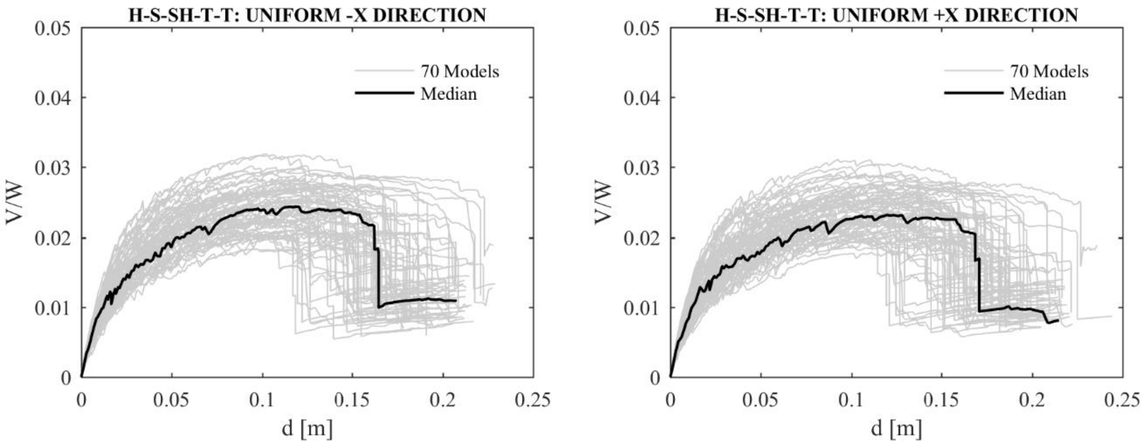

Figure D.5 – Pushover curves for H-S-SH-T-T: Uniform –X direction (left) and +X direction (right)

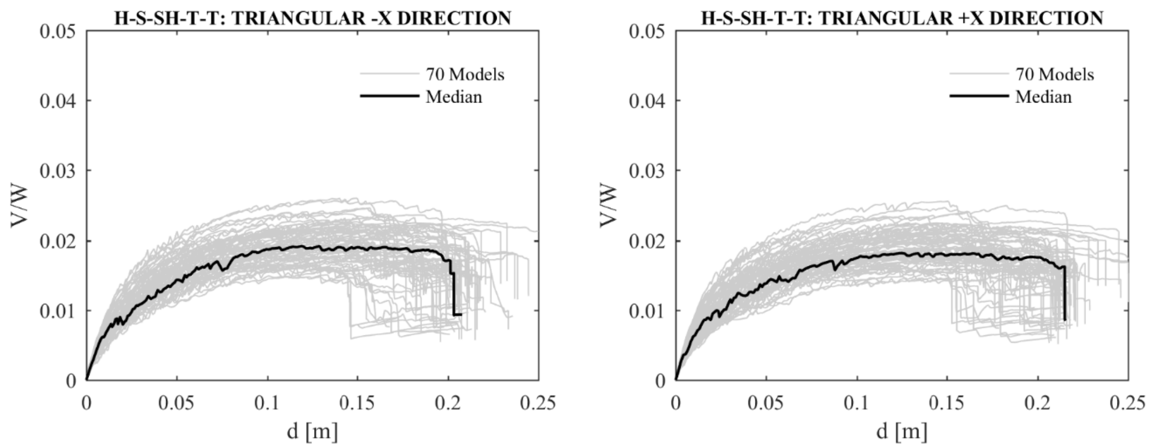

Figure D.6 – Pushover curves for H-S-SH-T-T: Triangular –X direction (left) and +X direction (right)

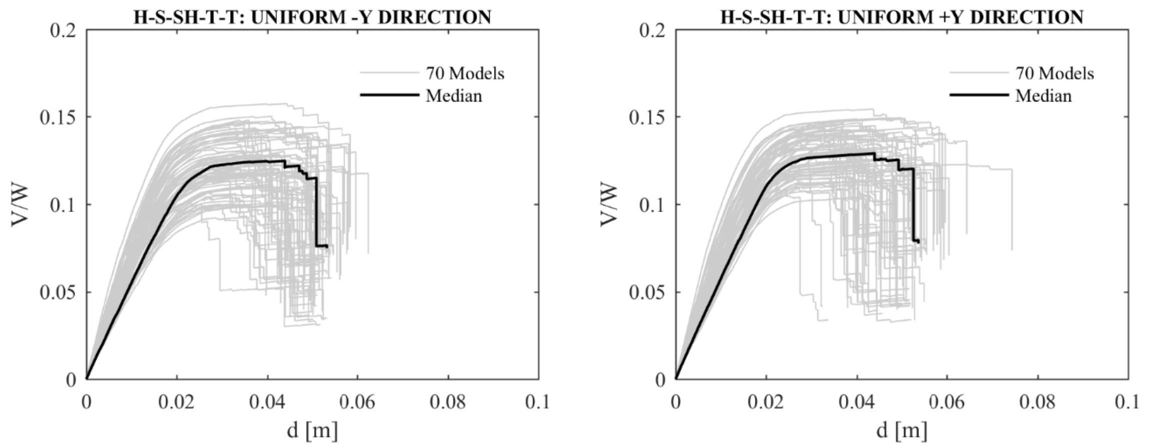

Figure D.7 – Pushover curves for H-S-SH-T-T: Uniform –Y direction (left) and +Y direction (right)

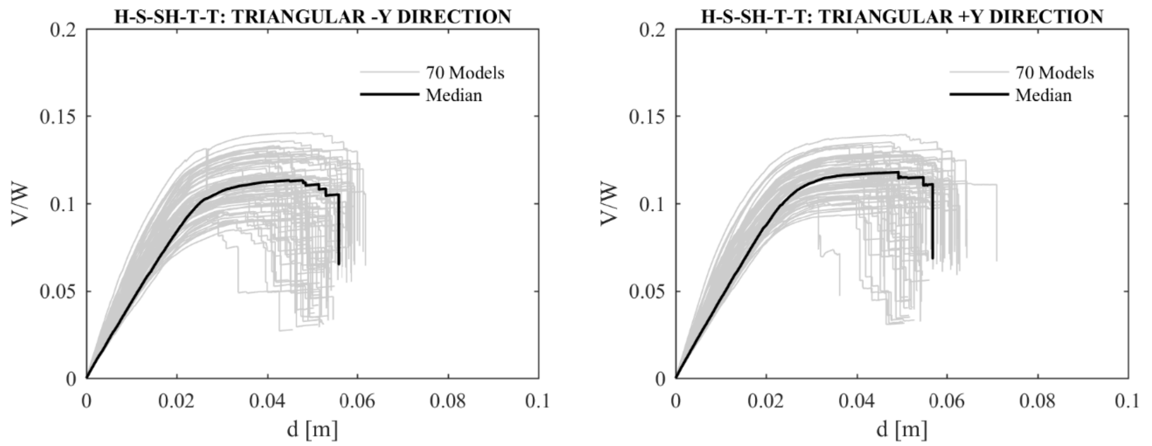

Figure D.8 – Pushover curves for H-S-SH-T-T: Triangular –Y direction (left) and +Y direction (right)

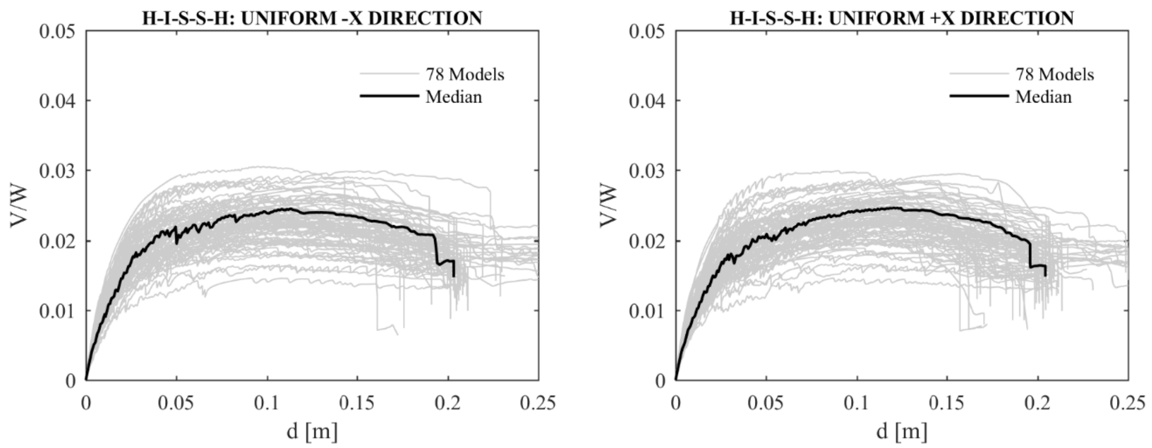

Figure D.9 – Pushover curves for H-I-S-S-H: Uniform –X direction (left) and +X direction (right)

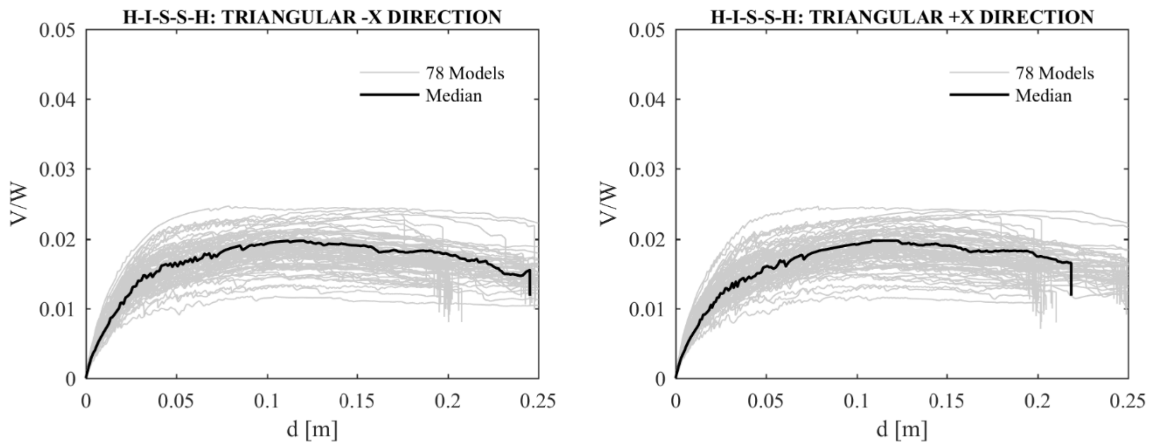

Figure D.10 – Pushover curves for H-I-S-S-H: Triangular –X direction (left) and +X direction (right)

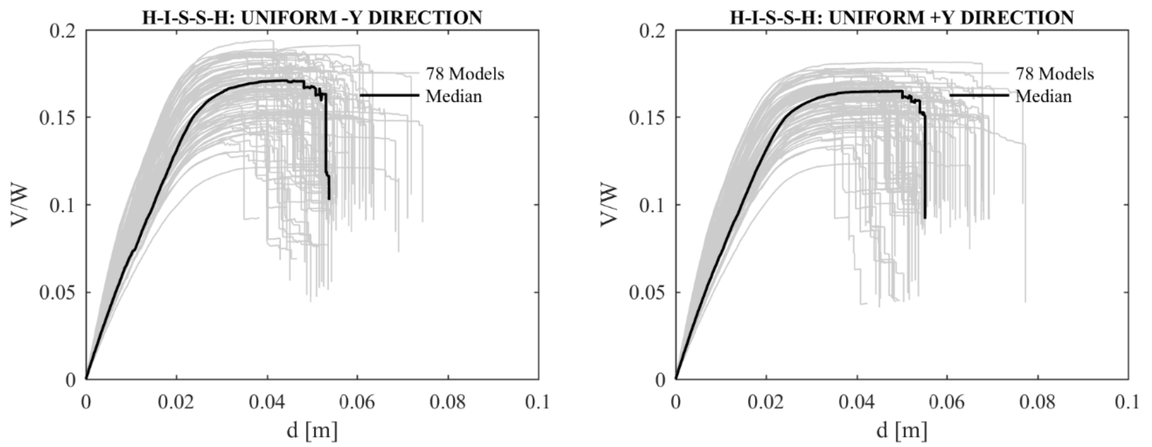

Figure D.11 – Pushover curves for H-I-S-S-H: Uniform –Y direction (left) and +Y direction (right)

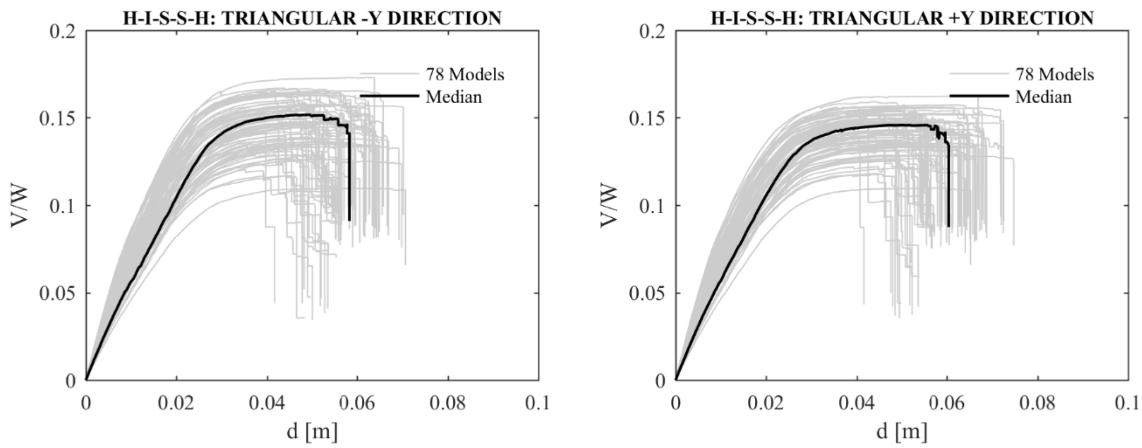

Figure D.12 – Pushover curves for H-I-S-S-H: Triangular –Y direction (left) and +Y direction (right)

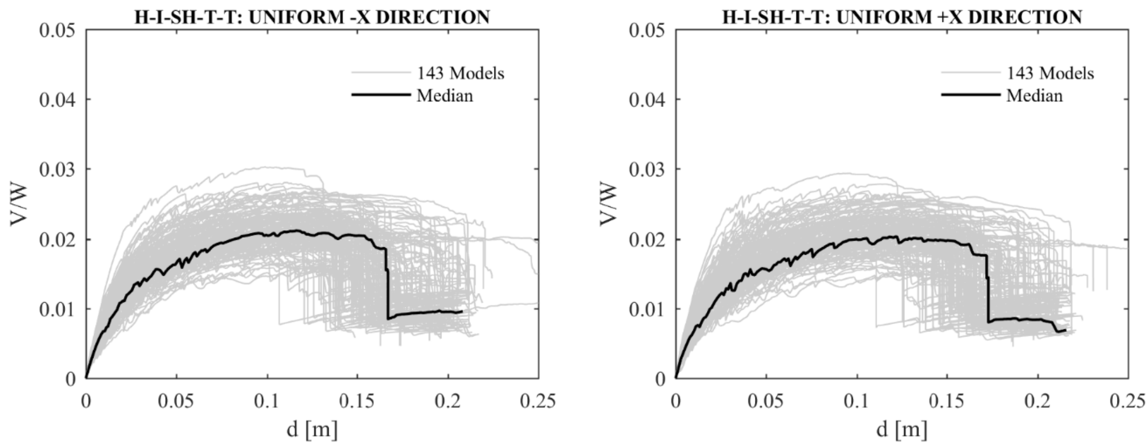

Figure D.13 – Pushover curves for H-I-SH-T-T: Uniform –X direction (left) and +X direction (right)

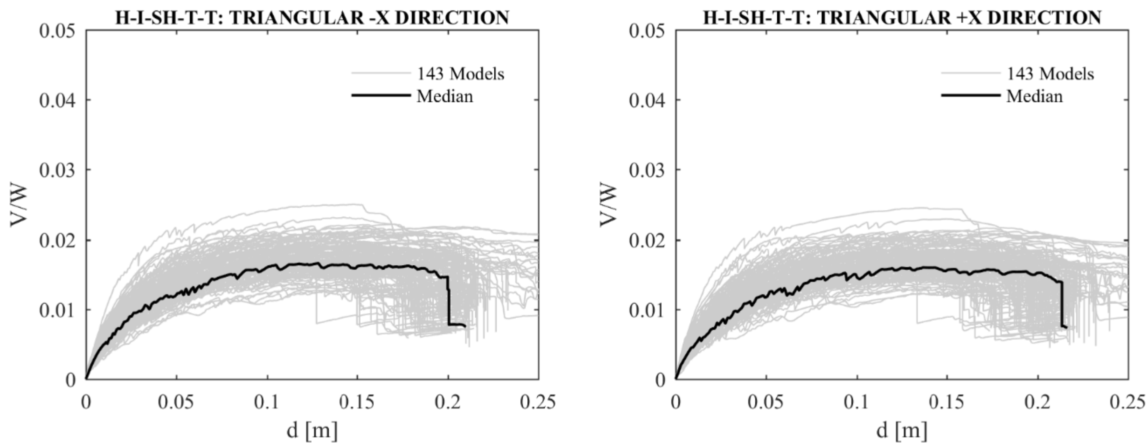

Figure D.14 – Pushover curves for H-I-SH-T-T: Triangular –X direction (left) and +X direction (right)

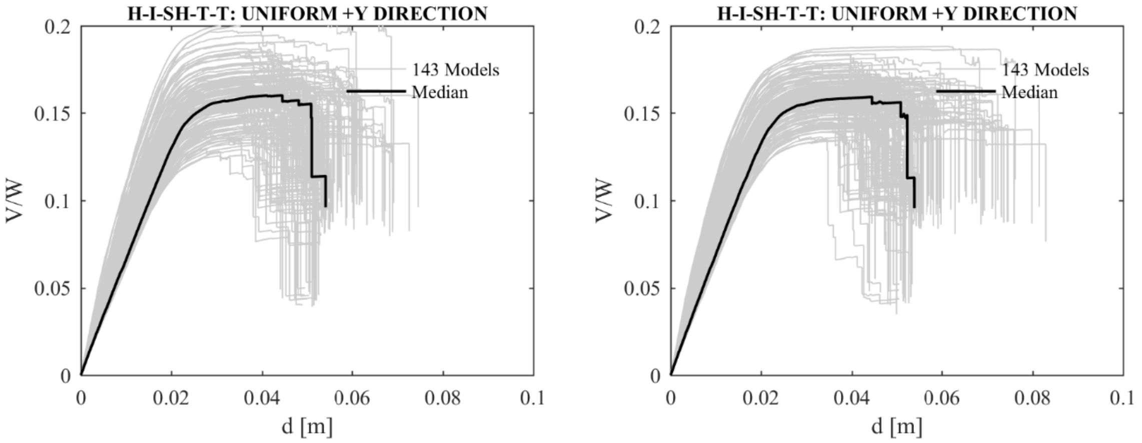

Figure D.15 – Pushover curves for H-I-SH-T-T: Uniform –Y direction (left) and +Y direction (right)

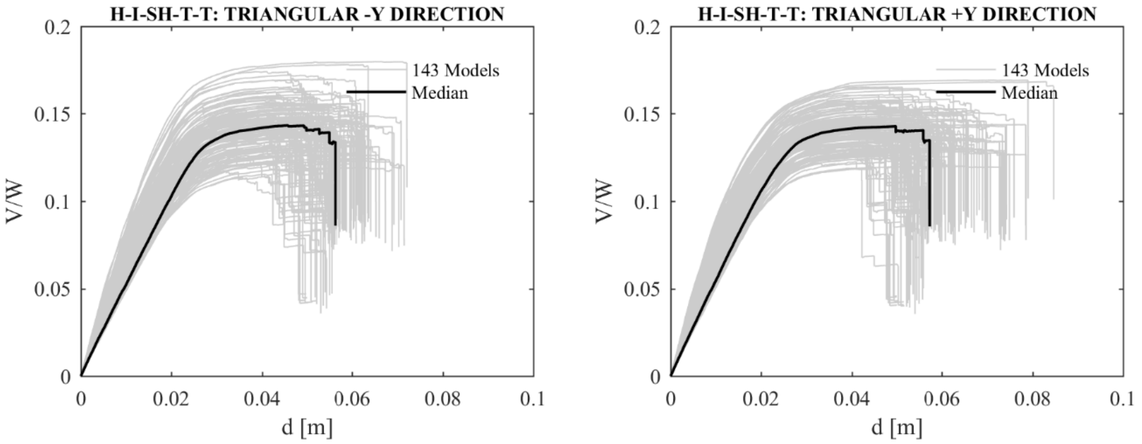

Figure D.16 – Pushover curves for H-I-SH-T-T: Triangular –Y direction (left) and +Y direction (right)

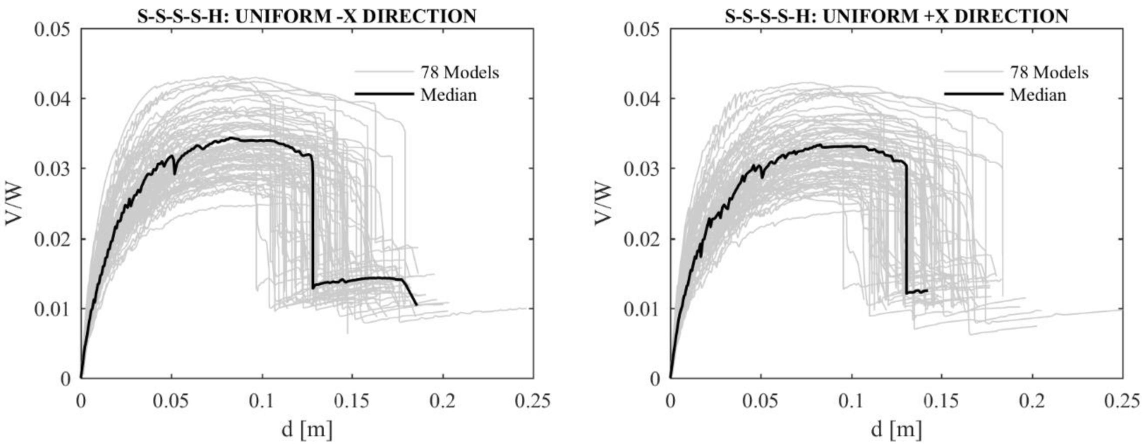

Figure D.17 – Pushover curves for S-S-S-S-H: Uniform –X direction (left) and +X direction (right)

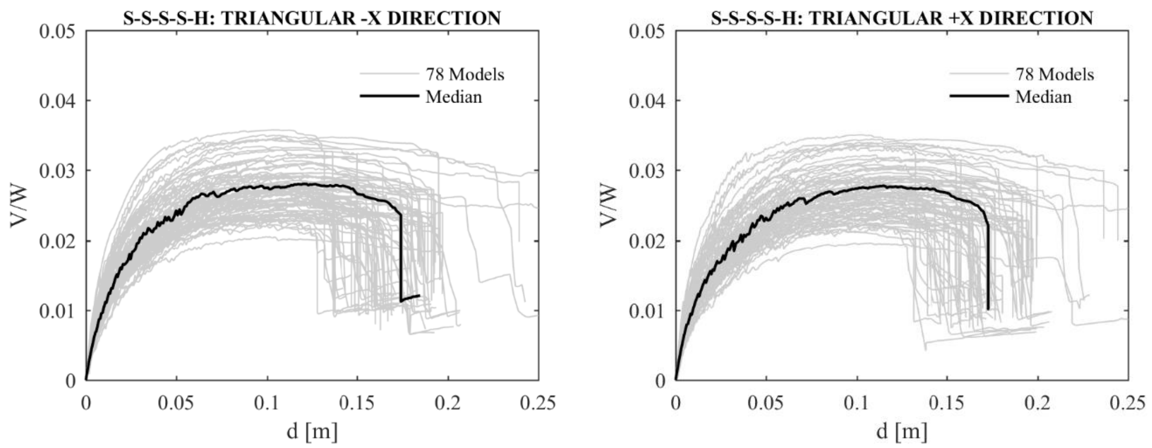

Figure D.18 – Pushover curves for S-S-S-S-H: Triangular –X direction (left) and +X direction (right)

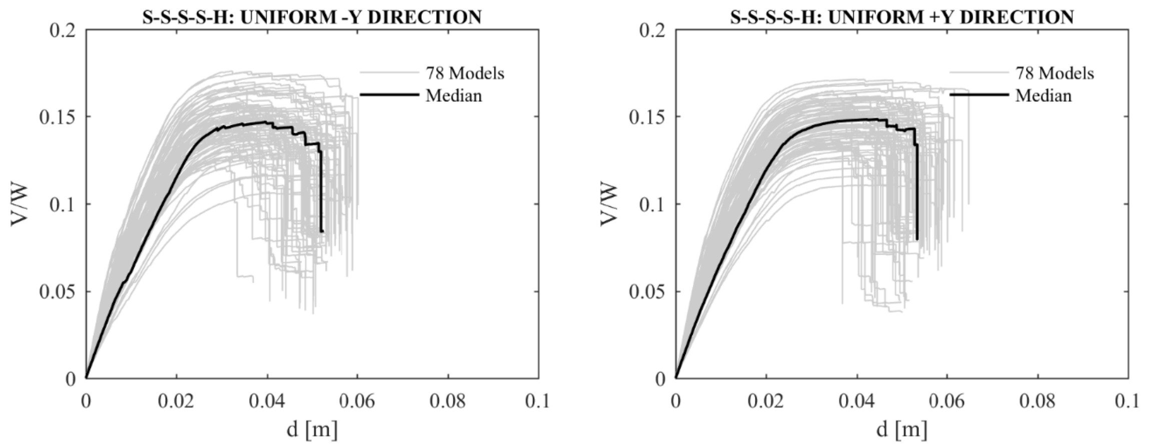

Figure D.19 – Pushover curves for S-S-S-S-H: Uniform –Y direction (left) and +Y direction (right)

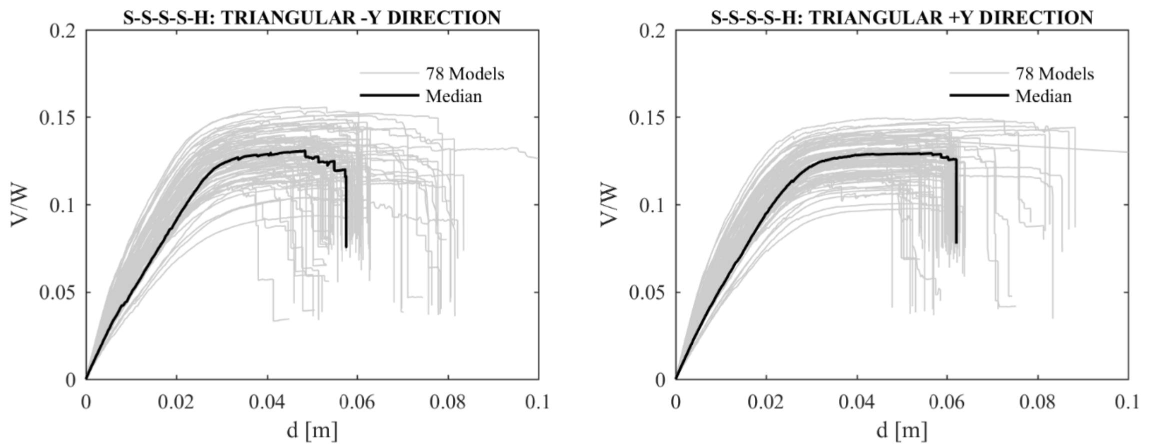

Figure D.20 – Pushover curves for S-S-S-S-H: Triangular –Y direction (left) and +Y direction (right)

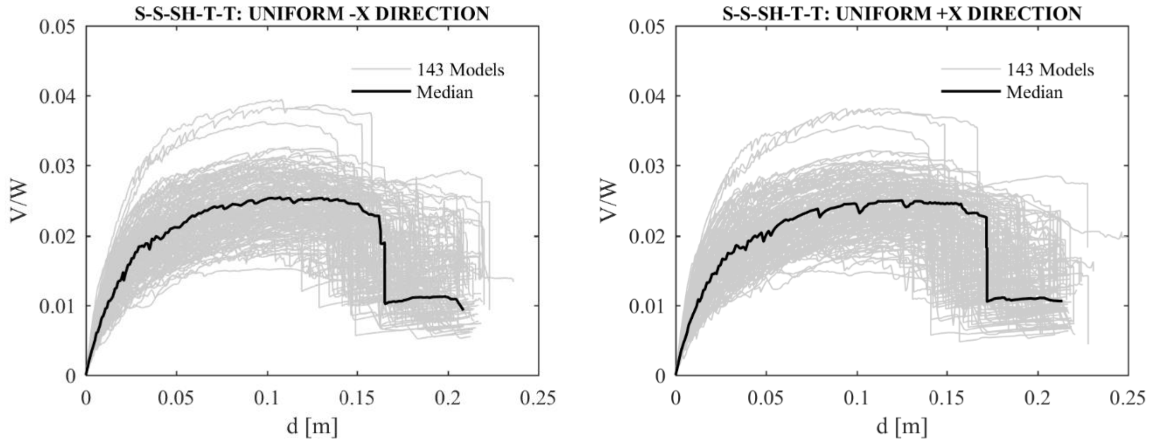

Figure D.21 – Pushover curves for S-S-SH-T-T: Uniform –X direction (left) and +X direction (right)

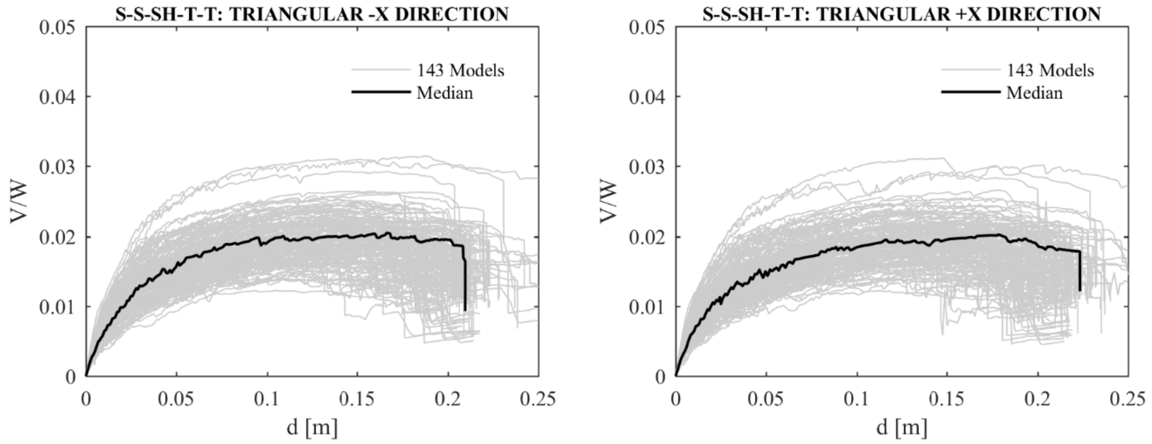

Figure D.22 – Pushover curves for S-S-SH-T-T: Triangular –X direction (left) and +X direction (right)

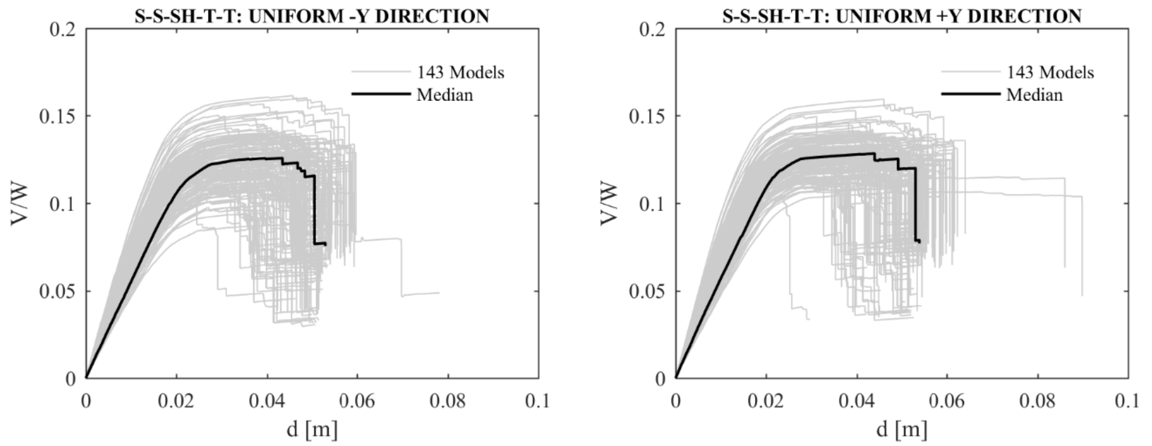

Figure D.23 – Pushover curves for S-S-SH-T-T: Uniform –Y direction (left) and +Y direction (right)

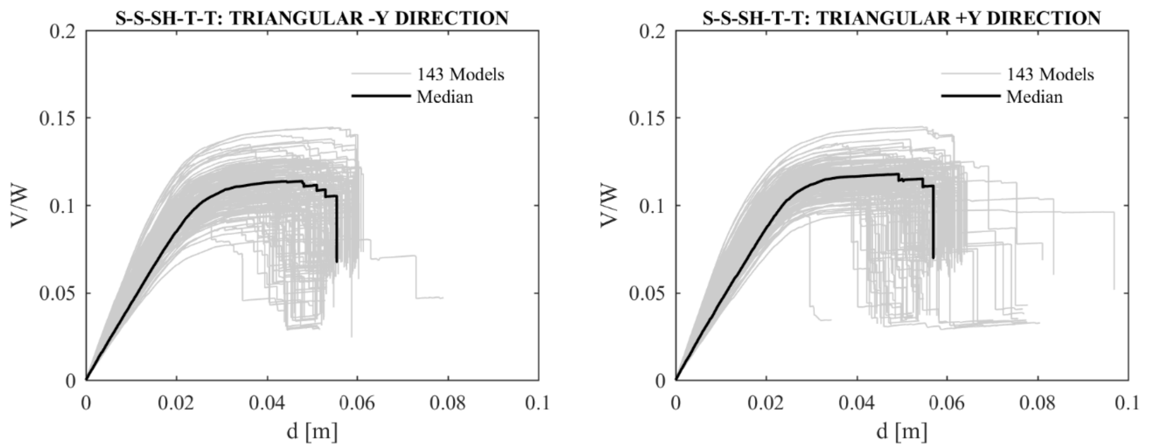

Figure D.24 – Pushover curves for S-S-SH-T-T: Triangular –Y direction (left) and +Y direction (right)

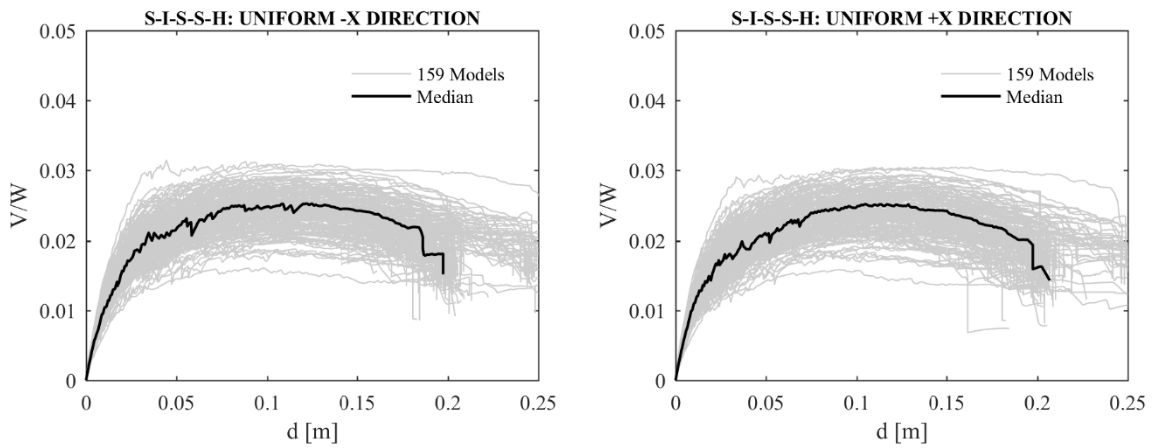

Figure D.25 – Pushover curves for S-I-S-S-H: Uniform –X direction (left) and +X direction (right)

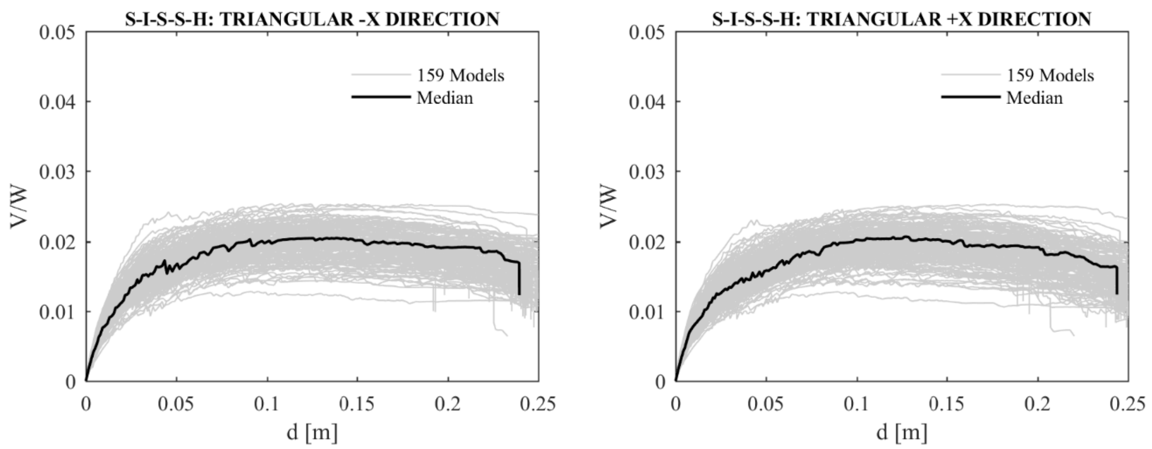

Figure D.26 – Pushover curves for S-I-S-S-H: Triangular –X direction (left) and +X direction (right)

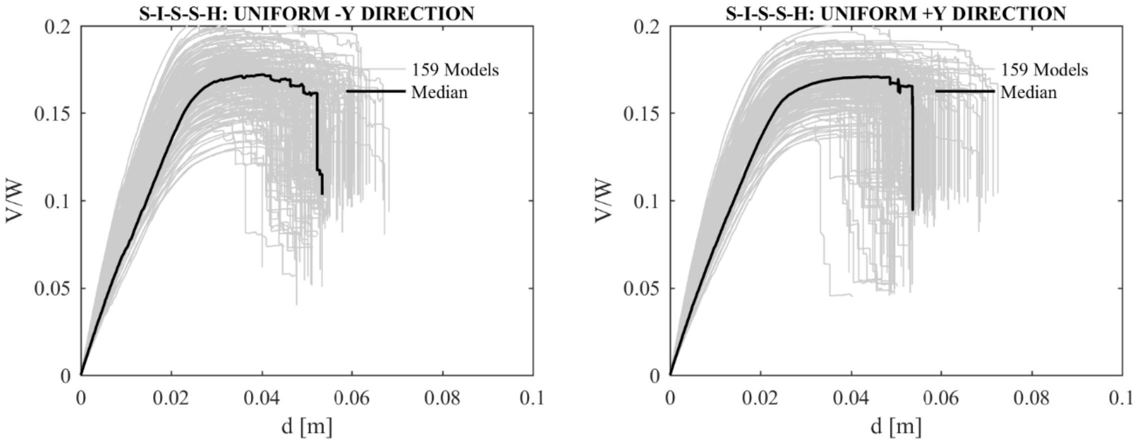

Figure D.27 – Pushover curves for S-I-S-S-H: Uniform –Y direction (left) and +Y direction (right)

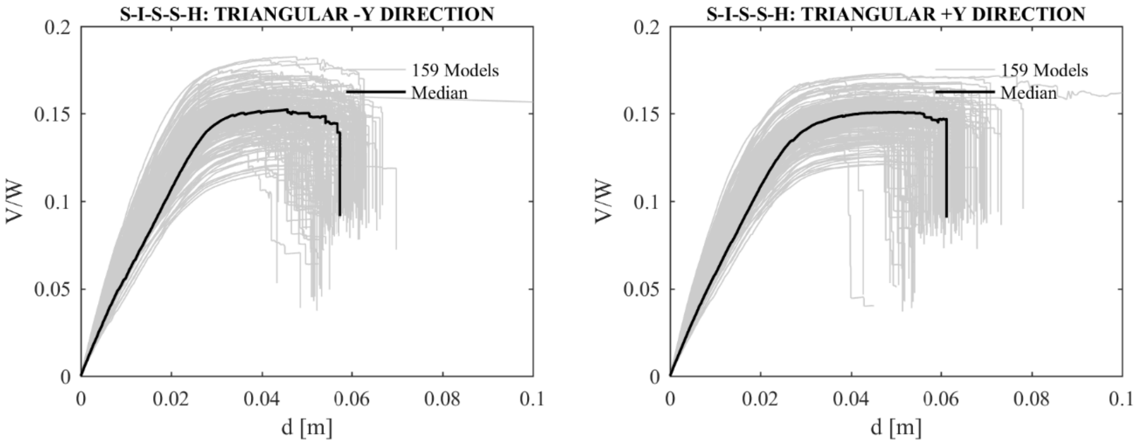

Figure D.28 – Pushover curves for S-I-S-S-H: Triangular –Y direction (left) and +Y direction (right)

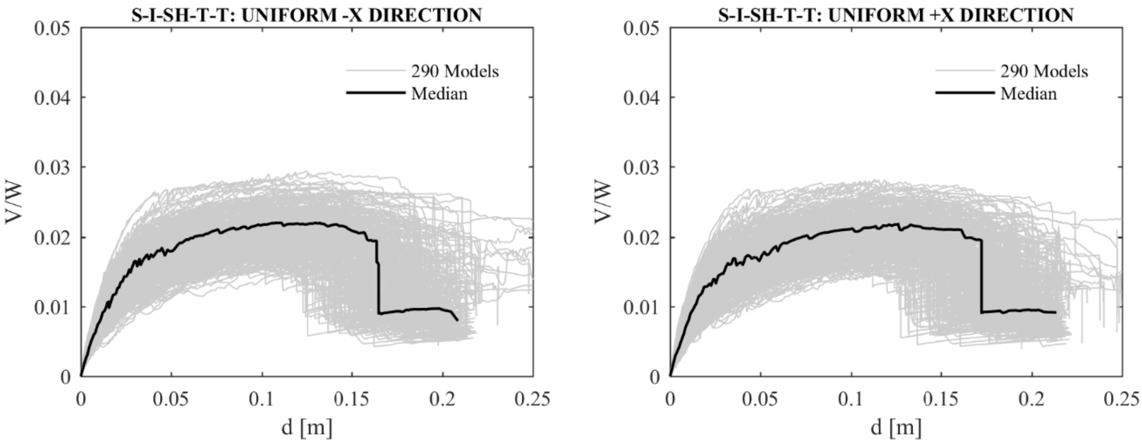

Figure D.29 – Pushover curves for S-I-SH-T-T: Uniform –X direction (left) and +X direction (right)

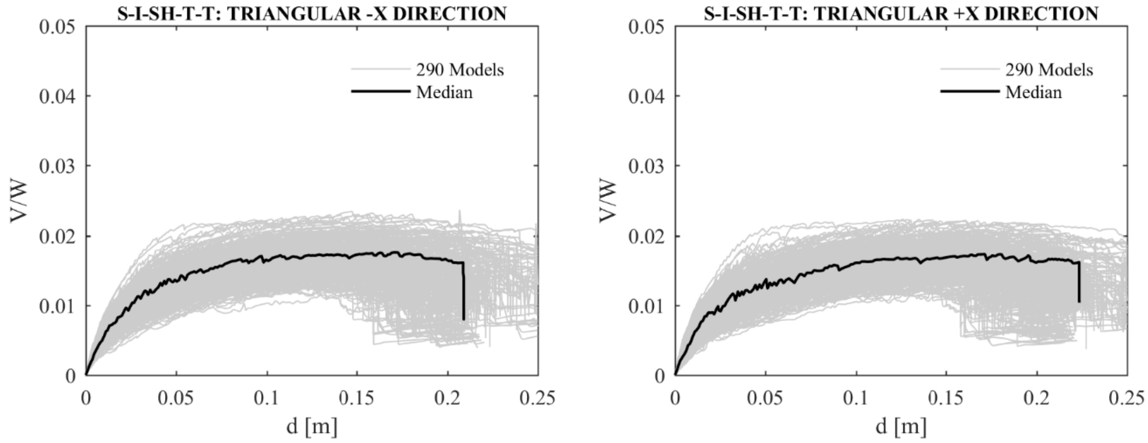

Figure D.30 – Pushover curves for S-I-SH-T-T: Triangular –X direction (left) and +X direction (right)

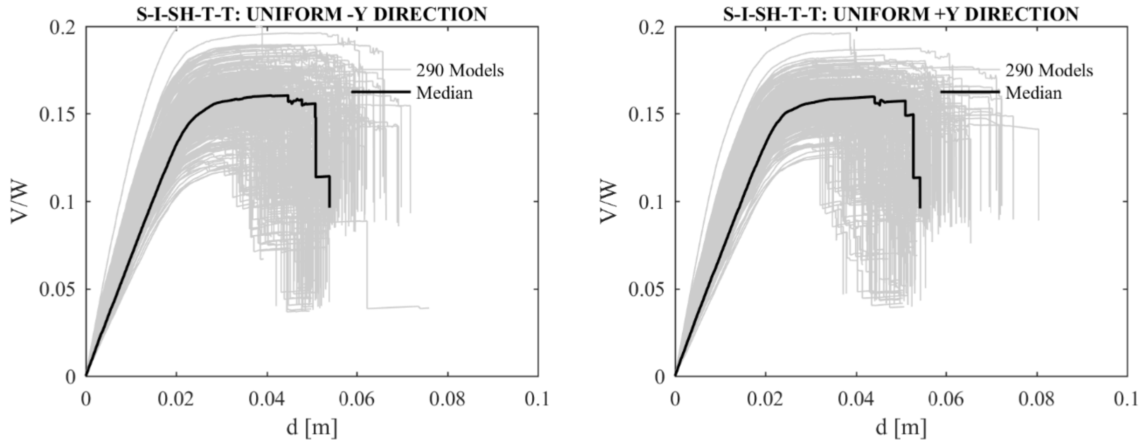

Figure D.31 – Pushover curves for S-I-SH-T-T: Uniform –Y direction (left) and +Y direction (right)

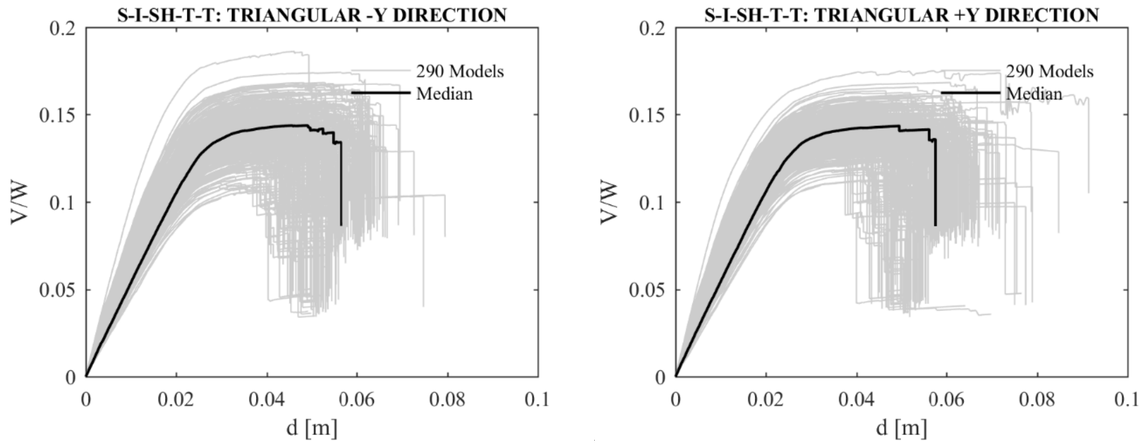

Figure D.32 – Pushover curves for S-I-SH-T-T: Triangular –Y direction (left) and +Y direction (right)

ANNEX E

In reference to §3.5.2, Figure E.1 to Figure E.4 plot the median values of PGA ($PGA_{50\%}$) values obtained with the 8 groups of building models determined with seismic action type 1 and type 2, while Figure E.5 to Figure E.8 plot the dispersion in the determination of the capacity (β_C).

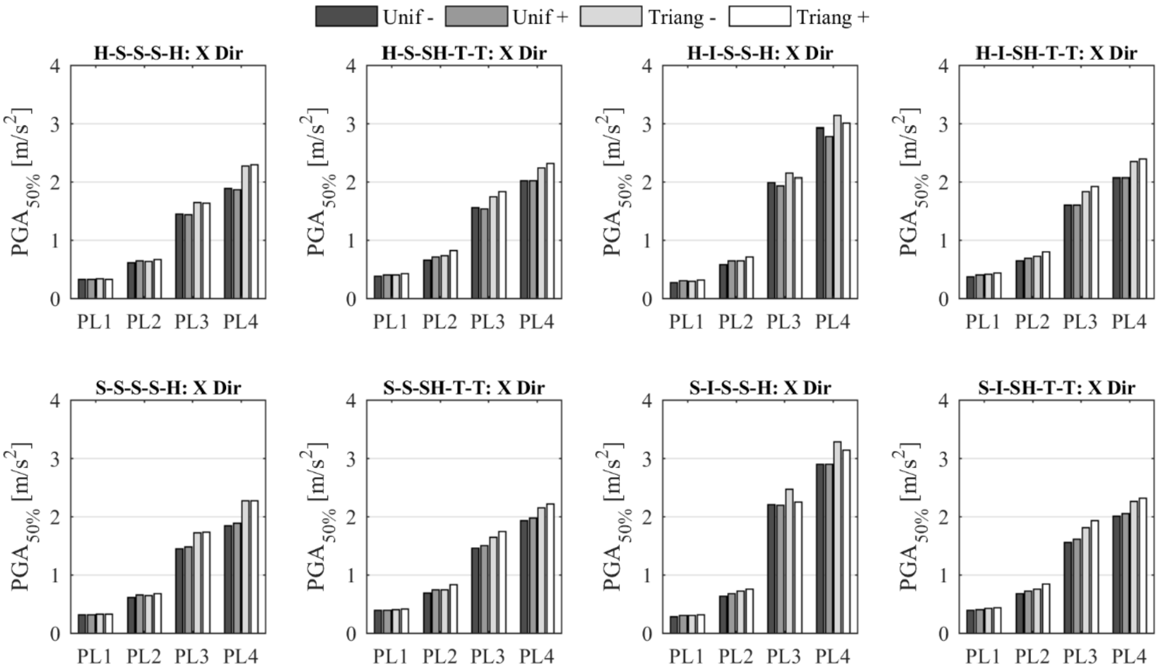

Figure E.1 – Median values of PGA obtained in the X direction: seismic action type 1

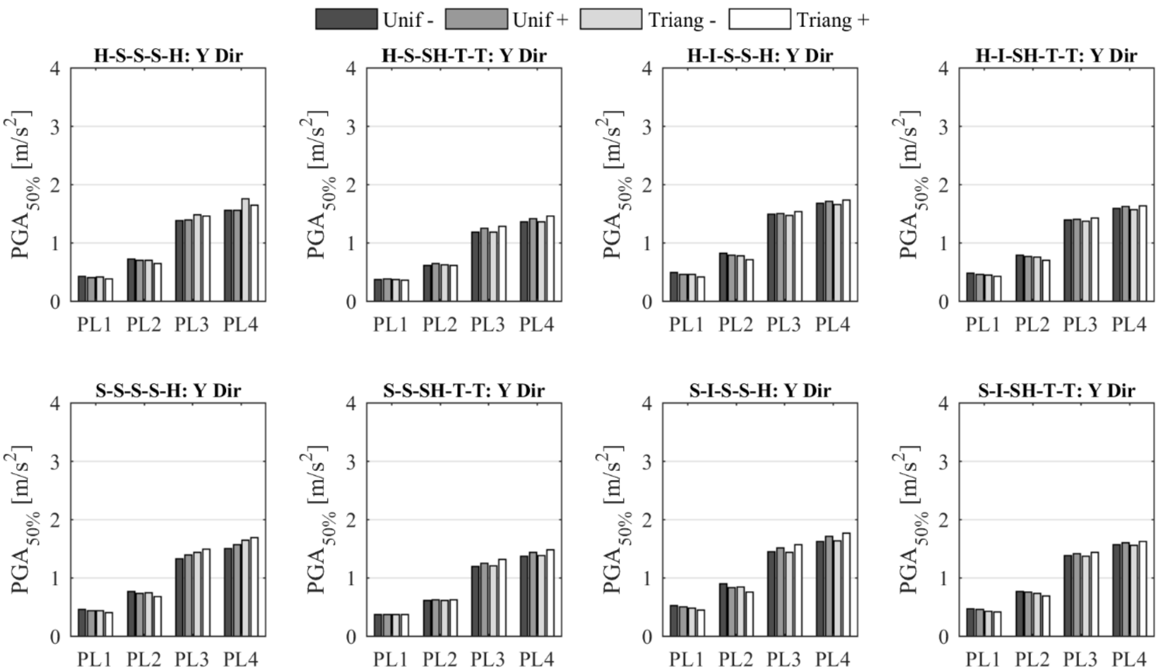

Figure E.2 – Median values of PGA obtained in the Y direction: seismic action type 1

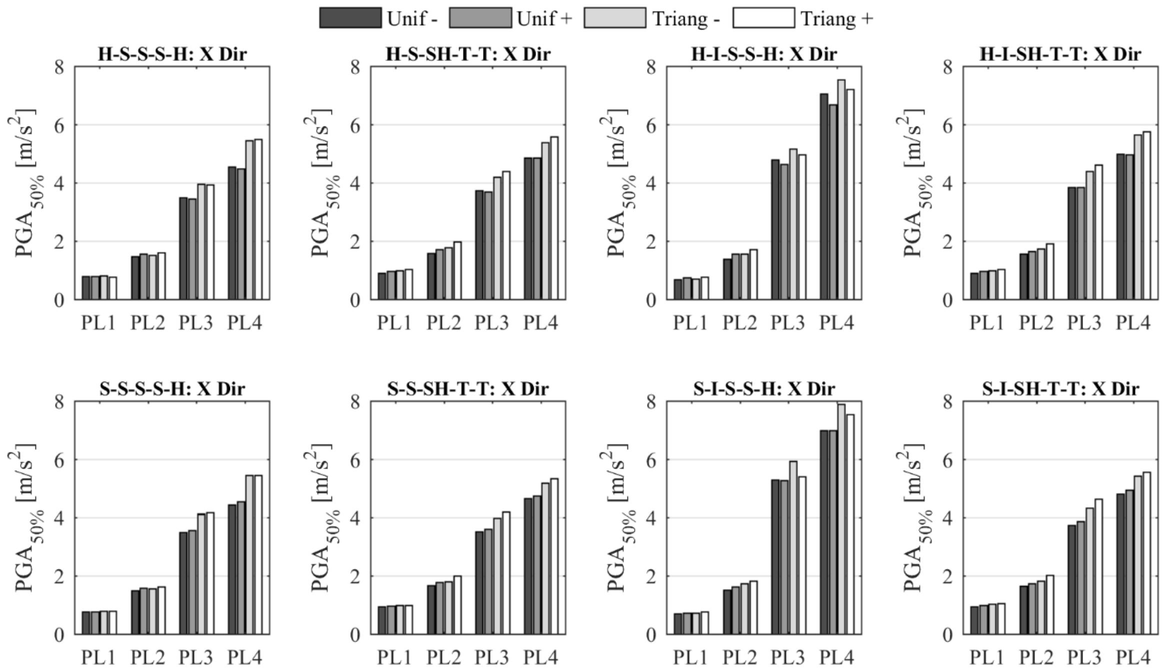

Figure E.3 – Median values of PGA obtained in the X direction: seismic action type 2

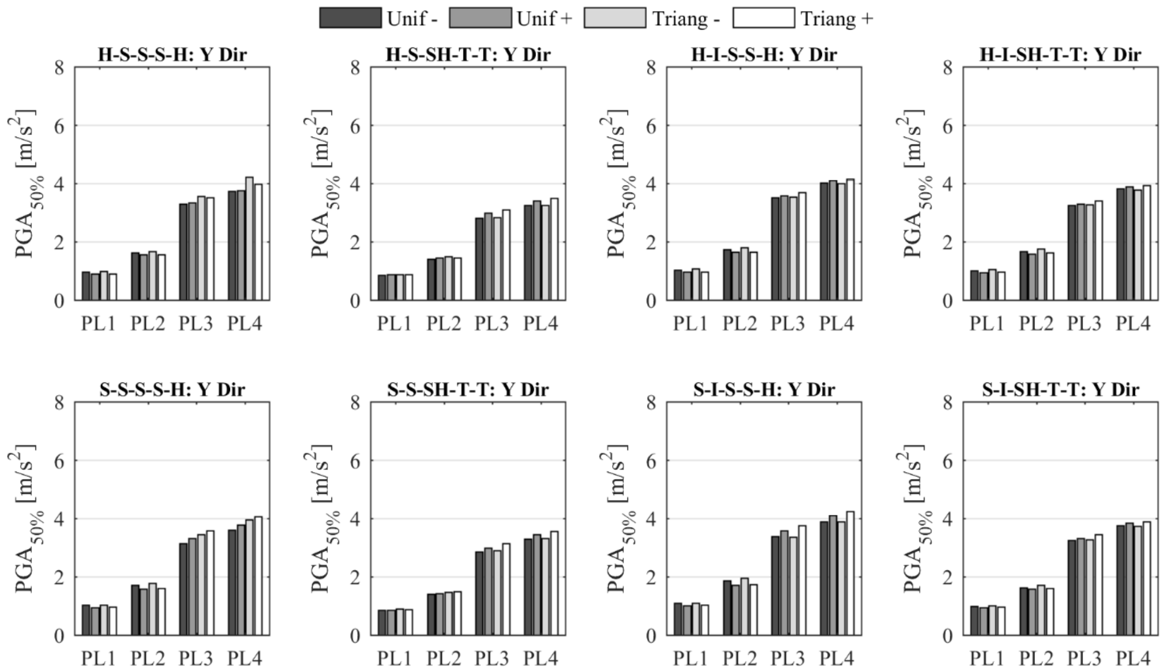

Figure E.4 – Median values of PGA obtained in the Y direction: seismic action type 2

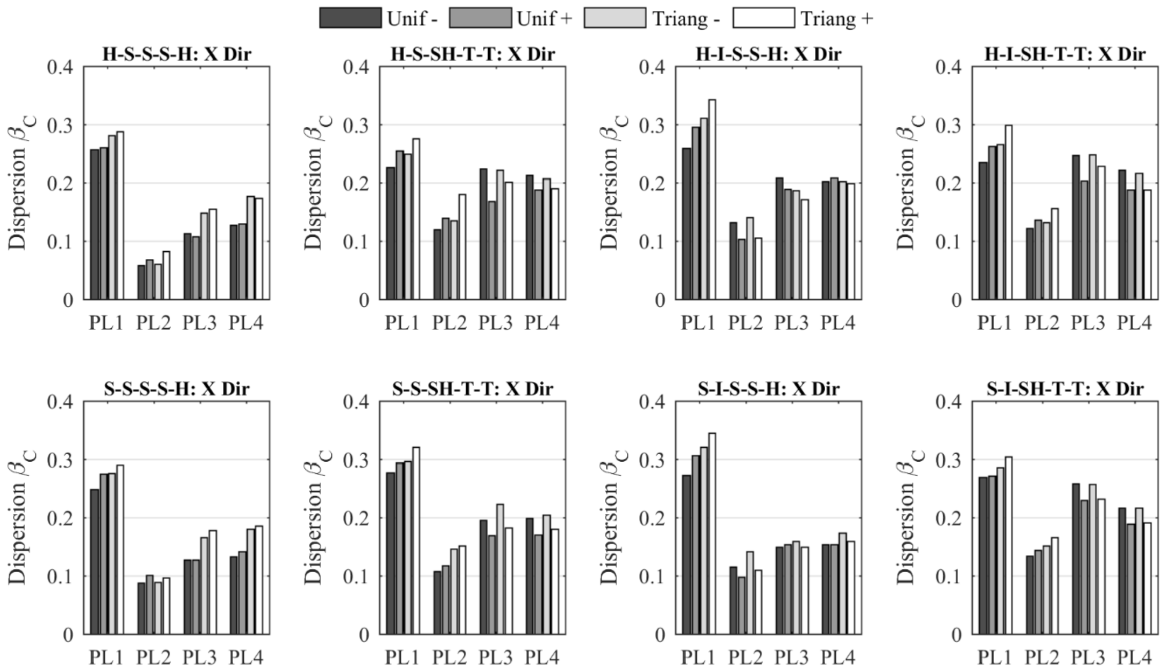

Figure E.5 – Dispersion in the capacity (β_C) obtained in the X direction: seismic action type 1

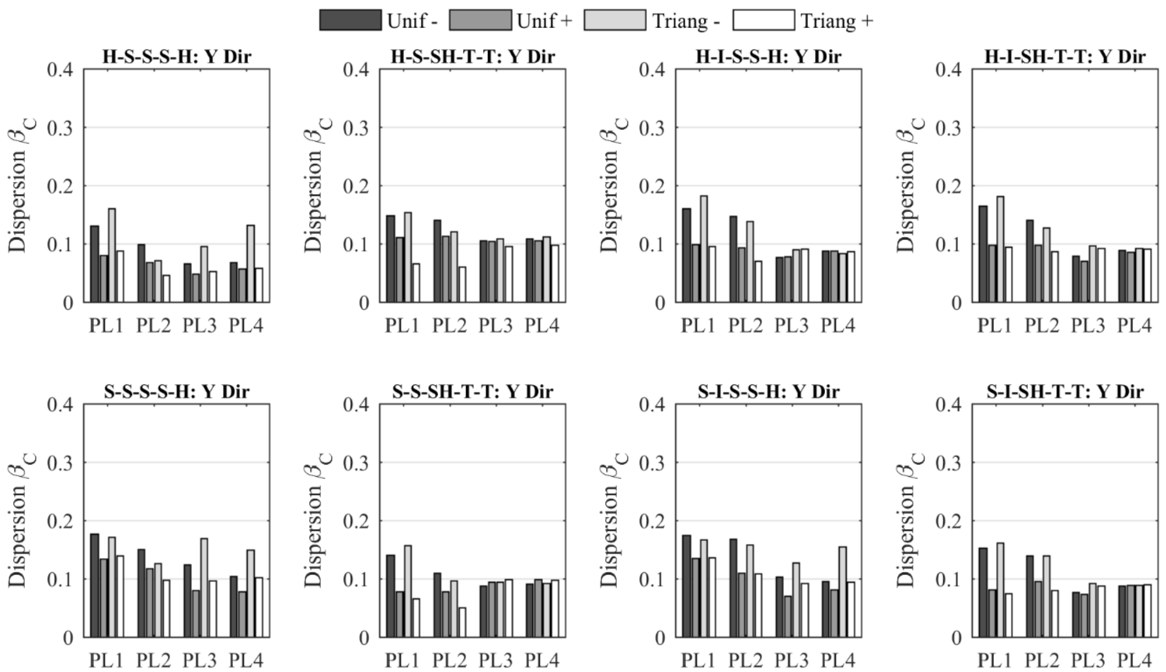

Figure E.6 – Dispersion in the capacity (β_C) obtained in the Y direction: seismic action type 1

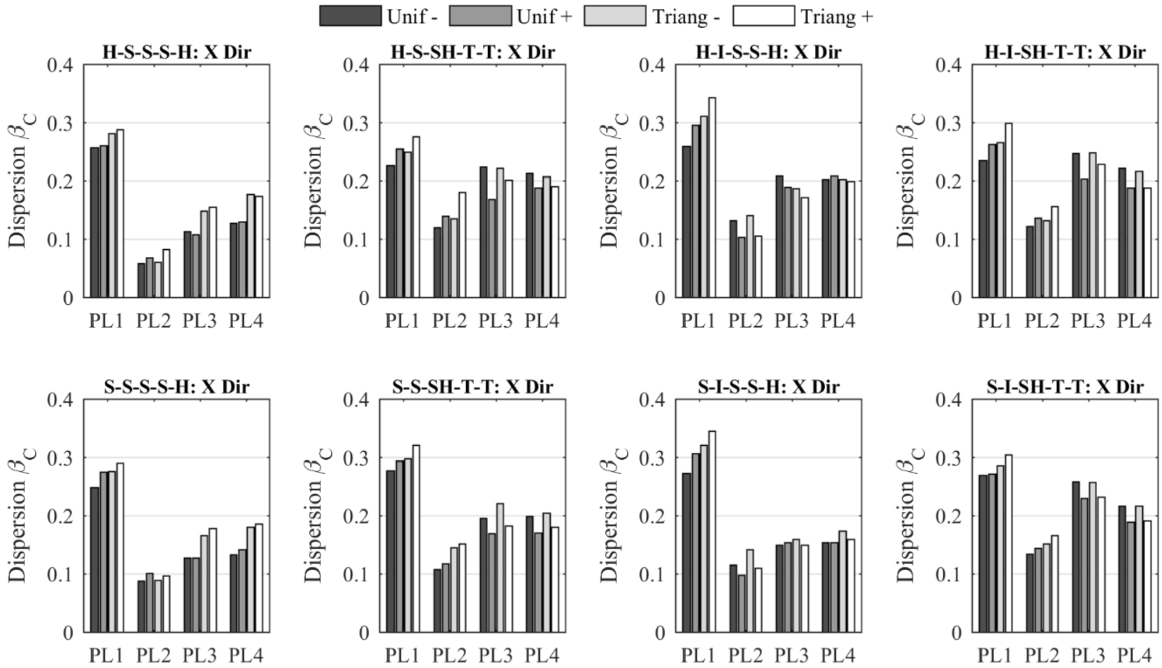

Figure E.7 – Dispersion in the capacity (β_C) obtained in the X direction: seismic action type 2

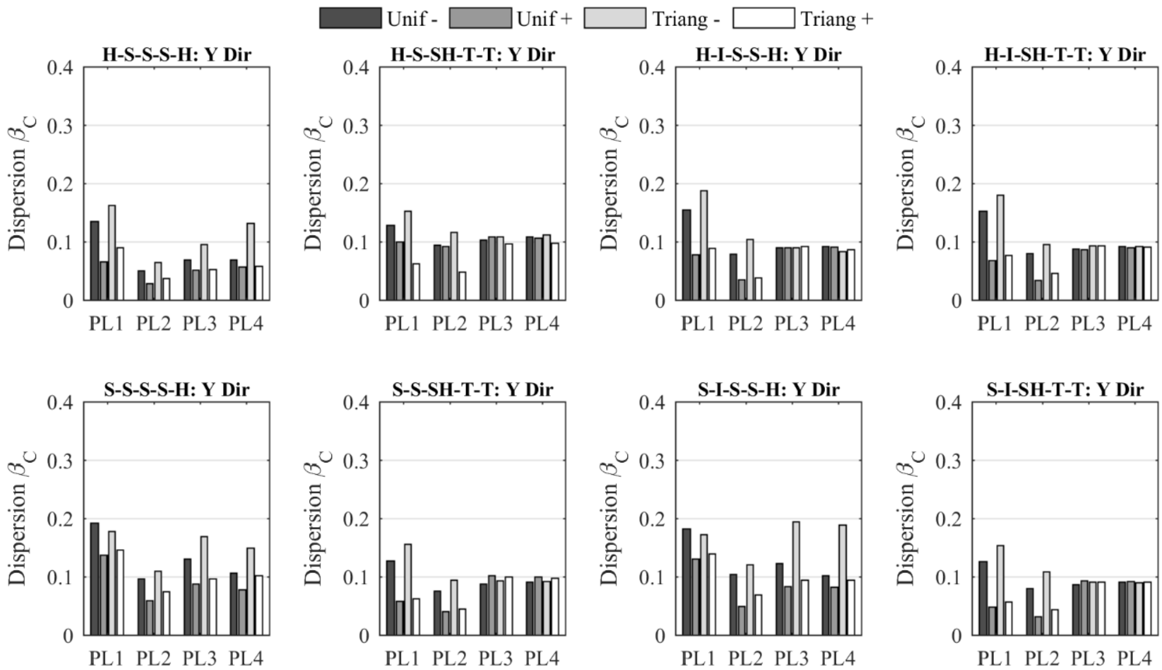

Figure E.8 – Dispersion in the capacity (β_C) obtained in the Y direction: seismic action type 2